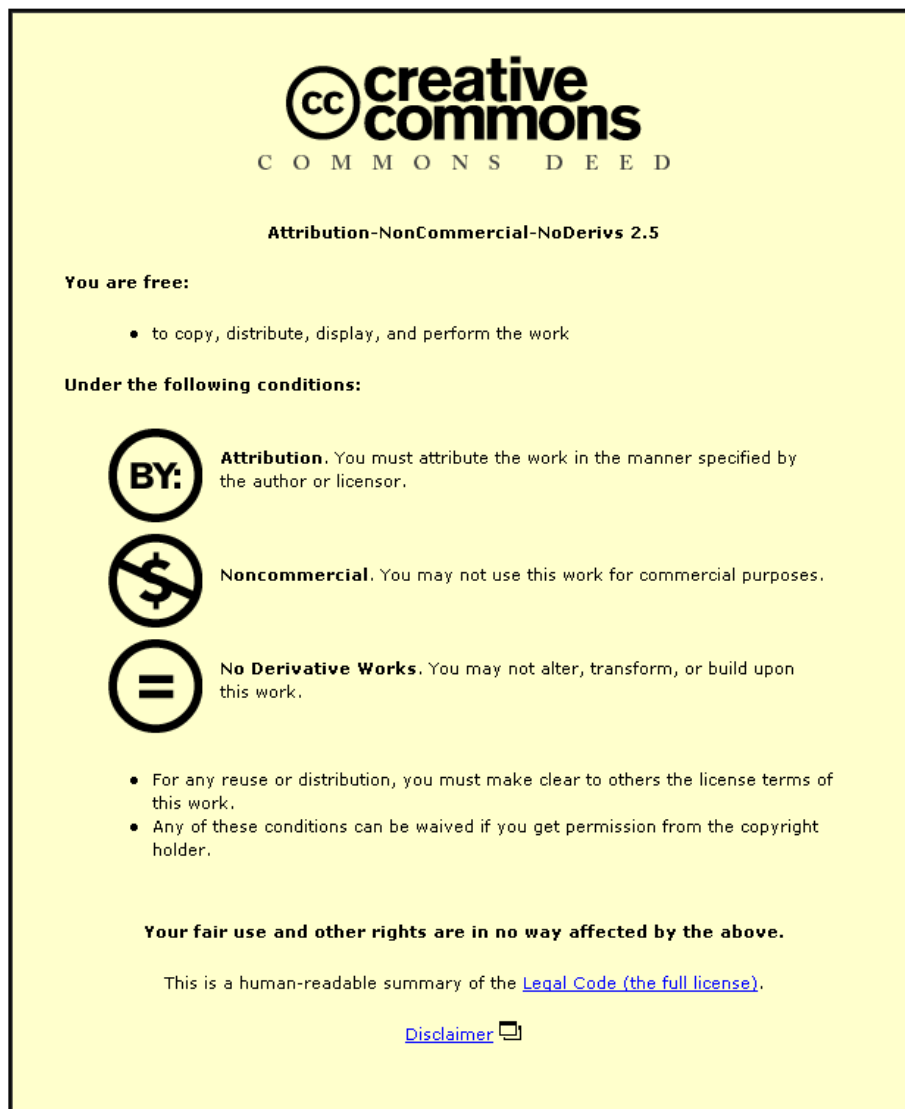


This item was submitted to Loughborough University as a PhD thesis by the author and is made available in the Institutional Repository (<https://dspace.lboro.ac.uk/>) under the following Creative Commons Licence conditions.



For the full text of this licence, please go to:
<http://creativecommons.org/licenses/by-nc-nd/2.5/>

**ADVANCED MEASUREMENT FOR SPORTS SURFACE
SYSTEM BEHAVIOUR UNDER MECHANICAL AND PLAYER
LOADING**

BY

XINYI WANG

A Doctoral Thesis Submitted in Partial Fulfilment of the Requirements for the
Award of
Doctor of Philosophy of Loughborough University

10th September 2013

© Xinyi Wang (2013)

Abstract

This research project has investigated the mechanical behaviour of artificial turf surface systems used for sports under a range of real player movements, and the contribution of component layers to the overall system response by developing advanced measurement systems and methods.

Artificial turf surface systems are comprised of a number of different materials and commonly with several layers, all of which contribute to their composite behaviour. During sports movements a player loads the surface, resulting in deformation that can change the surface behaviour, which in turn modifies the player biomechanical response. Improving the understanding of surface response to actual player loading is important for developing enhanced products for improving play performance. Likewise, by improving knowledge of surface effects on players, the understanding of injury risk can be improved. However, there is currently no published research to measure and analyse the behaviour of artificial turf system during real player locomotion. This research was undertaken to address this current lack of knowledge within the interaction between player and sports surface regarding the effects of player loading on the mechanical behaviour of artificial turf systems.

In addition to support player loading regime, mechanical behaviour of hockey and third generation artificial turf surface systems and their component shockpad layers (a rubber shreds bonded shockpad and a polyurethane foam shockpad) was examined through dynamic cyclic compressive loading using an advanced material testing machine in laboratory environment. Each layer and carpet-shockpad system was subjected to controlled loading designed with previous biomechanical data at various loading frequencies (0.9 Hz, 3.3 Hz and 10 Hz) and under two different contact areas (50 mm and 125 mm diameter) to simulate aspects of player walking, running and sprinting. All layers and surface systems tested showed nonlinear stress-strain behaviour with hysteresis. Increasing the contact area resulted in reduced surface vertical deflection and more linear response. Increasing the loading frequency led to stiffer response in the lower stress range (< 400 kPa) for all surface systems. The third generation artificial turf systems showed also an increase in stiffness at higher stress range (> 600 kPa) and a decrease in maximum strain as the loading frequency increased. Hysteresis loops obtained at different loading

frequencies indicated that the amount of energy lost at the same peak load of 1900 N in each surface system decreased with an increase in loading rate.

Player loading regime was performed to quantify the load/stress and the resulting surface deformation/strain under subject loading. Measurement systems including motion capture system, force plate and high speed were developed to characterise the response behaviour in a novel way. The mechanical behaviour of artificial turf surface systems under three player movement patterns (heel-toe walking, forefoot running and forefoot single leg landing) was measured. Boot-surface contact area of each movement varied during the stance. The heel-toe walking results indicated that the maximum applied stress and surface strain occurred in very early stance (first 10%) when the boot-surface contact area was small. For forefoot running and landing, the peak surface strain occurred around mid-stance concurrent with the time of peak applied stress. The maximum strain measured under running was smaller than under landing.

A ‘thin-film’ pressure sensing mat was used in both mechanical and player loading regimes and proved to be a useful tool for evaluating the pressure distributions and contact areas at different interfaces of the surface system. The applied stress on surface was observed to greatly reduce with depth over increasing contact area through the surface systems. Although the average pressure was reduced, pressure distribution contour showed directly under the surface load area the pressure at depth was still relatively large and that outside of this area the pressure was much lower.

A comparison of the mechanical behaviour of artificial turf systems in terms of compressive strain, modulus of elasticity, stress distribution and energy loss under mechanical cyclic loading, industry standard drop-weight impact tests and player loading was evaluated. Key loading parameters in different loading regimes and their influence on surface system response were determined. The structure and material intrinsic properties of shockpad were considered to further explain the observed surface system behaviour. Two mathematical models were used to fit through the experimental data and found to be able to describe surface system behaviour in the loading phase.

A breakthrough in understanding of the effects of real player loading on the mechanical behaviour response of artificial turf systems, and the contribution of the components to the whole system response has been achieved through the development of advanced measurement techniques.

Keywords: *Artificial turf system, mechanical behaviour, player loading, measurement system, stress distribution, modelling*

Acknowledgements

I would firstly like to express my thanks for the support, guidance and knowledge from my supervisors Dr. Paul Fleming and Prof. Neil Dixon. My thanks go to Dr. Steph Forrester for her expertise and support for processing the data from player loading experimental programme.

I also wish to thank other staff members and my fellow researchers from Sport Surfaces Research Group, Sports Technology Institute and Civil and Building Engineering for their assistance and help, in particular, Nick McLaren for his participation and effort in the player loading tests.

I would like to express my thanks to TigerTurf, AstroTurf, Recticel S.A., BSW Berleburger GmbH, Garside Sands and Murfitts Industries for their kindness and generosity to supply products and materials for testing purposes.

In addition to the academic help, my new friends that I met in the UK and old friends back in China have supported me over the last three years. Thanks to you all for your friendship and the precious memories we had together.

Special thanks go to my family, especially my parents Ming Wang and Mei Jin for their constant support and encouragement through my years at Loughborough.

Finally, a big thank you goes to my wife Zhen Sun whose love, encouragement and faith in me have given me the strength to reach this goal.

Table of Contents

Abstract.....	
Acknowledgements.....	iv
Table of Contents.....	v
List of Figures.....	viii
List of Tables.....	xx
1. Introduction.....	1
1.1 Background.....	1
1.2 Research approach.....	4
1.3 Aim and objectives.....	7
1.4 Thesis outline.....	7
2. Literature review.....	10
2.1 Chapter overview.....	10
2.2 Development of artificial turf surfaces.....	10
2.3 Construction and design of artificial turf pitches.....	12
2.3.1 Foundation layer.....	12
2.3.2 Shockpad layer.....	14
2.3.3 Carpet layer.....	16
2.4 Performance standards and mechanical test methods for artificial turf surfaces.....	19
2.4.1 Performance standards.....	19
2.4.2 Mechanical test methods.....	20
2.5 Player-surface interactions.....	25
2.5.1 Overview.....	25
2.5.2 Player loading characteristics.....	28
2.6 Material behaviour, measurement techniques and modelling.....	31
2.6.1 Overview.....	31
2.6.2 Material mechanical behaviour.....	33

2.6.3	Measurement techniques.....	40
2.7	Discussion	46
3.	Mechanical behaviour of artificial surface systems under controlled loading	63
3.1	Chapter overview	63
3.2	Experimental methodology	63
3.2.1	Surface samples	63
3.2.2	Mechanical loading methods	65
3.2.3	Equipment & measurement set-up.....	67
3.3	Results	74
3.3.1	Cyclic loading on individual layers	74
3.3.2	Surface system mechanical behaviour	77
3.3.3	Pressure distribution in surface system.....	85
3.4	Discussion	91
3.4.1	Effects of cyclic loading	91
3.4.2	Effects of loading frequency	92
3.4.3	Comparison between cyclic compression and the AAA loading	94
3.4.4	Stress distribution angle.....	95
4.	Mechanical behaviour of artificial surface systems under player loading.....	128
4.1	Chapter overview	128
4.2	Experimental methodology	128
4.2.1	Surface systems.....	128
4.2.2	Player, shoe and movement patterns.....	129
4.2.3	Equipment & measurement set-up.....	131
4.3	Results	135
4.3.1	Player movement patterns.....	135
4.3.2	Surface system mechanical behaviour	137
4.3.3	Pressure distribution in surface system.....	146

4.4	Discussion	149
4.4.1	Validity of boot segment plane	149
4.4.2	Stiffness of surface systems	151
4.4.3	Pressure contour	152
5.	Discussion	199
5.1	Chapter overview	199
5.2	Linking research findings	199
5.2.1	Differences between test approaches	199
5.2.2	Compressive strain	202
5.2.3	Chord modulus	203
5.2.4	Stress distribution	204
5.2.5	Energy behaviour	206
5.3	Modelling surface system mechanical behaviour	209
5.4	Summary	212
6.	Conclusions	221
6.1	Chapter overview	221
6.2	Conclusions	221
6.3	Study limitations	226
6.4	Recommendations	228
6.4.1	Further academic research	228
6.4.2	Industry	229
6.5	List of publications	230
	Reference	232

List of Figures

CHAPTER ONE: PAGE 9

Figure 1.1: Flow diagram illustrating the chapters of thesis interlinked with each other

CHAPTER TWO: PAGE 52 - 61

Figure 2.1: Three generations of artificial turf (TenCate, 2010)

Figure 2.2: Typical artificial turf pitch system structure (Synthetic Grass Info, 2010)

Figure 2.3: Typical structure of foundation layer for artificial sports pitches

Figure 2.4: Monofilament and Fibrillated turf blades (TenCate, 2010)

Figure 2.5: The structure of the Advanced Artificial Athlete (FIFA, 2012)

Figure 2.6: The Clegg Impact Hammer (Severn, 2010)

Figure 2.7: Ground reaction force components in three directions during running (Davidson, 2012)

Figure 2.8: Typical GRF profiles of rearfoot strike runner; (a) Fz, (b) FAP and (c) FML (Davidson, 2012)

Figure 2.9: Vertical ground reaction force of forefoot strike running (Lieberman et al., 2010)

Figure 2.10: Vertical ground reaction force curves of one runner performing 1 barefoot trial and 1 shod trial at the same velocity of 4.5 m/s (De Wit et al., 2000)

Figure 2.11: Vertical ground reaction force for a compliant and non-compliant surface (Young, 2006)

Figure 2.12: Closed-cell (left) and open-cell (right) polymer foam structures (Davidson, 2012)

Figure 2.13: Schematic compression stress-strain curves for a polymer foam

Figure 2.14: Example force-deflection data for compression of a viscoelastic material (Davidson, 2012)

Figure 2.15: Energy input, returned and lost in a sport surface. In each case the shaded region depicts the magnitude of the energy (Stefanyshyn and Nigg, 2003)

Figure 2.16: Three phases of shockpad behaviour under a compressive impact (Anderson, 2007)

Figure 2.17: Example plantar pressure map of a walking trial recorded by the Tekscan Matscan system (Zammit et al., 2010)

Figure 2.18: Tekscan Matscan system was mounted on top of a force plate (Carvalho et al., 2005)

Figure 2.19: Experimental setup used to apply pressure to Tekscan sensor using an Instron machine (Brimacombe et al., 2009)

Figure 2.20: Experimental setup of 3D-DIC system for the foam compression test (Jin et al., 2007)

CHAPTER THREE: PAGE 103 – 126

Figure 3.1: Instron ElectroPuls E3000 machine with sample

Figure 3.2: Representation of the sine wave loading cycles applied by the Instron machine

Figure 3.3: A picture of Tekscan pressure mat 3150E

Figure 3.4: Tekscan software calibration tool interface

Figure 3.5: Pressure mat calibration by Instron machine compressive loading

Figure 3.6: Schematic of the measurement system design, showing the surface system of carpet and shockpad and the compression dynamic mechanical loading

Figure 3.7: Schematic of pressure mat used between layers and under shockpad in the surface system under the dynamic compressive mechanical loading

Figure 3.8: Schematic of pressure mat used between layers and under shockpad in the surface system under the AAA test

Figure 3.9: Force-deflection relationship of 0.9 Hz cyclic loading with 50 mm loading foot on hockey turf (18 mm thick)

Figure 3.10: Force-deflection relationship of 0.9 Hz cyclic loading with 50 mm loading foot on 3G turf (32 mm infill depth)

Figure 3.11: Force-deflection relationship of 0.9 Hz cyclic loading with 50 mm loading foot on rubber shockpad (15 mm thick)

Figure 3.12: Force-deflection relationship of 0.9 Hz cyclic loading with 50 mm loading foot on foam shockpad (12 mm thick)

Figure 3.13: Force-deflection relationship of 3.3 Hz cyclic loading with 50 mm loading foot on hockey turf (18 mm thick)

Figure 3.14: Force-deflection relationship of 3.3 Hz cyclic loading with 50 mm loading foot on 3G turf (32 mm infill depth)

Figure 3.15: Force-deflection relationship of 3.3 Hz cyclic loading with 50 mm loading foot on rubber shockpad (15 mm thick)

Figure 3.16: Force-deflection relationship of 3.3 Hz cyclic loading with 50 mm loading foot on foam shockpad (12 mm thick)

Figure 3.17: Force-deflection relationship of 10 Hz cyclic loading with 50 mm loading foot on hockey turf (18 mm thick)

Figure 3.18: Force-deflection relationship of 10 Hz cyclic loading with 50 mm loading foot on 3G turf (35 mm infill depth)

Figure 3.19: Force-deflection relationship of 10 Hz cyclic loading with 50 mm loading foot on rubber shockpad (15 mm thick)

Figure 3.20: Force-deflection relationship of 10 Hz cyclic loading with 50 mm loading foot on foam shockpad (12 mm thick)

Figure 3.21: Force-deflection relationship of hockey turf with rubber shockpad system (green) and hockey turf with foam shockpad system (red) for 0.9 Hz loading with 50 mm (solid line) and 125 mm (dash line) diameters loading feet

Figure 3.22: Force-deflection relationship of 3G turf with rubber shockpad system (green) and 3G turf with foam shockpad system (red) for 0.9 Hz loading with 50 mm (solid line) and 125 mm (dash line) diameters loading feet

Figure 3.23: Stress-strain relationship of hockey turf with rubber shockpad system (green) and hockey turf with foam shockpad system (red) for 0.9 Hz loading with 50 mm (solid line) and 125 mm (dash line) diameters loading feet

Figure 3.24: Stress-strain relationship of 3G turf with rubber shockpad system (green) and 3G turf with foam shockpad system (red) for 0.9 Hz loading with 50 mm (solid line) and 125 mm (dash line) diameters loading feet

Figure 3.25: Force-deflection relationship of hockey turf with rubber shockpad system (green) and hockey turf with foam shockpad system (red) for 3.3 Hz loading with loading feet of 50 mm (solid line) and 125 mm (dash line) diameters

Figure 3.26: Force-deflection relationship of 3G turf with rubber shockpad system (green) and 3G turf with foam shockpad system (red) for 3.3 Hz loading with 50 mm (solid line) and 125 mm (dash line) diameters loading feet

Figure 3.27: Stress-strain relationship of hockey turf with rubber shockpad system (green) and hockey turf with foam shockpad system (red) for 3.3 Hz loading with 50 mm (solid line) and 125 mm (dash line) diameters loading feet

Figure 3.28: Stress-strain relationship of 3G turf with rubber shockpad system (green) and 3G turf with foam shockpad system (red) for 3.3 Hz loading with 50 mm (solid line) and 125 mm (dash line) diameters loading feet

Figure 3.29: Force-deflection relationship of hockey turf with rubber shockpad system (green) and hockey turf with foam shockpad system (red) for 10 Hz loading with loading feet of 50 mm (solid line) and 125 mm (dash line) diameters

Figure 3.30: Force-deflection relationship of 3G turf with rubber shockpad system (green) and 3G turf with foam shockpad system (red) for 10 Hz loading with 50 mm (solid line) and 125 mm (dash line) diameters loading feet

Figure 3.31: Stress-strain relationship of hockey turf with rubber shockpad system (green) and hockey turf with foam shockpad system (red) for 10 Hz loading with 50 mm (solid line) and 125 mm (dash line) diameters loading feet

Figure 3.32: Stress-strain relationship of 3G turf with rubber shockpad system (green) and 3G turf with foam shockpad system (red) for 10 Hz loading with 50 mm (solid line) and 125 mm (dash line) diameters loading feet

Figure 3.33: Intrusion effect of pressure mat inserted between hockey turf and rubber shockpad layers under 3.3 Hz loading at the first and last cycles

Figure 3.34: Intrusion effect of pressure mat inserted between hockey turf and foam shockpad layers under 3.3 Hz loading at the first and last cycles

Figure 3.35: Stitch lines across the backing of the 3G carpet

Figure 3.36: Pressure contour of 3G carpet at peak contact area under 3.3 Hz loading with 125 mm loading foot

Figure 3.37: Accumulation of residual strain for the layers under 3.3 Hz cyclic loading

Figure 3.38: Stress-strain relationship of hockey turf with rubber shockpad system for different loading frequencies with 50 mm loading foot

Figure 3.39: Stress-strain relationship of hockey turf with foam shockpad system for different loading frequencies with 50 mm loading foot

Figure: 3.40: Stress-strain relationship of 3G turf with rubber shockpad system for different loading frequencies with 50 mm loading foot

Figure 3.41: Stress-strain relationship of 3G turf with foam shockpad system for different loading frequencies with 50 mm loading foot

Figure 3.42: Stress-strain relationship of hockey turf systems for 10 Hz loading and the AAA impact

Figure 3.43: Stress-strain relationship of 3G turf systems for 10 Hz loading and the AAA impact

Figure 3.44: Stress distribution angle Θ through surface

Figure 3.45: Pressure mappings for hockey turf (above) and the 3G turf (below) under 50 mm diameter loading foot

Figure 3.46: Pressure contour at peak stress of 3.3 Hz compressive loading recorded at the bottom of hockey turf + rubber shockpad system under 50 mm diameter loading foot. The high pressure region is displayed by warm colour cells and outlined by the red line.

CHAPTER FOUR: PAGE 160 - 196

Figure 4.1: Test locations for infill height (numbered cells) and the AAA (numbered circles)

Figure 4.2: Picture of the soccer boots used in the experiment programme

Figure 4.3: Schematic graph (above) and picture (below) of the pressure mat position in the measurement set-up

Figure 4.4: Screen-shot of the layout of 12 Vicon cameras and capture volume including the force plate and markers in the centre of laboratory floor map

Figure 4.5: The static stage of calibration of the Vicon system to set the global coordinates system

Figure 4.6: Position of markers on the left boot of player in the pilot experiment

Figure 4.7: Improved markers configuration of the left boot with four additional markers (red)

Figure 4.8: High speed camera with lighting system orientated laterally to the surface system

Figure 4.9: Measurement set-up for player loading tests in laboratory

Figure 4.10: Multi-output trigger box for various devices (Vicon, force plate, pressure mat and high-speed camera)

Figure 4.11: Static trial capture with player standing alongside the force plate and labelled markers

Figure 4.12: Representative vertical impact force (F_z) and CoP (x,y)-time history profiles for heel-toe walking with images from high-speed camera taken at the frames of touchdown, first peak, second peak and toe-off

Figure 4.13: Representative vertical impact force (F_z) and CoP (x,y)-time history profiles for forefoot running with images from high-speed camera taken at the frames of touchdown, peak force and toe-off

Figure 4.14: Representative vertical impact force (F_z) and CoP (x,y)-time history profiles for forefoot landing with images from high-speed camera taken at the frames of touchdown, peak force and toe-off

Figure 4.15: A plane fitted through the 5 forefoot markers (black) in the static trial

Figure 4.16: Vertical deflection (green curve) of hockey turf + rubber shockpad system (a) and hockey turf + foam shockpad system (b) under player forefoot running

Figure 4.17: Vertical deflection (green curve) of 3G turf + rubber shockpad system (a) and 3G turf + foam shockpad system (b) under player forefoot running

Figure 4.18: Force-deflection relationship of player forefoot running on hockey turf + rubber shockpad system

Figure 4.19: Force-deflection relationship of player forefoot running on hockey turf + foam shockpad system

Figure 4.20: Force-deflection relationship of player forefoot running on 3G turf + rubber shockpad system

Figure 4.21: Force-deflection relationship of player forefoot running on 3G turf + foam shockpad system

Figure 4.22: Boot contact area-time relationship of player forefoot running

Figure 4.23: Stress-strain relationship of player forefoot running on hockey turf + rubber shockpad system

Figure 4.24: Stress-strain relationship of player forefoot running on hockey turf + foam shockpad system

Figure 4.25: Stress-strain relationship of player forefoot running on 3G turf + rubber shockpad system

Figure 4.26: Stress-strain relationship of player forefoot running on 3G turf + foam shockpad system

Figure 4.27: Vertical deflection (green curve) of hockey turf + rubber shockpad system (a) and hockey turf + foam shockpad system (b) under player forefoot landing

Figure 4.28: Vertical deflection (green curve) of 3G turf + rubber shockpad system (a) and 3G turf + foam shockpad system (b) under player forefoot landing

Figure 4.29: HSV footage shows the large surface deflection on 3G turf system at touchdown where the boot was inclined to the horizontal and boot-surface contact area was small

Figure 4.30: Force-deflection relationship of player forefoot landing on hockey turf + rubber shockpad system

Figure 4.31: Force-deflection relationship of player forefoot landing on hockey turf + foam shockpad system

Figure 4.32: Force-deflection relationship of player forefoot landing on the 3G turf + rubber shockpad system

Figure 4.33: Force-deflection relationship of player forefoot landing on 3G turf + foam shockpad system

Figure 4.34: Boot contact area-time relationship of player forefoot landing

Figure 4.35: Stress-strain relationship of player forefoot landing on hockey turf + rubber shockpad system

Figure 4.36: Stress-strain relationship of player forefoot landing on hockey turf + foam shockpad system

Figure 4.37: Stress-strain relationship of player forefoot landing on 3G turf + rubber shockpad system

Figure 4.38: Stress-strain relationship of player forefoot landing on 3G turf + foam shockpad system

Figure 4.39: Planes fitted through 5 forefoot markers (yellow), 5 rear and mid foot markers (blue) and 3 heel markers (red) in the static trial

Figure 4.40: Vertical deflection (green curve) of hockey turf + rubber shockpad system measured at 0-10%, 10%-55% and 55%-100% of ground contact under player heel-toe walking

Figure 4.41: Vertical deflection (green curve) of hockey turf + foam shockpad system measured at 0-10%, 10%-55% and 55%-100% of ground contact under player heel-toe walking

Figure 4.42: Vertical deflection (green curve) of 3G turf + rubber shockpad system measured at 0-10%, 10%-55% and 55%-100% of ground contact under player heel-toe walking

Figure 4.43: Vertical deflection (green curve) of 3G turf + foam shockpad system measured at 0-10%, 10%-55% and 55%-100% of ground contact under player heel-toe walking

Figure 4.44: Force (red dash curve) and deflection (green curve) in touchdown phase (10%), mid-stance phase (10%-55%) and push-off phase (55%-100%) during ground contact of player heel-toe walking on hockey turf + rubber shockpad system

Figure 4.45: Force (red dash curve) and deflection (green curve) in touchdown phase (10%), mid-stance phase (10%-55%) and push-off phase (55%-100%) during ground contact of player heel-toe walking on hockey turf + foam shockpad system

Figure 4.46: Force (red dash curve) and deflection (green curve) in touchdown phase (10%), mid-stance phase (10%-55%) and push-off phase (55%-100%) during ground contact of player heel-toe walking on 3G turf + rubber shockpad system

Figure 4.47: Force (red dash curve) and deflection (green curve) in touchdown phase (10%), mid-stance phase (10%-55%) and push-off phase (55%-100%) during ground contact of player heel-toe walking on 3G turf + foam shockpad system

Figure 4.48: Boot contact area-time relationship of player heel-toe walking

Figure 4.49: Stress-time and strain-time histories of player heel-toe walking on the hockey turf + rubber shockpad surface system

Figure 4.50: Stress-time and strain-time histories of player heel-toe walking on the hockey turf + foam shockpad surface system

Figure 4.51: Stress-time and strain-time histories of player heel-toe walking on the 3G turf + rubber shockpad surface system

Figure 4.52: Stress-time and strain-time histories of player heel-toe walking on the 3G turf + foam shockpad surface system

Figure 4.53: Pressure maps recorded at the bottom of hockey turf + rubber shockpad system and between the two layers. Larger high pressure region (warm colour) measured at the bottom than between the layers over similar contact area

Figure 4.54: Pressure contours show the peak contact area between the layers and underneath the 3G turf systems under player running (above) and walking (below)

Figure 4.55: Valid surface vertical deflection for player walking on hockey turf + rubber shockpad system (black), hockey turf + foam shockpad system (green), 3G turf + rubber shockpad system (red) and 3G turf + foam shockpad system (blue). All show the mean (solid/dashed line) \pm SD (shaded area)

Figure 4.56: Valid surface vertical deflection for player running on hockey turf + rubber shockpad system (black), hockey turf + foam shockpad system (green), 3G turf + rubber shockpad system (red) and 3G turf + foam shockpad system (blue). All show the mean (solid/dashed line) \pm SD (shaded area)

Figure 4.57: Valid surface vertical deflection for player landing on hockey turf + rubber shockpad system (black), hockey turf + foam shockpad system (green), 3G turf + rubber shockpad system (red) and 3G turf + foam shockpad system (blue). All show the mean (solid/dashed line) \pm SD (shaded area)

Figure 4.58: The active boot segment angle in sagittal plane for walking on hockey turf + rubber shockpad system (black), hockey turf + foam shockpad system (green), 3G turf + rubber shockpad system (red) and 3G turf + foam shockpad system (blue). All show the mean (solid/dashed line) \pm SD (shaded area)

Figure 4.59: The active boot segment angle in sagittal plane for running on hockey turf + rubber shockpad system (black), hockey turf + foam shockpad system (green), 3G turf +

rubber shockpad system (red) and 3G turf + foam shockpad system (blue). All show the mean (solid/dashed line) \pm SD (shaded area)

Figure 4.60: The active boot segment angle in sagittal plane for landing on hockey turf + rubber shockpad system (black), hockey turf + foam shockpad system (green), 3G turf + rubber shockpad system (red) and 3G turf + foam shockpad system (blue). All show the mean (solid/dashed line) \pm SD (shaded area)

Figure 4.61: A comparison of force-deflection relationship for the push-off phase of walking on hockey turf + rubber shockpad system (black), hockey turf + foam shockpad system (green), 3G turf + rubber shockpad system (red) and 3G turf + foam shockpad system (blue)

Figure 4.62: A comparison of force-deflection relationship for running on hockey turf + rubber shockpad system (black), hockey turf + foam shockpad system (green), 3G turf + rubber shockpad system (red) and 3G turf + foam shockpad system (blue)

Figure 4.63: A comparison of force-deflection relationship for landing on hockey turf + rubber shockpad system (black), hockey turf + foam shockpad system (green), 3G turf + rubber shockpad system (red) and 3G turf + foam shockpad system (blue)

Figure 4.64: Contact area measured by pressure mat at boot-surface interface and delineated by a polygon. The CoP was indicated by the black and white square.

Figure 4.65: Pressure contour measured at the carpet-shockpad interface (left) and the bottom of hockey turf + rubber shockpad system (right), with the impact area polygon and the CoP position

Figure 4.66: In hockey turf + rubber shockpad system, the pressure history measured at carpet-shockpad interface over whole contact area (red) and polygon area (magenta), and at the bottom of the surface system over whole contact area (green) and polygon area (cyan)

CHAPTER FIVE: PAGE 216 – 218

Figure 5.1: Stress-strain relationship of hockey turf surface systems for 3.3 Hz mechanical loading with 50 mm test foot (solid lines) and player forefoot running impact (dashed lines)

Figure 5.2: Stress-strain relationship of 3G turf surface systems for 3.3 Hz mechanical loading with 50 mm test foot (solid lines) and player forefoot running impact (dashed lines)

Figure 5.3: Comparison of stress-strain models for 3.3 Hz mechanical loading with 50 mm diameter loading foot on the hockey turf systems

Figure 5.4: Comparison of stress-strain models for 3.3 Hz mechanical loading with 50 mm diameter loading foot on the 3G turf systems

Figure 5.5: Comparison of stress-strain models for player forefoot running on the hockey turf systems

Figure 5.6: Comparison of stress-strain models for player forefoot running on the 3G turf systems

CHAPTER SIX: PAGE 229

Figure 6.1: Angled load platens design facilitating simultaneous application of multiple GRF components (modified from Davidson, 2012)

List of Tables

CHAPTER TWO: PAGE 50 – 51

Table 2.1: Field tests and requirements of artificial turf pitch for soccer (FIFA, 2012a)

Table 2.2: A summary of player movement classification (El Kati et al., 2009)

Table 2.3: Peak force and contact time measurements for various authors (updated from Severn, 2010)

CHAPTER THREE: PAGE 96 – 102

Table 3.1: Specifications of products used in this project

Table 3.2: Instron ElectroPuls E3000 key specifications (Davidson, 2012)

Table 3.3: Key parameters of the compression test methods compare to player walking, running and sprinting movements

Table 3.4: Peak vertical deflection and key stiffness values for all surface systems under 0.9 Hz 2nd loading cycle

Table 3.5: Peak vertical deflection and key stiffness values for all surface systems under 3.3 Hz 10th loading cycle

Table 3.6: Peak vertical deflection and key stiffness values for all surface systems under 10 Hz 20th loading cycle

Table 3.7: Results of the AAA tests on individual layer samples and carpet-shockpad systems

Table 3.8: Peak contact area and stress (+ standard deviation) measured by the pressure mat placed under individual layer samples and at two different positions in the surface systems under 0.9 Hz loading

Table 3.9: Peak contact area and stress (+ standard deviation) measured by the pressure mat placed under individual layer samples and at two different positions in the surface systems under 3.3 Hz loading

Table 3.10: Peak contact area and stress (+ standard deviation) measured by the pressure mat placed under individual layer samples and at two different positions in the surface systems under 10 Hz loading

Table 3.11: Peak contact area and stress (+ standard deviation) measured by the pressure mat placed under individual layer samples and at two different positions in the surface systems under the AAA impacts

Table 3.12: Average stress distribution angles of individual layers and surface systems under compressive loading at different frequencies with 50 mm loading foot and the AAA impacts

CHAPTER FOUR: PAGE 153 – 159

Table 4.1: Averaged infill height and force reduction measured on the test locations (marked in Figure 4.1) of the 3G turf surface systems before and after player testing trials

Table 4.2: Player movement patterns/surface systems tested in the laboratory

Table 4.3: A summary table linking the measurement methods to the results

Table 4.4: A summary of peak vertical force and contact time for each player movement pattern on each surface system with pressure mat placed at the bottom

Table 4.5: A summary of peak vertical force and contact time for each player movement pattern on each surface system with pressure mat placed between the layers

Table 4.6: Player movement repeatability analysis for all the trials

Table 4.7: Maximal vertical deflection for each surface system under player forefoot running

Table 4.8: Maximal vertical deflection for each surface system under player forefoot landing

Table 4.9: Vertical deflection of each surface system during three phases of player heel-toe walking

Table 4.10: Peak contact area and stress (+ standard deviation) measured by the pressure mat placed at different positions in the surface systems under three player movement patterns

Table 4.11: Average stiffness of surface systems under different player movements in the range of vertical force from 600 N to peak

CHAPTER FIVE: PAGE 214 - 215

Table 5.1: Summary table of compressive properties for each surface system under different loading types

Table 5.2: Parameters and error values for stress-strain models to describe the loading phase of the 10th cycle of 3.3 Hz mechanical loading with 50 mm diameter foot on each surface system

Table 5.3: Parameters and error values for stress-strain models to describe the loading phase of player forefoot running movement on each surface system

1. Introduction

1.1 Background

Artificial turf surfaces became recognised in 1965 when AstroTurf™ was installed at the Astrodome in Houston, Texas. The use of this artificial sports surface spread widely in the 1980's and was installed in both outdoor and indoor stadiums for football and baseball in North America. Artificial surfaces were introduced as an alternative to natural turf in an attempt to overcome the issues such as shortage of water, increased participation in sports and high operational and maintenance costs. The acceptance of artificial turf surface varies with different sports. The transition from natural to artificial turf surface has completed for the game of field hockey as the majority of top level competitions are played on artificial turf (FIH, 2008). In other sports such as soccer and rugby, this transition has been much slower. However, since the 1990's, the newer (third) generation of artificial turf offers playing characteristics closer to natural turf and has permitted its use for professional and international matches sanctioned by international governing bodies. Many sports worldwide have now adopted artificial turf into the laws of their game. Future generations of players accustomed to artificial turf surfaces at school and continuing development of the products will surely lead to further popularity and acceptance of artificial turf.

Although the artificial turf surfaces available on market vary in design and materials for different sports applications, most of the surfaces are of similar structure comprising the key components of an artificial carpet layer (with or without infill), a shockpad layer and an engineered foundation. A number of different materials involved in each constituent layer and each component with its own properties, all together they provide the acquired playing characteristics for specific sports or multiple uses. International sport governing bodies have set assessment requirements that comprise mechanical test methods and specifications that state performance limits for artificial turf pitches in terms of play performance, safety and durability. These requirements have in general been set by measuring the play performance properties of natural turf, and applying the test limits for compliance to a level considered to 'replicate' good quality natural turf. In general standards for community use have wider limits of acceptability for many tests compared to standards for professional level. The current industry standard test applied for compliance to governing body standards have been widely criticised as not simulative of either the player loading during interaction or of the typical ball movements during play. These

current industry standard tests are useful for construction compliance but increasingly are scrutinised for their applicability to predict or benchmark surface behaviour in relation to player performance or risk of injury.

The increasing popularity of artificial turf surfaces, their inclusion into the professional sporting world, and advances in many aspects of sport science associated with improving human performance and understanding/preventing injury has drawn the attention of academic and industry researchers to attempt to better understand the interactions of the player and ball with artificial surfaces. The surface is a form of sport equipment, and has attracted similar themes of research with regard mechanical testing, for performance and durability and also player perception. Negative player perception has been an important factor in the slow introduction of artificial turf into professional soccer in Europe, for example.

However, it is clear that in spite of technological developments in artificial turf systems, and studies largely carried out by well-resourced sport governing bodies, many scientific questions remain regarding how artificial surfaces (and natural ones) behave during the player and ball interactions. The technology drive for improving sporting boots and shoes has driven much work into shoe-surface interaction over a number of years (Muller et al., 2010; McGhie and Ettema, 2013; Grund and Senner, 2010). In most cases this has focussed on shoe outsole design and not the surface properties or indeed the interaction mechanisms. The terms used in sports engineering related publications rarely deconstruct terms such as the 'traction' resistance into material properties such as stiffness, strength, or fundamental friction values.

There exists a collective body of previous research into the interaction between the player and artificial turf system using human subjects, usually with a primary biomechanical focus on the effects of the surface on the subject wherein the surface is a generic type or is categorised based on the industry tests for shock absorbency or traction. These studies rarely provide any insight into the surface behaviour or response or attempt to investigate the influence of the surface design in any detail. Where the research studies have attempted to link the findings to potential injury risk (Andersson et al., 2008; Ford et al., 2006; Brachet, 2004; Stiles and Dixon, 2006; Twomey et al., 2012) the link has been primarily empirical, attempting to test out hypotheses of greater injury incidence on harder and/or higher traction surfaces for example. These epidemiological studies have in general again

provided little information on the characteristics of the surfaces selected or encountered such that there is a lack of clear evidence of any conclusive relationship between player response/injury and the surface design or condition at the time. There is an ongoing reliance, in general, on benchmarking surface state by the governing body standard test methods. These tests have been in existence for around 30 years or more and have not advanced significantly, such that there is a clear gap between what is now understood about player loading on a surface and what the (simple) tests can and do replicate. The current status quo is such that without mechanical test methods that better replicate player loading little advance is likely in measuring the performance or injury related surface behaviour. However, there are currently limited research efforts to improve understanding.

What is increasingly clear is that there is little published literature that describes measurement of the effect of the player loading on the sport surface's engineering behaviour. As more new technology is used in surface system design, and the desire to manufacture better safer surfaces that last longer, there is an increased demand for developing new knowledge of how the surface system responds to real player loading scenarios and how to use this knowledge to enhance artificial turf design. In general the current methods used in laboratory studies, drop-weight impact tests and material testing machines are considered inappropriate to accurately represent player loading occurring in real situations (Dura et al., 2002; Miller et al., 2000; Baroud et al., 1999; Nigg et al., 1984; Dixon et al., 1999; Young and Fleming, 2007) and are applied to whole surface systems such that the properties of the components are not investigated nor their interaction understood.

It is proposed that further scientific investigation of the effects of real player loading on the mechanical behaviour of sport surface systems, using more advanced measurement techniques and test approaches is required to develop new knowledge to enhance surface system design and testing. More detailed experimental data describing the sport surface material behaviour is useful for assisting academic research into mathematical modelling of surface interactions which can provide a powerful virtual tool to extend the applicability of experimental studies.

This research programme is thus focussed on developing measurement techniques to investigate the artificial turf surface behaviour under load.

1.2 Research approach

This research area, comprising the behaviour of sport surfaces under loading, is applied in nature and previous research has primarily adopted quantitative methodologies to explore research questions and hypotheses – usually with a clear focus on either impact related behaviour or friction/traction related behaviour. This differentiation is reflected in the current industry mechanical test methods employed to simulate either player to surface interaction or ball to surface interaction. Subject testing has to some extent also followed this differentiation with either studies on straight line running or a jump landing, or a cutting or turning manoeuvres. Mechanical tests for friction/traction measurement have largely adopted a static normal load, and data from subject testing clearly shows this is not the case throughout the ground contact time.

Sport surfaces clearly deform under load, and their design using thin layers of elastomeric materials dictates that the surface response is composed of the interaction of the material layers. The deformation behaviour under vertical load is of interest for many aspects of interaction, players and balls and other external loads such as maintenance equipment. It is unclear currently, however, how the deformation may change under varying load intensity. The compression of many elastomeric materials promotes non-linear response and also a viscous response (damping or hysteresis). The compression of particulate materials promotes densification and closer particle packing, also leading to stiffening and increases in shear strength which is related to resistance to stud traction. It is also clear that the more intrinsic engineering properties of stiffness and strength are not only related to load but also to the area of loading, i.e. the applied stress. Current research into sport surfaces engineering behaviour through mechanical and subject testing has largely been focussed on forces and deformations, and less so on stresses and strains. This has made the evaluation of engineering properties more challenging from previous work.

The approach taken in this work is that the behaviour of the surface systems under vertical loading is an area for further research. As the literature review demonstrates, it is currently unclear as to how much surfaces deform (or strain) under real in-game loading, and what the effects of load magnitude, area of loading and rate of loading are on the deformation response. This may be due to challenges in measuring the effect of these variables in the past, or the perpetuation of the focus on the rather simplistic industry tests regarding ‘fit for purpose’ rather than material behaviour.

The research approach taken is centred on this key question of quantifying the deformation response, and the contribution of the constituent layers to the surface deformation. It was also considered to evaluate the possibilities of extending the forces and deformations, into measurements of stress and strain, and energy absorption, storage and return. These parameters are relevant to the engineering quantification of the elastic and viscous properties of the materials, and relevant in principle to the users.

It is identified from previous studies that the behaviour of a surface under (vertical) subject loading, is not well simulated or achieved by the current industry test methods. Furthermore the variation in contact variables during player-surface interaction has not been previously married to evaluation of the materials response used in surfaces.

In summary, the approach of this research programme was to investigate both the actual surface deformations and strains under subject loading, and to develop enabling measurement systems to characterise the response behaviour in a novel way. However, subject loading is in general considered to be of poor repeatability and it was thus decided to evaluate behaviour under controlled laboratory testing conditions to explore using more advance mechanical testing to simulate aspects of subject loading.

Mechanical loading regime (Chapter 3) was employed to evaluate the surface system behaviour as they produce high levels of repeatability and have the ability to control several variables isolating individual remaining variable to be assessed. These variables included loading magnitude, loading frequency and contact area. An advanced material testing machine was utilised to deliver vertical cyclic loading and measure the stress-strain behaviour of the artificial turf systems at different loading conditions and identify the factors that affect the surface response. Biomechanical data from previous research was used to define the loading variables. Industry standard tests were used alongside aiding the evaluation to be comparable with the performance standards set by the sport governing bodies.

Subject (player) loading regime (Chapter 4) showed the novelty of measuring the surface system behaviour under real player movements. Subject based tests are less repeatable as results can vary between any two subjects. As this research was not focused on comparing the biomechanical data of players in response to surface, the variability introduced by the use of multiple players was minimised. Thus, the choice was made to use only one male soccer player with regular training and match playing experience on artificial turf pitch to

practise selected movements to represent typical player loading conditions on surface systems. In order to assess the feasibility of measurement systems and methods developed, and considering the player's safety performing on instrumented surface systems and limitations of equipment, three basic movement patterns involved in sports generating moderate forces and rates of loading (heel-toe walking, forefoot running and forefoot single leg jump landing) were selected. The speed, jump height, technique and external factors such as fatigue and footwear were controlled to help the player complete required movements. Measurement systems used for data collection in player loading test included motion capture system, force plate and high speed camera. Motion capture system was used to track the foot strike on the surface system and thereby determine the vertical deflection of the surface. In addition, a high speed camera was used for additional image feedback on the foot impact to correlate to the different phases during a ground contact. Force plate was widely used in biomechanical research and here to provide force and centre of pressure data during player movements.

The original idea to evaluate the stress and strain in the whole systems and within layers was, after evaluation of current technologies, somewhat ambitious. Attempt was made to measure how the applied stress is distributed through the layers within the surface system and evaluate the contribution of individual layers to this behaviour by using a 'thin film' pressure transducer at carpet-shockpad interface and at the bottom of surface system. This sensing device offered a solution to illustrate how the stress developed and was distributed. It was used in both mechanical and player loading test programmes as a novel way of measuring the stress variation with time and the contact area under load, and further analysing the interaction between the system layers.

It was expected that the behaviour observed would be able to be described with simple mathematical models such that the effect of changes in loading regimes could be predicted (Chapter 5). Preliminary modelling work was considered by using mathematical equations to fit through the experimental data obtained from this research. This attempt could be the logical first step to producing more complex numerical models (3D finite element analysis) for further theoretical study of surface system behaviour prediction under player interaction scenarios.

This research was aimed to develop measurement methods to enhance current provision for the evaluation of mechanical behaviour of artificial turf system under load, and the aims

and objectives stated in the following Section 1.3 reflect this aspiration, and set out the scope and focus of the research programme that evolved. The relationship between the set objectives and the following chapters is presented in Section 1.4.

1.3 Aim and objectives

This research project aimed to develop measurement systems and methods to improve understanding and quantify the effects of real player loading on the mechanical behaviour response of sports surface systems, and the contribution of the components to the whole system response. This overall aim is achieved through a number of objectives, outlined below.

1. Review current knowledge on sports surface system design and industry test standards, and surface properties and material behaviour under compressive loading
2. Review mechanical test methods, player loading characteristics and measurement systems/equipment in order to design and develop test approaches for mechanical behaviour assessment of sport surface system
3. Investigate the mechanical behaviour of the selected individual components and surface systems under dynamic cyclic compressive loading
4. Develop measurement system and methods for measuring force/stress applied and resulting surface deformation/strain under player movements
5. Evaluate the surface system response to player loading parameters
6. Develop mathematical models to describe the surface system behaviour
7. Distill the findings into implications for academia and industry

1.4 Thesis outline

Figure 1.1 illustrates the thesis structure which consists of four main stages; literature review and research definition, experimental work, discussion and conclusions. Key research needs are identified from the literature review (Chapter 2) and then used to define the focus of this project and the research approach in Chapter 1. Chapter 3 and 4 present the experimental programmes which use controlled mechanical loading and actual player loading tests to evaluate the artificial turf systems behaviour respectively. Each of these two chapters contains its own detailed experimental methodology, results and discussion. Chapter 5 discusses and compares the findings from Chapter 3 and 4, forming a wider integrated discussion and providing mathematical models to describe the system behaviour.

Finally, Chapter 6 draws the key conclusions addressing the research objectives, recognises aspects of limitations of the work, and recommends avenues of further work that could be undertaken.

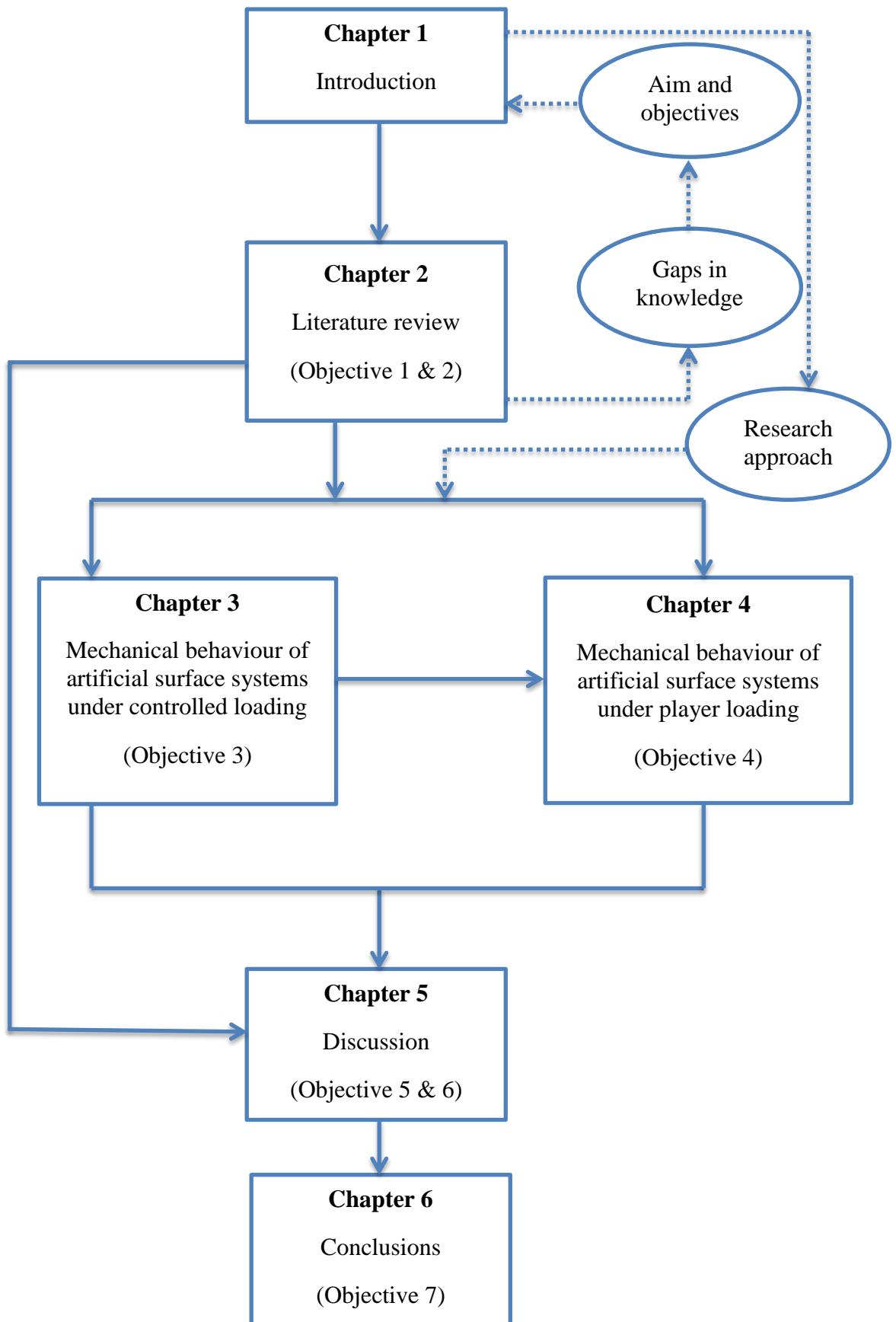


Figure 1.1: Flow diagram illustrating the chapters of thesis interlinked with each other

2. Literature review

2.1 Chapter overview

This chapter covers selected aspects of artificial turf sports surface systems and the component materials relevant to this research. The review of published literature encompasses relevant journal and conference papers, books and theses. This review aims to determine the current state of knowledge regarding artificial turf systems, and identify key gaps in knowledge for the development of this research programme to ensure an original and relevant contribution to this field.

Firstly, the history of artificial turf surfaces and key areas of construction and design are presented, providing necessary background information. Standards used to classify artificial turf pitches are then introduced. A critical review of current mechanical test methods for assessing properties/performance of sports surfaces is presented with particular focus on player-surface interactions. Following this, an in-depth examination of player-surface interactions concerning various movement patterns and loading characteristics in terms of both performance and safety is provided. Measurement techniques with experimental approaches for the mechanical assessment of sports surfaces and materials properties/behaviour and modelling methods used within literature are detailed. These are reviewed with focus on force-deformation/stress-strain relationship and pressure distribution. This comprehensive review of literature addresses objectives 1 and 2 (Chapter 1) of this thesis. The key points raised from the literature are discussed regarding test methods, measurement systems, effects of loading on the behaviour of surface systems and modelling. The discussion highlights areas for further research that form the basis of aims and objectives for this investigation set out in Chapter 1.

2.2 Development of artificial turf surfaces

Artificial turf surfaces, as an alternative to natural turf, have been applied in many sports and have undergone 50 years of development since their invention. Artificial turf became recognised for elite level sport in 1965 when AstroTurf™ was installed at the Astrodome in Houston, Texas. The use of this artificial sports surface spread widely and was installed in both outdoor and indoor stadiums used for football and baseball in North America. The first artificial turf surface installed in the UK was a football pitch at Caledonian Park, London in 1971 (Tipp and Watson, 1982; Crawshaw, 1989). This type of artificial turf surface is known as the first generation surface which made from fibres of a height 10-12

mm and with high density. In this early artificial turf system no infill between fibres and no shockpad was employed (Severn, 2010).

In the late 1970s there was an increasing demand for sports facilities which encouraged the growth of artificial turf surfaces (Tipp and Watson, 1982). In response to the shortage of available resources (e.g. water and land) and the difficulties of maintaining natural turf, the demand for artificial surfaces was further amplified in sports development. The artificial surfaces benefit from their ability to sustain a high level of use, required low maintenance, and yet provide consistent surface that offers desirable performance characteristics. In 1976, Montreal Olympics field hockey used an artificial turf surface for the first time in an international competition. Since then, field hockey has completely adopted this type of surface and has competed on it by both elite and recreational players. It was a sand filled system which is known as the second generation surface. Sand infills and shockpad were starting to be used to improve the interactions between surface and player/ball. The pile height was generally 20-25 mm, higher than the first generation products.

In the late 1990s, a development in artificial turf is the long pile carpet varying from 50 mm up to 65 mm in length and filled with rubber or a combination of sand and rubber crumb infills to a designed height in order to provide more cushioning and traction to the system. Furthermore, instead of polypropylene, the yarn is usually made from polyethylene (PE), which is softer and less abrasive to skin. This type of surface system is widely known as the third generation (3G) system and is commonly used for soccer and rugby. Due to the improved qualities of the 3G artificial turf systems, in 2004, the Federation Internationale de Football Association (FIFA) announced that the Laws of the Game included artificial turf surface as an acceptable field of play as long as it meets the requirements of the FIFA Quality Concept for Artificial Turf or the International Artificial Turf Standard (FIFA, 2012). The idea to accept artificial turf surface in international competitions was to provide a choice for the countries in climatic extremes or financial difficulties to have quality recognised playing surfaces other than natural grass pitches (Cotton, 2008). The different design of the artificial turf of the three generations is illustrated in Figure 2.1.

Some innovations of hybrid turf system and reinforced natural turf system have emerged in recent years. They have similar structures which natural grass roots become intertwined with the synthetic tufts and grow downward into the foundation material below. A dual-component backing combines biodegradable fibres and a plastic mesh is used. The tough

plastic mesh plays as an anchor for the components above and provides additional load bearing capacity and horizontal subsurface strength. GrassMaster (Desso, 2007) is a reinforced natural grass system which has been used successfully at 2010 FIFA World Cup in South Africa. It is the first time that FIFA World Cup matches have been played on pitches that are partly made up of artificial turf. The enhancements of this system are 20 million polyethylene fibres vertically injected 20 cm deep into the established natural grass pitch. Only 3% of the pitch is composed of artificial turf, so players have a similar experience to playing on a natural grass field. On the other hand, the artificial turf element provides better drainage performance and less damage from play. The hybrid system of artificial fibre materials and natural grass is seen as a new trend of the development of artificial turf surface.

2.3 Construction and design of artificial turf pitches

The artificial pitches are designed according to the desired application either specifically for individual sports or as multi-sports surfaces. Artificial turf system is an installation composed of several layers, and each layer is made from different materials. However, all the outdoor pitch systems share a basic structure, as shown in Figure 2.2. The system can be split into three major groups: foundation layer, shockpad layer and carpet layer. They are distinguished by their functions in the pitch performance and materials used for their construction (Anderson, 2007). The design of the installation before starting foundation layer construction is of great importance. In order to produce a site specific design, a site investigation and topography survey are vital for earthworks (SAPCA, 2005). According to individual sport governing federation's requirement, the base should be engineered with certain rate of gradients to meet the drainage demand for surface water runoff and also in some cases consistent ball roll characteristics. Foundation layer is constructed as a flat stable platform, its surface evenness and compaction should be checked before the shockpad layer is installed. The shockpad layer and artificial carpet layer together provide the particular playing characteristics (Fleming, 2011). In the following sections, the three layers are discussed in detail respectively.

2.3.1 Foundation layer

A stable and well-constructed foundation layer is highly important for the overall quality of artificial pitch and its service life (UEFA, 2003). From the bottom-up in Figure 2.3, the foundation layer of an artificial soccer pitch generally consists of consolidated subgrade, a geotextile membrane, load-bearing crushed stone sub-base, water-permeable base and

provides an even surface. Pitches need to be founded on hard-compacted ground. It is suggested (SAPCA, 2005) that the formation is based on natural ground as soil is usually stronger when it is not disturbed. In order to improve the ground strength, usually a 'cut to solid' process is conducted which excavates all the unwanted topsoil, turf and vegetation down to the solid natural ground.

An arrangement of suitable drainage system should be installed during construction. Drainage pipes made by perforated plastic are laid diagonally across the pitch and sheltered below the frost zone. The channels are then backfilled with clean stone and gravel. Finally, a vibrating roller is employed to compact the overall sub-base (Young, 2006). According to the local weather conditions, the pipes' diameter could vary greatly.

Depending on the level of frost penetration and load bearing capacity, it is recommended by UEFA (2003) that the average thickness of sub-base should be 30 cm to 100 cm. The main function of the sub-base is to support and transmit all the loads (especially high loads from construction and maintenance vehicles) on the artificial surface without causing permanent deformation of the site. It is preferable that a geotextile membrane covered on the formation ground to prevent contamination from the natural ground underneath can be used before the installation of the sub-base (SAPCA, 2005). On top of it, the first layer of sub-base consists of coarse broken stone is placed, and then a second layer of fine aggregates is laid to achieve the required thickness and evenness (Young, 2006). Weather conditions also need to be taken into consideration in design, for example, underground heating system is suggested to ensure a playable condition of a pitch in countries with a cold climate. UEFA produce a requirement on the ground heating system which demands the field to achieve a surface temperature of ± 0 to $+ 2$ °C. Pitches built in countries with a hot climate are recommended to have water-sprinkling systems to reduce the heat of the sun by spraying water evenly on the playing surface. In order to cooperate with the water-sprinkling system, instead of traditional water-permeable wearing course, it is recommended to construct impervious infrastructure to maintain water longer in the shockpad layer (UEFA, 2003). However, UEFA suggest professional advice is sourced from specialists in heating and water sprinkler systems.

Generally, the top of the foundation is comprised of a bound or unbound (dynamic) construction. Bound base, like concrete or asphalt, provides a well-engineered smooth surface. The pitch type and local environment condition determines the use of asphalt due

to its porosity. For example, water-based hockey pitches demand a much faster rate of drainage than typical sand-based pitches. Artificial turf pitches in excessive rainfall areas require more porous asphalt layer than pitches built in dry climatic condition. The asphalt is mostly installed in two layers. The base course is usually thicker to provide a stable platform. A typical base course asphalt layer is around 40-60 mm thick. The next layer of asphalt is called finish course which is typically 25 mm thick in the UK. The bound base needs to be constructed to meet the surface slope requirement defined by related sport governing body in order to provide perimeter drainage for the artificial pitch (Tipp and Watson, 1982). Unbound, often termed ‘dynamic base’ has two alternative structures: stone/sand mixture or lava/rubber mixture (SAPCA, 2005). Unbound constructions are claimed to have more natural feeling due to their shock absorbency characteristic under impact (Watson, 1986; Crawshaw, 1989; Anderson, 2007). On the other hand, this feature also influences the ultimate player and ball interactions of artificial surface system, so the choice of the grade of stone, its degree of compaction and the thickness should be carefully designed (Tipp and Watson, 1982; Sport England, 2003; SAPCA, 2005; Anderson, 2007).

Evenness is another important criterion in the top base construction. The current technique of installing the foundation’s top layer uses laser-controlled paving machines (SAPCA, 2005), which could achieve the evenness requirement in the majority area of surface. But from the industrial construction experience of the author, usually it is difficult to control evenness within the required tolerance in corner areas of pitch. A gateway for all vehicles used in the construction to access to the site is mostly opened in one of the corners of the pitch. Paving machines cannot install this area precisely meanwhile exiting the pitch backwards. The common way is to lay the courses manually on this area. Consequently, evenness is more likely to exceed the tolerances in this region.

2.3.2 Shockpad layer

The shockpad layer, known as the elastic layer in some literature, is not only used to create preferred playing characteristics for the particular sport but also to retain the initial qualities of artificial pitch over a long period of time (Brown, 1987; UEFA, 2003). There are three basic types of shockpad available on market nowadays: prefabricated, integral and in-situ shockpad (SAPCA, 2005; Anderson, 2007)

Prefabricated shockpads are manufactured in factory environment according to specific requirements. The major advantage of this kind of shockpad is the uniformity of property

and thickness due to the controlled production environment. In most instances, prefabricated shockpads are packed as rolls to deliver to sites. Many other forms of prefabricated shockpads are also available on market, for example pads of closed-cell foam, nylon filament and pre-formed mat/tile, etc (SAPCA, 2005). In the case of prefabricated system, shockpads can only be produced in single rolls or pieces. Therefore laying process and joint work are essential to the quality of this layer. Experience has shown that there are mainly two kinds of problem with this technology, shift movements of carpet and shockpad, and shrinkage or expansion between joints. If the carpet is not strongly attached to shockpad with minimum of distortion, there is a considerable chance of movements between the two layers after long period of using. Because the elastic materials used in shockpads are responsive to temperature variations, shrinkage and expansion usually cause clefts and ridges in joint areas (Anderson, 2007).

Integral shockpads are produced as part of the carpet system attached to artificial turf backing. Before providing the pad, one more application of back finish is needed to lock the tufts (Crawshaw, 1989). Prefabricated shockpads and integral shockpads are constituted of similar materials, e.g. polyurethane and closed cell foam neoprene (Anderson, 2007). Combinations of integral shockpads with prefabricated or in-situ shockpads are used to achieve preferred level of cushioning for artificial pitches.

The most popular in-situ shockpad for artificial turf pitch is known as resin-bound rubber crumb system (often called 'wet-pour' in the industry). Typical components of in-situ shockpad systems are recycled polyurethane rubber crumb from tyre carcass or sealing strip used in windows of vehicles mixed with a resin binder (Tipp and Watson, 1988). In-situ shockpads generally have a thickness in the range of 10 mm to 35 mm (SAPCA, 2005). The consistency in the mix ratio of rubber to binder is very important to the quality of shockpad. It is described by Fleming et al (2002) as the different densities caused by inconsistencies in the mix ratio could influence the tensile and compressive strength of the shockpad. The advantages of this cast in-situ shockpads are porosity and the potential of recovering minor unevenness flaw in the foundation layer (Watson and Tipp, 1987). Because the installation is operated in outdoor environment, weather condition and contamination could affect the shockpad quality. Careful quality control and monitoring procedures during construction are necessary to ensure the property of overall shockpad layer and compliance with the design (SAPCA, 2005). Thickness can be varied, as can binder content, to suit specific requirements.

Young (2006) identified the relationship between shockpad thickness and its impact absorption property. His test results demonstrate an increase in thickness improves the shockpads impact absorption and therefore an increase in force reduction. Rebound resilience is the ratio of the energy returned on recovery from deformation to the energy required to produce the deformation. This property of shockpad has close connection with player safety and ball interactions. Higher rebound resilience would cause higher ball rebounds (Watson, 1986). For player safety, the level of rebound resilience should be designed to a moderate value, so that it is neither too high to cause direct injury nor too low to cause fatigue and predispose to injury (Bartlett, 1999).

The properties of shockpad must be retained over the range of environmental conditions and possible mechanical loading throughout its effective life (Anderson, 2007). Different materials have their own disadvantages concerning degradation. Polyurethane (PU) shockpads are subject to degradation in conditions of high humidity and temperature. Shockpads made by expanded low-density polyethylene (LDPE) has good energy dissipating characteristics. However, it has relatively inferior recovery from a static load. Therefore, if a maintenance machine or other heavy equipment is left in one position for several hours, could cause permanent deformation of the shockpad at that spot (Tipp and Watson, 1982).

2.3.3 Carpet layer

Carpet layer generally consists of artificial fibres tufted, weaved or knitted on a backing sheet. For an infilled artificial turf surface, such as the 3G turf system, the carpet layer also includes the infills used between the carpet fibres.

There is a large diversity of materials used to produce carpet fibres. Traditionally, polyamides are usually chosen to produce fibres for hockey and multi-use games fields; polyolefines are widely used for soccer applications (Innovene, 2006; Hitoshi, 1995). Compared with polyolefin fibres, polyamide fibres have better fibrillation resistance and resilience (Schoukens, 2009). These properties are importance for non-filled hockey or tennis fields. But if the rigidity and friction coefficient of fibres are too high, the risk of injury caused by skin abrasion on the artificial turf surface is increased. There are several different polyolefines such as polypropylene and polyethylene. The mechanical characteristics of the polyolefines are defined by their structure and certain degree of crystallisation (Schoukens, 2009). Polypropylene has relatively higher strength and

stiffness than polyethylene. In order to reduce the possible occurrence of burns of the skin when sliding is performed. Some polyolefines with a low coefficient of friction characteristic are used for the soccer artificial turf application, e.g. high density polyethylene (HDPE) and polypropylene (Brandrup and Immergut, 1975). Additives are usually used to improve the polymers resistance to ultraviolet light (UV) and harsh temperature (Severn, 2010). A balance of all the material properties of fibres is essential for different artificial turf applications (Schoukens, 2009).

The selected polymer is then extruded as fibres with required thickness and width. Two types of turf blades are popular in market: monofilaments and fibrillated fibre, as in Figure 2.4. There is some disagreement on the subject of which one is the better design for turf carpet. The ball roll distance is a key performance criteria closely related with turf blades or yarns type and its resilience resistance. It is observed from author's site testing experience that fibrillated fibres have better resilience behaviour and provide more resistance during ball roll performance than monofilament fibres. But many manufacturers prefer to use monofilament in their carpet products, because its appearance looks more like nature turf and has wider selections of material.

The tufting method is the most common way in recent times to stitch the fibres into a prefabricated backing sheet to produce artificial turf carpet. The backing of the artificial turf could be made of different plastic material, for example a non-woven fabric that is saturated with latex (UEFA, 2003; Schoukens, 2009). The numbers of filaments per tuft and tufts per square metre can vary widely depending on the specific sport or purpose the turf carpet designed for. The carpet backing needs to be UV resistant and provides dimensional stability and strong attachment of the turf fibres. Turf withdrawal force is a required measurement by industry standards (FIFA, 2012).

Today's 3G artificial turf sport surface is a type of system which combines sand infills to stabilise the carpet by its weight and rubber infills to improve the playing characteristics of the surface. It is suggested by UEFA (2003) that round silica quartz sand with particle diameter larger than 0.5mm should be spread over the bottom of the turf for extra dimensionally stability. The thickness of this sand infill layer is generally between 10 and 15 mm. On top of the sand infills, the rubber granules are laid as the second layer of infills. Three types of rubber granules are commonly available on the market nowadays: styrene-butadiene rubber (SBR), ethylene-propylene-diene copolymer (EPDM) and thermoplastic

elastomers (TPE) (Torres et al, 2010). SBR granules are the most frequently used products that derived from vehicle tyres and other industrial waste rubber, due to its low cost. However, recent concern about the potential health and environmental risks of SBR infills prompted a large number of relevant studies. These researches are focused on problems including skin contact and possible latex allergy, volatile organic compounds (VOCs) and creation of dust (Vetrano, 2009). Other problems are the difficulties of quality control of this kind of infills, and no guarantee to the consistency of raw materials. Coloured EPDM rubber is particularly developed product for sports use. Compared with SBR granules, EPDM rubber granules are more stable under UV radiation and less absorption of the heat from sun, but more expensive. In addition, it has lower health and environmental risks and more adopted with the national legislations (UEFA, 2003). The new type of infill such as TPE product is still not a mature alternative to the existing systems. Hence there is few published research or technical information could be found. The advantages of TPE compared with EPDM are its properties can be tailored to specific requirements in the blending process and similar in cost (Severn, 2010).

The infills of sand and rubber together generally reach to 2/3 of the pile height (SAPCA, 2005). These infills systems provide traction of footwear studs and some of the shock absorbency for the loading applied to surface. A number of variables of the infills can affect its mechanical behaviour and the interaction with player/ball, e.g. particle size, material, quantity, bulk density and compaction condition. This is discussed further in Section 2.5. Free piles (piles above any infill as defined by FIFA) together with rubber infill would influence on the ball-surface interactions. Alcantara et al. (2009) reported the size of rubber infills used in a carpet layer affected the vertical ball rebound measured. The results indicated that the ball bounce height increased as increasing the ratio between the minimum and maximum diameter rubber infills used.

Different testing methods and many of the previous studies focus on differentiating and rating the performance of the composite artificial turf systems but do not explain in any detail the performance and contribution of each layer/material. In contrast, some previously published papers have described aspects of behaviour and measured properties of individual layer or material (e.g. rubber infill) but these have not attempted to make the link or correlation to their role in the artificial turf surface system overall behaviour.

2.4 Performance standards and mechanical test methods for artificial turf surfaces

2.4.1 Performance standards

The artificial sport surface system is designed to meet the specific play performance requirements of the specific sport (unless it is a multi-use facility), safety and durability to ensure a level of quality and consistency in construction (Severn, 2010). An important decision to be made early on for the client is to decide the primary use and level of use the system chosen will be required to meet (SAPCA, 2005).

International sport governing bodies including FIFA, International Hockey Federation (FIH) and International Rugby Board (IRB) produced their own series of requirements, called play performance standards. Artificial pitches must conform to the standard, and be tested and certified, if a certain level of competition needs to be performed. FIFA and FIH have introduced different grades of standards for pitch quality classification related to level of competition. FIFA developed two categories of performance: FIFA Recommended Two Star and FIFA Recommended One Star, with the former one being the higher category for professional play. The performance requirements of field test set by FIFA are listed in Table 2.1. In April 2008 the FIH updated its handbook such that instead of having three levels of standards, namely Global, Standard and Starter, (FIH, 1999) , the new handbook laid down two certification levels as requirements for installed pitches, termed class 1 and class 2. FIH world-level competitions are required to be played on ‘class 1’ level certified pitches, class 1 being more rigorous than class 2 aimed at community and recreational use.

In general, the standards set assessment requirements for artificial turf pitches from five specific aspects, namely player-surface interactions; ball-surface interactions; construction tests; durability tests and product identification tests. Player-surface interactions are assessed by measuring the shock absorbency and deformation ability of the surface to reduce the vertical loads applied and the linear and rotational resistance force to horizontal movements. These characteristics of sports surface conditions have been identified not only to impact the performance of the player, but also been linked to factors associated with injury, particularly the lower limb (Orchard, 2002; Petrass and Twomey, 2013), however not from a fundamental understanding point of view. Ball-surface interactions are determined by measuring ball rebound height, velocity and rolling resistance through three methods: vertical ball rebound, angle ball rebound and ball roll. Construction tests include

the surface evenness, dimension and slope check. Durability of the surface is predicted by using laboratory based climatic resistance test and mechanical wear simulation test. Product identification tests aim to confirm the surface system installed matches the products tested in the laboratory.

The introduction of standards and classifications has regulated the quality of products on market and narrowed the differences in surface system performance. However, it is possible that many surface systems have been designed just to ensure the governing body limits are achieved in order to be accredited, instead of providing optimum playing characteristics and safety for players. Furthermore, there is little information or clear justification from sports governing bodies on how their performance standards have been determined (Severn, 2010), in general this appears to be wholly empirical, and therefore raises the question as to their suitability in terms of providing the guidelines for ideal surface response for in-service play conditions.

Tests used to assess artificial turf pitches are often similar across the sport specific standards, but the limits of acceptability can be different between sports depending on the specific nature of the sport (Severn, 2010). The common industry tests and some alternative mechanical test methods and procedures used to measure and assess player-surface interactions are reviewed in the following subsection.

2.4.2 Mechanical test methods

Player-surface interactions are usually tested in two aspects, the effect of vertical impact force on the surface measuring shock absorption (Shorten et al., 2003) and the effect of horizontal force measuring resistance between shoe outsole and surface to movement (Villwock et al., 2008). In Chapter 3 and 4, mechanical behaviour of surface systems in response to vertical force from compressive mechanical and player loads is studied. Therefore, in this subsection current available test methods to measure surface behaviour under vertical force are reviewed in detail.

Vertical impact tests

Surface mechanical behaviour under vertical force is generally determined using drop tests. They measure the amount of absorption to impact a surface provides by measuring the peak impact force (Severn, 2010). Since its introduction the FIFA quality concept for football turf has done a number of revisions with developments in test methods and equipment. The latest revision, January 2012, the Advanced Artificial Athlete (AAA)

replaced the Artificial Athlete Berlin (AAB) to measure shock absorption and vertical deformation. The shock absorption ability of sports surface is determined by the 'Force Reduction' value which is calculated by comparing the percentage reduction in peak impact force measured on the test surface relative to a reference force (6760 N, fixed theoretical force on concrete). The force reduction is calculated using Equation 2.1 and 2.2 (FIFA, 2012; IRB, 2012).

$$F_{max} = mG_{max} + mg \quad (2.1)$$

Where:

F_{max} = Peak force on sports surface (N)

G_{max} = Peak deceleration during impact (m/s^2)

m = Weight of the falling mass unit (kg)

g = Acceleration by gravity (m/s^2)

$$F_{red} = \left(1 - \frac{F_{max}}{F_{ref}}\right) \times 100\% \quad (2.2)$$

Where:

F_{red} = Force reduction

F_{max} = Peak force on sports surface (N)

F_{ref} = 6760 N theoretical force on rigid concrete

The AAA (as in Figure 2.5) consists of a falling mass incorporating a metal spring with a stiffness of 2000 ± 100 N/mm over the range 0.1 to 7.5 kN and a lower side rounded test foot with a diameter of 70 ± 1 mm, having a total weight of 20 ± 0.1 kg. The integrated falling mass is released electronically from a drop height of 55 mm and falls onto the surface sample. A piezo-resistive accelerometer is used to measure the peak deceleration G_{max} during the impact. Compared with AAB, the integrated falling mass unit makes the AAA more portable and efficient.

The compliance of the sports surface can be quantified by the measurement of surface deformation under the controlled application of load. Vertical deformation is defined as the displacement of the surface and calculated as the displacement of the mass after moment of

impact subtracting the compression of the spring (Equation 2.3). The displacement of the mass is calculated by the double integration of the acceleration signal on the time interval from the moment the mass reaches the maximum velocity in the downwards direction to the moment maximum velocity in the upwards direction reached (Equation 2.4). The compression of the spring is given by Equation 2.5 (FIFA, 2012; IRB, 2012).

$$D_v = D_{mass} - D_{spring} \quad (2.3)$$

$$D_{mass} = \iint_{T_2}^{T_1} g dt \quad (2.4)$$

$$D_{spring} = \frac{mgG_{max}}{C_{spring}} \quad (2.5)$$

Where:

D_v = Vertical deformation (mm)

D_{mass} = Displacement of the mass (mm)

D_{spring} = Compression of the spring (mm)

t = Time (s)

C_{spring} = Spring constant (N/mm)

Other symbols are explained in Equation 2.1

An alternative device, the Clegg Impact Hammer (CIH), has been adopted as a comparison to the Artificial Athlete (Figure 2.6). The CIH initially developed for civil engineering purposes for monitoring compaction of surfaces (Clegg, 1976). It is also drop tester and records the maximum deceleration upon impact with surface in the reading termed as Clegg Impact Value (CIV) where 1 CIV unit equals to 10 gravities. The main differences compared with the AAA (AAB) are lighter falling mass (0.5, 2.25 or 4.5 kg), higher drop height (45 cm) and no spring involved (El Kati, 2012). Previous research by Fleming et al. (2004) and Young (2006) demonstrated that a strong correlation was found between the Artificial Athlete and the 2.25 kg CIH for measuring non-infilled water-based hockey pitches, with shorter contact time (in the region of 10 ms dependent on the surface under investigation) recorded with the CIH. An extended range of artificial sports surfaces including 3G turf, athletics track and tennis surface was tested by Young and Fleming

(2007) to further study the relationship between the CIH and the AAB. A good correlation ($r^2 = 0.9781$) was identified between these two devices over the range of samples tested showing the potential of using the CIH as a simplified method for sports surface classification. The 0.5 kg CIH was used by Carré and Haake (2004) to test different designs of artificial cricket pitch, with a complete time history of the acceleration being collected over the duration of impact using an analogue/digital converter. The readings of peak deceleration of the pitches were compared and noted to be insufficient for assessing the (ball) playing performance using this parameter alone. It was concluded that for accelerometer tests to be useful, all the acceleration-time data during the impact needed to be analysed, rather than the peak value alone.

The drop tests used by the industry and sports governing bodies have the advantages of portable for use, repeatable, easy to operate and relatively low cost. However, to determine the mechanical behaviour of sport surfaces under vertical impacts, they have the following shortcomings. Firstly, impact force peaks from the drop tests showed little correlation with the impact force peaks during actual player movements (e.g. running) (Nigg and Yeadon, 1987; Nigg, 1990). Secondly, the contact durations of drop tests (commonly in a range from 10 – 40 ms) were much shorter than the contact time during a ground contact in running or sprinting (over 100 ms) (Kolitzus, 1984; Nigg et al., 1984; Baroud et al., 1999). Thirdly, in most of the tests, only the peak magnitudes were considered, which have the disadvantage of lost important information for surface nonlinearity analysis (Dura et al., 2002; Carré and Haake, 2004). Fourthly, using the standard drop tests was inappropriate for simulating interactions of differing movement patterns and individuals with surface (Dixon, 1999).

In recent studies, dynamic material testing machines have been used to measure the sports surface's engineering behaviour to overcome some of the shortcomings presented above by determining the force-deflection (stress-strain) relationship and energy performance of surface (Miller et al., 2000; Dura et al., 2002; Allgeuer et al., 2008). These methods and surface behaviour are introduced in Section 2.6.2 of this chapter.

Horizontal friction/traction tests

As a player carries out a sports movement, both vertical force and horizontal forces often occur simultaneously when the foot is planted onto the surface. These two components are often measured separately by different mechanical test methods. Horizontal forces

produced at the foot-surface interface can be either translational (resistance to sliding) or rotational (resistance to turning) (Severn, 2010). They are the key parameters identified by sports governing bodies in their suite of tests for performance, and by biomechanical and medical researchers investigating lower limb injury.

Translational force is commonly tested in standards by pendulum swing testers. The pendulum Skid resistance tester was originally designed to measure the slip resistance of floors in business premises and roads. It has been adopted by the International Association of Athletics Federations (IAAF) for testing athlete tracks. FIFA also uses a modified version of this tester with studs on the test foot for artificial turf surface. The concept of the Skid tester is based on the Izod principle, with a specified rubber (studded in the case for FIFA) foot attached to the head of the pendulum which is released from a horizontal position and rotates about a vertical spindle to strike the sample surface. The Skid resistance value read directly from the scale relates to the friction coefficient. FIH employs another pendulum tester known as the modified Leroux to measure underfoot friction in its protocol (FIH, 2008).

Rotational resistance (traction) has been widely evaluated due to the perception that non-contact injuries in sports such as anterior cruciate ligament (ACL) injuries can be caused by excessive rotational movements at the knee (Livesay et al., 2006); however insufficient traction can result in slipping and sliding and loss of performance (Young, 2006; Severn, 2010). An increased research has been carried out into the rotational resistance of artificial turf surface in recent years with several different methods used. The rotational torque test used by FIFA aims to simulate the resistance of rotational movement of a studded foot on surface with a simple mechanical device. A studded test foot loaded with a weight of 46 ± 2 kg is dropped from 6.0 ± 0.5 cm above from the specimen and rotated manually at a speed of rotation of 12 rev/min until the test foot moves and reaches a minimal rotation of 45° .

Machine controlled devices also have been used to measure rotational resistance between shoe and surface in previous studies (Wannop et al., 2010; Stefanyshyn et al., 2010; Severn, 2010). These devices use different commercial soccer boots as test feet, with some using the forefoot part of the sole of soccer boots and others using complete boots. Furthermore, some devices use boots placed in an angle to the surface (El Kati, 2012). Either surface

sample on the platen or the boot rotates to measure the peak rotational traction value (Nm) as the key parameter.

Other research by Livesay et al. (2006) and Villwock et al. (2009) used devices that were able to measure the rotational traction throughout the entire rotation. The advantage was to determine the rotational stiffness of the surface at different rotation angles/torque values in addition to the peak rotational traction. Severn (2010) reported that the rotational resistance properties were mainly affected by the carpet layer condition with no effects from the shockpad.

2.5 Player-surface interactions

2.5.1 Overview

In biomechanical and sports engineering studies, the interactions between player and surface have been the focus of much research over recent years because the correct evaluation of player-surface interactions is important for developing the knowledge in the aspects to improve player comfort and safety, reduce injury, and enhance the performance of sports surface. The interaction is a complex function of surface mechanical properties, human perception and player biomechanical response. It is also a two-way interaction, the surface appearance and mechanical behaviour modifies the human biomechanical response, which in turn loads the surface, resulting in deformation and energy flow that can change the surface behaviour and appearance (Stiles et al., 2009; Davidson et al., 2009). With regard to the player, the factors that can affect the surface behaviour are thought to include, but are not limited to, movement type, direction of movement, velocity of movement, loading rate and the weight of player (Munro et al., 1987; Dixon et al., 1998). With regard to the surface, the variables considered to affect and influence the response of player loading include the mechanical properties of the surface system, such as force absorption, hardness and traction/friction, and the conditions at the time affecting its state may also include the surface temperature, degradation level, contamination and moisture degree. There are also some additional modifiers such as the athlete's footwear (Nigg and Anton, 1995), fatigue and protection equipment that are at the interface of interaction. To analyse player-surface interactions, it is necessary to quantify both surface mechanical and biomechanical parameters (Zanetti et al., 2013), and control the relevant modifiers.

The described mechanical tests in Section 2.4.2 are simplifications of the player-surface interactions. Young and Fleming (2007) identified that these tests have limitations in their

replication of actual player loading. In ‘real’ scenarios, variations in player movement patterns are expected to affect the sports surface behaviour as the loading rate, magnitude and direction of forces are variable. Therefore, for characterising the mechanical behaviour of sports surface, it is necessary to link with the effects of measured biomechanical loading parameters of the corresponding movement pattern to support the analysis of player-surface interactions. Sports (i.e. soccer, hockey and rugby) played on artificial turf surface consist of numerous movement patterns. Researchers studying in different fields usually categorise player movement in different ways. Three types of studies considering sports movements are time-motion analysis, injury studies and biomechanics (El Kati, 2012).

Generally, studies related to individual’s performance (injury) and time-motion analysis tend to use a comprehensive classification system. It is a collection of movement types used in specific sport or common actions in multiple sports. An example of this approach is ‘Bloomfield movement classification’ designed by Bloomfield et al (2004) after observation in multiple sports. In this classification, there are general movement patterns such as landing, walking, jumping, sliding etc. and particular actions with ball such as passing, dribbling, shooting. Studies focused on individual sport add some sport specific actions in their classifications, for example, lineout and scrummage are typical rugby actions. Other time-motion analysis studies refer to player movement patterns in match (competition) scenarios. However, they mainly focus on the velocity, distance covered and cumulative time spent on specific movement type (Duthie et al., 2003; Andersson et al., 2008; Macleod et al., 2009; Petersen et al., 2010). These research studies help the athlete and coach to evaluate the athletic performance in the game and refine training programmes to meet the competition demands. El Kati (2012) developed a summary (see Table 2.2) of movement classification based on the information gathered from literature. For each movement there are modifiers that can affect the movement, with an additional overall ball modifier for the movements performed with or without a ball. Some sport specific movements were added for contact and ball activities by the author.

In terms of movements discussed in biomechanical and injury studies, usually several representative movements such as running, jumps and landings, and turning/cutting manoeuvres are considered. These movements are selected because they are closely related with player musculoskeletal system loading assessment which is associated with injury risk. It has been suggested that the introduction of artificial turf surfaces, especially the first and second generation products, increased the injury risk and overall rate of injury compared

with natural grass across a number of sports (Williams et al., 2011). Despite differences in injury type, the rate of injury for 3G and natural grass surfaces has been shown to be comparable (Dragoo and Braun, 2010). Some studies claim that there is no evidence that playing on artificial turf surface leads to a higher risk of injury (Ekstrand et al., 2006; Fuller et al., 2007). Meyers and Barnhill (2004) suggested that artificial and natural turf had similar injury risks, but a higher incidence of muscle-tendon overload injuries was found on the artificial turf surface, while for natural grass a higher incidence of ligament tears occurred. However, most of this previous research provides little or no information on the characteristics of the surfaces used in the study. Some of these studies mention only the generic type of surface (i.e. 3G) (Fuller et al., 2007; Ekstrand et al., 2006), and some included details of the generic type of infill and if the surface was in a dry/wet condition (Hagel et al., 2003; Meyers and Barnhill 2004). Therefore, due to the lack of standardised practice for the routine measurement of ground conditions in injury studies there is limited quantitative evidence of the relationship between injury and surface conditions (Petross and Twomey, 2013).

Current player-surface interaction analysis is predominantly restricted to controlled laboratory environments with small surface samples. Laboratory offers more reproducible testing conditions, but suffers from a limited range of player motion and test repetition on few surface samples (Kirk et al., 2007). Most biomechanical studies focussed on one or two movement patterns practised by more than one participant to assess impact forces, rates of loading and joint movements/acceleration/angles (Stiles and Dixon, 2007; Kaila, 2007; Lieberman et al., 2010). Previous research effort has been primarily made on comparing the player response for a variety of generic surfaces (Andersson et al., 2008; Ford et al., 2006; Brachet, 2004; Stiles and Dixon, 2006) and for footwear design (Muller et al., 2010; McGhie and Ettema, 2013; Grund and Senner, 2010) again on types of surface without details of the surface properties. Many studies have used only a single parameter such as 'peak impact force' or 'surface hardness' to distinguish between the surfaces that movements were performed on, with very little literature attempting to explain the effect player loading had on sports surfaces or described how the surfaces behaved under player loading. In addition, it is clear that with relatively rapidly changing surface technologies, such as artificial fibres, it is challenging to compare surface related studies in great detail as the effect of these specific changes is unknown. Therefore, there is a clear imbalance in

research for the analysis of player-surface interactions from the perspective of the surface behaviour.

Previous research results of player performance can however help to select the representative and frequently used movement patterns in sports. Then the measurement of artificial turf surface system is focused on its behaviour under the selected movements and the effects of key player loading parameters.

2.5.2 Player loading characteristics

This subsection gives details of the range of player movements with key parameters (loads, contact times, loading rate, speed and direction) from a review of previous biomechanical research related to playing surfaces.

The resultant force acting between a player and the ground during locomotion is one of the key parameters commonly used to evaluate the interaction between player and sports surface. This high compressive force has normally been reported as ground reaction force (GRF) and can be measured using a force plate (FP) (Nigg et al., 1986; Dixon et al., 1998). During ground contact phase (e.g. running), GRF occurs in both vertical and horizontal directions, as shown in Figure 2.7, the vertical component (F_z) which acts normal to the ground, the anterior-posterior component (F_{AP}) which acts parallel to the running direction and the medial-lateral component (F_{ML}) which acts perpendicular to the running direction (Davidson, 2012). Depending on which region of the foot experienced the initial contact, there are three foot strike patterns during running movement: rearfoot, midfoot and forefoot strikes (Lieberman et al., 2010). Figure 2.8 shows typical FP outputs of GRF profiles for an individual exhibiting a rearfoot strike running. Force is specified in terms of body weight (BW). The vertical component has two distinct peaks and is divided into passive and active phases. The first peak in Figure 2.8 (a) corresponds to the initial impact of the heel on the ground (passive phase), whilst the active phase relates to the second peak during runner push-off. The F_{AP} component also has two phases including the braking phase of heel-strike, opposite to the forward motion of the runner and the propulsion phase of push-off, in line with the direction of movement. In running, F_{AP} peaks were reported in the region of 0.5 BW and the magnitude of F_{ML} was smaller compared to F_{AP} (Cavanagh and LaFortune, 1980; Munro et al., 1987). The vertical GRF profile can be different for other foot strike patterns, for example for forefoot strike running shown in Figure 2.9 exhibiting a single peak vertical force.

Loading rate represents how quickly the peak impact force is achieved. It equals the peak magnitude divided by the time between foot initial contact and occurrence of the peak force. Previous studies have identified that during rearfoot strike running the passive and active peaks occur within the first 50 ms and latter within 80 to 90 ms respectively (Nigg and Yeadon, 1987; Munro et al., 1987). Gotschall and Kram (2005) identified average values of loading rate associated with the passive phase during running of approximately 35 kN/s. De Wit et al (2000) reported higher average loading rates during running up to approximately 65 kN/s. High loading rates have been associated with the occurrence of overuse injuries such as stress fractures, tendonitis and damage to articular cartilage (Cavanagh, 1980; Dixon et al., 1998; Nigg and Bahlsen, 1988).

Table 2.3 summarises the GRF and contact time produced by subjects carrying out various movements collated from previous studies by a number of authors (updated from Severn, 2010). Adrian and Xu (1990) performed comprehensive research on various player movement patterns and reported the magnitudes for vertical and horizontal forces and contact time. The velocity of the subject was not specified for each movement pattern however, only described as a 'typical' movement speed of hockey or basketball. In addition, the subject was in contact with a rigid surface, different from the surface used in field hockey. Korhonen et al. (2010) investigated the GRF and temporal-spatial stride parameters of sprinting with both young and older male subjects. The data indicated an increase in the maximum vertical and horizontal forces in a shorter contact time compared to running at a slower speed. The difference was especially significant for young subjects. The maximum vertical force yielded an average of 3.34 BW for the young subjects sprinting at 9.5 m/s, whilst the magnitude during running was mostly in the order of 2 to 3 times BW. The ground contact time for sprinting was approximately 0.1 s which was 1/3 of the contact time during running recorded by Adrian and Xu (1990).

GRF is a function of several factors such as player body weight, movement speed, footwear and surface (Brachet, 2004). Munro et al (1987) showed that for running velocities between 3 and 5m/s, the average vertical GFR and loading rate both increase with running velocity and that foot contact time decreased. Nigg et al (1981) reported athletes produced 8.3 BW vertical GRF during long jump take-off at an 8.0 m/s approach speed. Footwear worn by player can also influence GRF, as shown in Figure 2.10. Barefoot heel-toe running is observed to generate a significantly higher loading rate than shod

running, but little difference is shown between the magnitudes of maximum vertical GRF (De Wit et al., 2000; Lieberman et al., 2010).

The level of cushioning (hardness) provided by a surface has been described as the effectiveness of the surface to reduce the magnitude of the impact peak (passive phase) (Nigg et al., 1995; Young, 2006). Generally, a non-compliant material provides less cushioning than a relatively compliant material (Dixon et al., 1998). Figure 2.11 highlights the differences between a compliant and non-compliant surfaces and how they influence the vertical GRF acting on a runner. The review of literature shows a lack of research on the player loading patterns on artificial turf surface, and the surface effects on the player. The study on cutting action carried out by Blackburn et al (2005) on 3G artificial turf pitch included only one specific cutting movement and the pitch condition was not reported in detail. Therefore, the connection between the player performance and surface influence couldn't be built to determine the player-surface interaction. Stiles and Dixon (2006) identified a tennis-specific movement on artificial turf and compared it with three other surfaces: a rigid force plate as the baseline condition, a carpet and an acrylic. Players from world-ranked to recreational level performed eight trials of running forehand foot plant at a sub maximal self-selected speed. The group mean peak vertical impact force on artificial turf was 2.88 BW measured by a FP, which was similar to other surfaces except for the baseline rigid condition. The artificial turf system used in their research was a sand-filled turf laid over a 5 mm thick acrylic surface. It was reported as 'high cushioning ability' as categorised using guidelines from the International Tennis Federation (ITF, 1997), but without any data to quantify its properties. El Kati (2012) studied the movement of 'stop and turn' based on 16 subjects on four 3G turf systems with different hardness (measured by the industry standard AAA) and traction. The averaged peak vertical GRF was 1.26 BW with averaged ground contact time in the range of 0.47 – 0.51 ms. Higher F_z (0.08 BW) was found on the soft-high traction surface (force reduction 68% and traction 38 Nm, tested using FIFA standard) during mid-stance and a higher F_z (0.067 BW) on the hard-low traction surface (force reduction 52% and traction 29 Nm, tested using FIFA standard) during push-off. These findings indicated the influence of surface properties on the magnitude of GRF. The research also criticised the AAA as not matching the player loading in vertical direction.

However, several other studies have showed no effects of surface hardness on the magnitude of vertical GRF during running/sprinting and turning (Dixon et al., 2000; Stiles

et al., 2011). These studies suggested that players were making kinematic adjustments to account for the different mechanical properties of surfaces to maintain the similar vertical impact peaks in running (Bobbert et al., 1992; De Wit and De Clercq, 1997).

The recent application of pressure insoles placed within footwear to measure loads at the foot plantar level and pressure distribution has provided an alternative methodology for measurement of player loading than using FP. Ford et al (2006) compared the in-shoe loading patterns on natural grass and artificial turf during cutting movements and found that the plantar loading at the forefoot and toes regions was affected by different types of surfaces used. The assessment of pressure distribution highlighted the potential of pressure data to detect different surface cushioning and study the surface effects on player loading (Stiles et al., 2009). The pressure measurement techniques used in previous research are detailed in subsection 2.6.3.

In summary, there is a lack of understanding on the parameters of sports related movements on artificial turf system. Previous research mainly focused on assessing the adaptation of player movement techniques for various surfaces and/or conditions (Stiles et al., 2009; Ford et al., 2006) and comparing the effects of different surfaces on the human body during movements (Kim and Voloshin, 1992). However, there is limited attempt in the research published to explain the effect of player loading on the artificial turf system's behaviour or to describe how the individual components of the surface system contribute to the system's response.

2.6 Material behaviour, measurement techniques and modelling

2.6.1 Overview

Artificial sports surfaces are commonly composed with various materials and several layers. Polymer foams (e.g. PU) as effective energy absorbers are frequently used as shock absorbing layers in artificial sports surfaces. Most foams produce a cellular structure during manufacture which can be primarily classified as a closed-cell or an open-cell structure. If the cell walls surrounding each air pocket remain intact, the foam has a closed-cell structure with discrete air pockets (see Figure 2.12 a). If the walls are ruptured, it has an open-cell structure of interconnecting struts with a continuous gas phase (see Figure 2.12 b) (Davidson, 2012). The mechanical properties of the foam are controlled by the intrinsic properties of the polymer and its cellular structure formed during foaming. Key variables in this respect include density, cell size, cell shape and degree of anisotropy

(Eaves, 2004). Figure 2.13 shows the typical compression characteristic for polymer (elastomer) foam exhibiting the stress-strain relationship with strong nonlinearity. It suggests viscoelastic performance of the material which means it returns to its original shape completely or almost completely when the deforming load is removed (elastic response), but the resumption of its shape is time dependent (viscous component to the response). If shape resumed only partially (residual deformation), the material has been deformed plastically, i.e. permanently due to molecules position change from their original position (Göbel, 1974). The stress-strain curves of loading and unloading result from the material's ability to absorb energy and to release part of this energy on retraction. The energy behaviour depends on several factors including the type of polymer, elastic buckling and fracture of solid matrix, coupled with viscous air flow in open-cell and air compression in closed-cell structures (Davidson, 2012).

Mechanical properties of sports surfaces and materials used in composite surface systems have been examined using various test methods. The tests that appear in literature can be divided into two categories. There are tests that measure mechanical properties by describing only a single data point during loading or unloading, presenting a measurement of force, acceleration or deformation – usually as a result of a drop test (as presented in Section 2.4); a second category of tests study the mechanical behaviour of materials and include the whole relationship between force and deflection (or stress and strain) and may also analyse the energy behaviour by reporting the loading and unloading phases of an impact or compression test (Anderson, 2007). The shortcomings of the sports industry mechanical measurement methods are shown in subsection 2.4.2. However, some researchers have adapted the industry tests to measure the whole impact signal for more detailed analysis (e.g. Carré and Haake, 2004; Anderson, 2007). Mathematical modelling also has been used to assess and predict the behaviour of sports surfaces during loading. Models detailed in literature range in complexity and accuracy. The most basic model contains a linear spring to represent force-deflection behaviour, and more advanced models containing a combination of nonlinear spring and damper in different configuration to represent the elastic and viscous components of sports surface.

Many sports surfaces show nonlinear force-deflection (stress-strain) behaviour with hysteresis and exhibit viscoelastic behaviour under compressive loading (Miller et al., 2000; Walker, 2003). Sports surfaces are complex systems with several layers and combined materials, all of which contribute to their composite behaviour (Bartlett, 1999).

Therefore, the mechanical behaviour of surfaces to interactions from players is difficult to assess fully. Identifying factors that can influence or control their performance is essential to comprehend the mechanical behaviour of the sports surfaces (Young, 2006). In subsection 2.6.2, mechanical behaviour of sports surfaces and relevant materials measured and modelled previously are discussed.

The forces applied upon the underlying sports surfaces are not applied at a single point, but are distributed over the area of impact which result surfaces deforming in different ways dependent on the structure and materials used. DIN standard classifies surface systems (mainly indoor floors) into three different types namely point elastic surface, area elastic surface and combined elastic surface. Point elastic surface only deforms under or close to the area of impact, for example synthetic playing surface installed on concrete. Area elastic surface deflects over a relatively larger area around the contact area during impact such as basketball wooden floor. Combined elastic surface represents a combination of both localised deflection and deflection over a wider area, usually structured with an area elastic base and a point elastic top layer. Technological advances in pressure-sensing technology, enabling the quantification of the vertical component of the forces and the contact area at specified locations of interest under the impact, have become commercially available for research and clinical applications (Zammit et al., 2010). Using pressure measurement system provides data of pressure distribution and change of contact area during loading which supports the analysis of sports surface response and elastic (deflection) type under load. Subsection 2.6.3 presents techniques of measuring pressure and material deformation under loading.

2.6.2 Material mechanical behaviour

2.6.2.1 Experimental approaches

Various authors have conducted quasi-static (Walker, 1996) or dynamic (Dura et al., 2002; Allgeuer et al., 2008) compression tests using servo-hydraulic test machines. The machine actuator in these tests was programmed to follow a specific force-time function to load and unload the test specimen via a platen/loading foot. Controlled energy impact tests such as ball and weight drop tests have also been used to produce vertical impacts and determine the response of surface (Carré et al., 2004; Anderson, 2007).

The force-deflection history is commonly presented to show the surface response and if contact area is recorded or interpreted then either in force-deflection or stress-strain graph.

Figure 2.14 shows an example of a viscoelastic material response under vertical load and unload in force-deflection relationship. Generally, the mechanical properties and behaviour are assessed deriving the following parameters: peak deflection; stiffness or spring rating; and some form of energy stored or loss related behaviour.

Peak deflection is extracted directly from the graphical data showing the material's ability to deform under load. The changing gradient during loading and unloading demonstrates stiffening of the material with increasing load, termed nonlinear behaviour. Different approaches have been used to establish an average or representative stiffness value for this nonlinear behaviour. Walker (2006) used the gradient of the tangent to the force-deflection curve at peak force as indicated in Figure 2.14 (f/d), whereas Schwanitz et al (2008) calculated secant stiffness across two specified load ranges (200 – 400 N and 1000 – 1500 N). Energy behaviour is determined by considering the area under or enclosed by various portions of the force-deflection curve (Davidson, 2012). With reference to Figure 2.15, the area under the loading curve represents the energy input during compression. The area under the unloading curve is equivalent to the energy returned as the surface returning to its original shape. The hysteresis demonstrates energy lost during the compression/impact. Numerical integration using trapezium rule is often used to calculate the magnitude of energy in Joules.

Anderson (2007) attempted to explain the somewhat complex process of shockpad behaviour under a dynamic compressive load in terms of shockpad structure and material from micro perspective. The behaviour of a cast in-situ recycled rubber (SBR) polyurethane bonded shockpad was described by dividing the loading section of force-deflection relationship into three phases as shown in Figure 2.16. Phase one, air void compression, is the initial phase characterised by high amounts of deformation for small loads and relatively lower stiffness compared to later phases. Phase two is a transition from lower to higher stiffness where shockpad deformation transitions from compression of air voids to compression of the rubber particles. Phase three is characterised by small deformations for high applied loads and therefore higher stiffness where compression resistance of rubber particles and internal friction of the binder are the primary functions.

Allgeuer et al (2008) examined the stress-strain behaviour of various shockpads (closed-cell PE, PU and SBR) under compression at low strain rate (around 0.004 Hz) and the permanent deformation of shockpads after cyclic loading at a higher strain rate (at 0.5 Hz).

The density of shockpad was found to be the key parameter driving the nonlinear behaviour and permanent deformation of shockpads. With decreasing density, the shockpads entered more rapid stiffening (densification) stage at a lower stress. It was concluded that lower density polyethylene foams were less suitable for shockpads in application than elastomeric foams. However, specification details of the samples, such as size and thickness, and the impact area of the compression loading were not stated. The design of the cyclic loading test at higher strain rate was aimed to simulate repeated impacts of the FIFA shock absorption test (refer to Section 2.4.2) and not loading inputs adopted from biomechanical data, which suggested the results measured could provide guidance for building products to meet the FIFA requirements but not permit the understanding of shockpad behaviour under real player loading.

McCullagh and Graham (1985) tested three artificial sports surfaces (rubberised outdoor surface: 6 mm, polymeric indoor surface: 6 mm and athletic track surface: 11 mm) using cyclic compressive loading to analyse their energy absorption at different loading rates. Tests were conducted to simulate a typical distance running impact with a maximum applied force of 2 kN at rates in the range of 0.001 to 2 kN/s on samples of size 50 mm × 50 mm approximates the area of the human heel. The amount of energy lost in each material was found to decrease as the loading rate increased, which suggested a viscosity property for each material. They observed an initial permanent ‘set’ deformation during the cyclic loading activity for all the materials after approximately three cycles.

Dura et al (2002) applied a viscoelastic linear model and frequency analysis to study the behaviour of three different materials used in sport surfaces. Material behaviour at six different cyclic loading frequencies from 5 to 35 Hz was analysed. An Instron machine was used to deliver eight consecutive impacts for each measure in each sample to maximum force of 500 N at a rate of loading of 10 N/millisecond. The sample size was 100 cm² and the impact area was a circle of 50 mm diameter, stated as similar to a heel. Two key properties, loss tangent (the ratio of lost energy to the stored energy) and dynamic rigidity (stress to strain ratio), were studied as functions of the loading frequency. There was no clear conclusion stated for the evolution of loss tangent with the change of frequency in the tested range. Both the PVC and thin rubber surface materials showed an increase of dynamic rigidity with increasing frequency. In comparison to the force reduction result of each material tested according to IAAF standard, this study discussed two strategies for achieving the level of shock absorption measured by the ‘Artificial

Athlete': high loss tangent and low dynamic rigidity. Limitations of this study were identified in the load history applied to simulate real player impact and the preload for test control. Maximum vertical force of 500 N was much lower than the majority of loads applied by player in real conditions. The preload used in the tests was 300 N, more than half of the maximum load, which could introduce residual stress and consequently change the material properties. Hence this loading regime was designed primarily based on the capacity of the testing machine and not simulating either the industry impact test or the player loading condition. New testing machines with improved dynamic control were expected by the authors to reduce the preload and improve the test.

A bespoke falling weight impact test device was used by Yukawa et al. (2011) to measure the response of athletic track surface under vertical impacts with eight different sizes of test feet ranging from 30 to 59.5 mm in diameter (7 to 28 cm²). A falling mass weighted 5 kg was dropped onto each test foot to load the surface from various heights to provide different impact velocity and hence impact energy intensity. A sensor unit consisted of accelerometer, force transducer and displacement sensor collecting corresponding data during an impact. Force-deflection relationship measured during loading showed an increase in surface stiffness and decrease in deformation as the impact area increased. It indicated the impact area was a factor influencing the surface mechanical response. However, the connection between the design of test loading inputs and actual player/ball in-play performance is unclear. This limitation suggests that results of surface tested may reflect more the set-up of the experiment and not the actual sports surface behaviour in-service (Baroud et al., 1999).

Recent research carried out by Zanetti et al (2013) tried to combine mechanical loading and biomechanical tests together to support the analysis of player-surface interaction. Two artificial turf carpets with different infills and one natural field were tested using quasi-static loading. Peak acceleration data in three directions during player performing football actions (e.g. straight and zig-zag running) was recorded by three accelerometers placed in correspondence of the ankle. Mechanical loading tests loaded the samples for 5 cycles with a 70 mm diameter test foot (same as the AAA foot size) to three magnitudes (1 kN, 2 kN and 3 kN) at three velocities (0.33 mm/s, 0.67 mm/s and 1 mm/s). Although the loading magnitudes were comparable with player vertical GRF in running, a limitation of this study was pointed out as the loading speeds were much slower than the peak impact speed in the foot landing phase due to the limited capabilities of the testing machine. Results indicated

load speed had no influence on surface stiffness for the tested velocity range and energy loss increased with increase in loading magnitude. Increasing load speed was found to reduce the energy loss. They concluded that peak vertical accelerations in player testing were affected by the energy storage and loss capabilities of surfaces. However, the findings were based on relative comparison between the three surfaces' performances and not confirmed quantitatively.

Investigations conducted by Nigg (1990), Carré et al (2004) and Anderson (2007) using drop test methods and studies using material testing machines (Allgeuer et al., 2008; Dura et al., 2002; Zanetti et al., 2013) showed the force-deflection behaviour of sports surface to be dependent on boundary conditions such as loading magnitude, loading rate, impactor shape, impact area, and specimen geometry (Miller et al., 2000). But these impact conditions were not fully detailed in most of previous studies, so the effect of each impact variable on surface behaviour has not been systematically analysed. In order to adequately determine the material properties of sports surface, the stress-strain relationship of a material is necessary to be quantified using different types of tests to understand its elastic and viscous properties. In addition, better understanding the mechanical behaviour of surfaces to interactions from players requires an integrated approach where both biomechanical and mechanical aspects are assessed. Therefore, further research is needed to measure the load/stress of actual player loading and the resulting surface deformation/strain simultaneously.

2.6.2.2 Modelling

Mathematical modelling has been used to assess and predict the force-deformation behaviour of sports surfaces during ball/weight drop impacts. It can be helpful to understand the energy behaviour of the impacted surface, and to inform the design of surface to ensure it is fit for purpose.

Rheological models characterise the surface in terms of elastic and viscous parameters. The elastic spring component, in which impact force is related to depth (displacement) of impact, models the elastic energy stored in the surface that will be returned to the impacting object. The viscous damper component, in which impact force is related to velocity of impact (and in some cases also depth of impact), represents energy not returned to the impacting object – energy that may instead be retained as plastic deformation or dissipated as heat (Davidson et al., 2009). Kelvin-Voigt Model is represented by a linear

spring and damper in parallel configuration as given by Equation 2.6. This model has been used by McCullagh and Graham (1985) as a first generation model to describe elastomeric sports surfaces and provided to be able to reproduce the hysteresis loop, but could not adequately represent the material force-deformation behaviour due to the constant stiffness of the spring. Peikenkamp et al. (2002) used a linear spring and damper model to describe an area-elastic surface response during an athlete's landing, but this model generates an unrealistic instantaneous impact force.

$$F = kx + c\dot{x} \quad (2.6)$$

Where:

F = Force (N)

k = Spring stiffness (N/m)

x = Displacement (m)

c = Damping coefficient (N.s/m)

\dot{x} = Velocity (m/s)

Sports surfaces behaviour under impact is fundamentally nonlinear. Shorten and Himmelsbach (2002) provided a model based on Hertzian contact theory to describe this nonlinear behaviour of a playground surface and an in-filled synthetic carpet as shown in Equation 2.7, where n represented a nonlinear coefficient. The nonlinear spring stiffness depended on the surface's elastic modulus and the geometry of the impactor. The nonlinear coefficient n was a positive number and claimed to be dependent on surface properties and contact geometry. This model encompassed linear impacts ($n = 1$), Hertzian contact ($n = 3/2$) and materials that stiffen ($n > 1$) or soften ($n < 1$) when compressed. However, without considering the effect of damping, this model was limited to describing only the loading phase of impacts.

$$F = kx^n \quad (2.7)$$

A combination of nonlinear spring in parallel with a viscous damper provided a more accurate model for describing the behaviour of sports surfaces and showed promise for the assessment of surface energy absorption (Carré et al., 2006; Anderson, 2007). However, stiffness, nonlinear and damping coefficients were dependent on surface thickness and impactor type (mass and contact area), thus no set of model coefficients could be used to describe surface behaviour independently of design. Another limitation is the models have only been tested for low-impact situations such as ball-surface impacts with impact kinetic energy less than 14 J.

Anderson (2007) also presented a similar stress-strain model as given by Equation 2.8. It was used to determine an equation to describe shockpads behaviour independent of their thickness. But this model displayed too much variability to accurately determine a set of coefficients to describe generic shockpad behaviour.

$$\sigma = E \varepsilon^\alpha + d \dot{\varepsilon} + \sigma_0 \quad (2.8)$$

Where:

σ = Applied stress (Pa)

ε = Strain

E = Modulus (Pa)

d = Damping coefficient (strain) (N.s.m⁻²)

α = Nonlinear coefficient (strain)

$\dot{\varepsilon}$ = Strain rate (s⁻¹)

σ_0 = Stress offset (Pa)

A model incorporating an exponential function to represent the nonlinear elastic and nonlinear viscous elements for the simulation of impact tests on viscoelastic sports surfaces was developed by Kobayashi and Yukawa (2011). The advantages of this model were the capability of representing the complicated viscous force by using deformation and deformation velocity, and stability of simulation. Davidson et al (2009) compared various aforementioned spring-damper models reported in the literature to evaluate their ability to reproduce the experimental acceleration-time and force-deformation impact curves. The

impact situation analysed was of a head form dropped at various heights impacting a gymnastic mat. Force- deformation curves were generated from the experimental data, with force being calculated from the measured acceleration values and surface deformation derived as the second integral of the accelerations. An exponential spring and depth damper combination (Equation 2.9) was found to best replicate the force-deformation relationship of the mats tested, and to demonstrate their energy behaviour. $1/b$ was related to the curvature of the elastic component of the force-displacement graph, similar as nonlinear coefficient n in power model. c was related to the energy absorbed (Davidson et al., 2009).

$$F = A \times \exp(x/b) - A + c\dot{x} \quad (2.9)$$

Where:

A = Exponential amplitude constant (N)

b = Exponential depth constant (m)

Other symbols are explained in equation 2.6

This model may be applied to describe the behaviour of sports surfaces under a range of player movement patterns apart from short duration impacts, and simulate player-surface interactions with different intensities and loading durations. However, no investigation could be found in literature using these advanced models for assessing the behaviour of sports surfaces during actual player movements such as walking and running.

2.6.3 Measurement techniques

2.6.3.1 Pressure measurement under loading

Pressure measurement systems employed by researchers include insole systems (Novel Pedar, Tekscan F-scan, RS-Scan Insole and IVB Bio-foot etc.) and mat systems (Novel Emed, RS-Scan Footscan and Tekscan Matscan). Capacitive and force sensitive resistor are two commonly used transducer types for pressure measurement. In capacitive transducers, such as Novel Pedar, two capacitor plates are separated by a compressible rubber dielectric material. When pressure is applied, the two plates are pushed closer resulting in an increase of capacitance which is calibrated in units of pressure. Pressure

measurement sensors, such as those made by Tekscan Inc. (South Boston, MA), comprise a matrix of electrically isolated force sensing elements (sensors) based on the use of conductive or semi-conductive inks sandwiched between thin, flexible polyester sheets. Electrically conductive pathways are imprinted on the polyester sheets and the conductive ink is deposited between the upper and lower sheets at locations at which the pathways intersect. The ink provides an electrical connection between the upper and lower conductors. The resistance of this connection changes with an applied compressive force. Knowing the spatial dimensions and resolution of the sensors, the measured force data can be converted into a pressure profile. By varying the spacing and patterns of the conductive pathways, manufacturers have produced sensors of various shapes, sizes and sensor resolution (Murin et al., 2001).

Commercially available pressure mat systems used in previous studies, such as XSENSOR, RS-Scan Footscan and Tekscan Matscan, have their own strengths and limitations of temporal and spatial resolution and physical characteristics. The advanced capacitive sensor mat XSENSOR is flexible with the sensing area thickness around 1 mm. However a disadvantage of low sampling rate was identified from the previous publications (Webster and Roberts, 2010; Halkon et al., 2012). This problem limited the application of the XSENSOR pressure mat in the dynamic measurements. Therefore, it was mostly used in static measurements such as automotive seating and sleep pressure imaging evaluations. The dimension range of RS-Scan Footscan system is from 0.5×0.4 m to 2.0×0.4 m, which makes it possible for assessing multiple footsteps. Current Footscan systems can be used for dynamic measurement at a sampling rate up to 500 Hz. But the RS-Scan pressure mat is a nonflexible rigid plate with a minimal thickness of 8 mm. So it was usually used on top of a rigid surface such as force plate to compare the plantar pressure values with human movements (De Wit et al., 2000; Willems et al., 2005). The uses of Tekscan pressure measurement systems are presented in the following details.

Tekscan pressure sensors are appealing for biomechanics research and widely used in previous studies because they are thin, flexible, light weight, high resolution and conform to contoured surfaces. Contact pressure profiles between two opposing surfaces offer real-time dynamic feedback of visual and quantitative descriptions of how the vertical force is distributed and surfaces are loaded during contact. The recorded data is often presented as 2D or 3D colour-coded maps (as shown in Figure 2.17) which may represent a particular time instant or be a composition of all data recorded for the contact duration (Davidson,

2012). The real advantage of the pressure sensing system, in comparison to the traditional load measurements made on force plate, is to determine the pressure variation with time and the area of loading under controlled (mechanical) and uncontrolled (human) loading, whereas force plate has no distribution measurement capabilities (Barnett et al., 2001).

Reliability of the pressure measurement systems in terms of accuracy, sensitivity, repeatability and durability has been determined by several authors in a range of biomechanical applications. There are several factors that affect the sensor output, consequently the reliability of the pressure measurement, including variations in sensitivity across individual sensels; creep in the output with constant applied pressure over time, leading to hysteresis in the dynamic response; temperature; contact surface curvature; contact surface compliance and noise introduced by the system hardware (Bryant et al., 1999; Luo et al., 1998; Murin et al., 2001). For pressure insole systems, they function in a more challenging environment which tends to cause sensor inaccuracy and deterioration in sensitivity, either due to temperature or moisture variability or creasing of sensor matrix within the shoe (Barnett et al., 2001; El Kati et al., 2010). Tekscan Matscan system displayed moderate to good reliability for the variables of maximum force, peak pressure and average pressure for assessing human barefoot walking taken in one week apart (Zammit et al., 2010).

Several validation studies have been published to determine the appropriate calibration procedures for Tekscan pressure sensors and investigate the effects of the aforementioned factors on the measured output. Prior to calibration the insole size sensor could be equilibrated in Tekscan software by applying a constant, predetermined pressure to the entire sensing area by means of an instrumented air bladder in order to equalise the sensitivity across individual sensels (Halkon et al., 2012; El Kati et al., 2010; Pain et al., 2008). For pressure mat sensor, this procedure is carried out by manufacturer in factory, but it is difficult to perform it in laboratory due to the larger size of the sensing area. Mueller and Strube (1996) suggested for comparing absolute measures between different Tekscan F-Scan insoles or across days, external calibration from a stable output source such as a force plate was recommended. They also pointed out the reliability might be further improved by placing the sensor inside the shoe for 5-10 min prior to the subject weight static calibration to allow the sensor to be loaded repeatedly and the temperature to stabilise to the environment of the shoe. It suggested in this study the sensor needed a 'warm-up' period before calibration. Carvalho et al (2005) used a force plate with the same

dimensions as Tekscan Matscan sensor (as shown in Figure 2.18) to correctly calibrate the Matscan sensor for the pressure distribution analysis of cows' hooves under dynamic conditions (stance phase). However, the calibration process was not detailed.

Using statically calibrated Tekscan pressure sensor followed the procedure outlined by the manufacturer for short duration human impact measurements showed the sensor consistently underestimated the dynamic peak force values. It was noted that the loading rate of applied force played a significant role in the output of the sensor and, for this reason, a dynamic way to calibrate the sensor for such data collection is required (Halkon et al., 2012; Pain et al., 2008). Force values from an external source such as FP or load cell were linearly regressed against the Tekscan sensor static calibrated force data. Each regression line was fitted through the origin and the gradient of the regression line was used as the calibration coefficient (conversion factor) for the Tekscan data, thereby enabling the Tekscan reading to be representative of the actual force experienced. Murin et al (2001) reported the effects of contact surface compliance on Tekscan sensor output. It was found that linear calibration slopes and sensor outputs were lower for the sensor located over more compliant surfaces (Luo et al., 1998). The decrease of sensor output was explained by the fact that the deformation of compliant material caused shear force around the curved edge of the contacting surface under the impactor, and the force normal to the sensor experienced by the sensels was lower, hence a lower output. Another source of variability was the non-uniformity of the compliant surfaces. It indicated that calibration of Tekscan sensor should be performed under conditions that are as close as possible to the actual measurement conditions in order to obtain reliable results. Brimacombe et al (2009) conducted a validation study to determine the effects of different calibration algorithms on sensor accuracy by comparing two standard Tekscan calibration options (single-point linear and two-point power calibrations) to two user-defined calibration algorithms (ten-point cubic polynomial and three-point quadratic polynomial calibrations). For conditioning, calibration and loading cycles, an experimental setup (Figure 2.19) used an Instron material testing machine to load material (polyethylene) and Tekscan sensor representing actual experimental conditions. Calibrations were performed by increasing the force linearly over 10 s, holding it constant for 5 s, and decreasing it to zero linearly over 10 s. The results indicated the power calibration yielded more accurate pressure measurements between the standard Tekscan calibration options for this testing configuration showing under 3% RMS error across the full sensing range. Both user-

defined calibration methods yielded more accurate results than the Tekscan methods over the full range, with the ten-point cubic calibration yielding the most accurate pressure measurements. The importance of selecting optimal calibration points to obtain accurate results within the pressure range of sensor used was highlighted. A limitation of this study was other factors (as discussed above) known to affect Tekscan accuracy were not quantified.

2.6.3.2 Deformation measurement under loading

The current method employed by the industry (FIFA, 2012) to measure vertical deformation of artificial turf surfaces was introduced in Section 2.5.1. But only the deformation at peak deceleration is reported according to the standard. In research, in order to describe the surface behaviour during the entire loading event, it is useful to analyse all the deformation-time data rather than the peak value alone. In the accelerometer impact tests carried out by Carré and Haake (2004) using a CIH, the complete time history of the acceleration of the mass during impact with the surface was collected. These data were then integrated twice with respect to time to produce velocity and displacement information. Taking acceleration as a function of force and assuming the mounted accelerometer displacement was equal to the surface vertical deformation, a plot of force-deformation was produced to describe the key parameters of surface response. Anderson (2007) converted the filtered vertical GRF-time output of a ball impact on shockpad from a force plate to shockpad vertical deformation-time data using a series of integrations. Acceleration data was obtained by using Newton's Second Law of Motion as the mass of the ball remained constant and the mass of shockpad undergoing deformation was considered negligible. Then the same approach as Carré and Haake's was taken to integrate the acceleration data twice to obtain vertical deformation-time data using trapezium method. Measuring surface deformation from acceleration data involved several assumptions and simplifications, but it is a common method used for ball/weight impact tests.

In order to measure real-time deformation of material/surface under dynamic loading without altering the strain response of the sample and the loading behaviour, non-contact optical motion analysis systems were also used in previous research. Anderson (2007) investigated the impact of a hockey ball with a shockpad or shockpad-carpet surface system using high speed camera to capture images throughout the impact which were used to digitally measure vertical deformation-time behaviour. The camera was placed in line

with the upper surface of the sample to avoid parallax errors and captured a marked ball at a rate of 2100 frames per second (fps). The first point of contact between the surface and the ball was selected visually and set this frame as the origin for time and displacement of the coupled ball-surface. Three black marker points closest to the centre of the ball were selected for digitising each impact. An average of the vertical coordinates for the three markers on the image was used to measure vertical displacement, with change in this coordinate from the first frame equal to surface vertical deformation. The errors produced in visual identification of the initial contact frame and manual digitisation of markers on the ball were estimated to produce a maximum of 20% difference in deflection measurements, which was considered to be significant.

3-dimensional digital image correlation (3D-DIC) photogrammetry was proved to be a useful tool for the full-field surface deformation measurement with sub-pixel resolution in biomechanics and materials engineering aspects, providing 3D measurement of the specimens under dynamic loading (Tyson et al., 2003). This optical technique is independent of the material that it is measuring, providing a non-contact measurement which can be easily integrated in existing experimental environments. Jin et al (2007) demonstrated that the 3D-DIC technique was able to obtain accurate full-field deformation of PU foams and strain concentrations during compression tests showing the effects of loading configurations on deformation and strain concentration in foam specimens. The 3D-DIC system was composed of two CCD cameras with a resolution of 1280×1024 pixels. The frame rate used in the tests was 25 fps because the compression was quasi-static about 1.27 mm/s. The maximum frame rate was up to 500 fps at full resolution for high strain rate tests. A random speckle pattern with good contrast to the surface of foam specimen was painted, which deformed with the specimen under loading. The deformation and strain fields were then computed in the three-dimensional Cartesian coordinates from the image pairs acquired from the two cameras before and after deformation. Figure 2.20 shows the experiment setup. The keys to 3D-DIC measurement are the deformation can only be tracked when the specimen speckled surface remains within the field of view of the cameras and the cameras need to be ideally set to be both normal and close to the observed surface. It is difficult to use this technique for measuring surface vertical deformation especially for 3G turf system because it is hard to set the cameras normal to the deformation in vertical direction and applied the speckle pattern due to the infills in carpet.

Vicon is a passive motion analysis system which tracks the location of retroreflective markers in real-time using cameras equipped with infrared light-emitting diodes (LEDs) (Tsu, 2010). Each marker visible with multiple cameras reflects this light relaying information about its position in 3D. This system was mainly used to capture the movements of human based on markers placed on the body. From these markers, kinematic data such as joint angles and rotational angular velocity could be determined (Tsu, 2010; El Kati, 2012; Ahmadi et al., 2010). Compared to other non-contact optical motion analysis methods, the main advantage of Vicon system is the much larger capture volume created by more than 10 cameras used which makes the markers visible within the view of at least two cameras throughout the entire motion in various experimental conditions. Attention should be paid to the attachment of markers. Possible errors could be introduced by local marker movement (wobbling) due to stretch or deformation of the surface it attached to. Although there is currently no publication available using this measurement method for surface/material deformation analysis, it has the potential to be employed in this application by comparing the positions of tracked markers on an impactor between frames.

2.7 Discussion

This section provides a discussion of the current state of knowledge regarding tests methods for artificial turf surfaces, player-surface interactions and techniques used in relevant areas for assessing material behaviour. The main areas identified from the discussion requiring further investigation are then highlighted.

The construction of an artificial turf pitch can be divided into two main sections, the foundation layer and the surface system. The surface system usually comprises a shockpad layer and an artificial turf layer (with or without infill) that together provide the required playing characteristics (Fleming, 2011). The review of literature showed a large variety in materials used and design and therefore the overall system exhibits different mechanical behaviour in-service. Sports governing bodies have implemented performance requirements to try and limit the differences between surfaces constructed for a specific sport. Artificial turf surface systems are currently classified and compared using a number of mechanical test methods. However, these methods are too simplistic to properly quantify the behaviour of the surfaces (Miller et al., 2000). Many of these mechanical tests have been criticised for their lack of ability to simulate real movements that occur in sport (Dixon et al., 1999), however in their current state they are easily repeatable and portable

for use in field testing and are useful for indexing sports pitches by sports governing bodies. Shortcomings of vertical impact tests used to determine compliance and energy characteristics of surfaces in terms of little correlation with impact force peaks during locomotion (Nigg et al., 1987) and much shorter contact durations than ground contact durations in player movements (Kolitzus, 1984; Nigg et al., 1984) are presented in subsection 2.4.2.

A range of player movement patterns analysed in previous studies has been classified in Section 2.5.1, and frequently used general movement patterns in multiple sports can be identified. Key loading parameters such as GRF, loading rate, contact time, and velocity of movement are commonly used to evaluate the interactions between player and sports surface. A lack of research to obtain these loading parameters that enable a number of sport-specific movements performed on an artificial turf surface system to be characterised has been identified. These parameters are identified as having the potential to influence mechanical behaviour of sports surface. However, understanding player-surface interactions has in general received more research effort focussed on biomechanical aspects, and little regarding the effects of player loading on the surface's mechanical behaviour. The gaps in knowledge are partly caused by the fact that some biomechanical studies failed to characterise the surface properties (Blackburn et al., 2005; Stiles and Dixon, 2006; McGhie and Ettema, 2013), whereas other studies that did quantify the surface/material properties provided limited biomechanical data (Yukawa et al., 2011; Allgeuer et al., 2008; Dura et al., 2002).

Most of sports surfaces and component materials (e.g. rubber particles and polymer foam) exhibit nonlinear viscoelastic response under compressive loading tested by material testing machines (Walker, 2003). The use of mechanical compression tests enables control over several variables in comparison to subject testing and therefore has ability to evaluate the effect of individual variables in isolation. McCullagh and Graham (1985) found that the amount of energy absorbed by each material decreased with the increase in loading rate. Dura et al (2002) showed an increase of dynamic rigidity (stiffness) with increasing loading frequency for the surfaces tested. Yukawa et al (2011) exhibited the force-deflection relationship of surface sample showing an increase in surface stiffness and decrease in deformation as the impact area increased. Zanetti et al (2013) found that energy loss of artificial turf surfaces increased with increasing vertical load and reducing load speed respectively.

A limitation in common for previous research was the loading inputs of test control were not relevant to actual or closely simulated player movements performed on sports surfaces. In addition, current sport surface studies using drop tests and material testing machines have mainly determined the force-deformation behaviour of various materials. The force-deformation behaviour is a structural property, which depends on boundary conditions such as loading magnitude, loading frequency and rate, contact area, impactor shape and velocity, and specimen geometry. The stress-strain relationship of a material is considered to be able to describe the material behaviour independent of boundary conditions such as geometry (Miller et al., 2000). Therefore, further research is required to design appropriate mechanical loading methods using biomechanical data (e.g. loading magnitude, rate, area and contact time) for evaluating the mechanical behaviour of sports surfaces (e.g. surface deflection, stiffness and energy behaviour) and identifying loading parameters that can influence or control their performance.

Nigg and Yeadon (1987) suggested that to understand the performance aspects of a surface material tests need to be complemented with subject tests. To the author's knowledge, there is no published data quantifying the previously discussed real-time mechanical behaviour of artificial turf surface systems under actual player movements and the corresponding effects of influential loading parameters. Advanced measurement techniques for assessments of force, pressure and deformation under dynamic compressive loading were introduced in this review of literature. Force plate and pressure sensors have been widely used in biomechanical research. Force plate is commonly considered as the 'gold standard' for measuring GRF during dynamic sports movements. Using pressure sensors enables the quantification of the vertical component of forces and the contact area at specified locations of interest under the impact. The additional information of contact area reveals how the applied load is distributed over the area. Most of previous research regards the surface system as a single element. Further research into the component layer behaviour of artificial turf surface system is required to provide a greater understanding of how these components behave individually in terms of load spreading and contribute to the composite surface system's response. Pressure sensing mat technology provides the opportunity to quantify the loads/pressures experienced at each level of the carpet/shockpad system (Stiles et al., 2009). Motion analysis system such as Vicon, tracking marker displacement by multiple cameras with LEDs in 3D, offers potential for measuring real-time surface deflection under actual player movements. In comparison to

other optical motion analysis systems, it has the advantages of recording at high sampling rate without extra illumination, providing much larger capture volume and eliminating parallax errors and observation blind area (e.g. blocked by the carpet fibres) that may occur when using single or dual cameras.

Experimental studies provide useful information about the effects of changing surface material properties. For new product design and construction, it might be more satisfying to be able to predict its mechanical behaviour before it is manufactured; however, in reality, it is often necessary to reverse-engineer prototype models with the ‘trial and error’ method to discover why particular, often poorly understood features have proven successful or otherwise (Miller et al., 2000; Thomson et al., 2001). Mathematical modelling and computer simulation provide the opportunity to study new designs and constructions with much less time and expense. The development of rheological models for sports surfaces would help to describe characteristics of mechanical behaviour such as nonlinearity and hysteresis and explain how the load/impact is absorbed by the materials and their energy behaviour (McCullagh and Graham, 1985; Anderson, 2007). In order to develop an appropriate model comprised of components of elasticity and viscosity for sports surfaces, elastic and viscous properties of the surfaces must be quantified using different types of tests (Miller et al., 2000). The review of literature found no suitable stress-strain model to accurately describe and predict nonlinear mechanical behaviour of artificial turf systems by fitting to the experimental data obtained from actual or accurately simulated player interactions with the surface systems.

In summary, artificial turf surface systems can be comprised of a number of different materials and composed of several layers and therefore the mechanical behaviour of surface systems to interactions from players is complex and difficult to assess. Current industry mechanical tests described in Section 2.4 fail to represent player loading and incorporate the complexities of player movement and therefore are not considered to be appropriate for measuring the behaviour of surface system in-service conditions. Player-surface interaction is two-way and studies that provide details of the mechanism by which variation in player loading affect artificial turf system performance are lacking. Hence research is needed to better understand the load/stress and the resulting surface deformation/strain under real player loading. In addition to support this, the mechanical behaviour of the component layers and systems is required to be evaluated by mechanical loading tests using biomechanically validated design. This will benefit the sports surface

industry by providing a clearer understanding of the mechanical behaviour of component layers and overall surface system that influence player-surface interactions enabling better judgements and decisions to be made when designing a surface system to provide the desired playing characteristics, and consequently benefiting the artificial turf surface users.

Table 2.1: Field tests and requirements of artificial turf pitch for soccer (FIFA, 2012)

Characteristic	Test Method	Requirement			
		FIFA Recommended Two Star		FIFA Recommended One Star	
Vertical ball rebound	FIFA 01	60cm - 85cm		60cm - 100cm	
Ball roll	FIFA 03	Initial assessment	4m - 8m	Initial assessment	4m - 10m
		Re-tests after 12 months play	4m - 10m	Re-tests after 12 months play	4m - 12m
Shock Absorption	FIFA 04a	60% - 70%		55% - 70%	
Vertical Deformation	FIFA 05a	4mm - 10mm		4mm - 11mm	
Rotational Resistance	FIFA 06	30Nm - 45Nm		25Nm - 50Nm	
Surface regularity of playing surface	FIFA 12	<10mm		<10mm	

Table 2.2: A summary of player movement classification (El Kati, 2012)

Movements/actions	Modifiers	Additional
Linear movements		
Stand still	Direction	Overall ball modifier
Walk	Forwards/Backwards	Ball involved: Yes/No
Jog	Forwards/Backwards diagonally right/left	
Skip	Arc forwards left to right/right to left	
Shuffle	Arc backwards left to right/right to left	
Run	Arc sideways left to right/right to left	
Sprint	Intensity	
Accelerate	Low, medium, high, very high	
Decelerate		
Jump		
Change of direction		
Swerve	Direction	
Turn- /twist	Left/Right	
Crossover cut	Angle	
Side-step cut	30°, 60°, 90°, etc.	
	Intensity*	
	Low, medium, high, very high	
Contact		Sport specific movements
Impact	Type of impact	Rugby
Slide	Deliver/Receive: push, pull, tackle	Ruck/maul
Dive	Intensity	Scrimmage
Land	Low, medium, high, very high	Football
Fall / Stumble		Block
Ball activity		
Pass	Pass/Shoot	Soccer
Receive	Long/short air, long/short ground	Throw in
Shoot	Method	Rugby
Trick / Fake	Right/left foot, head, chest, thigh, heel	Lineout
		Field hockey
		Push pass

Table 2.3: Peak force and contact time measurements for various authors (updated from Severn, 2010)

Author	Velocity	Surface	Move	Vertical Fmax	Horz. Fmax	Contact Time (s)
Adrain and Xu (1990)	Typical movement speed of hockey or basketball	Force Plate	walking	1.33 BW	0.25 BW	1.1
			Running	2.50 BW	0.33 BW	0.3
			Veering	2.00 BW	0.83 BW	0.3
			Cutting	2.00 BW	0.67 BW	0.65
			Stopping	2.67 BW	3 BW	0.5
			Dodging	2.67 BW	0.67 BW	0.9
			Pivoting	2.67 BW	0.17 BW	1
			Jumping	2.00 BW	0.33 BW	1
			Landing	3.33 BW	1 BW	0.5
			Lunging	2.67 BW	0.75 BW	1
Ozguven and Berne (1988)	N/A	Gym Mat	Jumping	5.70 BW ^a	N/A	N/A
Nigg and Yeadon (1987)	4 m/s	Track 1	Running	1458 N	N/A	N/A
		Track 2		1419 N	N/A	N/A
Munro et al (1987)	3 m/s	Force Plate	Running	1.57 BW	N/A	N/A
	4 m/s			1.95 BW	N/A	N/A
	5 m/s			2.32 BW	N/A	N/A
Dixon et al (2000)	3 m/s	Asphalt	Running	1.6 BW	N/A	N/A
		I.A.A ^b	Running	1.58 BW	N/A	N/A
Blackburn et al (2005)	N/A	3G Pitch	45° Cut	3250 N	2000 N	0.225
Stiles et al. (2007)	3.83 m/s	Natural Clay	Running	2.53 BW	N/A	N/A
		Natural Sandy		2.47 BW	N/A	N/A
		Natural Rootzone		2.50 BW	N/A	N/A
Korhonen et al. (2010)	9.5 m/sec ^a	Indoor Synthetic Track	Sprinting (young subjects)	3.34 BW ^a	1.42 BW ^a	0.102 ^a
	7.3 m/sec ^a		Sprinting (older subjects)	2.82 BW ^a	0.88 BW ^a	0.129 ^a

Note: BW – body weight, a – mean results, b – Impact absorbing asphalt



First generation synthetic turf



Second generation synthetic turf



Third generation synthetic turf

Figure 2.1: Three generations of artificial turf (TenCate, 2010)

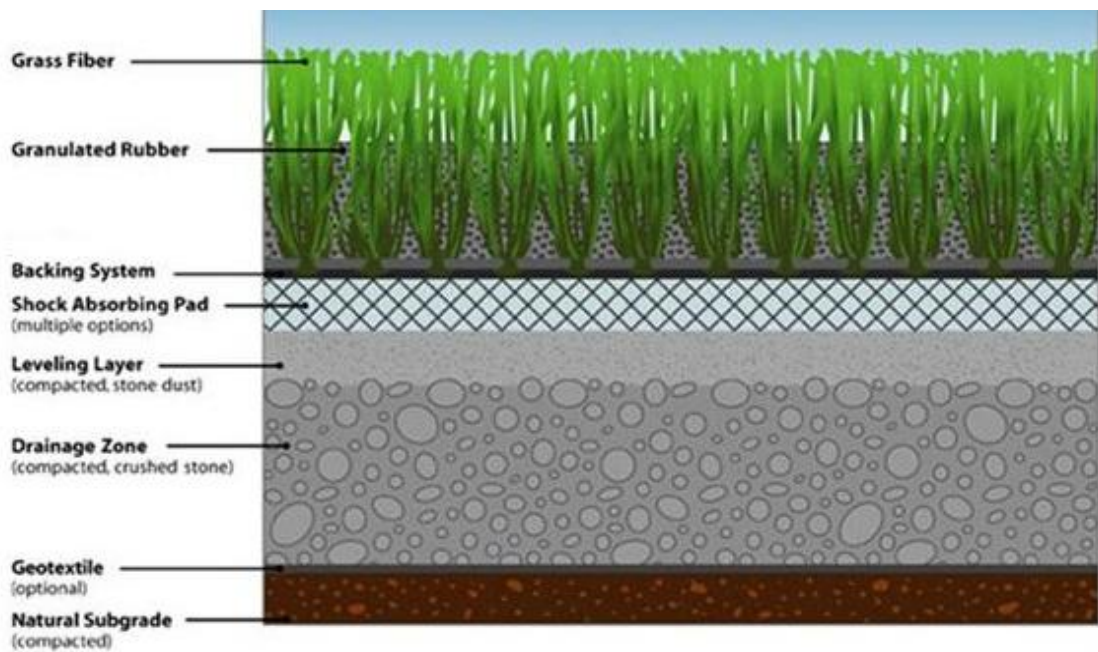


Figure 2.2: Typical artificial turf pitch system structure (Synthetic Grass Info, 2010)

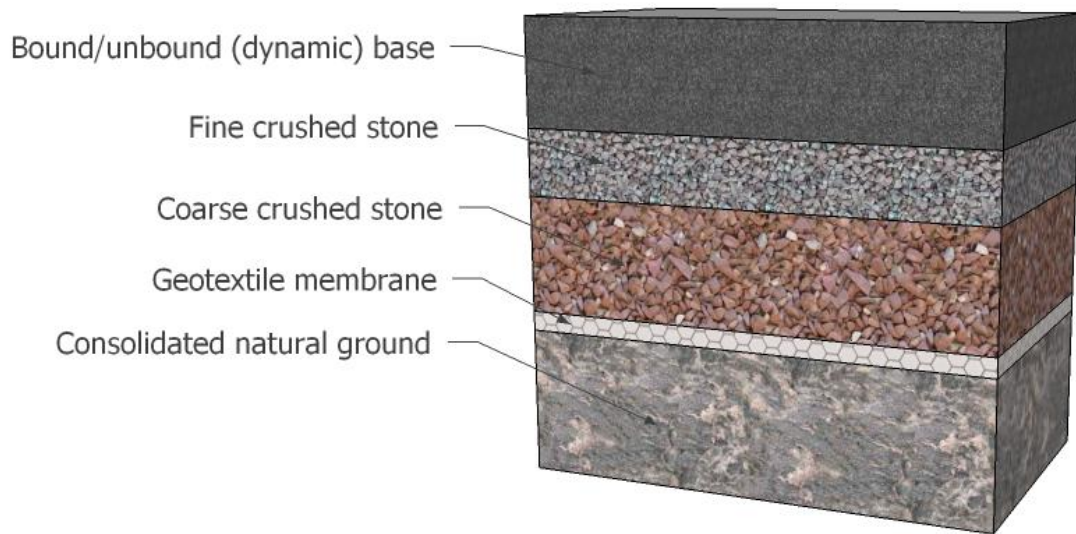


Figure 2.3: Typical structure of foundation layer for artificial sports pitches

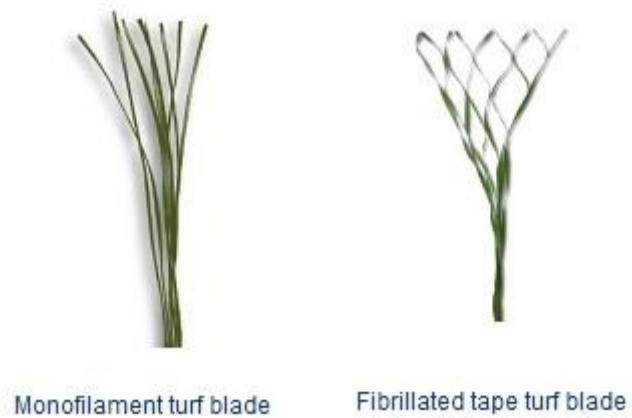
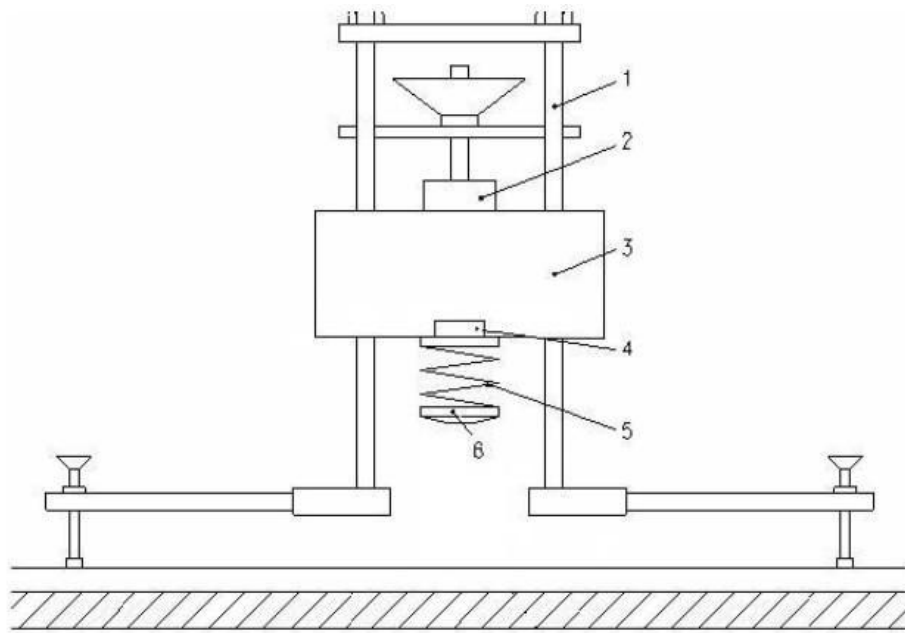


Figure 2.4: Monofilament and Fibrillated turf blades (TenCate, 2010)



- 1 guide for the falling mass;
- 2 electric magnet;
- 3 falling mass;
- 4 accelerometer;
- 5 spring;
- 6 test foot.

Figure 2.5: The structure of the Advanced Artificial Athlete (FIFA, 2012)



Figure 2.6: The Clegg Impact Hammer (Severn, 2010)

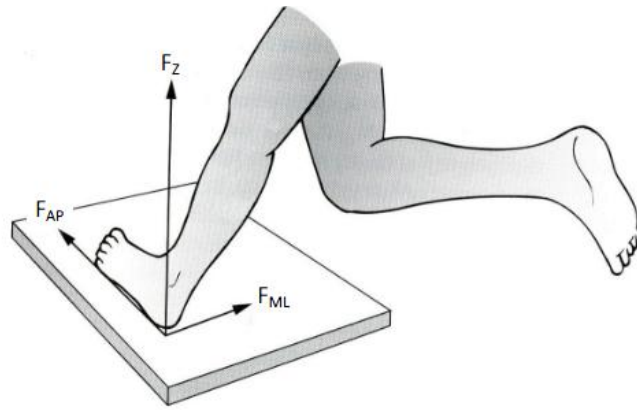


Figure 2.7: Ground reaction force components in three directions during running (Davidson, 2012)

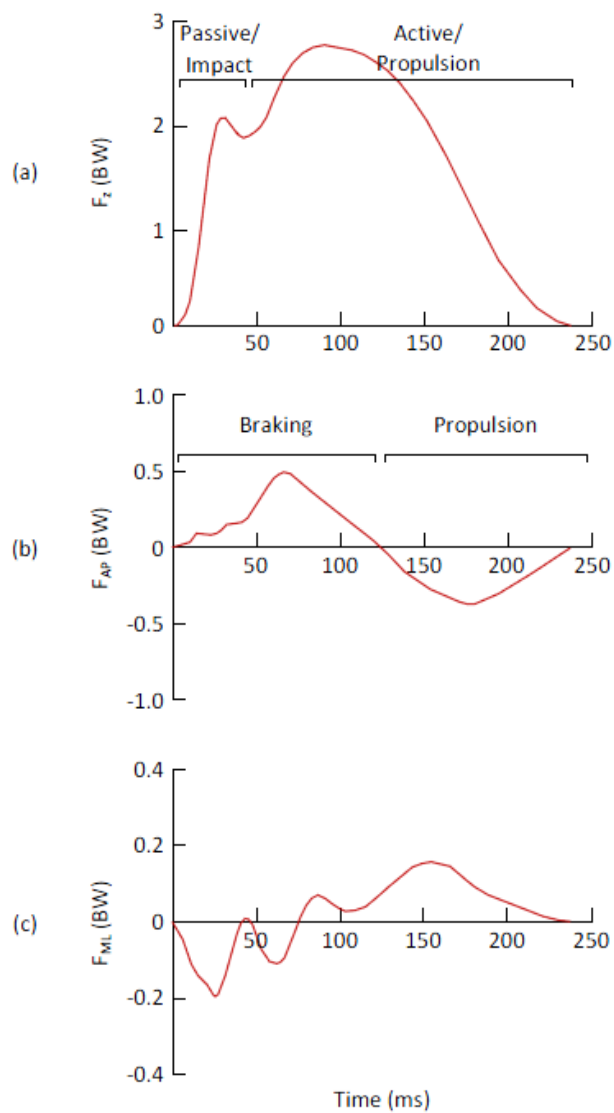


Figure 2.8: Typical GRF profiles of rearfoot strike runner; (a) F_z , (b) F_{AP} and (c) F_{ML} (Davidson, 2012)

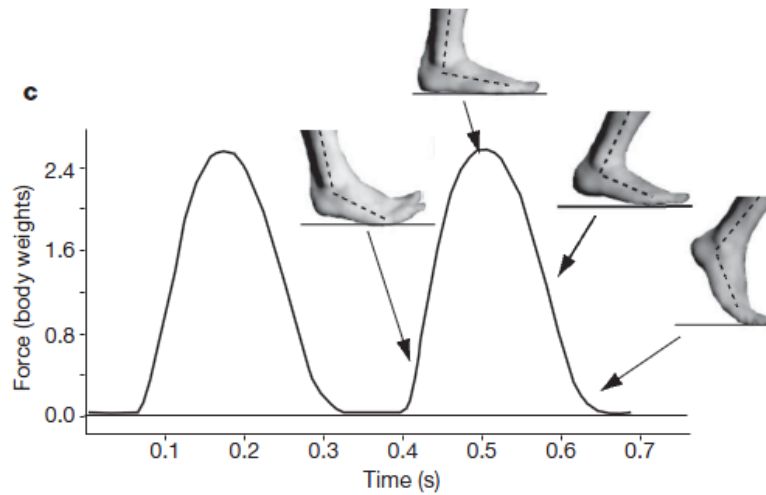


Figure 2.9: Vertical ground reaction force of forefoot strike running (Lieberman et al., 2010)

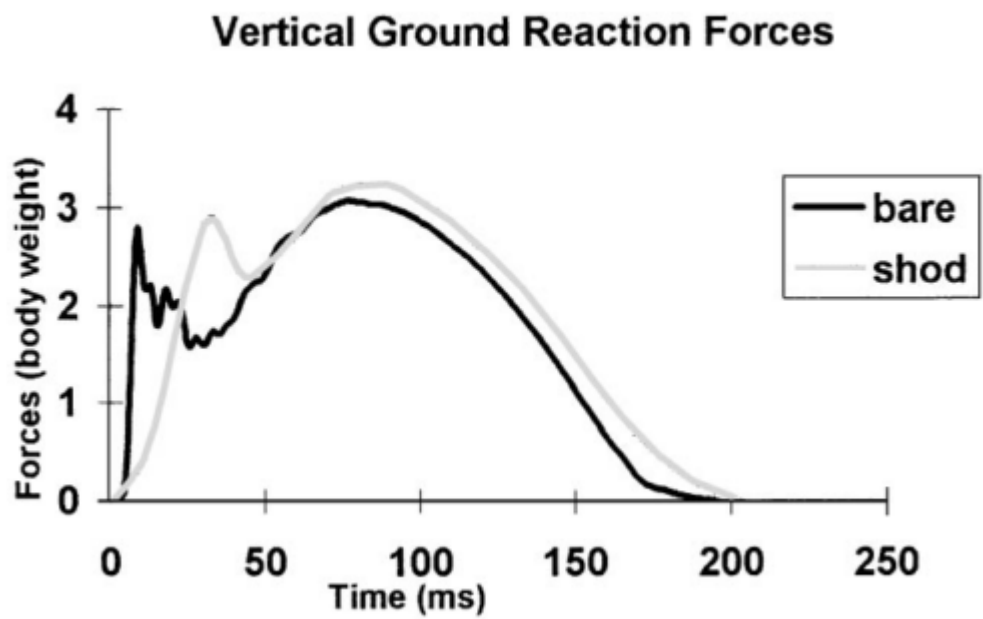


Figure 2.10: Vertical ground reaction force curves of one runner performing 1 barefoot trial and 1 shod trial at the same velocity of 4.5 m/s (De Wit et al., 2000)

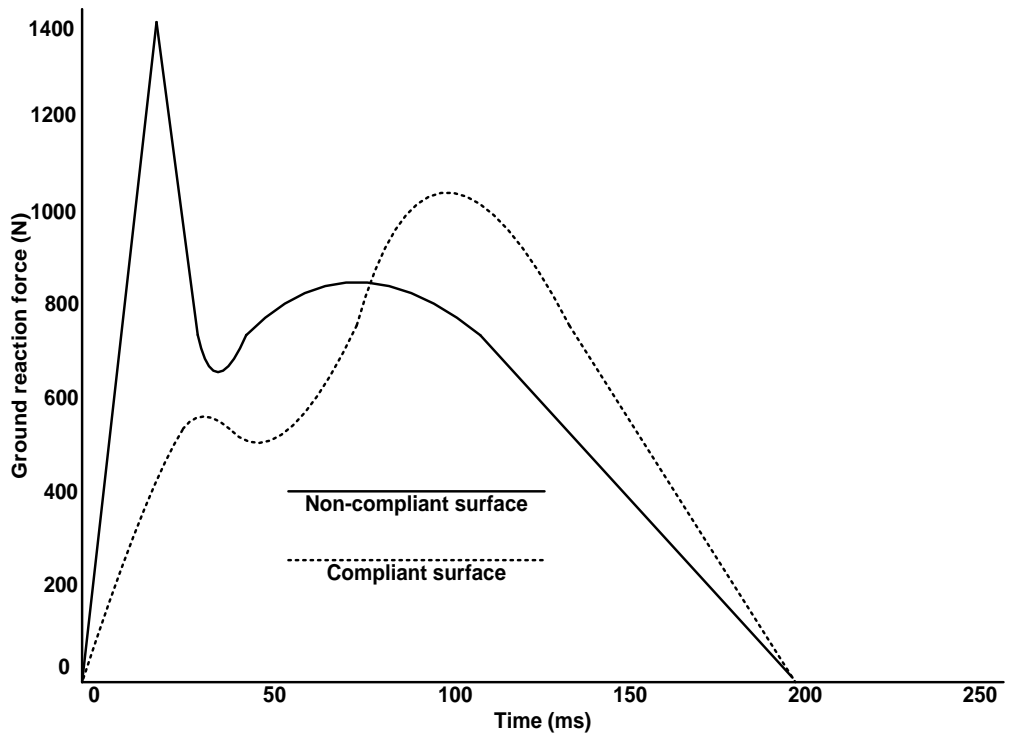


Figure 2.11: Vertical ground reaction force for a compliant and non-compliant surface (Young, 2006)

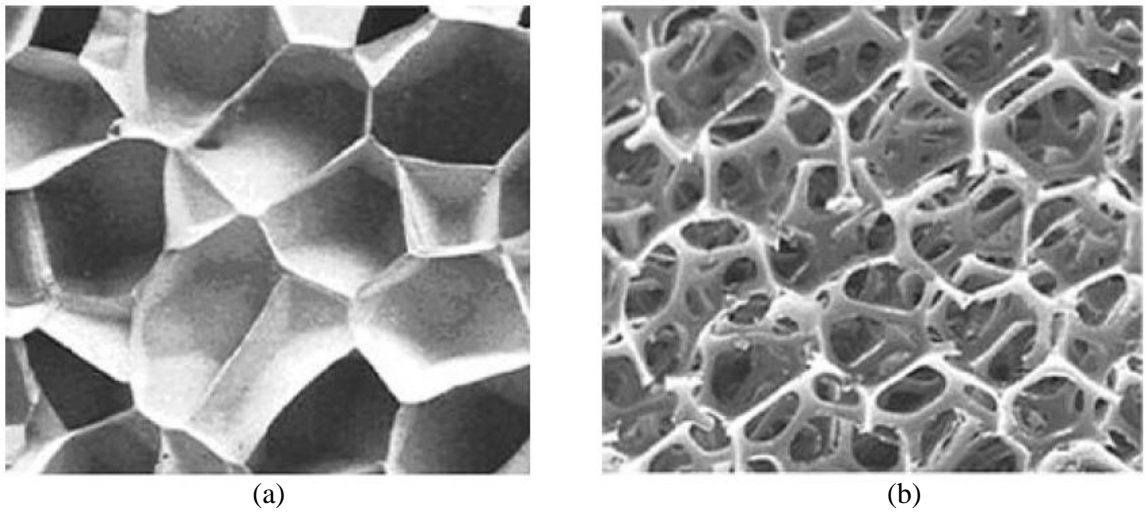


Figure 2.12: Closed-cell (a) and open-cell (b) polymer foam structures (Davidson, 2012)

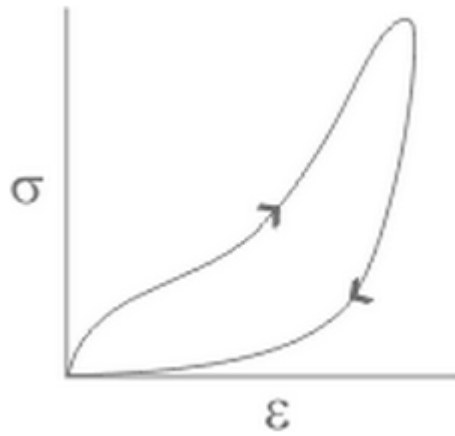


Figure 2.13: Schematic compression stress-strain curves for a polymer foam

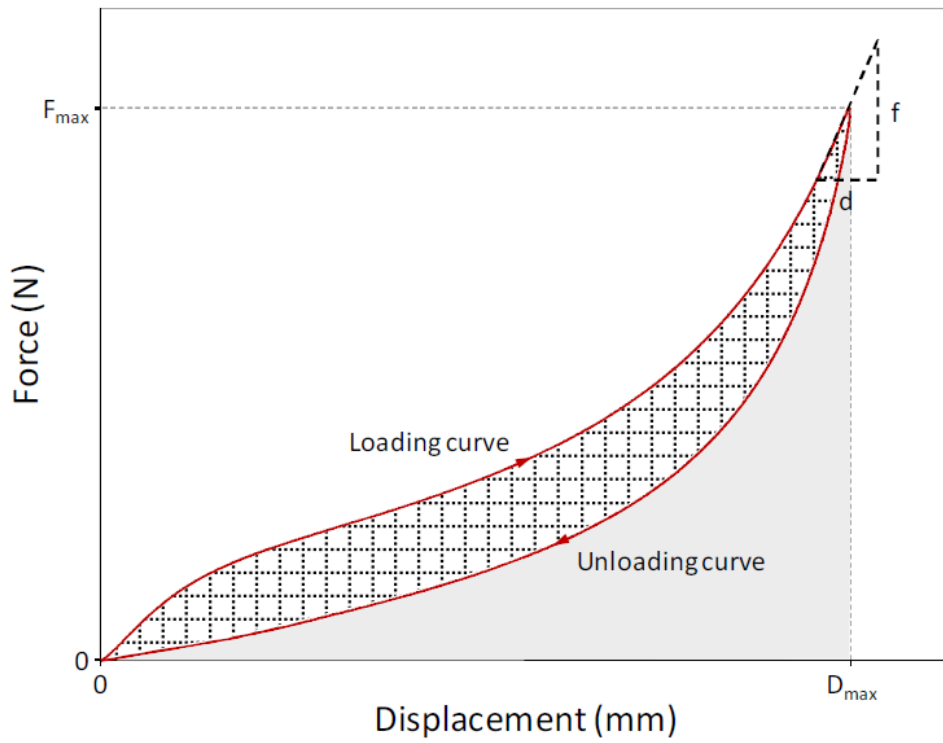


Figure 2.14: Example force-deflection data for compression of a viscoelastic material (Davidson, 2012)

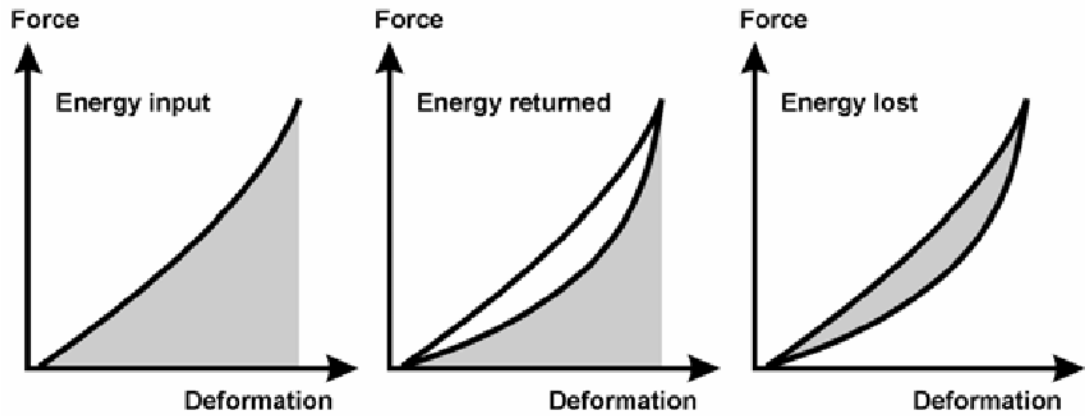


Figure 2.15: Energy input, returned and lost in a sport surface. In each case the shaded region depicts the magnitude of the energy (Stefanyshyn and Nigg, 2003)

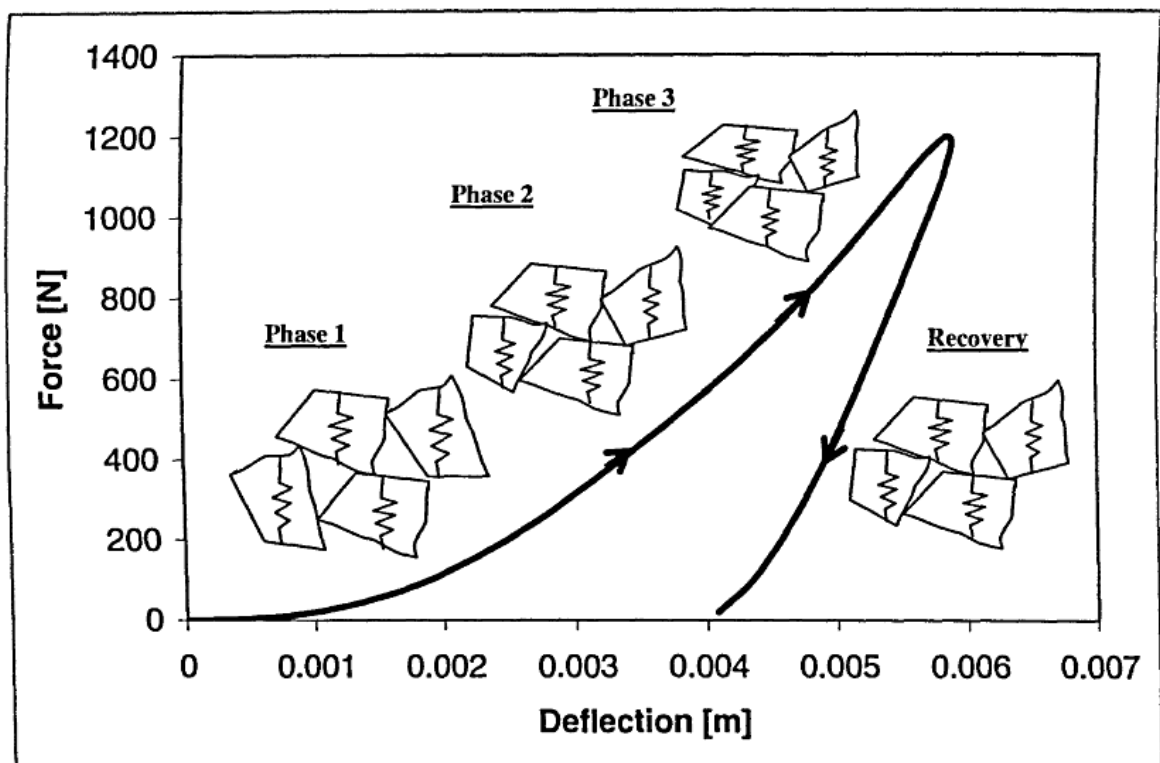


Figure 2.16: Three phases of shockpad behaviour under a compressive impact (Anderson, 2007)

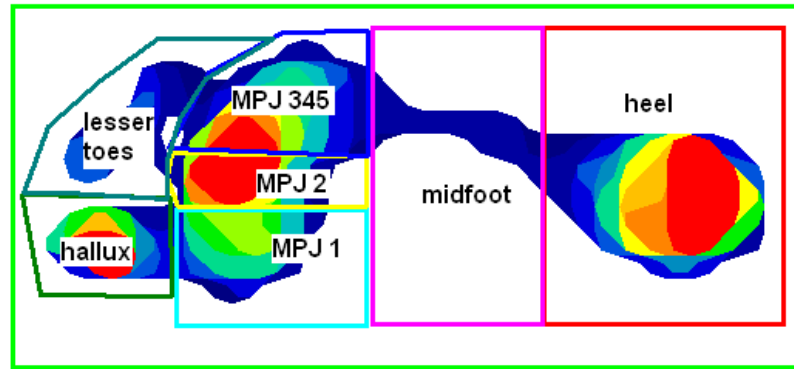


Figure 2.17: Example plantar pressure map of a walking trial recorded by the Tekscan Matscan system (Zammit et al., 2010)



Figure 2.18: Tekscan Matscan system was mounted on top of a force plate (Carvalho et al., 2005)

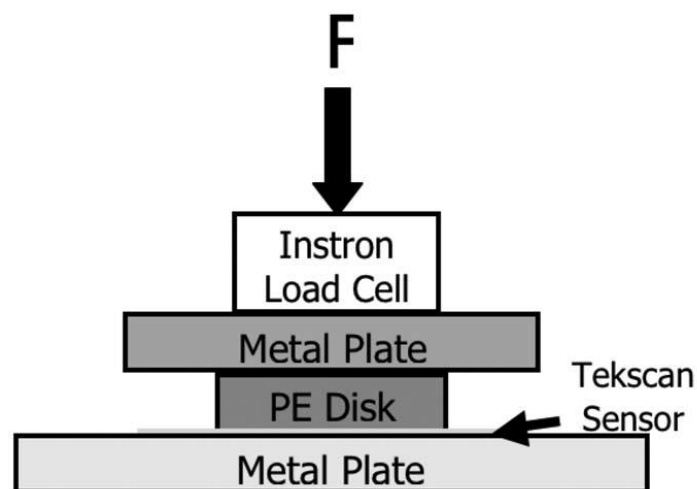


Figure 2.19: Experimental setup used to apply pressure to Tekscan sensor using an Instron machine (Brimacombe et al., 2009)

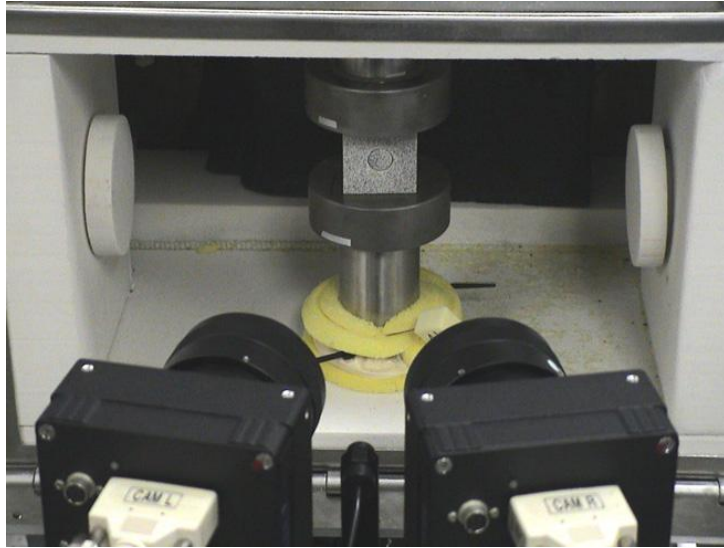


Figure 2.20: Experimental setup of 3D-DIC system for the foam compression test (Jin et al., 2007)

3. Mechanical behaviour of artificial surface systems under controlled loading

3.1 Chapter overview

Chapter 2 identifies the current construction and design of artificial turf surface systems and mechanical test methods for quantifying sports surface properties and categorising products according to sports governing bodies' standards. However, in order to more comprehensively understand their mechanical behaviour and functional performance, artificial turf systems need to be tested under conditions representative of in-service use, especially with the approach to better simulate player interaction. This chapter aims to investigate the mechanical behaviour of a range of surface systems and the individual components under dynamic compressive loading, which addresses objective 3 set in Chapter 1 of this thesis.

Drawing and expanding upon the literature reviewed in Chapter 2 concerning the presently available test methods and measurement techniques, the design of the new controlled cyclic loading test methods which simulate the vertical loads and contact durations of three player movements is presented in Section 3.2. A pressure sensing mat was used as a novel way of determining the pressure distribution in surface system and the change of contact area under loading. Following this, data obtained from tests has been interpreted to analyse fundamental mechanical properties including nonlinear stiffness and stress-strain relationship of the selected surface samples under different loading methods. The final part of this chapter discusses the variables that affect surface system mechanical behaviour and the applicability of the current industry impact related measurement techniques in the standards used.

The implementation of simulated player interaction testing using a dynamic material testing apparatus in this chapter provided useful information for developing the experiment method with real player loading in Chapter 4. Results in this chapter are then compared with data from the player testing in Chapter 4, in the discussion in Chapter 5.

3.2 Experimental methodology

3.2.1 Surface samples

The review of literature shows that the player-surface interactions are mainly influenced by the shockpad and carpet layers of an artificial turf surface system (Young, 2006). Widely

used products in the market were sourced from different industry manufacturers including prefabricated shockpads, infill materials, 3G soccer turf and hockey turf carpets. General and technical specifications of these products are provided in Table 3.1. All the products used as testing samples meet the requirements of relevant industrial standards. The details of the selected products are specified in the following paragraphs.

Prefabricated shockpads were selected for this research mainly because the advantages of their controlled manufacturing environment produce shockpads with good uniformity and consistency. The prefabricated shockpads were supplied in rolls directly from the factories, such that it was easier to cut them into desired size and install in the laboratory, than the cast in-situ shockpads. Two different types of shockpad were selected to compare their own mechanical behaviour and their contribution in the carpet-shockpad systems.

Regupol[®] 6010 SP with a thickness of 15 mm is a premanufactured mat made from selected rubber shreds bonded with polyurethane and termed ‘rubber shockpad’ throughout the remainder of this thesis. Re-bounce[®] uni F82.16 shockpad with a thickness of 12 mm consists of polyurethane flexible open-cell foam and is termed ‘foam shockpad’ throughout the remainder of this thesis. Besides the differences of material and structure, bulk density in construction is different for the rubber and foam shockpad. The density of rubber shockpad is 550 kg/m³, more than twice of the foam shockpad, according to the manufacturers’ technical sheets.

Round silica sand size range from 0.2mm to 0.7mm was sourced from Garside 2EW and used as stabilising infill in the 3G carpet surface. SBR rubber infill was identified as the most commonly used performance infill in the UK among the choices of SBR, EPDM and TPE. Therefore, a batch of SBR rubber granules size grading 1 -3 mm was selected for the test programmes.

A great variety of turf carpets are available in the market nowadays, as discussed in Section 2.3.3. Two distinct carpet products designed for hockey and soccer respectively were selected to investigate their mechanical behaviour under loading. Test programmes first started with the short pile (12 mm), non-infill water based hockey carpet (termed as ‘hockey turf’ in this thesis) because its mechanical behaviour was more consistent and easier to analyse without the infills variables (Young, 2006). This is a necessary preparation before testing more complex infilled 3G carpet to improve test design and methods. Dry Hockey turf samples without watering were tested because the level of

mechanical impact energy applied in this test programme was only influenced by the dissipation of energy caused by the water to a small extent, hence the mechanical behaviour of the dry sample tested was considered to be representative of the behaviour of the saturated surface in match condition (Young, 2006). Monofilament long pile (50 mm) 3G soccer carpet (termed as ‘3G turf’) filled with sand and rubber was also tested. The 3G turf samples were prepared in laboratory with selected sand and SBR infills. The amounts of infill materials used to fill the carpet were taken from the specification of a recent associated PhD study on biomechanical loading, 10 kg/m² of each sand and rubber (El Kati, 2012). The measurements of sand infill depth and total infills depth were carried out three times at each location for the centre and four corners of each 3G turf sample to check the uniformity and repeatability of the carpet filling. The carpet samples were not conditioned and infills kept in loose condition before testing.

3.2.2 Mechanical loading methods

The following section describes the experimental methods designed to measure the mechanical behaviour of individual surface layers and shockpad-carpet systems. Mechanical loading procedures were designed to simulate different player movements in terms of vertical load magnitude and contact duration, and measure the behaviour of each component layer and combined surface system.

3.2.2.1 Instron machine

Mechanical loading applied by a material testing machine is widely used to study material behaviour because of its controllability and repeatability (Ronkainen et al., 2010). A cyclic compressive loading test programme was developed to measure the mechanical behaviour of the individual layers and combined surface systems. An advanced Instron dynamic compression machine (ElectroPulsTM E3000, Norwood, MA, USA, shown in Figure 3.1) was utilised to load the samples at different frequencies. Key machine specifications are listed in Table 3.2. The machine was controlled to provide vertical compressive cyclic loading (using the Console v8.1 and WaveMatrixTM v1.2 software) onto the surface through a sine wave. Key machine specifications are presented in subsection 3.2.3.1.

Design of loading inputs

The review of literature in Section 2.5.1 showed that for each movement pattern, different mass of the player, velocity of the movement and habit of foot strike produced different load magnitude, contact duration and time to peak force. Adrian and Xu (1990) and

Korhonen et al. (2010) provided comprehensive magnitudes for vertical and horizontal force and contact duration for various player movement patterns. For this mechanical loading test programme, the vertical peak force and contact duration results of walking and running from Adrian and Xu (1990) and sprinting of young (23 ± 4 yr) subjects from Korhonen et al. (2010) were used to develop the test methods for the simulated loading cycles. The results presented in both research papers were in units of body weight. Because of the test apparatus set in load control mode, the biomechanical data was required to be converted into unit of force. The literature review showed male athletes/soccer players having an average mass of around 80 kg (Adrian and Xu, 1990; Korhonen et al., 2010; Andersson et al., 2008). Therefore, a body weight of 80 kg was used to represent a typical male player. The parameters determined for the simulated loading methods to control the test apparatus listed in Table 3.3. The impact frequency of the sine wave for each loading cycle was determined by the contact duration of a player foot strike (Anderson, 2007). Contact duration varies from 0.1 to 1.1 seconds depending on the movement patterns. Thus, the frequencies of walking, running and sprinting simulated loading cycles were set at 0.9 Hz, 3.3 Hz and 10 Hz respectively.

The load transducer has an absolute capacity of ± 5 kN, but the dynamic test capacity is ± 3 kN (see Table 3.2). The presented player vertical force ranged from 1000 to over 2600 N for different movement patterns. Preliminary tests indicated that the desired peak force of 2626 N for sprinting case could not be implemented on the test apparatus, because it became progressively unstable and target loading profile parameters could not be repeatedly achieved at the high frequency within acceptable tolerances. In order to avoid damage to the actuator and vibration of the load frame when applying accelerated loading frequency test, the peak vertical force was set at 1900 N for all the three loading conditions ensuring validity in comparison (see Table 3.3). The sine wave patterns of cyclic loading produced by the machine are shown in Figure 3.2.

Two sizes of circular loading feet, 50 mm and 125 mm diameters were used to simulate a shod adult's heel and forefoot respectively (Dura et al., 2002). Preliminary tests showed that a steady state for the cyclic loading (to achieve the set peak force) was quickly reached within 10 initial cycles for the 0.9 Hz and 3.3 Hz loadings, hence 20 and 40 total loading cycles were applied in the 0.9 Hz and 3.3 Hz loadings respectively. For the 10 Hz loading, circa 20 initial cycles were needed to reach the steady state; therefore, 60 cycles were applied for each trial. The test apparatus could not operate at zero load and therefore a pre-

load was required to ensure continuous contact between the actuator and specimen during unloading. The pre-load also ensured no movement of the specimen occurred during testing, avoiding the need for additional fixture method (Davidson, 2012). The higher the loading frequency, the larger the pre-load needed for the machine to control the actuator. Insufficient pre-load value resulted in overshoot of the pre-set target load value to a momentary no-load state, which caused an emergency stop of the test apparatus. The finalised pre-load applied for each test method was shown in Table 3.3.

3.2.2.2 Advanced Artificial Athlete

This AAA impact test was employed as a recognised industry standard test to correlate with the cyclic compressive loading test. This mechanical drop test, similar to its previous version AAB reportedly reproduces the general pattern of force time history of a player heel impact during running (Dixon et al., 1999). It is appointed by the FIFA quality concept (2012) to measure the force reduction and vertical deformation of an artificial turf system. The force reduction is reported in percentage as the peak impact force recorded by an accelerometer on the sports surface compared with the reference peak force at 6760 N on a rigid concrete surface using Equation 2.2 (refer to Section 2.4.2).

The AAA raw measurements from the acceleration sensor are filtered to remove noise using a 2nd order low-pass Butterworth filter with a cut-off frequency of 600 Hz (FIFA, 2012). The size of the test foot is 70 mm in diameter, larger than the heel size test foot used in dynamic cyclic loading tests. Three repeat AAA drops on the same location are the practice indicated in the FIFA standard (2012), peak impact force, vertical deformation and force reduction were recorded the Gforce software. The average of results from the 2nd and 3rd drops was reported and compared to the results using the cyclic loading test methods presented in Section 3.2.2.1. The measurement set-up is described in Section 3.2.3.4.

3.2.3 Equipment & measurement set-up

3.2.3.1 Instron machine

The Instron ElectroPuls (E3000) machine was instrumented with the load cell mounted to the base and the supporting platen was fixed on top of the load cell. The platen was made from steel, had a size of 400 mm * 600 mm and weighed approximately 4 kg (see Figure 3.1). After the testing sample was placed on the platen, the load cell was balanced to zero and the amount of pre-load listed in Table 3.3 was applied to the sample once the test was started. Force and displacement data output by the test apparatus was recorded at the

sampling rate of 1000 Hz by a computer to provide sufficient number of data points during the impacts. The vertical displacement was measured by both an LVDT (position channel) and an incremental optical encoder device (digital position channel) installed in the test apparatus. The two sets of data were comparable with small difference of less than 0.1 mm. It is suggested by Instron and previous research, the digital position measurement provides more accurate displacement data, and therefore was used for surface vertical deflection and strain calculations (Davidson, 2012).

The load cell was checked and calibrated by the manufacturer with a calibration certificate provided. A known weight was used to check the load cell before placing the testing sample on the supporting platen.

3.2.3.2 Pressure mat

General

Pressure mat is commonly utilised in industrial, clinical and biomechanical research environments for measuring pressure distribution and contact area under static loading. In comparison to FP measurement systems, the pressure sensing systems have the advantages of thin, light weight, deformable and pressure distribution mapping indication.

The review of literature concerning pressure measurement techniques in Section 2.6.2 indicates three key factors in the choice of pressure mat for sports surface systems behaviour measurement are sampling rate, measuring range and size. High sampling rate is important for evaluating dynamic loading events and enables the output recorded with sufficient data points without missing key information such as peak or trough value. Adequate measurement range should be provided by the pressure sensor to accommodate the range of pressure applied by different player movement patterns. Chuckpaiwong et al. (2008) studied the total foot peak pressure during walking and running at certain speeds with adults with average weight around 81.5 kg. The total foot peak pressures of walking and running were 264.30 ± 49.0 kPa and 369.60 ± 6.8 kPa respectively. In the study of Queen et al. (2007), the pressure analysis was performed while the players doing side-cut, crossover-cut and acceleration tasks. The side-cut task resulted in the largest entire foot peak pressure of 690.06 ± 137.31 kPa. The peak pressure mean values of the crossover-cut and acceleration movements were similar, around 530 kPa. So ideally, the pressure mat for player loading measurement should cover the range from 200 kPa to 700 kPa. Tekscan pressure mat and insole used in previous studies could measure pressure up to 862 kPa.

Concerning the size of pressure sensor, the dimension of sensing area is necessary to be large enough for practising player movements without altering his/her gait when approaching the measurement system. The pressure sensor has to be thin and flexible to minimise the reinforcing effect when it is installed between two surface layers and limit the influence of sensor intrusion to the free-field strain response of the surface system.

A mat transducer (Tekscan Inc.) was selected to measure real-time pressure distribution under surface system and within its layers. The Tekscan Matscan 3150E transducer has a measuring range up to 862 kPa, a maximum sampling rate (scan speed) of 440 Hz, is 0.18 mm in thickness (with the protective cover removed, in Figure 3.3) and a spatial resolution of 1.4 sensing cells per cm². A total of 2288 sensing cells (52 * 44 cells) read alternately across the mat of 44 cm by 37 cm.

Equilibration is a preliminary procedure suggested by Tekscan to practise before calibrating the pressure sensor. It is used to normalise the digital output of all the sensing cells and compensate the sensitivity differences among them introduced from manufacturing. The equipment needed to perform this procedure is required to apply accurate and even pressure over the entire sensing area to different magnitudes. The air bladder system in the laboratory built for equilibrating pressure insoles could not be used in this study due to its limited size unable to cover the entire sensing area of the pressure mat. Water bladder equilibrators were considered, but even for the lowest equilibration point 138 kPa, 2.3 m³ of water was required to cover the sensing area of 1607.6 cm². It was impractical to build such a water bladder in the laboratory. Previous work on analysing the behaviour of Tekscan sensors under dynamic loading has demonstrated the difference between the raw outputs with and without equilibration was 1.5% ± 0.25 (Morvan, 2012). Therefore, in this application, the variations in the measurements due to lack of equilibration were considered to be insignificant.

Calibration procedure

The Matscan pressure mat uses resistive technology which means each sensing cell is a force sensitive variable resistor. It is designed to measure static/low dynamic human activities for clinical purpose. A reliable calibration procedure is an important preliminary step before testing in order to maximise the accuracy and repeatability of the absolute transient mechanical and player pressure measurement. The working principle of calibration is that a known force is applied to the sensor and changes the impedance of the

loaded sensing cells. Depending on the impedance value of each sensing cell, the analogue to digital converter assigns a digital (Raw) value between 0 to 255 (8 bit) (Tekscan, 2003). By using the calibration methods provided with the software (F-Scan mobile research v6.30), correlations between the digital output from the sensing cells to engineering units (pressure or force) are established. Since errors in calibration cause errors of the reported experimental results, calibration method should be selected according to the application parameters of the experiment and practiced correctly.

There are two basic concepts of pressure mat calibration, single load (linear) calibration and two-load (non-linear) calibration. Single load calibration assumes the digital output is zero with zero force applied on the pressure mat. A single calibration point can be defined when a known force is applied. Then a straight line is plotted from the zero point through the calibration point and ended at an extrapolated saturation pressure according to a digital output of 255. The equation used for single load calibration is shown as Equation 3.1 (Tekscan, 2003).

$$Y = AX \quad (3.1)$$

Where:

Y = Force or pressure

A = Calibration factor

X = Digital output

Single load calibration is a simple way to quickly prepare the pressure mat before testing and provides accurate results if the experimental load is close to the calibration load. Errors grow when the experimental load deviates from the calibration load.

Two-load calibration requires two calibration points created by two known loads applied on the pressure mat. For the same contact area, the larger load should be 2 to 3 times the magnitude of the smaller load, and the experimental load applied needs to be within this range. A power law, as given in Equation 3.2, is utilised to draw the calibration curve (Tekscan, 2003).

$$Y = AX^b \quad (3.2)$$

Y = Force or pressure

A = Calibration factor

X = Digital output

b = Exponent

The exponent b determines the non-linearity of the power law curve. Tekscan (2003) suggests a valid calibration should have the value of b between 0.6 and 2. Because the power law curve is the typical form of relationship of sensor digital output and applied pressure, so comparing to the single load calibration, two-load calibration provides greater accuracy, especially when the experimental load varies over a large range from the calibration load (Brimacombe et al., 2009). In the Tekscan software interface, as shown in Figure 3.4, there are four calibration methods available for selection namely Walk, Step, Point and Frame. Both Walk and Step are single load calibration methods. Point and Frame methods allow two-load calibration. A calibration curve, either linear or a power, is displayed at this interface according to the selected calibration method.

In the calibration process, it is also very important to mimic the application parameters used in experiments. Not only do the range of pressures applied in the calibration need to be close to the actual pressures in the experiment, the contact duration, material interface, interface profile and temperature should all be similar to those of the proposed application. As the pressure mat is designed for static or low dynamic measurement, the Step and Point calibration methods of the software only work in a static way which needs a stable load applied for 5 to 10 seconds. In accordance with previous research (Pain et al., 2008; Halkon et al., 2012), preliminary testing identified that using statically calibrated sensor to measure dynamic loads, e.g. mechanical simulated or actual player movements, underestimated the dynamic peak force by circa 30%, possibly due to its low sampling rate and multiplexing. Although Walk calibration method can be used in a dynamic walking scenario, it is a single load calibration based on the body weight and automatically estimated by computer. Hence Tekscan (2003) indicates Walk calibration is not an accurate calibration method to obtain absolute pressure values and used mainly in clinical purpose in consideration of efficiency.

For this experimental programme, two calibration procedures were practised. Prior to the measurements, the pressure mat was calibrated by the Step calibration method under different sample interfaces (hockey turf, 3G turf, foam and rubber shockpad) respectively

at laboratory temperature (21 ± 3 °C). The Instron test apparatus was instructed to apply a constant load of 1900 N with the 125 mm loading foot for 10 seconds before unloading the sample and pressure mat (as shown in Figure 3.5). In order to correct the under-evaluation of dynamic force, a dynamic calibration factor was derived from dividing the Instron load cell peak force value by the pressure mat 'Step' calibrated maximum force. The pressure mat force values obtained during loading period in testing were processed by multiplying the dynamic calibration factor, thereby improving the pressure mat force reading to be more representative of the actual force experienced (Halkon et al., 2012). By applying the dynamic calibration factor, the mean error was reduced to less than 5%. However, the problems with this calibration procedure were repeat trials were needed to get an averaged singular dynamic calibration factor and an individual dynamic calibration factor required for mechanical loading at each frequency (0.9 Hz, 3.3 Hz and 10 Hz) with every sample interface. Hence using this calibration procedure was time consuming and increased the data processing complexity.

A post calibration method, Frame calibration, was also used to calibrate the sensor after the experimental data had already been recorded. Instead of using a static load, the Instron was employed to carry out dynamic loading and impart a calibration force under testing conditions using the same material interface, loading magnitude and frequency. By synchronising the devices, the reference force from the load cell of Instron and raw digital output of pressure mat were interrelated by time (or frame number). To make a Frame calibration file for cyclic loading, two calibration points were created. The first point was identified by selecting a reference force value close to 700 N and assigning this value to the corresponding frame of the pressure mat recording. The second point was created by assigning the peak reference force value of load cell to the frame of the peak digital output of pressure mat. Then a power law calibration curve was drawn through these two points. For impact from the AAA, the pressure mat directly laid on top of FP under each layer sample was also post calibrated. A series of diminishing impacts delivered by the drop of mass was recorded by both devices. The peak force values of the first and third impacts by the FP were assigned to the first and third peak digital outputs (raw values) by the pressure mat. The values of exponent 'b' of Frame calibration curve in Equation 3.2 for all mechanical loading trials were in the range of 0.6 to 1.5, within the valid calibration range suggested by Tekscan (2003).

Murin et al. (2001) suggested that the best calibration procedure was the practice which matched its intended use conditions as close as possible. Therefore, due to the advantages of close to dynamic testing conditions and using two-load calibration concept, even without any correction by conversion factor, the difference between the calibrated force by Frame calibration and the reference force value from the load cell/FP was less than 7%. Thus, Frame calibration was used as the main calibration method of the pressure in this and subsequent chapter.

3.2.3.3 Force plate

The main uses of force plate (FP) under the AAA test were to provide force-time history of the whole impact event, validate peak force measured by the accelerometer of the AAA and calibrate the pressure mat with Frame calibration method using reference force from FP. A Kistler 9821B (600 mm * 400 mm) FP calibrated by the manufacturer was used. The measurement range was controlled by an 8-channel charge amplifier and set at 'Range 3' up to 2.5 kN to provide sufficient force measurement range. A quick calibration was conducted when the testing sample was placed on the FP prior to each trial. The recorded voltage with only surface sample and pressure mat on the FP was used to 'zero' the force reading by the software (i.e. set the recorded voltage corresponded to zero force) to remove the 'weight' of sample (Tsu, 2010). After this, the FP measured only the net force produced by the AAA impacts without the gravity of the objects placed on it.

3.2.3.4 Measurement set-up

Figure 3.6 shows the typical test set up of an artificial turf carpet-shockpad surface system placed onto the supporting platen of the Instron machine. Each mechanical compressive load was firstly performed on individual components, to compare the performance of two different types of shockpads (rubber shockpad and foam shockpad) and measure the mechanical behaviour of the two different carpets (hockey turf and 3G turf). Then the tests were repeated for the composite carpet- shockpad systems to examine the performance of the whole surface system. Four carpet-shockpad systems were tested, namely hockey turf + rubber shockpad (HT+RS), hockey turf + foam shockpad (HT+FS), 3G + rubber shockpad (3G+RS) and 3G + foam shockpad (3G+FS).

The pressure mat was connected to a laptop with USB 2.0 recording the data with the top sampling rate of 440 Hz. It was triggered to start and stop the recording manually. The pressure mat measured purely vertical forces produced by the loads, but the horizontal

friction forces at the surface sample and pressure mat interface due to surface material deformation and horizontal expansion could not be measured. Contact area was determined and then pressure contour map at each frame was created by the software. The time base of the pressure mat reading was synchronised to the data of load cell and the FP respectively.

To determine the pressure distribution through the individual surface layers and the artificial turf systems, the pressure mat was first placed under each sample layer, then under the combined carpet-shockpad systems. For measuring the pressure distribution at the interface between carpet layer and shockpad, the pressure mat was inserted between the two layers. Figure 3.7 and 3.8 show the installations under the cyclic compressive loading and the AAA test respectively.

Three locations on each individual layer and surface system were tested using the methods presented in subsection 3.2.2. The average and standard deviation are calculated for each parameter and presented in Section 3.3.

3.3 Results

3.3.1 Cyclic loading on individual layers

3.3.1.1 Cyclic loading at 0.9 Hz

Compressive behaviour of each individual layer was measured under cyclic loading from the test apparatus with the 50 mm diameter loading foot. Vertical deflection was calculated by Equation 3.3 using the digital position data.

$$D_v = D - D_{pre} \quad (3.3)$$

Where:

D_v = Vertical deflection (mm)

D = Displacement of the actuator (mm)

D_{pre} = Start position of the actuator when loading foot in contact with specimen (mm)

Force-deflection behaviour of hockey turf shows a strong trend of non-linear stiffness during loading and unloading, as shown in Figure 3.9. A total of 20 loading cycles were practised with the results of every 5 cycles plotted. At the maximum vertical force 1900 N, the vertical deflection measured 10-11 mm for all the cycles. At round 500 N, the curves

steepen significantly indicating the rapid increase of the stiffness response of specimen to increased load. It is observed that the deflection of the first cycle was around 0.5 mm smaller than the last cycle. This may be explained by the fibres of hockey turf flattening with increasing load cycles, resulting in an accumulation of permanent deformation of the specimen. This is further discussed in the following Section 3.4.1.

Force-deflection behaviour of 3G turf under 0.9 Hz cyclic loading is illustrated in Figure 3.10. The 3G turf reached large deflection at low force level and stiffened rapidly when the force was over 500 N. At the maximum force 1900 N, the average vertical deflection of the first cycle was 14.9 mm in comparison to the last cycle at 17 mm. A greater change in deflection measured in 3G turf than hockey turf due to a more marked compaction and some rubber infills around the edge of loading foot compressed beyond the loading area.

A comparison of force-deflection behaviour of rubber shockpad at the selected loading cycles is shown in Figure 3.11. The gradient of the first loading curve demonstrates the rubber shockpad could possibly accommodate further deformation without stiffening rapidly. The vertical deflections at peak measured at the first and last cycles were similar with a difference of only 0.3 mm. It suggests the rubber shockpad almost fully recovers instantaneously after each cycle at this loading frequency.

Force-deflection behaviour of foam shockpad under 0.9 Hz cyclic loading is illustrated in Figure 3.12, showing more nonlinearity than Figure 3.11. The average peak deflection of the first cycle was 7.5 mm in comparison to the last cycle at 7.7 mm. The applied force increased rapidly with minimal further deflection above a load of 1000 N. The permanent deformation of foam shockpad was small, around 0.2 mm, after 20 loading cycles.

3.3.1.2 Cyclic loading at 3.3 Hz

Under 3.3 Hz cyclic loading, the force-deflection behaviour of hockey turf is shown in Figure 3.13. A total of 40 cycles applied, the graph shows the curves of every 10 cycles. The sample was unloaded to pre-load, 40 N after each cycle. At 1900 N, the average vertical deflection measured 10.8-11.2 mm for all the loading cycles. However, the hockey turf behaved stiffer than under 0.9 Hz loading, especially at low force level (< 500 N). The amount of accumulated permanent deformation of hockey turf after 40 loading cycles was 0.6 mm.

Force-deflection behaviour of 3G turf is shown in Figure 3.14. The vertical deflection measured at peak force was smaller than under walking simulation (14.5 mm in comparison to 17 mm at the 20th cycle). The 3G turf demonstrated a higher stiffness response in the range of 100 N to 500 N compared to the behaviour under 0.9 Hz loading. The amount of accumulated permanent deformation of 3G turf after 40 loading cycles was 2.5 mm.

The force-deflection behaviour of rubber shockpad (Figure 3.15) was similar to the behaviour under walking simulation. The peak deflection at the 20th cycle was 6.2 mm which was slightly smaller than the deflection reached under 0.9 Hz loading. The shockpad showed a linear behaviour when applied force was less than 750 N and became non-linear at higher force level. The residual deformation of rubber shockpad was insignificant under this set of cyclic loading.

Force-deflection behaviour of foam shockpad is presented in Figure 3.16. The average peak deflection was 7.8 mm at 1900 N with small residual deformation over the test period. This shockpad showed a higher stiffness response at low force level (< 500 N) than under 0.9 Hz loading. At higher force level, the foam shockpad stiffened rapidly to increased load showing a much higher stiffness compared to the rubber shockpad.

3.3.1.3 Cyclic loading at 10 Hz

Force-deflection behaviour of hockey turf under 10 Hz cyclic loading is shown in Figure 3.17. A selection of cycles was plotted from a total of 60 cycles. As mentioned in Section 3.2.2.1, due to the accelerated loading frequency, approximately 20 initial cycles were required for the test apparatus to ‘ramp up’ reaching the set loading profile. Hence the peak force values of the first and 10th cycle shown in Figure 3.17 are lower than 1900 N. After the 30th cycle, the target peak force value was achieved. The deflection at 1900 N was 10.8 mm in the 30th cycle, less than under 3.3 Hz loading. It is observed that the loading curves are almost linear in this range of force and the amount of accumulated permanent deformation is around 0.7 mm.

Force-deflection behaviour of 3G turf under 10 Hz loading is shown in Figure 3.18. At 1900 N, the vertical deflection varied between 12 and 12.9 mm from the 1st to the 30th cycle, smaller than under 3.3 Hz loading. The 3G turf shows a stronger non-linear behaviour and lower stiffness than hockey turf in the range of applied force. Around 1.1 mm of accumulated deformation is calculated after 60 cycles.

Force-deflection behaviour of rubber shockpad is presented in Figure 3.19. The impact force increased from 500 N to 1900 N with a deflection of 1.9 mm, showing the shockpad stiffened significantly under accelerated frequency loading. The amount of accumulated permanent deformation is around 0.5 mm, slightly larger than under 0.9 and 3.3 Hz loadings.

Force-deflection behaviour of foam shockpad is shown in Figure 3.20. The vertical deflection measured at 1900 N was similar to under 0.9 and 3.3 Hz loadings. Foam shockpad behaved slightly stiffer than rubber shockpad in the range of applied force. Minimal accumulated deformation of 0.2 mm is calculated.

Overall, carpet layers measured larger accumulation of permanent deformation than shockpads under cyclic loading. The 3G turf had largest accumulated deformation for all loading frequencies. This effect of cyclic loading is described in further detail in Section 3.4.1. The graphs also show changes in stiffness of individual layers at given levels of force when the frequency of loading is varied. The effect of loading frequency on surface force-deflection behaviour is discussed in Section 3.4.2.

3.3.2 Surface system mechanical behaviour

This section examines the overall responses of combined carpet and shockpad surface systems (HT+RS, HT+FS, 3G+RS and 3G+FS) under controlled mechanical loading. All surface systems were subjected to cyclic loadings at different frequencies with the Instron in the laboratory temperature range of 22.5 – 25 °C, and subjected to impacts with the AAA in the laboratory temperature range of 24.5 – 28.5 °C. The resulting mechanical behaviour concerning force-deflection relationship was converted to stress-strain relationship to normalise for the thickness of surface systems. Force was converted into stress using the Equation 3.4. Strain (expressed as a decimal fraction) of the surface system was determined by Equation 3.5, where D_v is the vertical deflection calculated using Equation 3.3 and h is the total thickness of the surface system. For this investigation, the carpet-shockpad system was considered to be a single element to analyse the strain. The total thickness of hockey turf and shockpad systems was determined from the combined thickness of shockpad and height of carpet from the bottom of backing to the top of pile. The total thickness of the 3G turf and shockpad systems was measured from the combined thickness of shockpad and the infill depth in carpet before testing.

$$\sigma = \frac{F}{S} \quad (3.4)$$

Where:

σ = Stress (kPa)

F = Vertical force (N)

S = Contact area (cm²)

$$\varepsilon = \frac{D_v}{h} \quad (3.5)$$

Where:

ε = Strain

D_v = Vertical deflection (mm)

h = Total thickness of surface system (mm)

3.3.2.1 Loading at 0.9 Hz

Force-deflection relationship

Table 3.4 specifies the three test locations averaged values of peak vertical deflection and tangent stiffness at specified load for each surface system at the 2nd loading cycle under 0.9 Hz loading. Data from the 2nd loading cycle was used, because it was the earliest cycle as the target peak force reached and recorded the surface system behaviour without large accumulation of deformation.

A comparison of force-deflection relationship for two sizes of loading feet on HT+RS and HT+FS is shown in Figure 3.21. Load applied with 50 mm loading foot resulted 15.5 mm and 16.8 mm vertical deflection on HT+RS and HT+FS respectively at 1900 N. For both hockey turf systems, there was an initial stage where force was lower than 500 N the stiffness remained low as large deformation caused by minimal increase in force. The initial stiffness of HT+RS and HT+FS was 75 N/mm and 61 N/mm respectively. Both hockey turf systems behaved stiffer at higher force level when force was over 1300 N. The stiffness in the final loading stage increased to 338 N/mm and 367 N/mm for HT+RS and

HT+FS respectively. It is noticed that the stiffness of HT+RS is higher than HT+FS at lower force, however HT+FS is stiffer than HT+RS in the late loading stage. This suggests that hockey turf combined with rubber shockpad could accommodate larger deflection and stiffened slower than using foam shockpad at higher force level.

Compared with the strong nonlinear force-deflection relationship of hockey turf systems under the 50 mm loading foot, the hockey turf systems showed almost linear behaviour under the loading foot of 125 mm diameter. At peak vertical force of 1900 N, HT+RS reached a deflection of 7.5 mm, smaller than 8.8 mm for HT+FS. In the initial loading stage as force lower than 400 N, there is a fast change of stiffness along with the increase of force for both hockey turf systems. In the range of 400 N to 1900 N, the hockey turf systems became stiffer but with minimal change in stiffness. The final stiffness of HT+RS was 348 N/mm in comparison to 292 N/mm for HT+FS. During the whole loading event, HT+RS exhibited stiffer than HT+FS and the difference in stiffness increased along with the increase of force.

A comparison of force-deflection relationship of 0.9 Hz loading with two sizes of loading feet on 3G+RS and 3G+FS is shown in Figure 3.22. Load applied with the 50 mm loading foot at lower force level (< 400 N), the stiffness of 3G+RS was 81 N/mm compared with 62 N/mm for 3G+FS. At 1900 N, the vertical deflection of 3G+RS was 19.2 mm, the same value for 3G+FS. The stiffness in the final loading stage increased to 338 N/mm for 3G+RS and 3G+FS.

Both 3G turf systems showed the same force-deflection relationship in the initial stage of loading (< 400 N) under larger foot. Then 3G+FS deformed greater than 3G+RS in the rest of the loading event. The deflections where peak force occurred were 10.4 mm and 11.4 mm for 3G+RS and 3G+FS respectively. At the force range over 1000 N, the stiffness of 3G+RS was 461 N/mm compared with 365 N/mm for 3G+FS. Under larger loading area, 3G+RS showed higher stiffness than 3G+FS when the applied force was over 400 N. It is most likely explained that similar force-deflection relationship of the two 3G turf systems exhibit at lower force is mainly influenced by the same infilled 3G carpet layer used, thereafter, the different characteristics of two shockpads contribute to the varied stiffness reached as the increase of applied force.

Although force applied on a surface system was the same, the deflections of the surface system were notably different due to the different sizes of loading area. The deflection at

peak force of HT+RS under 50 mm loading foot was 8 mm larger than under 125 mm loading foot. The same amount of deflection increase was also found for HT+FS. The deflection at peak force applied with 50 mm loading foot was increased by 84% in 3G+RS and 68% in 3G+FS respectively. It is observed from Figure 3.21 and 3.22 that loading curves of surface systems were steeper under 125 mm foot in the force range lower than 1000 N. Surface systems were especially stiffer in the initial loading stage under 125 mm foot. The initial stiffness of HT+RS and HT+FS under 125 mm diameter foot were 293 N/mm and 240 N/mm respectively, which were approximately 3.9 times higher than the stiffness measured under 50 mm foot. Both 3G turf systems at round 400 N measured stiffness of 132 N/mm under 125 mm loading foot and a reduction in stiffness by 39% and 53% under 50 mm loading foot for 3G+RS and 3G+FS respectively.

Stress-strain relationship

Stress-strain relationship for the 0.9 Hz loading 2nd cycle on HT+RS and HT+FS is presented in Figure 3.23. Under the peak force of 1900 N, maximum applied stress of 968 kPa and 155 kPa were generated under 50 and 125 mm loading feet respectively. At 155 kPa, the strain of HT+RS was 0.23 under both loading feet. There was a small difference in the strain of HT+FS at 0.27 and 0.29 for under small and large loading foot respectively. Strain of hockey turf systems measured at the range of 0-155 kPa under the two loading feet has no discernible difference, as shown in Figure 3.23, indicating the contact area has no significant effect on the stress-strain relationship at this loading cycle. At 968 kPa, the strain of HT+RS and HT+FS was 0.47 and 0.56 respectively.

Figure 3.24 shows the stress-strain relationship for the 0.9 Hz loading 2nd cycle on 3G+RS and 3G+FS. At the range of 0-155 kPa, larger strain measured under 50 mm loading foot for 3G+FS whilst similar strain for 3G+RS under both loading feet. 3G+FS shows an increase in strain at 155 kPa by approximately 15% under 50 mm loading foot. At the peak stress of 968 kPa, the strain of 3G+FS was 0.47 compared to 0.35 for 3G+RS.

Under 0.9 Hz loading, the change of loading area has greater influence on the strain of 3G+FS than other surface systems. This may be explained by the stronger penetration in the infills of 3G turf systems and lower stiffness of 3G+FS at low stress level under 50 mm loading foot. For all surface systems tested, the largest strain was measured in HT+FS and 3G+RS had the smallest strain.

3.3.2.2 Loading at 3.3 Hz

Force-deflection relationship

Table 3.5 lists the values of peak vertical deflection and stiffness for each surface system at the 3.3 Hz loading 10th cycle. Data from the 10th loading cycle was used to compare the mechanical behaviour of surface systems given the target value of peak vertical force (1900N \pm 1%) was achieved after the initial 9 cycles.

A comparison of force-deflection relationship of HT+RS and HT+FS with two sizes of loading feet is shown in Figure 3.25. Load applied with the 50 mm diameter loading foot resulted 16.2 mm and 18 mm vertical deflection on HT+RS and HT+FS respectively at peak force. In the initial stage of loading when the vertical force was lower than 400 N, the stiffness of HT+RS was 124 N/mm, this was reduced to 108 N/mm for HT+FS. For both hockey turf systems, stiffness increased at constant gradient in line with the applied force and reached 413 N/mm and 516 N/mm in the final stage of loading (> 1200 N) for HT+RS and HT+FS respectively. The change between initial and final stage stiffness is more considerable for HT+FS by approximately 378% than 233% for HT+RS.

For both hockey turf systems, the surface deflection measured under the 125 mm loading foot was significantly smaller than under 50 mm loading foot. At peak vertical load, the vertical deflection of HT+RS was 8.7 mm compared to 10.3 mm for HT+FS. The force-deflection relationship displays a less marked nonlinear response during loading than under 50 mm foot, especially shows an apparent linear response in the range of 200 N to 800 N. In the range of 1200 N to peak, the final stage stiffness of HT+RS was 399 N/mm compared with 335 N/mm for HT+FS. The stiffness of HT+RS is higher than HT+FS during the whole loading event.

A comparison of force-deflection relationship of 3.3 Hz loading with two sizes of loading feet on 3G+RS and 3G+FS is shown in Figure 3.26. With the 50 mm loading foot, the exerted peak force resulted 16.9 mm and 17.8 mm vertical deflections on 3G+RS and 3G+FS respectively. Both 3G turf systems exhibit lower stiffness around 98 N/mm at low force level and display a continual increase of stiffness. In the final stage of loading when the vertical force was over 1200 N, the stiffness of 3G+RS was 436 N/mm, this was increased to 540 N/mm for 3G+FS.

The deflection of 3G+RS at peak vertical load under the 125 mm loading foot was 11.4 mm compared with 3G+FS deforming 13.8 mm. The difference between peak deflections of two 3G turf systems is 2.4 mm, markedly larger than 0.9 mm difference measured under small loading foot. For both 3G turf systems, the force-deflection relationship displays nonlinear behaviour from the outset to 800 N; however, a less noted change in stiffness occurs as load increases. In the late loading stage (> 900 N), the stiffness values were 472 N/mm and 380 N/mm for the 3G+RS and 3G+FS respectively.

Stress-strain relationship

Stress-strain relationship for the 3.3 Hz loading 10th cycle on HT+RS and HT+FS is presented in Figure 3.27. At the same stress range of 0-155 kPa, a change in mechanical response during loading is evident for both hockey turf systems under two loading feet showing the effect of contact area. For both systems, a leftward shift of the stress-strain profile occurs as enlarging the contact area, indicating a decrease in strain. At 155 kPa, the strain of HT+RS was 0.26 under 125 mm loading foot and 0.31 under 50 mm loading foot. The strain of HT+FS at this stress level was 0.34 under 125 mm loading foot compared to 0.4 under 50 mm loading foot. The difference in strain caused by changing contact area for both hockey turf systems is around 0.05. Higher stress reached with the same amount of load (1900 N) applied on the smaller foot, the strain of HT+RS at peak stress was 0.49, and the strain was 0.6 for HT+FS.

Figure 3.28 displays the stress-strain relationship of 3G+RS and 3G+FS under two sizes of loading feet. At the range of 0-155 kPa, the strain of 3G+RS increased by 10% under 50 mm loading foot compared to 0.22 under 125 mm loading foot, whilst the strain of 3G+FS showed an increase of 7%. At the peak stress of 968 kPa, the strain of 3G+RS was 0.37 compared to 0.43 for 3G+FS. For all surface systems tested, an apparent difference in strain at low stress level (< 155 kPa) is noted due to the load applied over two different contact areas. In comparison with 0.9 Hz loading, contact area has a more prominent effect on the stress-strain response of the surface systems under higher frequency running simulation loading.

3.3.2.3 Loading at 10 Hz

Force-deflection relationship

Table 3.6 specifies the values of peak vertical deflection and stiffness for each surface system at the 10 Hz loading 20th cycle. Data from the 20th cycle was used to compare the mechanical behaviour of surface systems in this section given the target value of peak vertical force (1900N \pm 2%) was achieved after more initial cycles as the loading frequency increased.

A comparison of force-deflection relationship of HT+RS and HT+FS for 10 Hz loading with two sizes of loading feet is shown in Figure 3.29. Under the 50 mm loading foot at peak force, the vertical deflection of HT+RS was 16 mm, 1.5 mm smaller than the deflection of HT+FS. As discussed in Section 3.2.2.1, larger pre-load required to remain on the samples for the machine to control the actuator at higher frequency loading. The stiffness of HT+RS at the range of 300 N to 900 N was 403 N/mm. At the same force range, the stiffness of HT+FS was 503 N/mm. In the final stage of loading (> 1500 N), both hockey turf systems exhibit a linear force-deflection response, with stiffness of 506 N/mm and 633 N/mm for HT+RS and HT+FS respectively.

Under the 125 mm loading foot at peak load, the vertical deflection of HT+RS was 8.8 mm compared to 10 mm for HT+FS. In the range of 200 N to 800 N, the stiffness for HT+RS was 388 N/mm and 330 N/mm for HT+FS. In the late stage of loading (> 1000 N), 486 N/mm and 410 N/mm were measured for HT+RS and HT+FS respectively.

Figure 3.30 displays the force-deflection relationship of 3G+RS and 3G+FS. The peak deflections under 50 mm loading foot were 16.7 mm and 17.3 mm for 3G+RS and 3G+FS respectively. For both 3G turf systems, stiffness increased gradually in the range of 300 N to 1000 N, after which it reached 493 N/mm and 619 N/mm for 3G+RS and 3G+FS respectively in the final loading stage (> 1500 N).

Under the 125 mm loading foot, the peak deflection of 3G+RS was 11 mm, reduced by 34% compared with this parameter under 50 mm loading foot. 3G+FS showed a peak deflection decrease of 30%, to 12.1 mm. In the load range 1000-1900 N, a less marked change in stiffness occurs as load increases. The stiffness of 3G+RS was 523 N/mm, higher than 445 N/mm for 3G+FS.

Stress-strain relationship

Stress-strain relationship for 10 Hz loading at the 20th cycle on HT+RS and HT+FS is presented in Figure 3.31. Because of the pre-load remained on the surface systems after

each cycle, the minimum stress under 50 mm loading foot was around 170 kPa, causing strain in HT+RS and HT+FS for 0.38 and 0.5 respectively. At peak stress, the strain increased by 28% and 16% for HT+RS (0.49) and HT+FS (0.58) respectively. The stress range under 125 mm loading foot was 10 – 155 kPa. Strain of HT+RS developed from 0.15 to 0.27 showing an increase of 80%, whilst the strain of HT+FS changed from 0.18 to 0.33 exhibiting a larger increase of 83%.

Figure 3.32 shows the stress-strain relationship of 3G+RS and 3G+FS under two sizes of loading feet. Under 50 mm loading foot at the minimum stress, the strain of 3G+RS was 0.29 compared to 0.35 for 3G+FS. At peak stress, the strain increased to 0.38 and 0.42 for 3G+RS and 3G+FS respectively. Under 125 mm loading foot, strain measured 0.23 and 0.26 for 3G+RS and 3G+FS respectively at 155 kPa. Although there is no data to compare at the same stress range for different contact areas, a leftward shift trend of the stress-strain profile is also expected as identified in Section 3.3.2.2 from 3.3 Hz loading. In addition, for all the surface systems, the separation between the stress-strain profiles measured with the two loading feet is anticipated to be more considerable due to even higher loading frequency applied.

3.3.2.4AAA impact

Averaged results of peak force, force reduction and vertical deformation (calculated as per Section 2.4.1) of three test locations on each sample measured by the AAA are listed in Table 3.7. Force-time profile of the AAA impact was also recorded by FP to validate the peak force with the result from the accelerometer of the AAA. Comparing the peak force measured by the AAA and the FP reading was within 1.8%.

For individual layers, peak force recorded on rubber shockpad was around 200 N lower than on foam shockpad. A difference of 385 N in peak force was measured between hockey and 3G carpet but with minimal difference in vertical deformation at 0.6 mm. Decreased variations were shown for the parameters of the combined carpet-shockpad systems. For HT+FS, at the lowest peak force of 2101 N, largest vertical deformation at 11.4 mm was recorded. The highest peak force of 2526 N was measured on 3G+RS with the smallest vertical deformation at 10.3 mm. It is anticipated that HT+FS demonstrates the highest shock absorbency showing a force reduction of 66% whilst 3G+RS being the least cushioning surface system exhibits the smallest force reduction of 59.7%.

As the nonlinear response of surface system under dynamic compressive loading at different frequencies presented before this subsection, showing only the peak force and vertical deformation values of an impact is insufficient to understand the change of stiffness during its loading phase and the energy characteristics of surface system. In Section 3.4.3, force and vertical deformation results at peak for surface systems under the AAA impacts are compared with the loading curves measured in Instron tests.

3.3.3 Pressure distribution in surface system

The pressure mat was placed under individual layers and at different interfaces of surface systems under the mechanical cyclic loading and the AAA impacts to measure the pressure distribution through single layers and within the surface systems. Two shockpads, two carpets and four carpet-shockpad combined systems were tested. Contact area and stress at peak were averaged from three locations of each specimen tested for the same selected loading cycle at each loading frequency as presented in Section 3.3.2. Step calibration was practised for the cyclic loading tests and validated with the load cell data comparing the peak loads within 2%. Frame calibration method was used for the AAA tests due to its higher accuracy than ‘step calibration’ at high rate of loading impacts. Both calibration procedures were introduced in Section 3.2.3.2. The time base of pressure mat recordings were synchronised to the Instron load cell and FP respectively.

3.3.3.1 Effectiveness of pressure mat

Although the pressure mat is very thin with a thickness of 0.18 mm, it is made by materials distinct from those used in artificial turf system. Hence using this sensor between two surface layers may have a reinforcement effect and alter the free-field strain response of the surface system, which needs to be evaluated.

Stress-strain relationship of HT+RS with the pressure mat between layers and without under loading at 3.3 Hz is presented in Figure 3.33. HT+RS with the pressure mat inserted between layers showed an overall reduction in strain during loading and unloading compared to the surface system without the pressure mat inserted. For the same loading cycle, HT+RS with pressure mat in between measured the strain at peak 0.02 smaller than without insert. A less marked change in strain occurred at pre-load. For HT+FS at peak stress, the strain without the pressure mat intrusion was also 0.02 larger than it with the pressure mat between layers (as in Figure 3.34). However, the difference in strain at pre-load was slightly greater than HT+RS, around 0.03.

Generally, the intrusion effect of pressure mat placed between layers in terms of surface system strain was insignificant. Strain of the tested surface systems with pressure mat between layers was reduced by less than 5% over the loading period regardless of the number of loading cycle.

Accuracy of results concerning contact area and pressure recorded by the pressure mat is related to the number of activated sensing cells and calibration method used. Results presented following in this section showed better reliability for the pressure mat reading under the 125 mm loading foot due to more sensing cells being activated, especially in the case of pressure mat inserted between layers. For faster loading events (high loading rate and short contact duration) such as 10 Hz cyclic loading and the AAA test, two-load frame calibration method provided more accurate stress values than using single-load step calibration method on account of the advantages introduced in Section 3.2.3.2. Thus, the frame calibration method is practised in the following experiment programme with player loading (Chapter 4).

3.3.3.2 Loading at 0.9 Hz

A summary Table 3.8 lists the average peak contact area and peak stress with standard deviation measured by the pressure mat. Under the 50 mm loading foot, the individual layer samples showed an increase in peak contact area ranging from 115% to 200%, with the largest increase for 3G carpet and the smallest increase for foam shockpad. For all carpet-shockpad surface systems, the peak contact areas measured at the bottom were increased over 4 times the size of the loading foot (20 cm²). 3G+FS showed the largest increase by a factor of 4.65 and HT+RS the least with a factor of 4.2. Surface systems with foam shockpad were observed at least 30% more increase in this parameter than systems with rubber shockpad.

Under the 125 mm loading foot, the scale of peak contact area increase was smaller, less than 90%. For individual layers, rubber shockpad showed the largest increase by 53.7% whilst foam shockpad and hockey turf showed similar increase by 43.1% and 44.7% respectively. Peak contact area recorded under 3G carpet only increased by 20.3% because it was affected by the parallel stitch lines across the carpet backing (see Figure 3.35). The sensing cells under the space between two convex stitch lines were not activated, so the reported contact area is smaller.

The applied load during compression on top of samples over the area of loading foot was distributed over an increasing contact area, reduced the stress through the surface layer. For individual layers loaded with the 50 mm loading foot, the magnitude of stress reduction was similar for both shockpads around 56%. Although a significant reduction in stress was measured with 3G turf, up to 76%, the inactivated sensing cells may cause under-estimation of stress. So the peak stress measured under 3G turf layer was considered to have lower reliability.

For all the surface systems, a marked reduction in stress by over 75% occurred, but the variation in this parameter between the surface systems was minimal. With the greatest enlarged peak contact area recorded at the bottom of 3G+FS, the applied stress was decreased by 77.9%. The peak stress measured at the bottom of HT+RS averaged 237 kPa showing the least reduction in stress of 75.5%.

Under the 125 mm loading foot, the reduction in stress varied between 21.3 – 35.5% for the four individual layers tested. Applied stress 155 kPa decreased to 100 kPa with rubber shockpad showing the largest reduction percentage whilst 3G turf exhibited the least reduction by 21.3%. Peak stress measured under foam shockpad and hockey turf was similar around 110 kPa showing a reduction of approximately 29%. For the surface systems, except 3G+RS measured the least reduction in stress at the bottom by 34.8%, other systems reduced the applied stress by more than 40%. The peak stress at the bottom of HT+FS averaged 84 kPa demonstrating the largest reduction by 45.8%. The stress reduction with HT+RS and 3G+FS was similar around 42%.

The pressure mat was also inserted between the carpet and shockpad layers. For HT+RS under 50 mm loading foot, the peak contact area measured between layers was slightly larger than it measured at the bottom of surface system by 2.4%. The average peak stress recorded between layers was 202 kPa showing a reduction from the applied stress by 79%. For HT+FS under 50 mm loading foot, the peak contact area between layers was 111 cm², 23.3% larger than at the bottom of surface system, showing a lower peak stress at 156 kPa compared with 220 kPa. Conversely, for both hockey turf systems under 125 mm loading foot, peak contact areas measured at the carpet-shockpad interface were smaller than at the bottom of systems by 6 – 8%. However, there was no discernible difference between the stress measured at the carpet-shockpad interface and at the bottom for both hockey turf systems. Due to the effect of unsmooth backing of 3G turf (as shown in Figure 3.35) on the

contact area and stress readings, results of these two parameters at the carpet-shockpad interface of 3G turf surface systems could not accurately be obtained from the pressure mat and therefore have been omitted from analysis.

3.3.3.3 Loading at 3.3 Hz

Average peak contact area and peak stress measured by the pressure mat under 3.3 Hz loading are summarised in Table 3.9. Under the 50 mm loading foot, the individual layer samples showed an increase in peak contact area ranging from 100 – 170%, with the largest change for hockey turf and the smallest change for foam shockpad. Both the rubber shockpad and 3G turf increased the peak contact area to 46 cm², by 130%. For the hockey systems, peak contact area recorded at the bottom of HT+FS was 91 cm², larger than 82 cm² for HT+RS. Peak contact area measured at the bottom of 3G+FS was increased by 370% as the largest change and 3G+RS the least with 305% in all the systems.

Under the 125 mm loading foot, the increase in peak contact area was less significant than under the 50 mm loading foot. Peak contact area at the bottom of foam shockpad increased by 44.7% compared with 36.6% for rubber shockpad. Hockey turf showed the largest increase of 47.2%. Figure 3.36 displays the pressure contour at peak contact area measured under 3G carpet showing only the sensing cells pressed by the stitch lines on the backing were activated, hence a much smaller average value of 147 cm² was recorded. The magnitude of increase in contact area at peak for HT+FS and 3G+FS was similar around 80%. Surface systems with rubber shockpad exhibited this increase by less than 70%.

For individual layers loaded with the 50 mm loading foot, the stress reductions varied between 51 – 65.2%. Applied stress reduced approximately by half with foam shockpad as the least decrease. A less marked variation in stress reduction was found between the surface systems varying in the range of 74.8 to 78.3%. Surface systems combined with foam shockpad exhibited slightly better stress reduction performance than those built with rubber shockpad.

Under the 125 mm loading foot, applied stress reduced by foam shockpad and hockey turf around 32%. The least reduction was recorded with 3G turf for only 14.2%. The same trend was found as under the 50 mm loading foot, surface systems with foam shockpad reduced the stress by over 44% whilst by less than 40% for systems with rubber shockpad.

There was no discernible difference between the peak contact area and stress measured at hockey turf and shockpad interface and these parameters at the bottom under loading with the 50 mm loading foot. Under the 125 mm loading foot, the pressure mat in between hockey turf and rubber shockpad recorded the peak contact area at 190 cm² reducing the applied stress to 96 kPa. At the interface between hockey turf and foam shockpad, the peak contact area increased to 205 cm² reducing the stress to 97 kPa. The results showed the applied stress first reduced by hockey turf for around 38%, and then reduced even further as penetrating the shockpad by 2.1 and 11.3% for rubber and foam shockpad respectively.

3.3.3.4 Loading at 10 Hz

A summary Table 3.10 lists the average peak contact area and peak stress measured by the pressure mat. Under the 50 mm loading foot, for the individual layer samples tested, the least increase in peak contact area was found with foam shockpad by 110% and hockey turf the largest by 170%. Peak contact area measured under rubber shockpad was 48 cm², 2 cm² larger than under 3G turf. For surface systems, 3G+RS enlarged the peak contact area at the bottom 4 times of the area of 50 mm loading foot (20 cm²). Other surface systems distributed the load over even larger areas, with HT+FS exhibiting the greatest increase by a factor of 4.65.

Under the 125 mm loading foot, rubber shockpad increased the peak contact area by 46.3% compared to 39% for foam shockpad. Peak contact area was recorded an increase by 41.5% under hockey turf, much larger than 18.7% increase for 3G turf. For carpet-shockpad systems, an increase by approximately 73% of peak contact area was measured for HT+FS and 3G+FS. HT+RS shows an increase by 69.1%, larger than 58.5% for 3G+RS.

All individual layers exhibit an overall reduction in peak stress by over 50% under the 50 mm loading foot. But it was noted that relatively lower peak stress (large reduction) was measured under 3G turf for the same amount of load over the specified contact area, which may be suggesting under-estimation of stress as pointed out in Section 3.3.3.2. The range of stress reduction for the surface systems was relatively narrow, 75.6 – 78.9%. Hockey turf and 3G turf systems with foam shockpad still showed slight larger reduction than those using rubber shockpad.

Under the 125 mm loading foot, rubber shockpad showed the greatest reduction in stress by 32.3% of all the individual layers. Foam shockpad and hockey turf demonstrated a similar reduction percentage around 29%. 3G turf only reduced the stress by 16.8%, to 129

kPa. Two hockey turf systems and 3G+FS showed similar stress reduction around 42% whilst 3G+RS had a lower stress reduction by 38.1%.

For both hockey turf systems, peak contact areas recorded at the carpet-shockpad interface were smaller than at the bottom of systems. But peak stress measured between layers under the 50 mm loading foot was around 20 kPa lower than it recorded at the bottom. This may be explained that due to higher loading frequency at 10 Hz and with less activated sensing cells under the 50 mm loading foot, greater errors occurred in the calculation of stress between layers. Under the 125 mm loading foot, HT+RS displayed a gradual reduction in stress from 155 kPa to 94 and then 90 kPa as the load distributed over an increasing area from 123 cm² (loading foot area) to 188 and then 208 cm². For HT+FS, the peak contact area was 203 cm² between the two layers, 10 cm² smaller than it recorded at the bottom of the surface system which led to a further reduction by 18% in stress through foam shockpad.

3.3.3.5AAA impact

The AAA tests were practised according to the requirements of FIFA Quality Concept (2012) as introduced in Section 2.4.2. The test foot of AAA is a lower side slight rounded disc with a diameter of 70 mm. Contact area on top of the specimens was taken as 38 cm². Table 3.11 summarises the peak contact area and stress measured by the pressure mat indicating pressure distribution of surface systems under the AAA impacts.

For all individual layers, peak contact area measured at the bottom increased by over 60%, with the greatest change for hockey turf and the smallest change for foam shockpad. Around 70 cm² peak contact area was recorded for rubber shockpad and also 3G turf. For surface systems, peak contact area was increased by 181.6% for HT+RS compared to 197.4% for HT+FS. Both 3G turf systems showed the same magnitude of increase in peak contact area at 221.1%.

Average peak stress applied was calculated from the average peak force of 2nd and 3rd impacts of the test locations recorded by FP. Applied stress on individual layers varied from 824 – 1001 kPa. Lower applied stress measured on hockey turf systems than 3G systems. The range of stress reduction with individual layers was 37.8 – 50.1%, with the largest reduction for hockey turf and the smallest for foam shockpad. All carpet-shockpad combined systems demonstrated a reduction in stress over 60%. The largest reduction of

69.1% was achieved with 3G+FS whilst HT+RS exhibited the least stress reduction of 64.4%.

The pressure mat was inserted between the layers of hockey turf systems. A gradual increase of peak contact area through the layers of HT+RS was recorded as 94 cm² measured at carpet-shockpad interface and then further developed to 107 cm² at the bottom. Similar peak contact area around 113 cm² was measured between the layers and at the bottom of HT+FS. The applied stress of 595 kPa reduced firstly by 59% through hockey turf and then had a further reduction of 64.4% through rubber shockpad. Unlike HT+RS, the difference in peak stress measured at the two interfaces of HT+FS was only 2 kPa.

3.4 Discussion

3.4.1 Effects of cyclic loading

Results presented in subsection 3.3.1 show a development of permanent surface deformation along with the increase of the applied number of loading cycles. Permanent surface deformation after each cycle is converted into residual strain of specimen in order to normalise the thickness. Residual strain is calculated using Equation 3.6.

$$R = \frac{D_{Fmin} - D_{pre}}{t_0} \quad (3.6)$$

Where:

R = Residual strain

D_{Fmin} = Position of the actuator when minimum force reached at each cycle (mm)

D_{pre} = Start position of the actuator when loading foot in contact with specimen (mm)

t_0 = Original specimen thickness (mm)

R has been calculated from the point minimum force (close to pre-load value) reached at each cycle, hence represents the instantaneous level of residual strain from the loading regime at this time (Davidson, 2012).

Accumulation of residual strain for the individual layers under 3.3 Hz cyclic loading with the 50 mm loading foot is compared in Figure 3.37. Rubber shockpad, hockey and 3G turf carpets demonstrate a gradual accumulation of residual strain during cyclic loading. There is no apparent accumulation of residual strain found for foam shockpad and the residual

strain of around 0.32 throughout the loading event is mainly caused by the pre-load remaining on the specimen. The accumulation of residual strain is less than 0.05 for hockey turf and rubber shockpad from initial loading cycle to the 40th. 3G turf exhibits a prominent accumulation of 0.12 in the 40 cycles. The residual strain of each tested layer is related to its stiffness at lower stress level (< 30 kPa). Due to higher initial stiffness of rubber shockpad, the average residual strain is much smaller than other layers.

Hockey carpet contains a turf surface with 12 mm long nylon fibres and an 6 mm integral foam pad underneath. As the characteristics of foam shockpad shown above, the integral foam pad of hockey carpet is also expect to show stable residual strain performance under cyclic loading. In addition, based on visual inspection the fibres were examined an apparent compaction at the loading completion. Low resistance of the fibres results the residual strain develops from 0.4 to 0.44 showing an accumulation of 0.04 solely caused by the compaction of fibres. The infilled 3G carpet exhibits a significant accumulation of residual strain under cyclic loading because of gradual compaction of the infill materials. The accumulation of 0.12 agrees with the change in infill depth at 4 mm measured by gauge after the completion of 40 cycles.

Recovery of residual strain of surface is time dependent which is not analysed in this research. However, for carpet layer especially compaction of infills in 3G carpet, usually it could not fully recover to its original thickness after repeated loading over time. The change in mechanical response of 3G carpet due to compaction effect is reported in previous research (Alcantara et al., 2009; Severn, 2010). The compaction of 3G turf surface leads to a reduction in impact attenuation performance, unless these changes can be well perceived by the player to make kinematic adaptations, it potentially increases the injury risk. Therefore, maintenance of artificial turf system is important to restore and maintain the mechanical performance after regular usage.

3.4.2 Effects of loading frequency

The results presented in Section 3.3.2 show that the changes in frequency of loading leads to a change in mechanical responses of all the surface systems tested. Previous studies implementing drop-weight procedures did not specify loading frequency (Young, 2006; Shorten and Himmelsbach, 2002). Others implementing force-controlled static/dynamic compression testing had used loading conditions that were not adopted from biomechanical data (Anderson, 2007; Dura et al., 2002; Allgeuer et al., 2008). There is no literature

specially discusses the effects of loading frequency on mechanical behaviour considering artificial turf system.

The three loading frequency conditions defined as in Table 3.3 were selected to represent realistic player walking (0.9 Hz), running (3.3 Hz) and sprinting (10 Hz) events. All conditions were applied to the four surface systems and the 19th cycle of each loading profile was selected to present the stress-strain relationship of each surface system. The chosen number of cycle was based upon considering the surface systems been conditioned to the same level (by previous cycles) and the target ranges of peak force, pre-load and time to peak to be achieved for all specimens and loading frequency conditions, thus ensuring validity in comparison. Maximum strain, stiffness values in initial stage (< 400 kPa) and final stage (> 600 kPa) at the selected cycle are compared to highlight the effects of loading frequency.

Figure 3.38 shows the stress-strain relationship of HT+RS for three loading frequency conditions. The maximum strain of HT+RS remains around 0.49 at the 19th loading cycle regardless of loading frequency. The stiffness in final stage for all loading conditions varies in a narrow range between 500 – 510 N/mm. However, HT+RS subject to 10 Hz condition exhibits the largest initial stage stiffness compared with other two conditions. For stress level below 200 kPa, the stiffness measured at 3.3 Hz is larger than at 0.9 Hz.

A comparison of stress-strain relationship of HT+FS at different loading frequencies is illustrated in Figure 3.39. Maximum strain varies in a relatively narrow range between 0.58 – 0.6 for the change in loading frequency. The final stage stiffness is in the range of 620 – 640 N/mm. The same trend as HT+RS is found considering initial stage stiffness with increased values for the accelerated loading conditions.

3G+RS shows an overall reduction in maximum strain as the increase of loading frequency (Figure 3.40). Similar maximum strain is observed at 3.3 and 10 Hz, but this is 11% larger for 0.9 Hz condition. There is an overall increase in stiffness in line with loading frequency.

The separation in maximum strain values at different loading frequency conditions is more pronounced for 3G+FS as shown in Figure 3.41. The maximum strain is 0.42 for 10 Hz, 6% and 24% smaller than 3.3 Hz and 0.9 Hz respectively. The same trend as 3G+RS is apparent considering stiffness increase for the accelerated conditions over the whole loading phase.

These results show that increased loading frequency leads to stiffer behaviour in the initial stage of loading at the same cycle for all surface systems. Concerning maximum strain and final stage stiffness, the increase of loading frequency has a more profound effect on 3G turf systems resulting decrease of maximum strain and increase of stiffness.

3.4.3 Comparison between cyclic compression and the AAA loading

The results of peak stress and vertical deformation of surface systems under the AAA testing are listed in Table 3.11 and 3.7, compared with the force-deflection data of the cyclic compressive loading. As presented in Chapter 2, the AAA has been designed to simulate the impact peak of a heel strike running. The values of rising time to peak force of the AAA impacts on the tested surface systems vary between 18 – 20 ms. Although it is not directly comparable to the mechanical loading conditions, the 10 Hz loading with the shortest rising time to peak force at 50 ms among the cyclic loading tests is selected to compare with the AAA impact.

Figure 3.42 shows stress-strain curve under the 3rd cycle of 10 Hz loading in comparison to the average data point of the 2nd and 3rd AAA impacts for hockey turf systems. Figure 3.43 shows data for 3G turf systems presented in the same way. At 595 kPa, the strain of HT+RS under the AAA impact is 0.32, 26% smaller than the strain measured under 10 Hz loading. For HT+FS at 551 kPa, the strain under the AAA impact is 27% smaller than under 10 Hz loading. The AAA impact peak stress on 3G+RS is 673 kPa resulting a strain of 0.21, 36% smaller than the strain at the same stress level under 10 Hz loading. The difference of strain measured under two loading patterns in 3G+FS is 37%. This reduction in strain recorded under the AAA impact may be explained by the rate of loading is much higher than it for the 10 Hz loading and the impact area of the AAA test foot (38 cm²) is larger compared to 20 cm² loading foot. It is noted that the hockey turf systems exhibit around 27% of reduction in strain whilst 3G turf systems show a reduction of around 37%. It is unclear that this trend of reduction is related with the type of surface system or the applied stress level.

The limitations of similar mechanical drop test (AAB) for the simulation of human interaction with a surface have been identified by Dixon et al. (1999). The results presented above suggest the AAA impact has much shorter rising time to peak force than 10 Hz sprinting simulation loading. Therefore, for the same amount of load, the rate of loading delivered by the AAA is higher which may result smaller surface strain measured in

comparison to the surface strain actually experienced under most of player ‘in-game’ movements. For the single point of stress-strain relationship at peak recorded by the AAA, only the secant stiffness of tested surface can be estimated from the origin to this given point. As the strong nonlinear behaviour of surface systems shown in Section 3.3.2, the AAA results are unable to show the change of stiffness of surface system during the loading period.

3.4.4 Stress distribution angle

In geotechnical engineering, stress distribution angle Θ (Figure 3.44) is used to determine the stress distribution in soil over an enlarged area at any depth as a vertical load applied on the soil surface over the loaded area. This parameter is employed to describe the stress distribution through the sports surfaces. The applied stress from the compressive mechanical loading on the surface layers/systems is distributed over increased areas measured by the pressure mat at the bottom, as presented in subsection 3.3.3. The enlarged circular contact areas recorded by the pressure mat are shown in Figure 3.45. A stress distribution cone at the cross-section can be constructed showing the stress spread out at an angle Θ from the edge of the loaded area to the edge of enlarged area at the total thickness of specimen. The values of stress distribution angle under compressive loading with the 50 mm diameter foot and the AAA are calculated using Equation 3.6 and the averages are compared in Table 3.12.

$$\theta = \arctan \frac{r_2 - r_1}{h} \quad (3.6)$$

Where:

Θ = Stress distribution angle (°)

r_1 = Radius of impact area (mm)

r_2 = Radius of enlarged contact area at the bottom of specimen (mm)

h = Total thickness (mm)

For individual layers under compressive loading at different frequencies, the stress distribution angle is in a relatively narrow range between 41.5° and 45° except for the 3G carpet. The angle calculated with the 3G carpet is less than 30° which is considered to be underestimated due to the unsmooth backing issue addressed in subsection 3.3.3 (Figure

3.45). For combined surface systems, the largest stress distribution angle is measured with HT+FS around 44° whilst the smallest angle with 3G+RS approximately 28° . It is noted that with the same carpet layer, surface systems using foam shockpad distribute the stress at larger angles than using rubber shockpad. The results show no discernible effect on stress distribution angle at different loading frequencies.

Under the AAA loading, the applied stress is distributed through the individual layers at an angle around 38° with the exception for the 3G carpet. The angles for combined surface systems vary in the range of $29.7 - 39.8^\circ$. It is observed that the stress distribution angle is not sensitive to the change of loading rate (frequency) in the compressive tests. Hence, the decrease of stress distribution angle may be explained as the increase of the impact area from 20 cm^2 to 38 cm^2 . Analysis of the stress distribution angle under the 125 mm diameter loading foot shows a further reduction in this parameter. For example, at the 10 Hz loading, the stress distribution angles reduce to 18.8° and 33.5° for the 3G+RS and HT+FS respectively.

Pressure contour recorded by the pressure mat indicates that the stress is not uniformly distributed over the enlarged areas below the layer/surface system. A high pressure region is located in the centre within an area similar to the size of the impact area. The high pressure region is surrounded by an annular region with relatively lower pressure. The pressure contour at peak stress of 3.3 Hz loading recorded at the bottom of HT+RS with the 50 mm loading foot is presented in Figure 3.46. The average stress over the whole contact area is 230 kPa whilst the average stress in the high pressure region (area within the red line) is more than 2 times higher, at 523 kPa. Significantly lower average stress is measured in the surrounding annular region at 116 kPa. The width of low stress annular region is 2.5 cm. This value agrees well with the increase in radius of contact area ($r_2 - r_1$). It suggests that the applied stress spread out through the surface system at the angle Θ with high stress mainly concentrated in the central region directly below the loaded area.

Table 3.1: Specifications of products used in this project

Sample	Product name	Sample size (mechanical loading test)	Sample size (player loading test)	Thickness	Material and structure	Manufacturer/supplier	Density
Rubber shockpad	Regupol® 6010 SP	300 * 300 mm ²	600 * 400 mm ²	15 mm	polyurethane bonded rubber shreds	BSW Berleburger GmbH	550 kg/m ³
Foam shockpad	re-bounce® uni F82.16	300 * 300 mm ²	600 * 400 mm ²	12 mm	polyurethane foam	Recticel S.A.	250±15% kg/m ³
Sand infill	N/A	0.2-0.7 mm	0.2-0.7 mm	N/A	Silica, round shape	Garside 2EW	N/A
Rubber infill	N/A	1-3 mm	1-3 mm	N/A	SBR	N/A	N/A
Hockey turf	System 5	300 * 300 mm ²	600 * 400 mm ²	18 mm total	12mm long nylon fibres, with a 6mm integral foam pad	McCardle AstroTurf	N/A
3G turf	Soccer Real 50 MS/55 MS*	300 * 300 mm ²	600 * 400 mm ²	50/55 mm (pile height)	Polyethylene, monofilament	TigerTurf	25200 (tufts/m ²)

Note: after mechanical loading test programme, Soccer Real 50 MS carpet was exhausted. TigerTurf replaced Soccer Real 50 MS with Soccer Real 55 MS in their catalogue. So the latter product was sourced and used in the player test programme. The only difference between the two products was the pile height changed from 50 mm to 55 mm. The quantities of infills used to prepare samples were kept the same for both carpets.

Table 3.2: Instron ElectroPuls E3000 key specifications (Davidson, 2012)

	Parameter	Value
Force	Load cell rating (absolute capacity)	± 5.0 kN
	Dynamic test capacity	± 3.0 kN
	Static test capacity	± 2.1 kN
	Measurement accuracy	± 0.5 % of actual value
	Measurement repeatability	< ± 0.25 % of reading (from 1 - 100 % of cell rating)
	Calibration frequency	Annually to UKAS standard
Displacement	Actuator stroke (maximum)	60 mm
	Actuator frequency	> 100 Hz (displacement dependent)
	Measurement accuracy	± 0.5 % of actual value
	Calibration frequency	Annually to UKAS standard
Data	Acquisition rate	up to 5 kHz

Table 3.3: Key parameters of the compression test methods compare to player walking, running and sprinting movements

	Researcher	Vertical force (BW)	Contact duration (s)	Max vertical force of 80 kg player (N)	Max vertical force applied by Instron (N)	Frequency (Hz)	Time to peak force (s)	No. of cycles	Pre-load (N)
Walking	Adrian and Xu (1990)	1.33	1.1	1043	1900	0.9	0.55	20	10
Running	Adrian and Xu (1990)	2.5	0.3	1960	1900	3.3	0.15	40	40
Sprinting	Korhonen et al. (2010)	3.35	0.1	2626	1900	10	0.05	60	100/300

Note: BW = body weight. For sprinting simulation (10 Hz), pre-load was set at 100 N for 125 mm diameter loading foot, 300 N for 50 mm diameter loading foot.

Table 3.4: Peak vertical deflection and key stiffness values for all surface systems under 0.9 Hz 2nd loading cycle

Surface system	Loading foot diameter (mm)	Peak vertical deflection (mm)	Initial stiffness (N/mm)	Final stiffness (N/mm)
Hockey turf + Rubber shockpad	50	15.5 ± 0.2	75 ± 3	338 ± 8
	125	7.5	293 ± 4	348 ± 9
Hockey turf + Foam shockpad	50	16.8 ± 0.1	61 ± 2	367 ± 9
	125	8.8	240 ± 3	292 ± 6
3G turf + Rubber shockpad	50	19.2 ± 0.4	81 ± 4	338 ± 10
	125	10.4 ± 0.1	132 ± 8	461 ± 13
3G turf + Foam shockpad	50	19.2 ± 0.5	62 ± 3	338 ± 9
	125	11.4 ± 0.2	132 ± 8	365 ± 12

Table 3.5: Peak vertical deflection and key stiffness values for all surface systems under 3.3 Hz 10th loading cycle

Surface system	Loading foot diameter (mm)	Peak vertical deflection (mm)	Initial stiffness (N/mm)	Final stiffness (N/mm)
Hockey turf + Rubber shockpad	50	16.2 ± 0.1	124 ± 5	413 ± 7
	125	8.7	252 ± 4	399 ± 5
Hockey turf + Foam shockpad	50	18 ± 0.2	108 ± 6	516 ± 10
	125	10.3	214 ± 3	335 ± 2
3G turf + Rubber shockpad	50	16.9 ± 0.3	98 ± 8	436 ± 6
	125	11.4 ± 0.1	230 ± 7	472 ± 5
3G turf + Foam shockpad	50	17.8 ± 0.2	98 ± 6	540 ± 9
	125	13.8 ± 0.1	197 ± 4	380 ± 4

Table 3.6: Peak vertical deflection and key stiffness values for all surface systems under 10 Hz 20th loading cycle

Surface system	Loading foot diameter (mm)	Peak vertical deflection (mm)	Initial stiffness (N/mm)	Final stiffness (N/mm)
Hockey turf + Rubber shockpad	50	16 ± 0.1	403 ± 11	506 ± 9
	125	8.8	388 ± 9	486 ± 6
Hockey turf + Foam shockpad	50	17.5 ± 0.1	503 ± 14	633 ± 18
	125	10 ± 0.1	330 ± 8	410 ± 7
3G turf + Rubber shockpad	50	16.7 ± 0.2	308 ± 12	493 ± 19
	125	11 ± 0.2	334 ± 16	523 ± 20
3G turf + Foam shockpad	50	17.3 ± 0.4	374 ± 28	619 ± 23
	125	12.1 ± 0.1	285 ± 9	445 ± 13

Table 3.7: Results of the AAA tests on individual layer samples and carpet-shockpad systems

	AAA		
	Fmax (N)	Force Reduction	Vertical Deformation (mm)
Rubber shockpad	3646.5 ± 22	48 ± 0.5 %	4.8 ± 0.2
Foam shockpad	3842.5 ± 38	45 ± 0.8 %	6.0 ± 0.3
Hockey carpet	3184 ± 40	55 ± 0.7 %	7.8 ± 0.2
3G carpet	3569.5 ± 72	49 ± 2 %	7.2 ± 0.6
Hockey turf + Rubber shockpad	2276.5 ± 23	69 ± 1 %	10.5 ± 0.3
Hockey turf + Foam shockpad	2101 ± 21	71 ± 0.9 %	11.4 ± 0.1
3G turf + Rubber shockpad	2526 ± 59	65 ± 1.1 %	10.3 ± 0.2
3G turf + Foam shockpad	2408 ± 68	67 ± 1.2 %	10.8 ± 0.3

Table 3.8: Peak contact area and stress (\pm standard deviation) measured by the pressure mat placed under individual layer samples and at two different positions in the surface systems under 0.9 Hz loading

Surface	Pressure mat results						Bottom area increase	Bottom stress reduction
	Peak contact area (cm ²)			Peak stress (kPa)				
	Top	Between	Bottom	Top	Between	Bottom		
Rubber shockpad	20	N/A	46	968	N/A	413 ± 4	130.0%	57.3%
	123	N/A	189 ± 1	155	N/A	100 ± 2	53.7%	35.5%
Foam shockpad	20	N/A	43 ± 1	968	N/A	428 ± 6	115.0%	55.8%
	123	N/A	176 ± 2	155	N/A	111 ± 1	43.1%	28.4%
Hockey carpet	20	N/A	53 ± 1	968	N/A	360 ± 6	165.0%	62.8%
	123	N/A	178 ± 1	155	N/A	109 ± 2	44.7%	29.7%
3G carpet	20	N/A	60 ± 2	968	N/A	231 ± 16	200.0%	76.1%
	123	N/A	148 ± 4	155	N/A	122 ± 4	20.3%	21.3%
Hockey turf + Rubber shockpad	20	86 ± 4	84 ± 1	968	202 ± 8	237 ± 7	320.0%	75.5%
	123	198 ± 1	211 ± 1	155	90 ± 1	90 ± 2	71.5%	41.9%
Hockey turf + Foam shockpad	20	111 ± 5	90 ± 4	968	156 ± 9	220 ± 10	350.0%	77.3%
	123	208	227 ± 1	155	86	84 ± 2	84.6%	45.8%
3G turf + Rubber shockpad	20	N/A	86 ± 1	968	N/A	229 ± 7	330.0%	76.3%
	123	N/A	194 ± 2	155	N/A	101 ± 1	57.7%	34.8%
3G turf + Foam shockpad	20	N/A	93 ± 2	968	N/A	214 ± 4	365.0%	77.9%
	123	N/A	212	155	N/A	89 ± 1	72.4%	42.6%

Note: 'Top' suggests the applied stress and the area of loading foot. 'Between' indicates the parameters measured as the pressure mat sandwiched between carpet and shockpad layer. 'Bottom' means the parameters measured as the pressure mat placed underneath the layer/surface system on top of the Instron platen.

Table 3.9: Peak contact area and stress (\pm standard deviation) measured by the pressure mat placed under individual layer samples and at two different positions in the surface systems under 3.3 Hz loading

Surface	Pressure mat results						Bottom area increase	Bottom stress reduction
	Peak contact area (cm ²)			Peak stress (kPa)				
	Top	Between	Bottom	Top	Between	Bottom		
Rubber shockpad	20	N/A	46 \pm 2	968	N/A	412 \pm 5	130.0%	57.4%
	123	N/A	168 \pm 2	155	N/A	112 \pm 2	36.6%	27.7%
Foam shockpad	20	N/A	40 \pm 1	968	N/A	474 \pm 3	100.0%	51.0%
	123	N/A	178 \pm 1	155	N/A	105 \pm 1	44.7%	32.3%
Hockey carpet	20	N/A	54	968	N/A	351 \pm 4	170.0%	63.7%
	123	N/A	181 \pm 1	155	N/A	104 \pm 1	47.2%	32.9%
3G carpet	20	N/A	46 \pm 4	968	N/A	337 \pm 12	130.0%	65.2%
	123	N/A	147 \pm 4	155	N/A	133 \pm 5	19.5%	14.2%
Hockey turf + Rubber shockpad	20	80 \pm 1	82 \pm 1	968	236 \pm 7	230 \pm 4	310.0%	76.2%
	123	190 \pm 1	208 \pm 1	155	96 \pm 1	94 \pm 1	69.1%	39.4%
Hockey turf + Foam shockpad	20	95 \pm 1	91 \pm 1	968	201 \pm 10	210 \pm 5	355.0%	78.3%
	123	205	221 \pm 1	155	97 \pm 1	86 \pm 1	79.7%	44.5%
3G turf + Rubber shockpad	20	N/A	81	968	N/A	244 \pm 10	305.0%	74.8%
	123	N/A	202 \pm 3	155	N/A	98 \pm 2	64.2%	36.8%
3G turf + Foam shockpad	20	N/A	94 \pm 2	968	N/A	211 \pm 9	370.0%	78.2%
	123	N/A	222 \pm 2	155	N/A	85 \pm 1	80.5%	45.2%

Note: 'Top' suggests the applied stress and the area of loading foot. 'Between' indicates the parameters measured as the pressure mat sandwiched between carpet and shockpad layer. 'Bottom' means the parameters measured as the pressure mat placed underneath the layer/surface system on top of the Instron platen.

Table 3.10: Peak contact area and stress (\pm standard deviation) measured by the pressure mat placed under individual layer samples and at two different positions in the surface systems under 10 Hz loading

Surface	Pressure mat results						Bottom area increase	Bottom stress reduction
	Peak contact area (cm ²)			Peak stress (kPa)				
	Top	Between	Bottom	Top	Between	Bottom		
Rubber shockpad	20	N/A	48 \pm 1	968	N/A	391 \pm 3	140.0%	59.6%
	123	N/A	180 \pm 1	155	N/A	105 \pm 1	46.3%	32.3%
Foam shockpad	20	N/A	42 \pm 1	968	N/A	451 \pm 6	110.0%	53.4%
	123	N/A	171 \pm 1	155	N/A	110 \pm 1	39.0%	29.0%
Hockey carpet	20	N/A	54 \pm 1	968	N/A	351 \pm 5	170.0%	63.7%
	123	N/A	174 \pm 1	155	N/A	109 \pm 1	41.5%	29.7%
3G carpet	20	N/A	46 \pm 2	968	N/A	330 \pm 8	130.0%	65.9%
	123	N/A	146 \pm 2	155	N/A	129 \pm 2	18.7%	16.8%
Hockey turf + Rubber shockpad	20	81 \pm 1	84 \pm 1	968	209 \pm 8	230 \pm 6	320.0%	76.2%
	123	188 \pm 1	208 \pm 1	155	94 \pm 2	90 \pm 1	69.1%	41.9%
Hockey turf + Foam shockpad	20	91 \pm 2	93 \pm 1	968	182 \pm 10	204 \pm 7	365.0%	78.9%
	123	203 \pm 1	213 \pm 1	155	108 \pm 1	89 \pm 1	73.2%	42.6%
3G turf + Rubber shockpad	20	N/A	80 \pm 1	968	N/A	236 \pm 7	300.0%	75.6%
	123	N/A	195 \pm 1	155	N/A	96 \pm 1	58.5%	38.1%
3G turf + Foam shockpad	20	N/A	85 \pm 1	968	N/A	222 \pm 5	325.0%	77.1%
	123	N/A	212 \pm 2	155	N/A	89 \pm 1	72.4%	42.6%

Note: 'Top' suggests the applied stress and the area of loading foot. 'Between' indicates the parameters measured as the pressure mat sandwiched between carpet and shockpad layer. 'Bottom' means the parameters measured as the pressure mat placed underneath the layer/surface system on top of the Instron platen.

Table 3.11: Peak contact area and stress (\pm standard deviation) measured by the pressure mat placed under individual layer samples and at two different positions in the surface systems under the AAA impacts

Surface	Pressure mat results						Bottom area increase	Bottom stress reduction
	Peak contact area (cm ²)			Peak stress (kPa)				
	Top	Between	Bottom	Top	Between	Bottom		
Rubber shockpad	38	N/A	71 \pm 1	970	N/A	518 \pm 3	86.8%	46.6%
Foam shockpad	38	N/A	61 \pm 1	1001	N/A	622 \pm 4	60.5%	37.8%
Hockey carpet	38	N/A	76	824	N/A	411 \pm 2	100.0%	50.1%
3G carpet	38	N/A	70 \pm 1	944	N/A	491 \pm 9	84.2%	48.0%
Hockey turf + Rubber shockpad	38	94	107	595	242 \pm 2	212 \pm 2	181.6%	64.4%
Hockey turf + Foam shockpad	38	114 \pm 1	113	551	184 \pm 2	186 \pm 2	197.4%	66.2%
3G turf + Rubber shockpad	38	N/A	122 \pm 2	673	N/A	213 \pm 3	221.1%	68.4%
3G turf + Foam shockpad	38	N/A	122 \pm 1	643	N/A	199 \pm 2	221.1%	69.1%

Table 3.12: Average stress distribution angles of individual layers and surface systems under compressive loading at different frequencies with 50 mm loading foot and the AAA impacts

Surface	Thickness (cm)	Stress distribution angle (°)			
		Compressive loading (impact area 20 cm ²)			AAA (impact area 38 cm ²)
		0.9 Hz	3.3 Hz	10 Hz	
Rubber shockpad	1.5	41.5	41.5	43.2	39.9
Foam shockpad	1.2	45.0	41.7	44.0	37.1
Hockey carpet	1.8	41.8	42.5	42.5	38.3
3G carpet	3.3	29.6	21.9	21.9	20.3
Hockey turf + Rubber shockpad	3.3	39.0	38.3	39.0	35.3
Hockey turf + Foam shockpad	3	43.6	43.9	44.4	39.8
3G turf + Rubber shockpad	4.8	29.7	28.2	28.0	29.7
3G turf + Foam shockpad	4.5	33.2	33.4	31.0	31.3



Figure 3.1: Instron ElectroPuls E3000 machine with sample

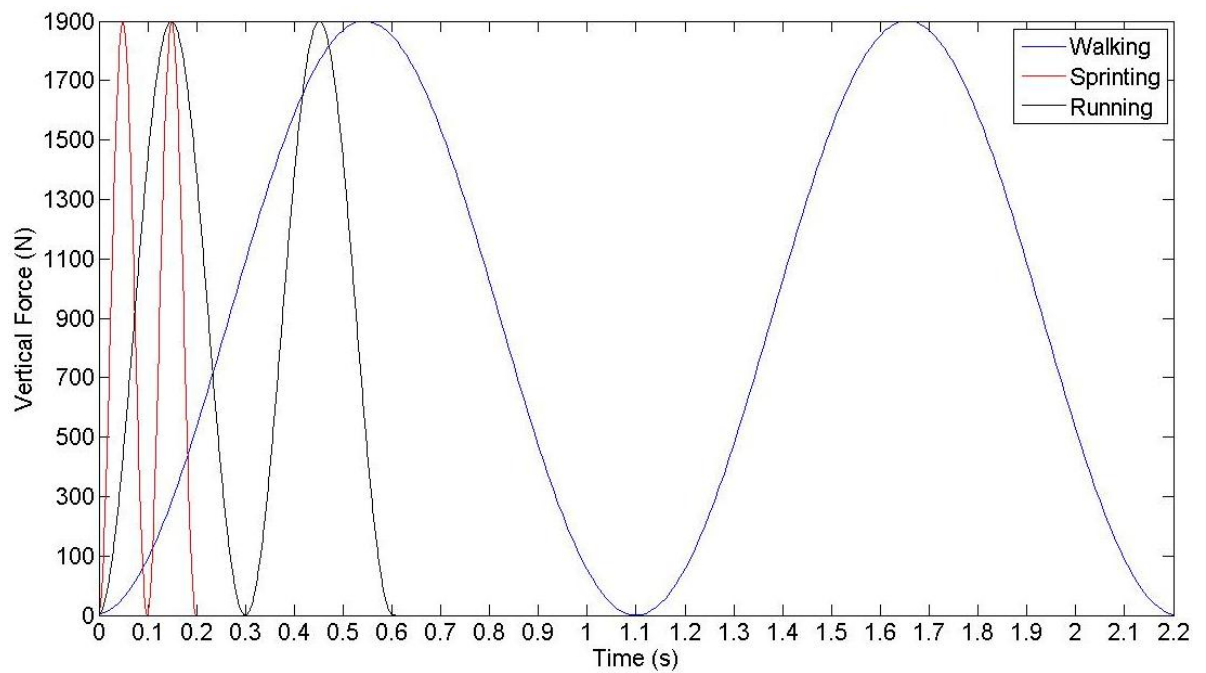


Figure 3.2: Representation of the sine wave loading cycles applied by the Instron machine

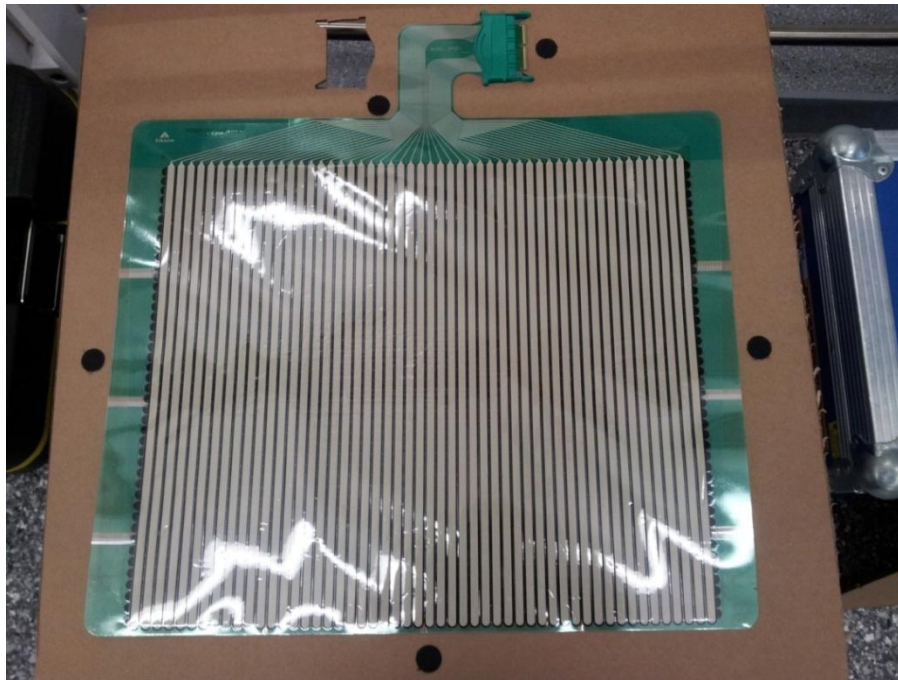


Figure 3.3: A picture of Tekscan pressure mat 3150E

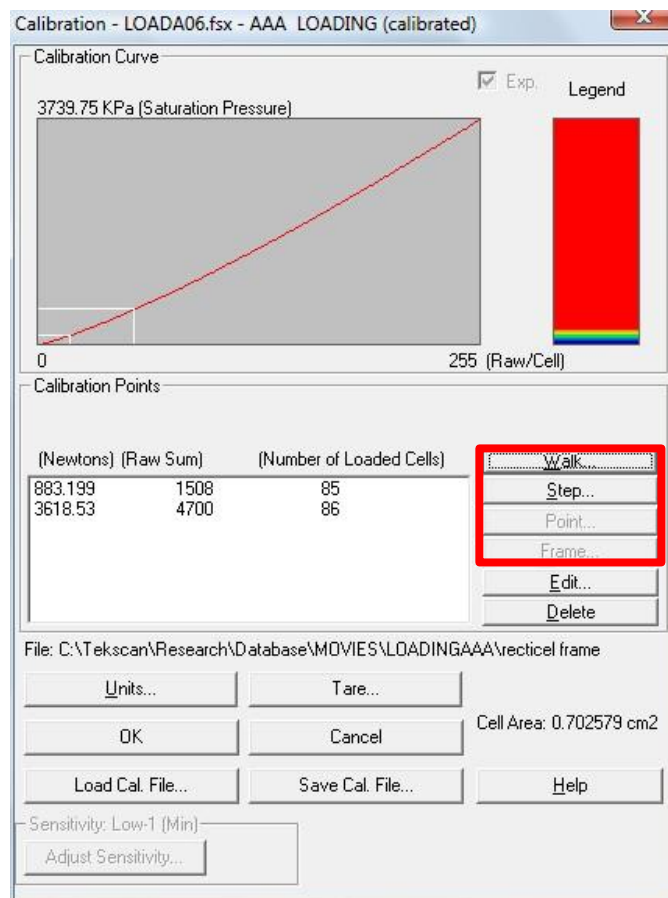


Figure 3.4: Tekscan software calibration tool interface

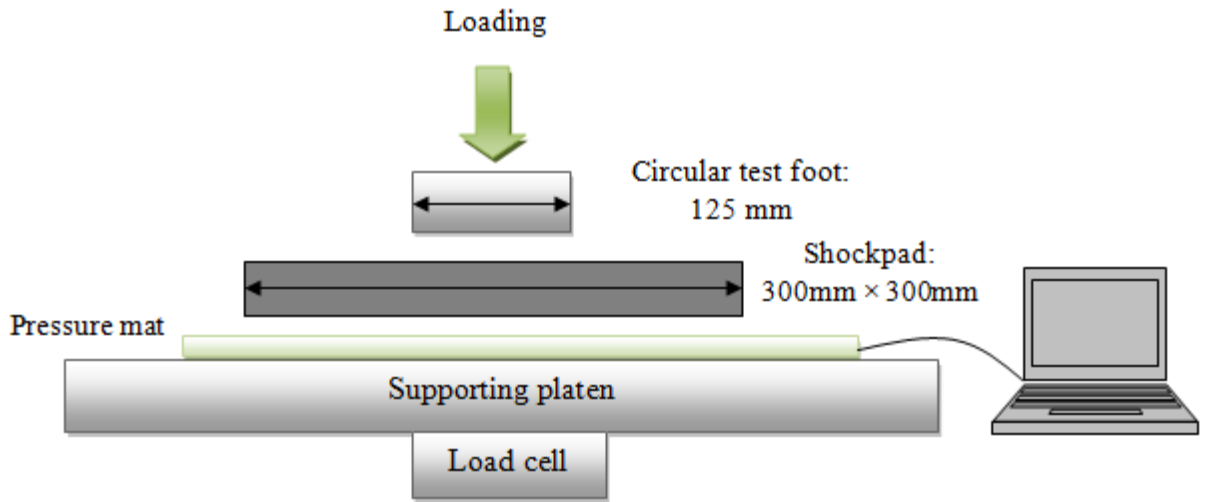


Figure 3.5: Pressure mat calibration by Instron machine compressive loading

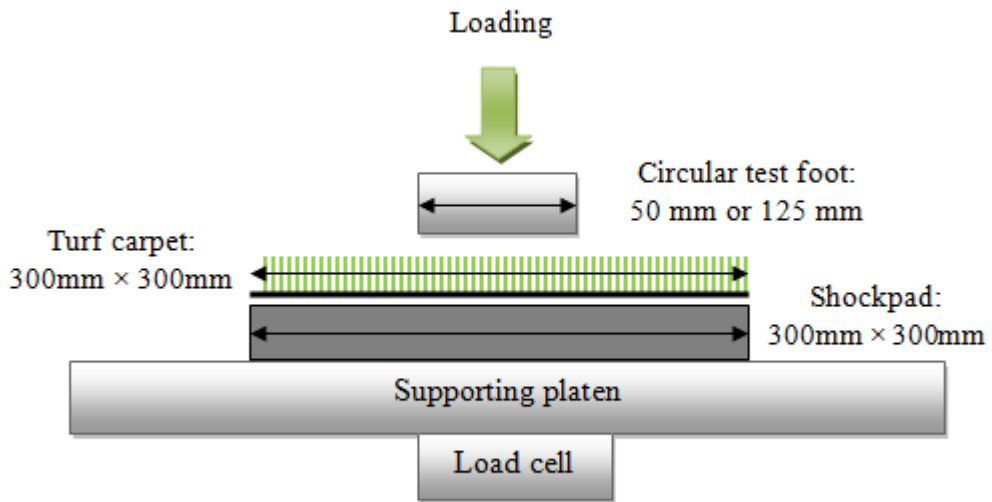


Figure 3.6: Schematic of the measurement system design, showing the surface system of carpet and shockpad and the compression dynamic mechanical loading

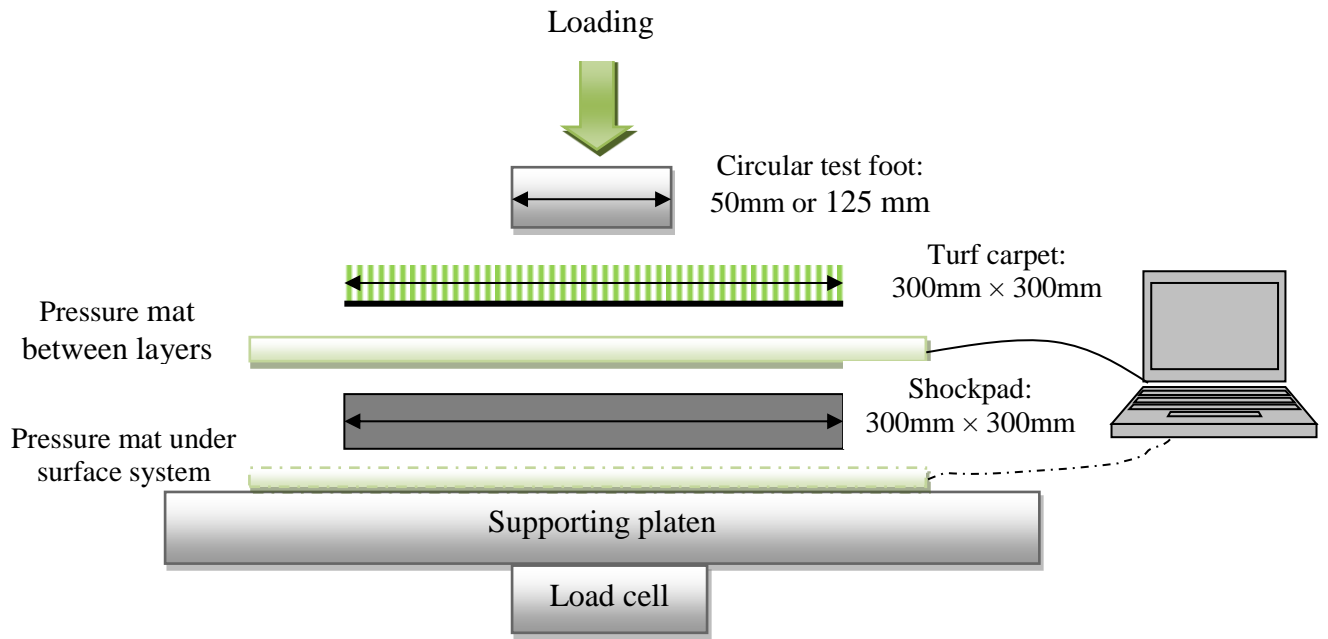


Figure 3.7: Schematic of pressure mat used between layers and under shockpad in the surface system under the dynamic compressive mechanical loading

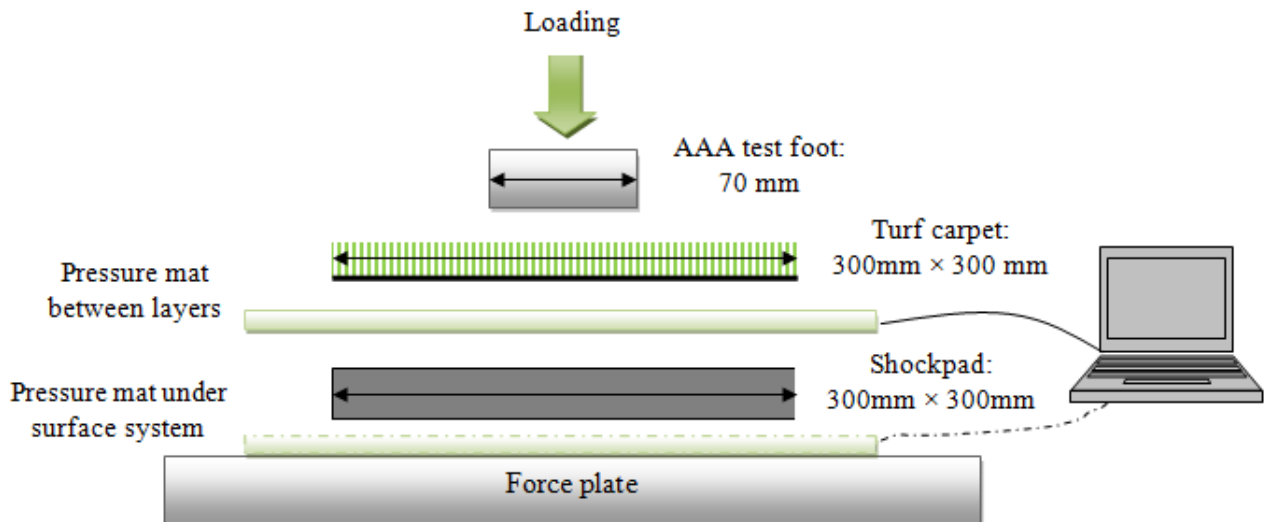


Figure 3.8: Schematic of pressure mat used between layers and under shockpad in the surface system under the AAA test

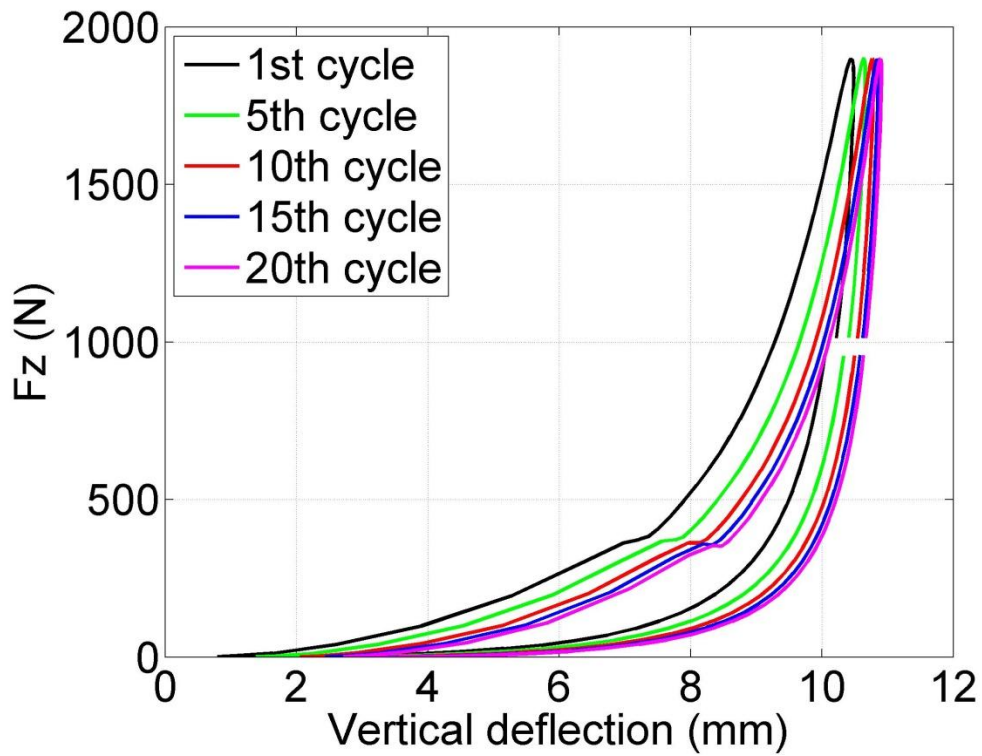


Figure 3.9: Force-deflection relationship of 0.9 Hz cyclic loading with 50 mm loading foot on hockey turf (18 mm thick)

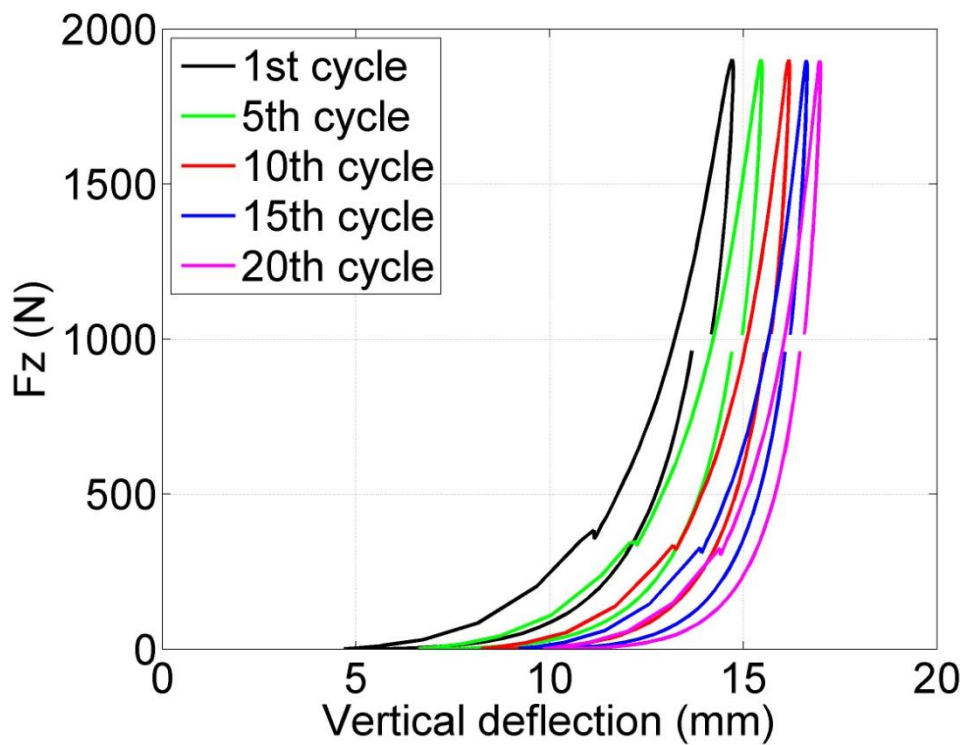


Figure 3.10: Force-deflection relationship of 0.9 Hz cyclic loading with 50 mm loading foot on 3G turf (32 mm infill depth)

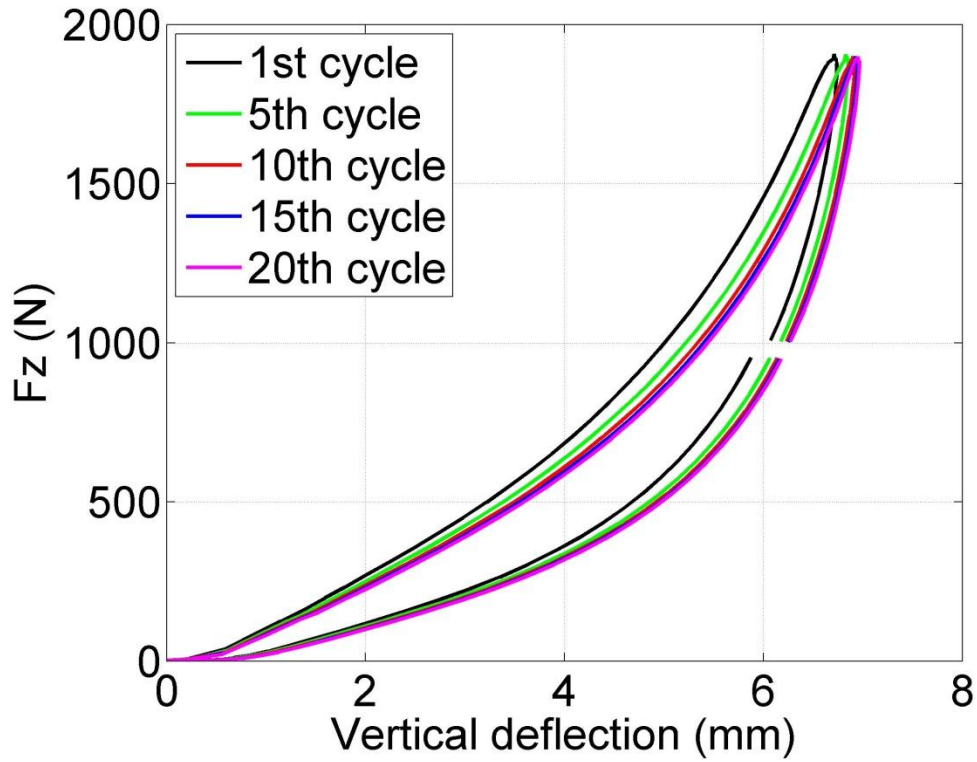


Figure 3.11: Force-deflection relationship of 0.9 Hz cyclic loading with 50 mm loading foot on rubber shockpad (15 mm thick)

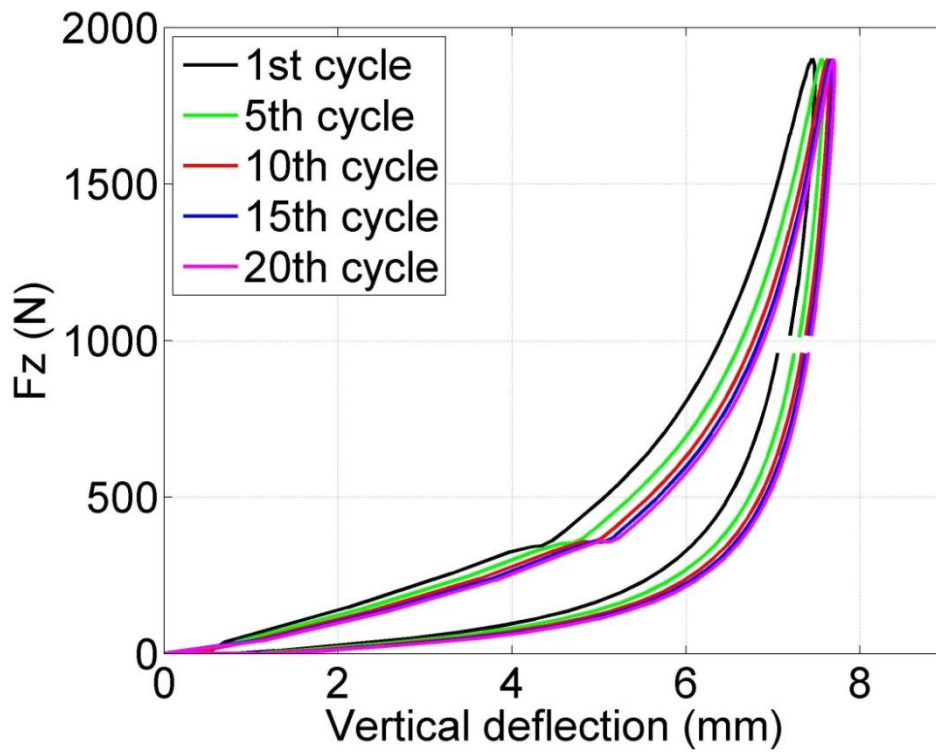


Figure 3.12: Force-deflection relationship of 0.9 Hz cyclic loading with 50 mm loading foot on foam shockpad (12 mm thick)

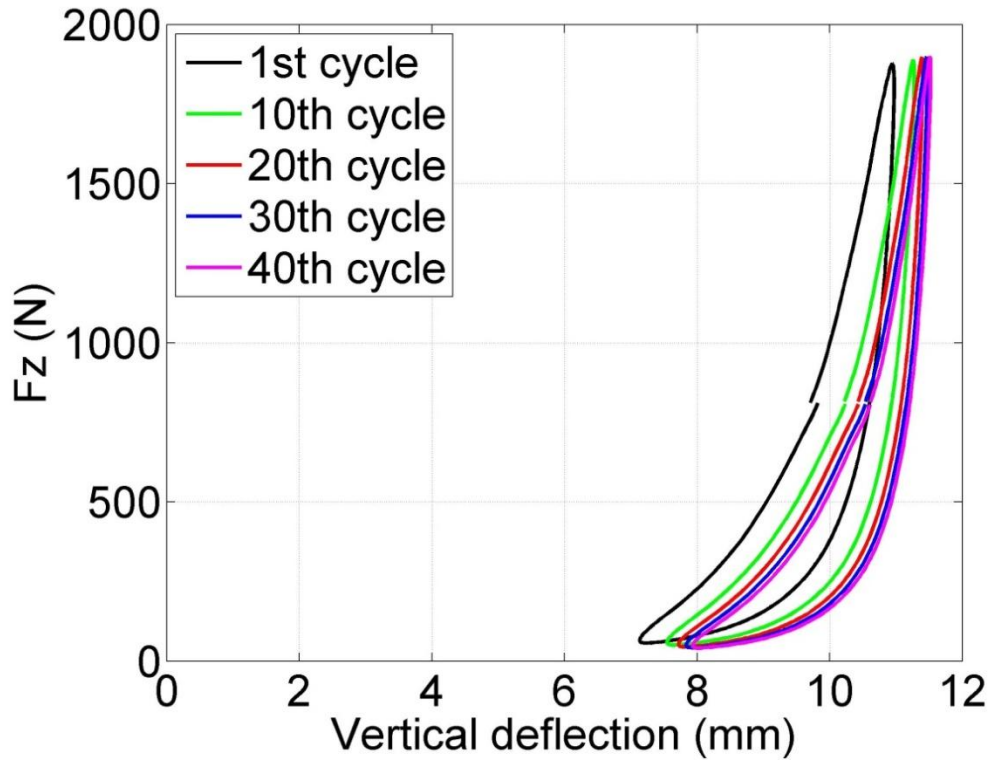


Figure 3.13: Force-deflection relationship of 3.3 Hz cyclic loading with 50 mm loading foot on hockey turf (18 mm thick)

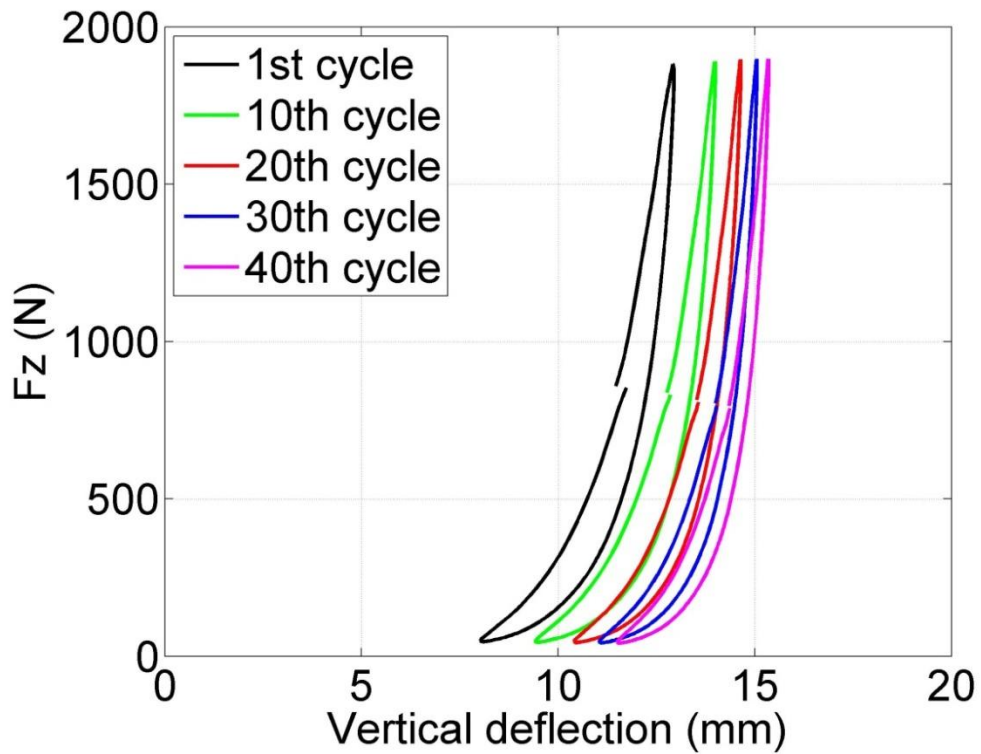


Figure 3.14: Force-deflection relationship of 3.3 Hz cyclic loading with 50 mm loading foot on 3G turf (32 mm infill depth)

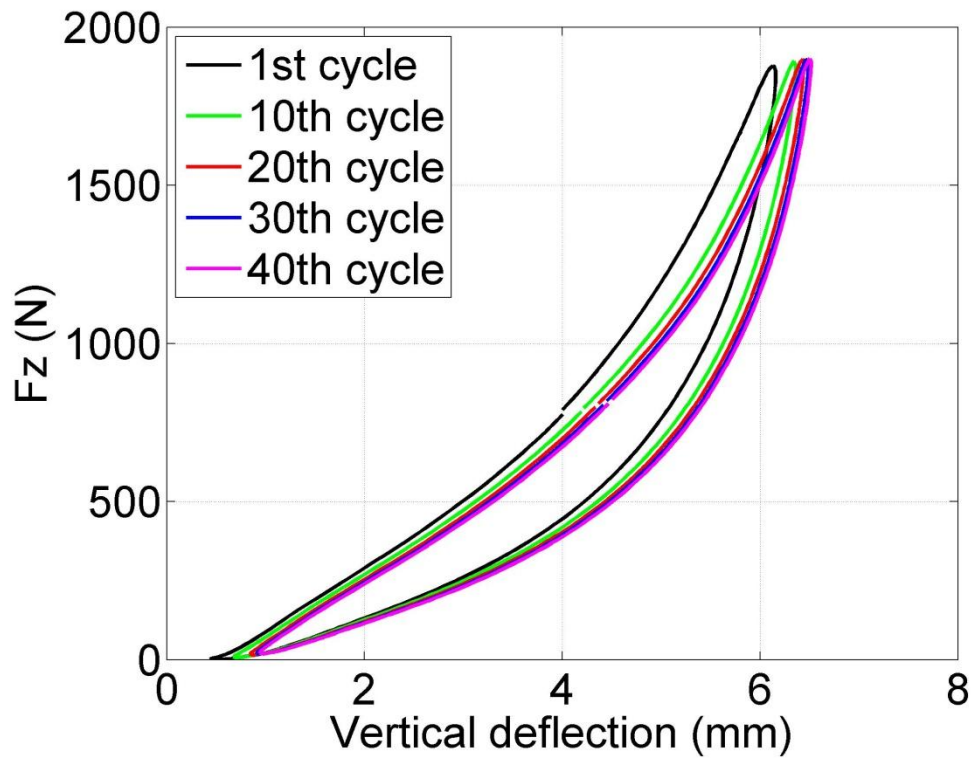


Figure 3.15: Force-deflection relationship of 3.3 Hz cyclic loading with 50 mm loading foot on rubber shockpad (15 mm thick)

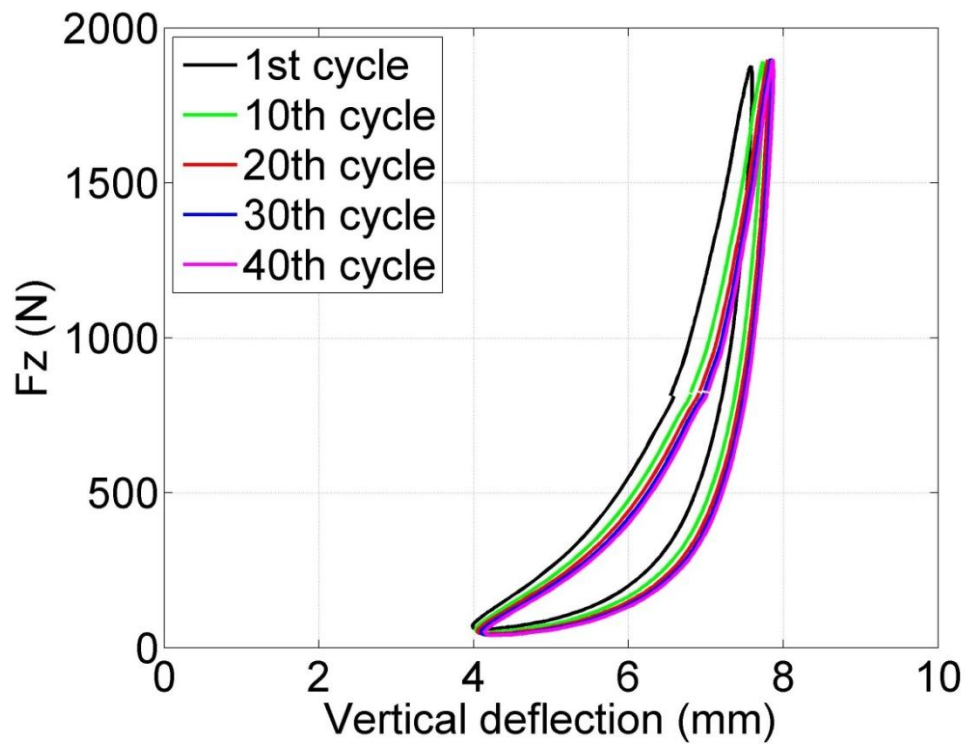


Figure 3.16: Force-deflection relationship of 3.3 Hz cyclic loading with 50 mm loading foot on foam shockpad (12 mm thick)

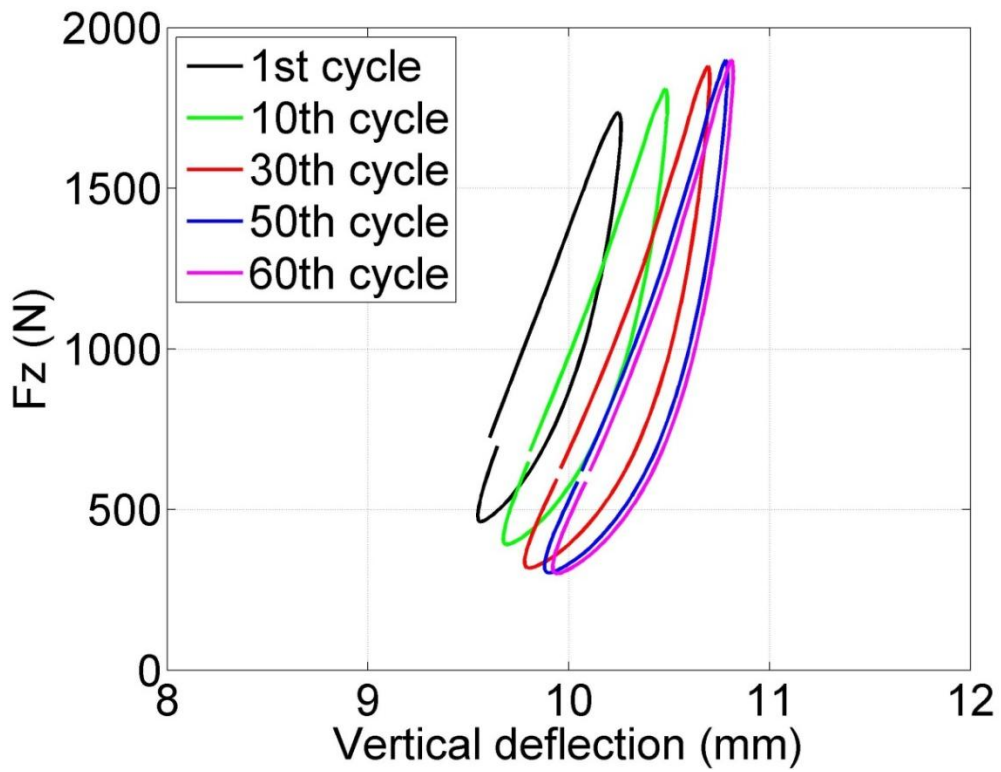


Figure 3.17: Force-deflection relationship of 10 Hz cyclic loading with 50 mm loading foot on hockey turf (18 mm thick)

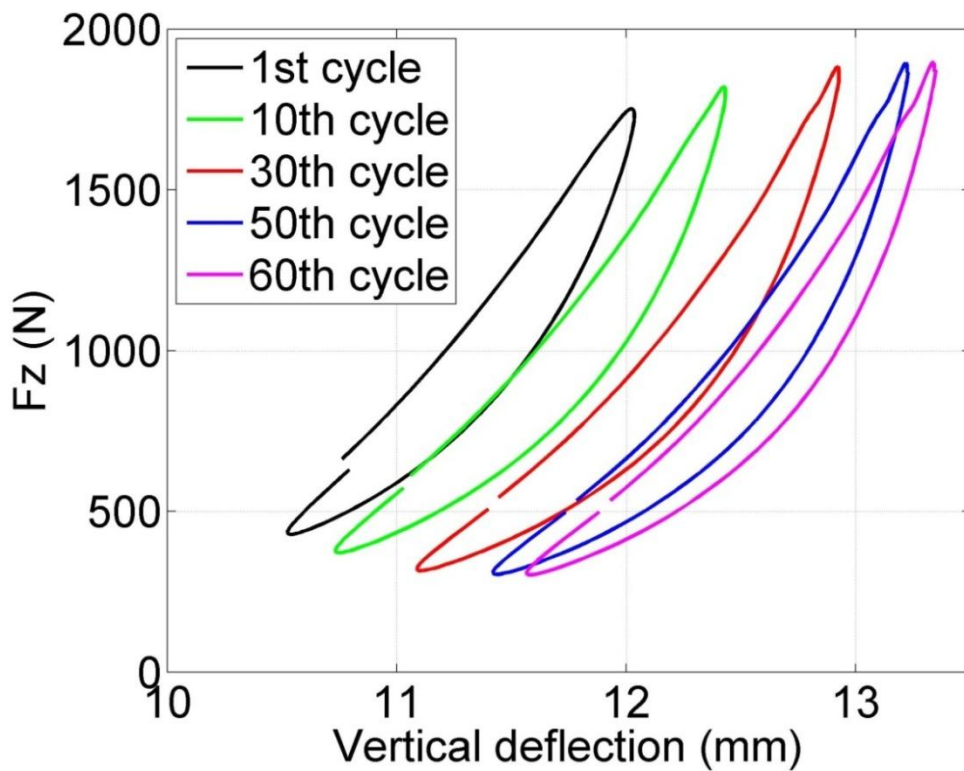


Figure 3.18: Force-deflection relationship of 10 Hz cyclic loading with 50 mm loading foot on 3G turf (35 mm infill depth)

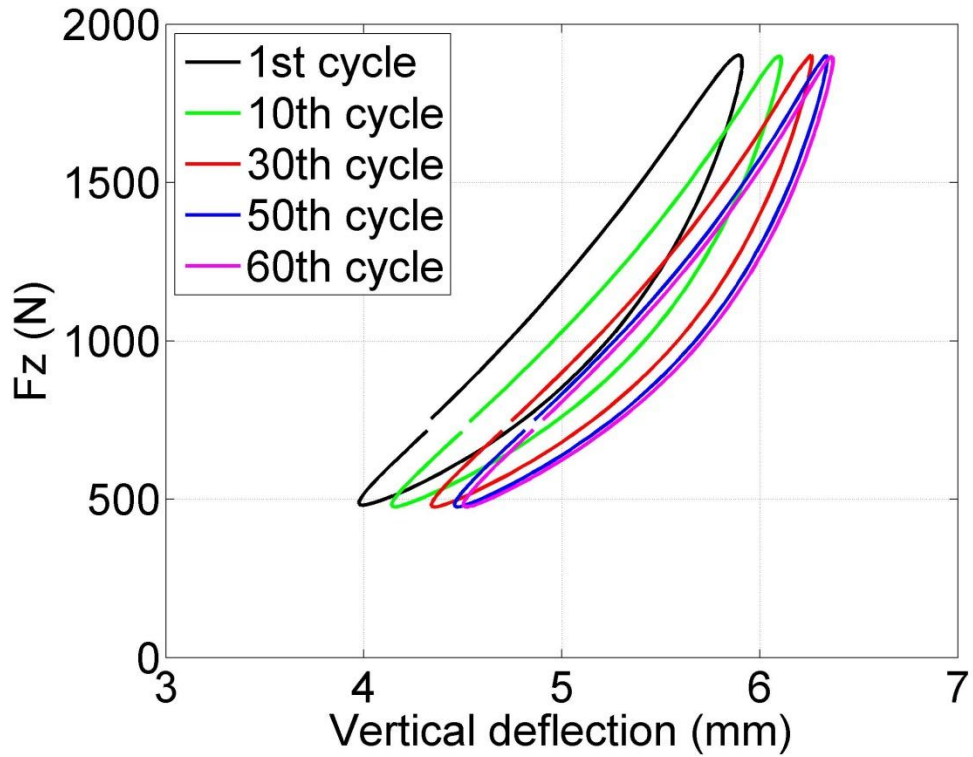


Figure 3.19: Force-deflection relationship of 10 Hz cyclic loading with 50 mm loading foot on rubber shockpad (15 mm thick)

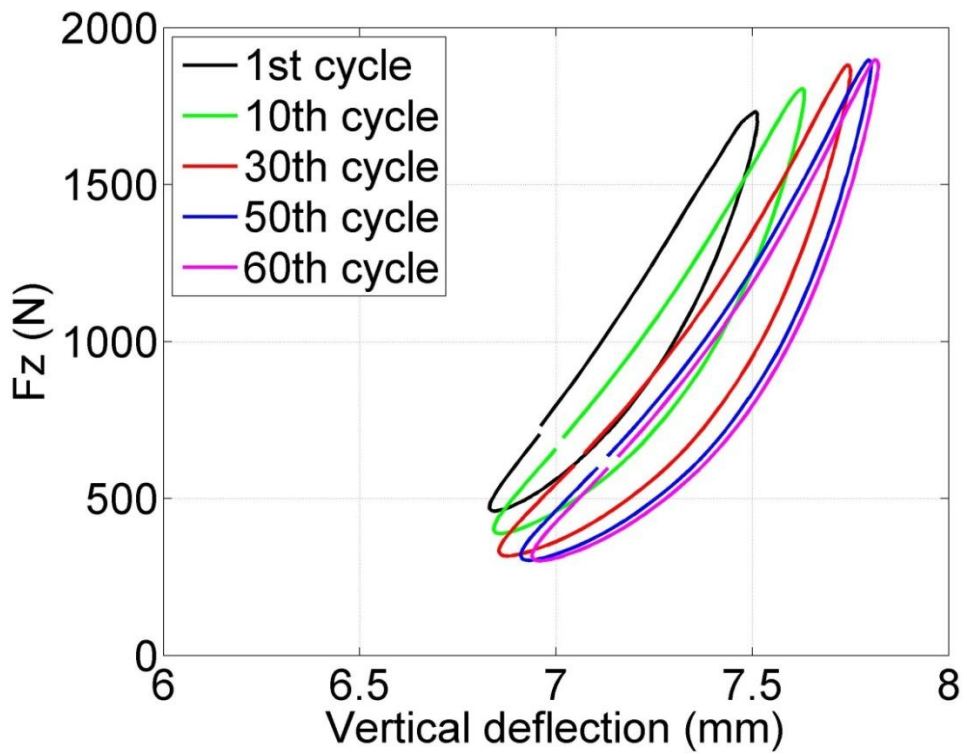


Figure 3.20: Force-deflection relationship of 10 Hz cyclic loading with 50 mm loading foot on foam shockpad (12 mm thick)

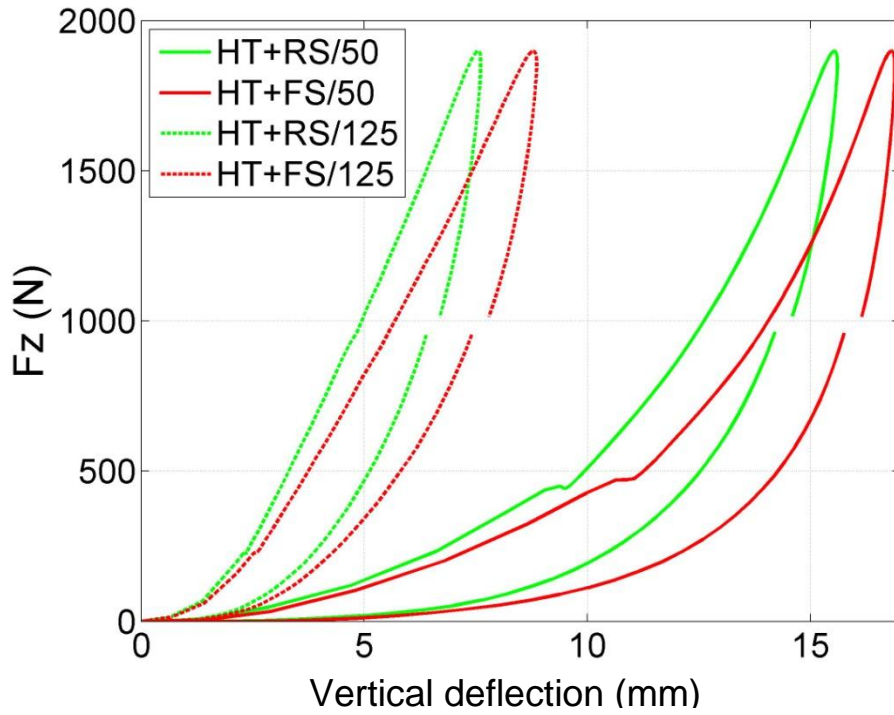


Figure 3.21: Force-deflection relationship of hockey turf with rubber shockpad system (green) and hockey turf with foam shockpad system (red) for 0.9 Hz loading with 50 mm (solid line) and 125 mm (dash line) diameters loading feet

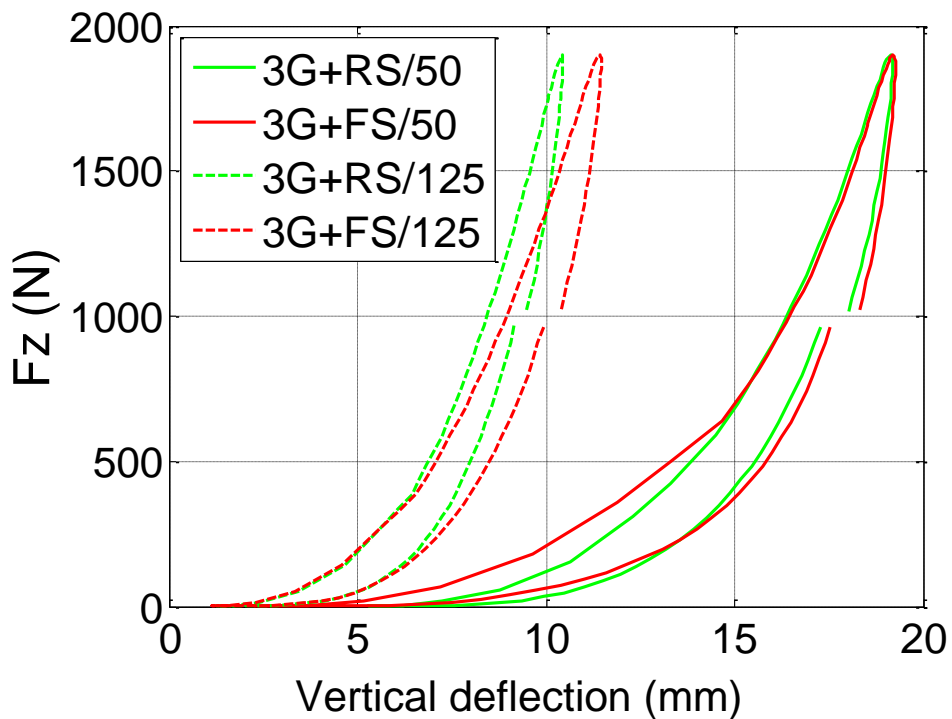


Figure 3.22: Force-deflection relationship of 3G turf with rubber shockpad system (green) and 3G turf with foam shockpad system (red) for 0.9 Hz loading with 50 mm (solid line) and 125 mm (dash line) diameters loading feet

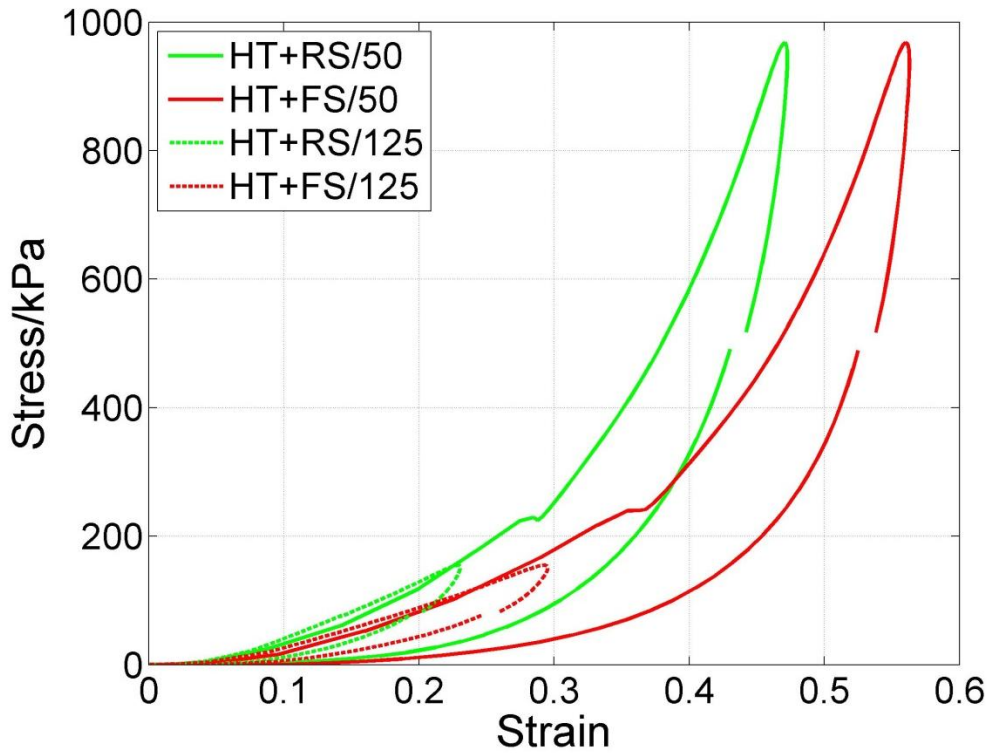


Figure 3.23: Stress-strain relationship of hockey turf with rubber shockpad system (green) and hockey turf with foam shockpad system (red) for 0.9 Hz loading with 50 mm (solid line) and 125 mm (dash line) diameters loading feet

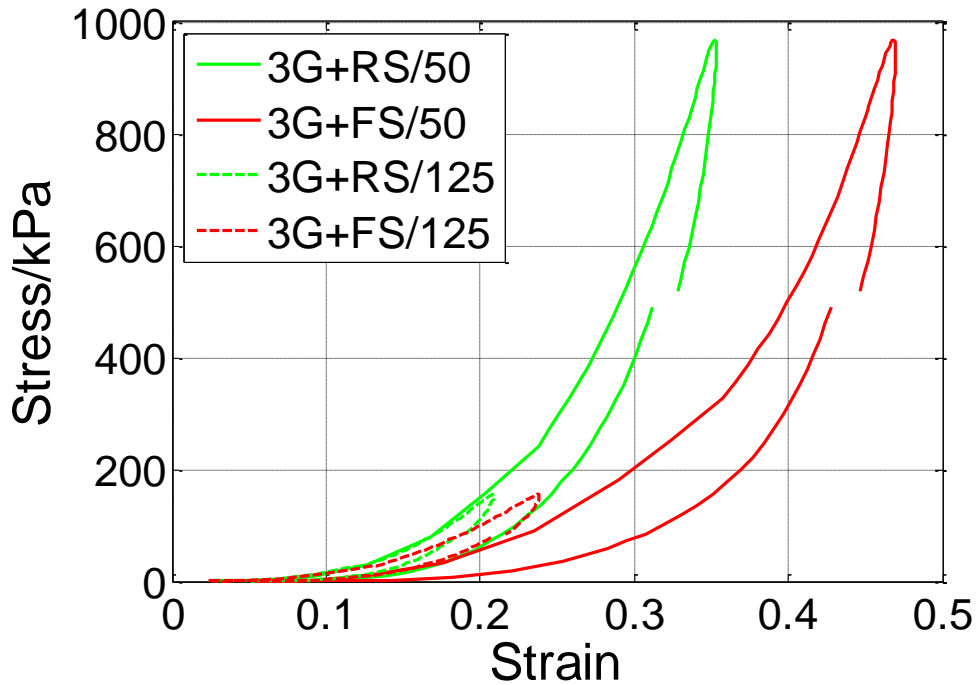


Figure 3.24: Stress-strain relationship of 3G turf with rubber shockpad system (green) and 3G turf with foam shockpad system (red) for 0.9 Hz loading with 50 mm (solid line) and 125 mm (dash line) diameters loading feet

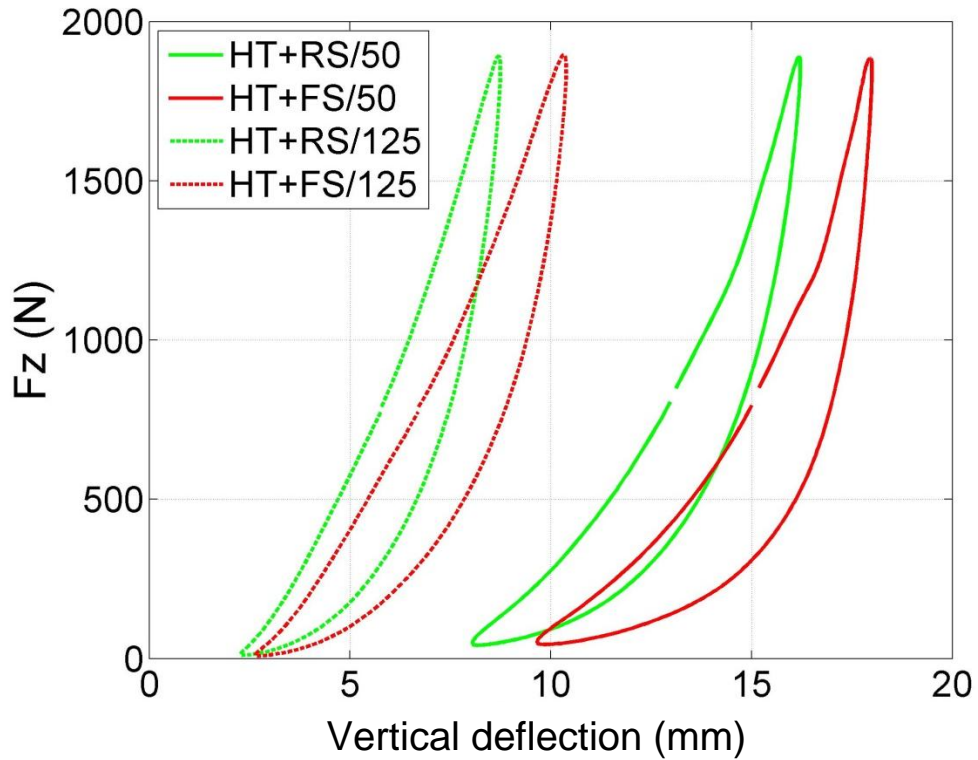


Figure 3.25: Force-deflection relationship of hockey turf with rubber shockpad system (green) and hockey turf with foam shockpad system (red) for 3.3 Hz loading with loading feet of 50 mm (solid line) and 125 mm (dash line) diameters

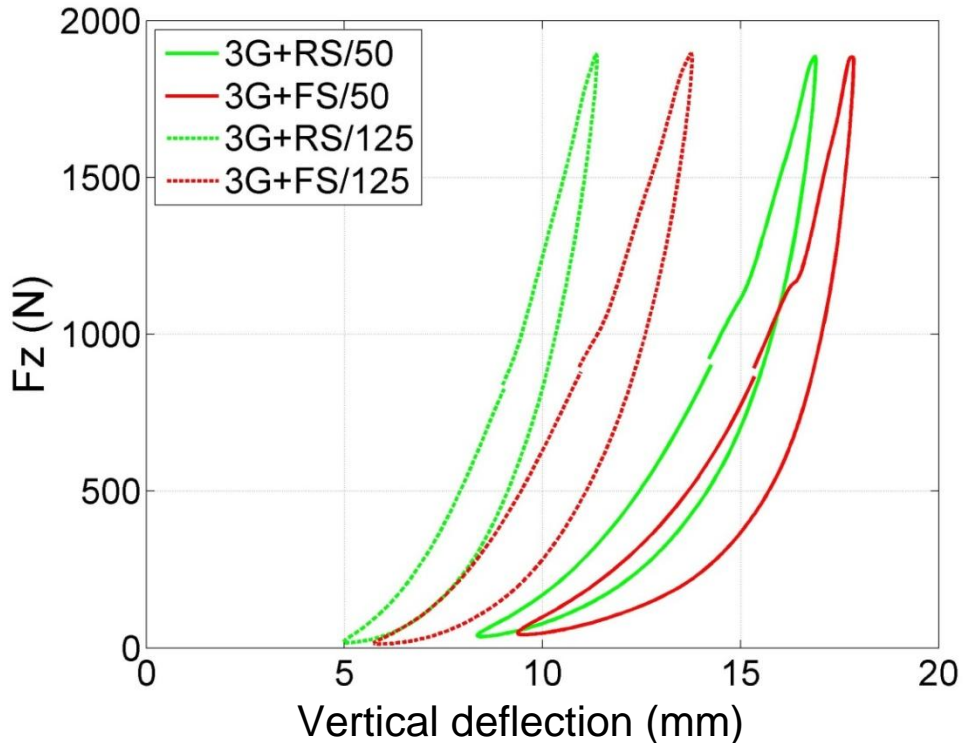


Figure 3.26: Force-deflection relationship of 3G turf with rubber shockpad system (green) and 3G turf with foam shockpad system (red) for 3.3 Hz loading with 50 mm (solid line) and 125 mm (dash line) diameters loading feet

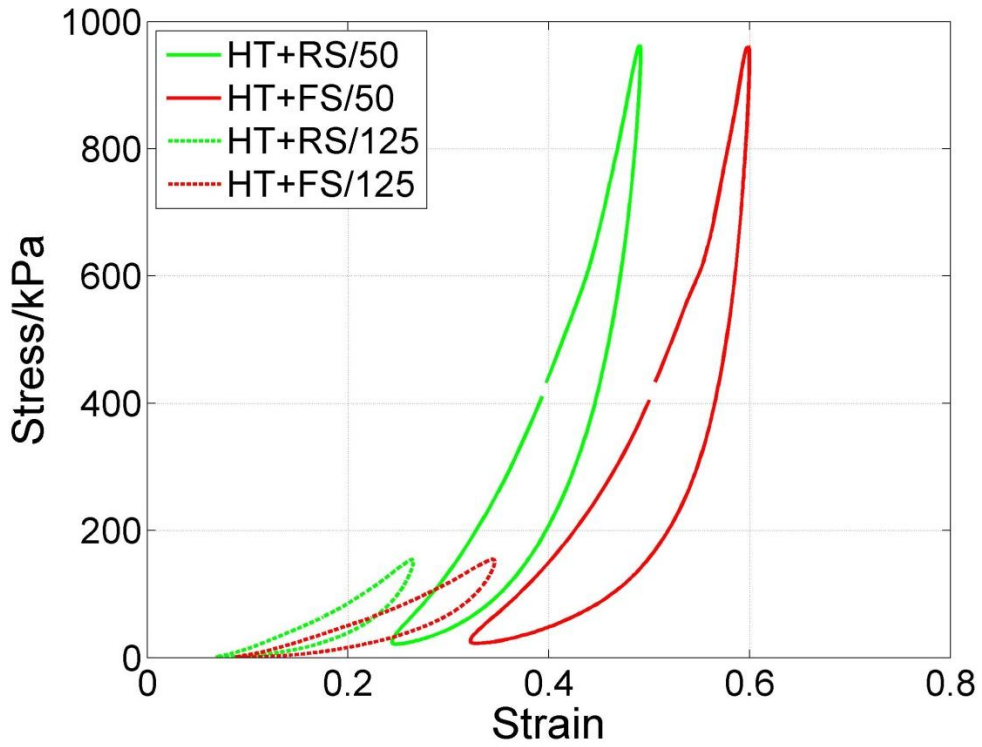


Figure 3.27: Stress-strain relationship of hockey turf with rubber shockpad system (green) and hockey turf with foam shockpad system (red) for 3.3 Hz loading with 50 mm (solid line) and 125 mm (dash line) diameters loading feet

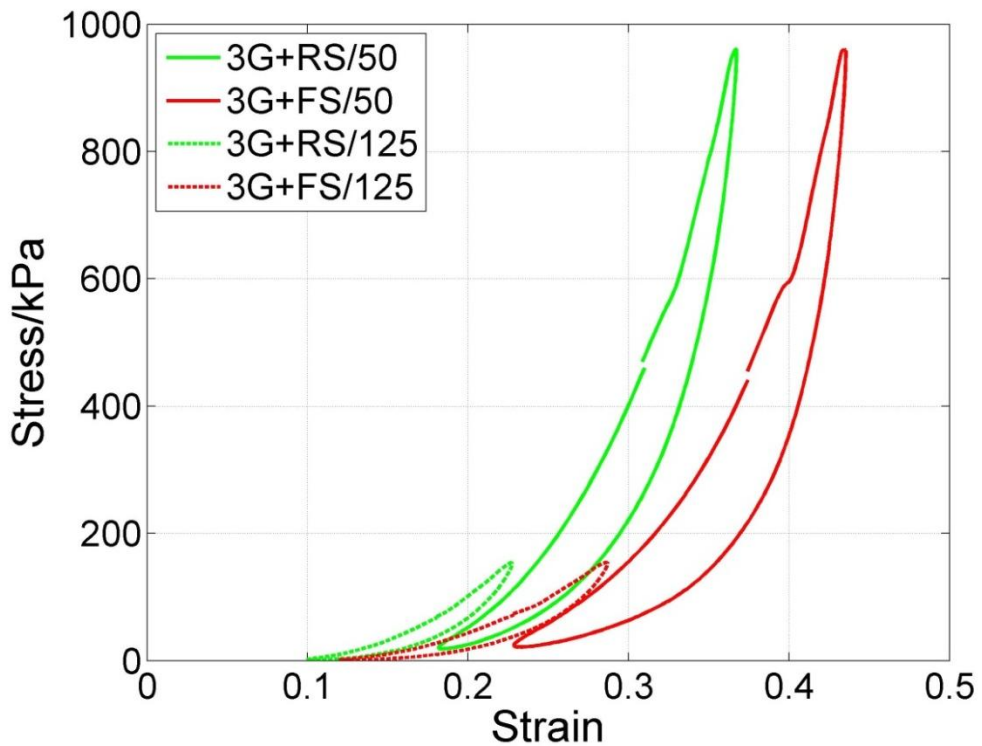


Figure 3.28: Stress-strain relationship of 3G turf with rubber shockpad system (green) and 3G turf with foam shockpad system (red) for 3.3 Hz loading with 50 mm (solid line) and 125 mm (dash line) diameters loading feet

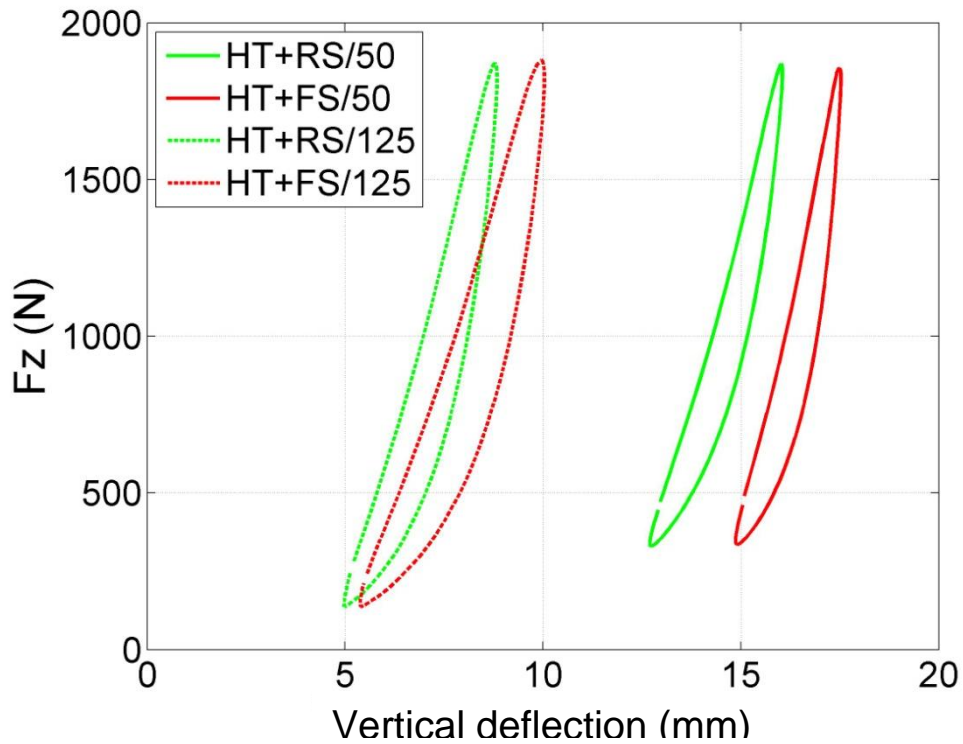


Figure 3.29: Force-deflection relationship of hockey turf with rubber shockpad system (green) and hockey turf with foam shockpad system (red) for 10 Hz loading with loading feet of 50 mm (solid line) and 125 mm (dash line) diameters

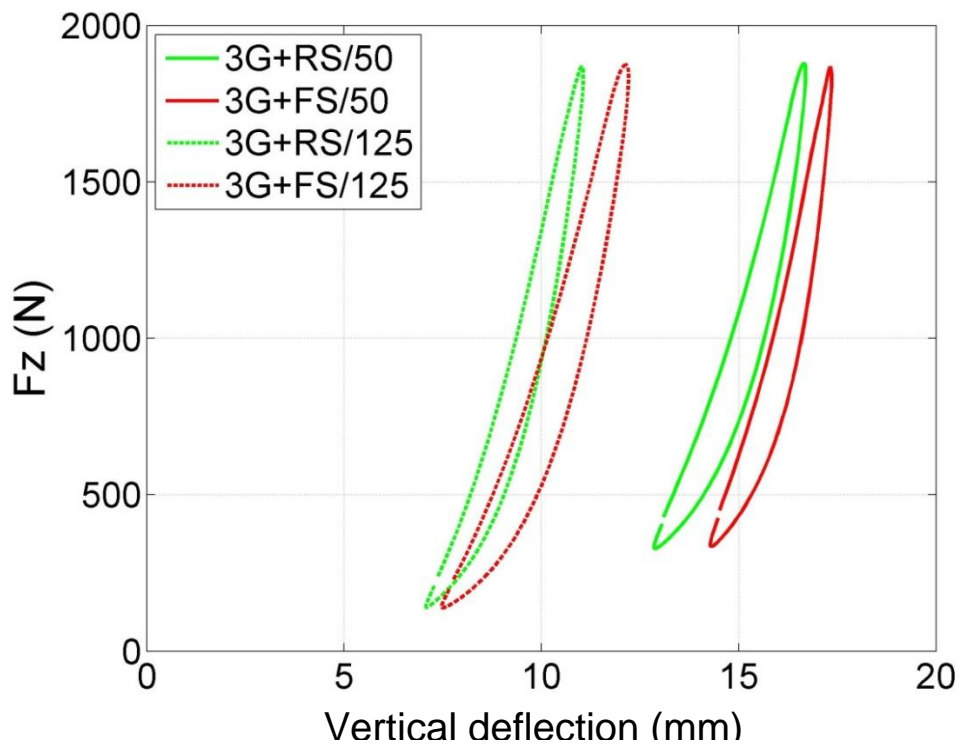


Figure 3.30: Force-deflection relationship of 3G turf with rubber shockpad system (green) and 3G turf with foam shockpad system (red) for 10 Hz loading with 50 mm (solid line) and 125 mm (dash line) diameters loading feet

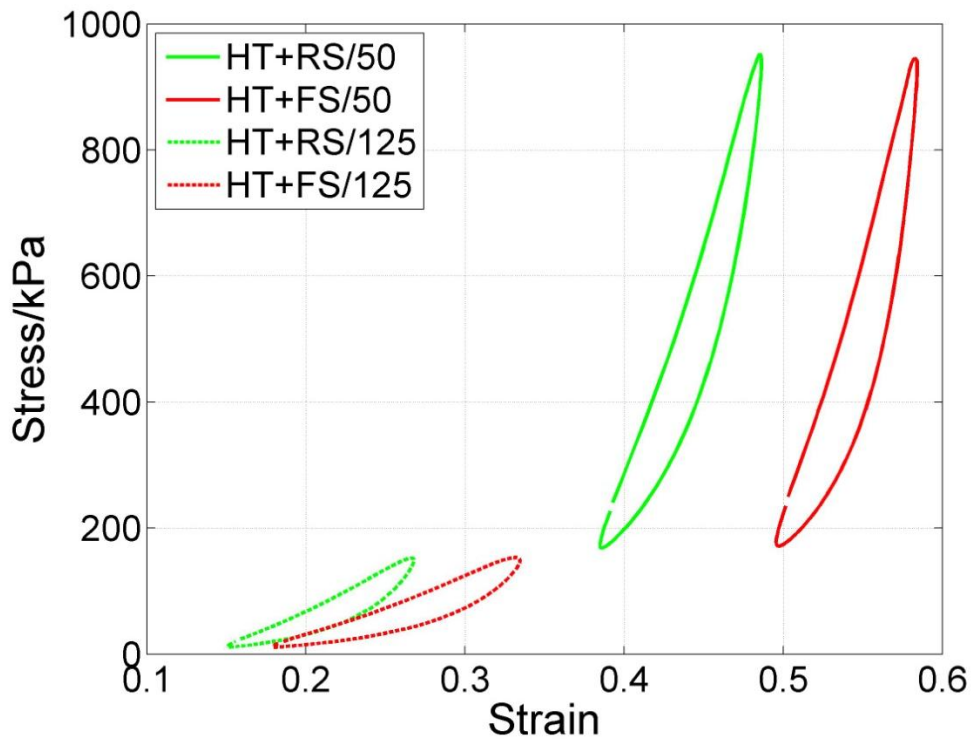


Figure 3.31: Stress-strain relationship of hockey turf with rubber shockpad system (green) and hockey turf with foam shockpad system (red) for 10 Hz loading with 50 mm (solid line) and 125 mm (dash line) diameters loading feet

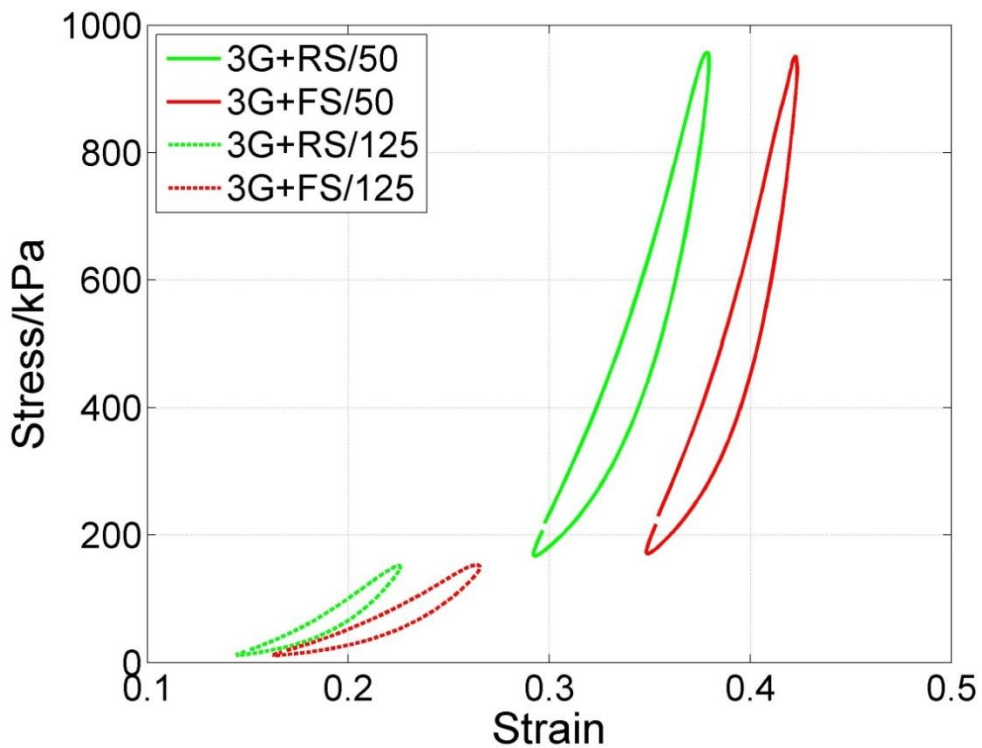


Figure 3.32: Stress-strain relationship of 3G turf with rubber shockpad system (green) and 3G turf with foam shockpad system (red) for 10 Hz loading with 50 mm (solid line) and 125 mm (dash line) diameters loading feet

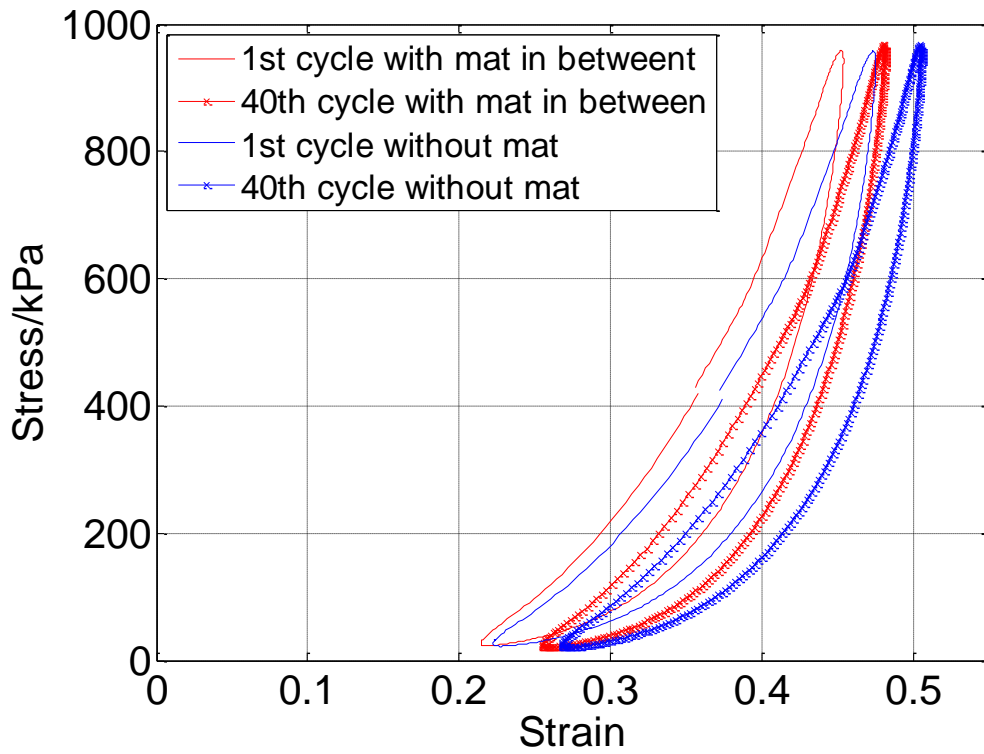


Figure 3.33: Intrusion effect of pressure mat inserted between hockey turf and rubber shockpad layers under 3.3 Hz loading at the first and last cycles

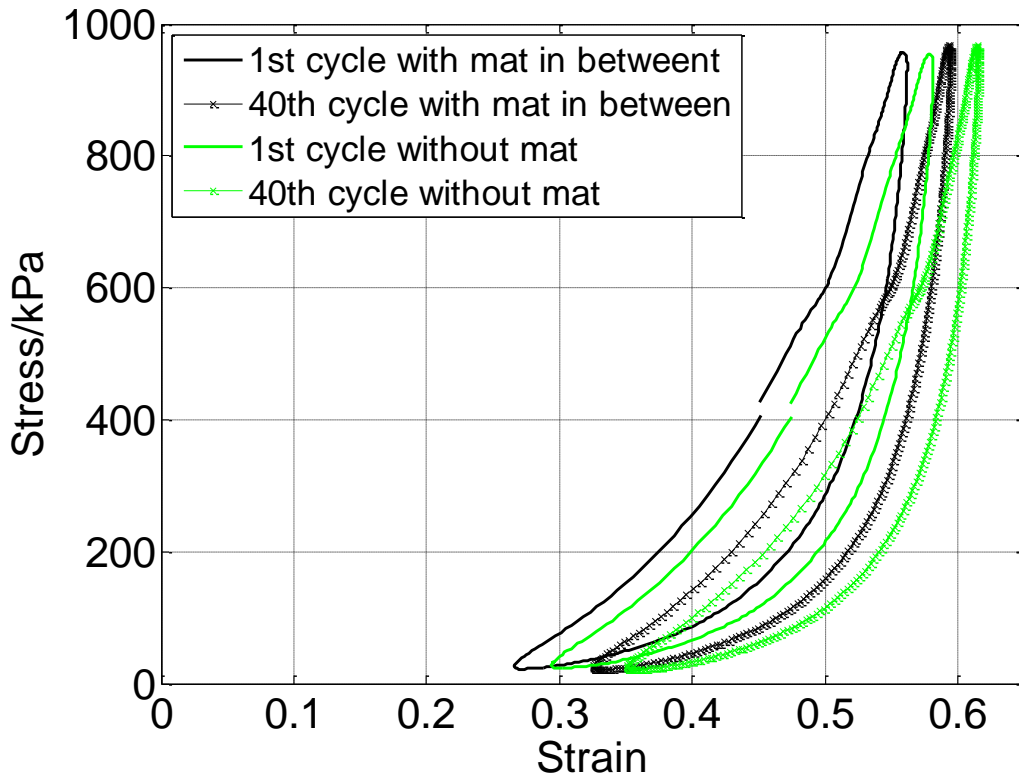


Figure 3.34: Intrusion effect of pressure mat inserted between hockey turf and foam shockpad layers under 3.3 Hz loading at the first and last cycles



Figure 3.35: Stitch lines across the backing of the 3G carpet

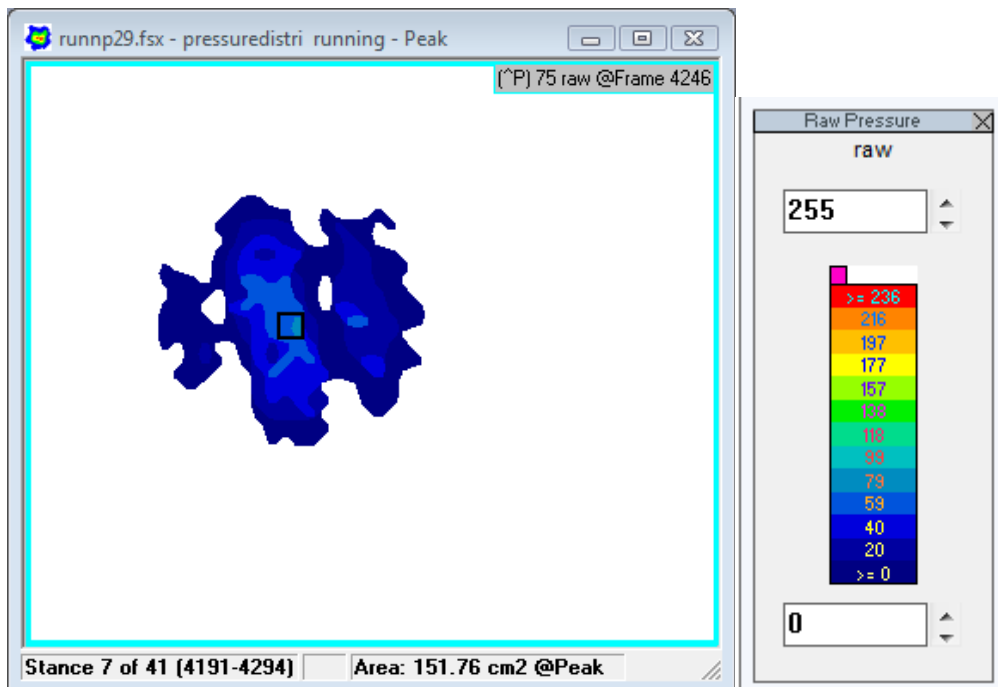


Figure 3.36: Pressure contour of 3G carpet at peak contact area under 3.3 Hz loading with 125 mm loading foot

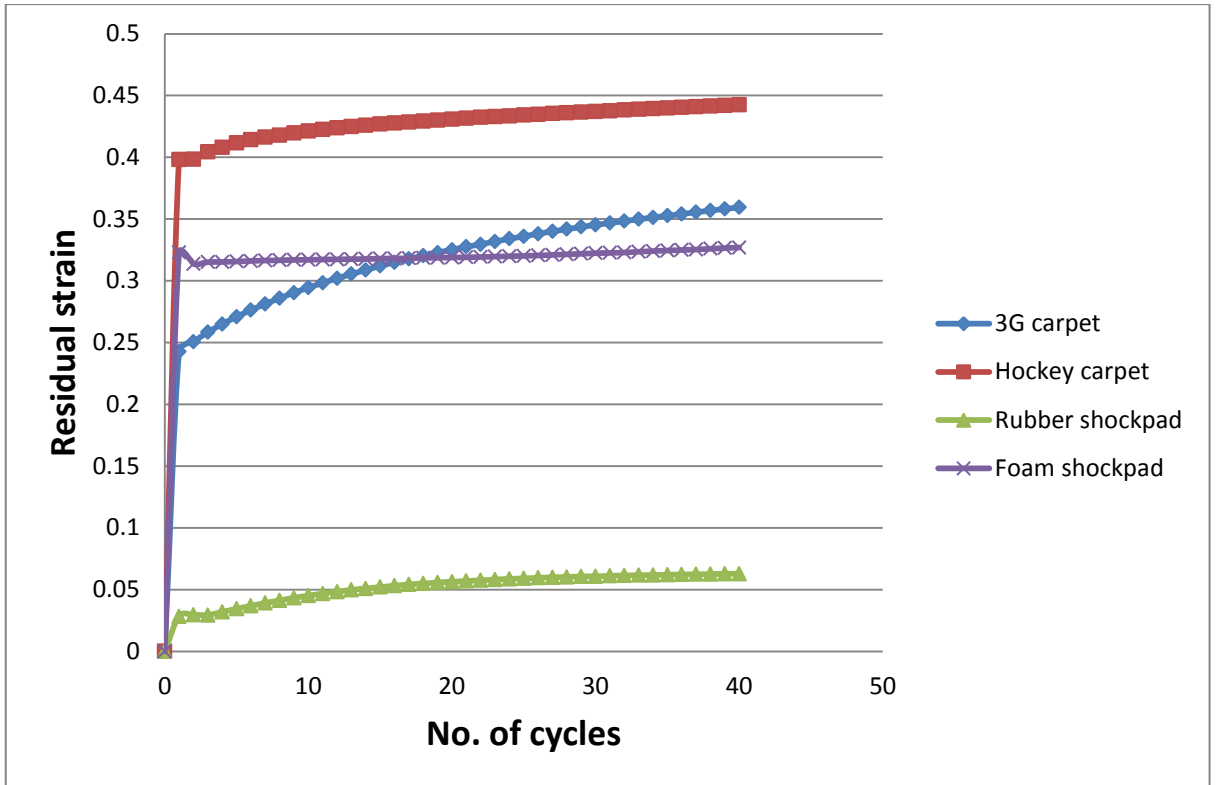


Figure 3.37: Accumulation of residual strain for the layers under 3.3 Hz cyclic loading

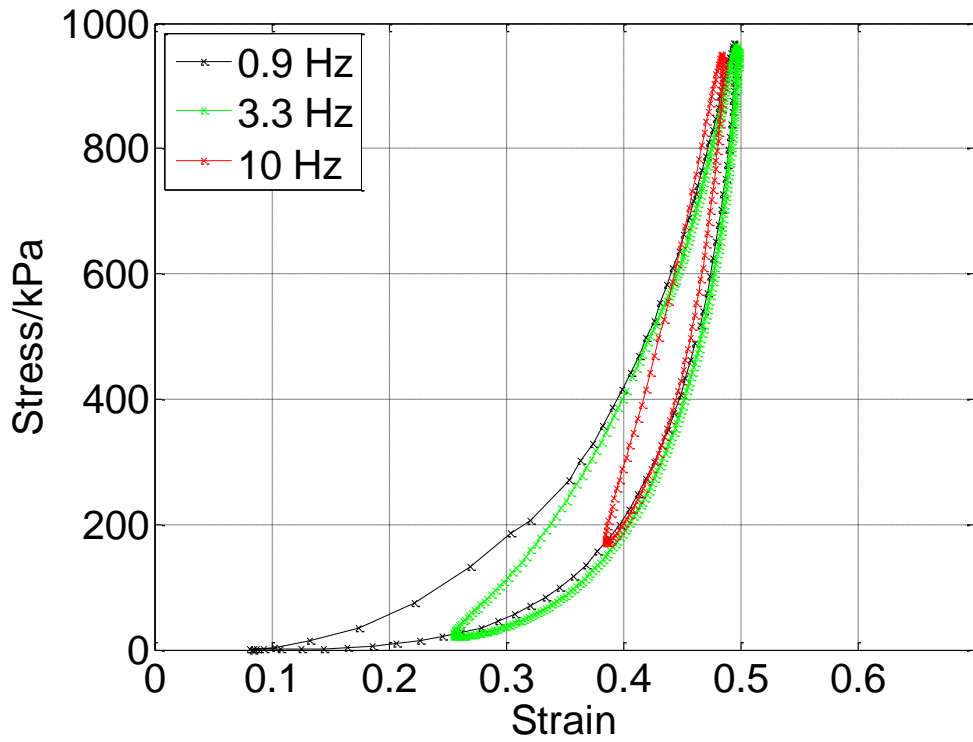


Figure 3.38: Stress-strain relationship of hockey turf with rubber shockpad system for different loading frequencies with 50 mm loading foot

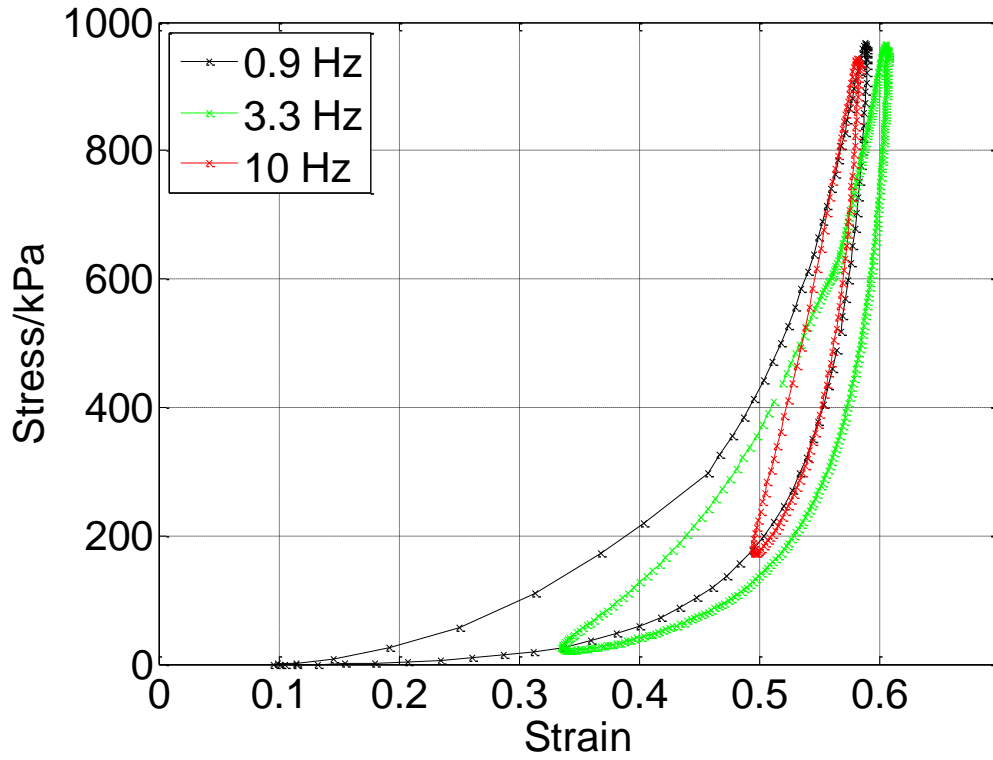


Figure 3.39: Stress-strain relationship of hockey turf with foam shockpad system for different loading frequencies with 50 mm loading foot

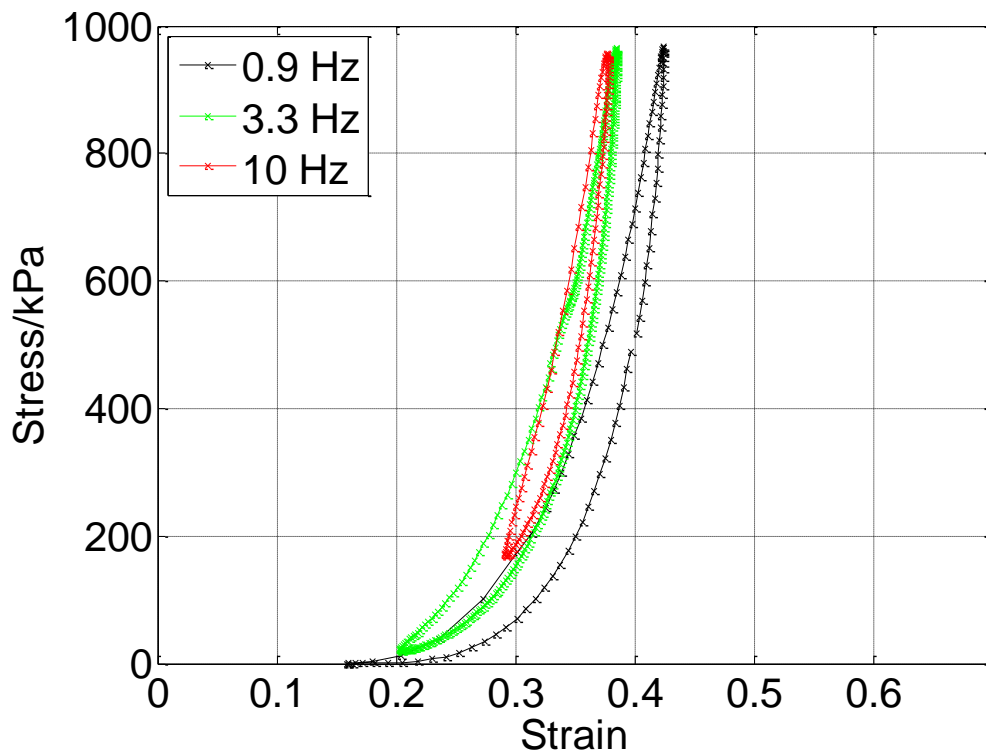


Figure: 3.40: Stress-strain relationship of 3G turf with rubber shockpad system for different loading frequencies with 50 mm loading foot

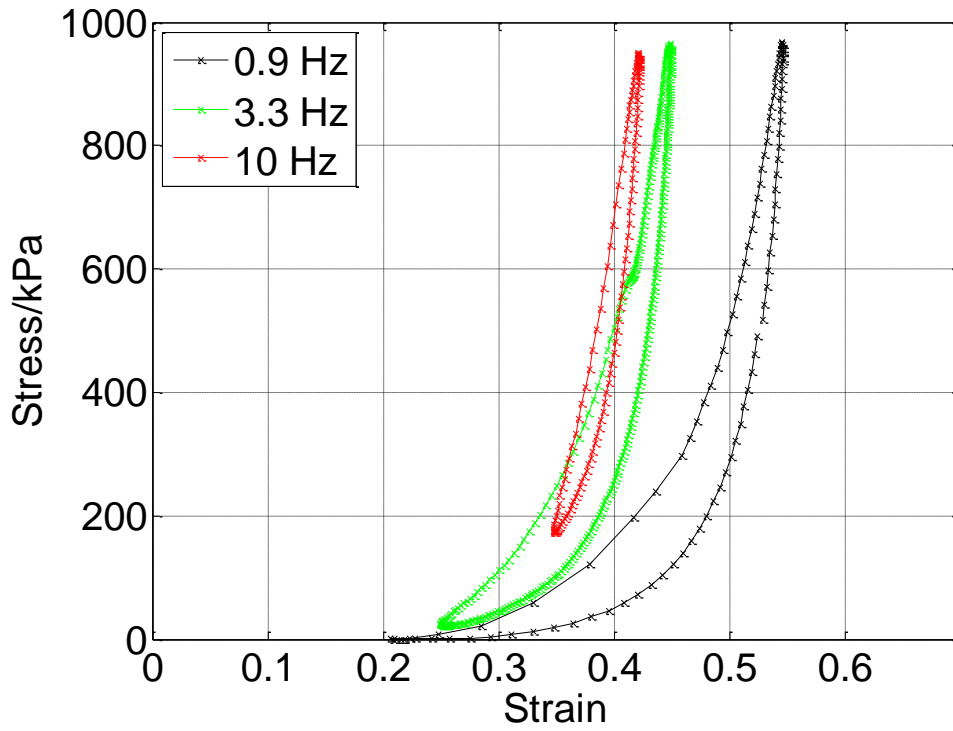


Figure 3.41: Stress-strain relationship of 3G turf with foam shockpad system for different loading frequencies with 50 mm loading foot

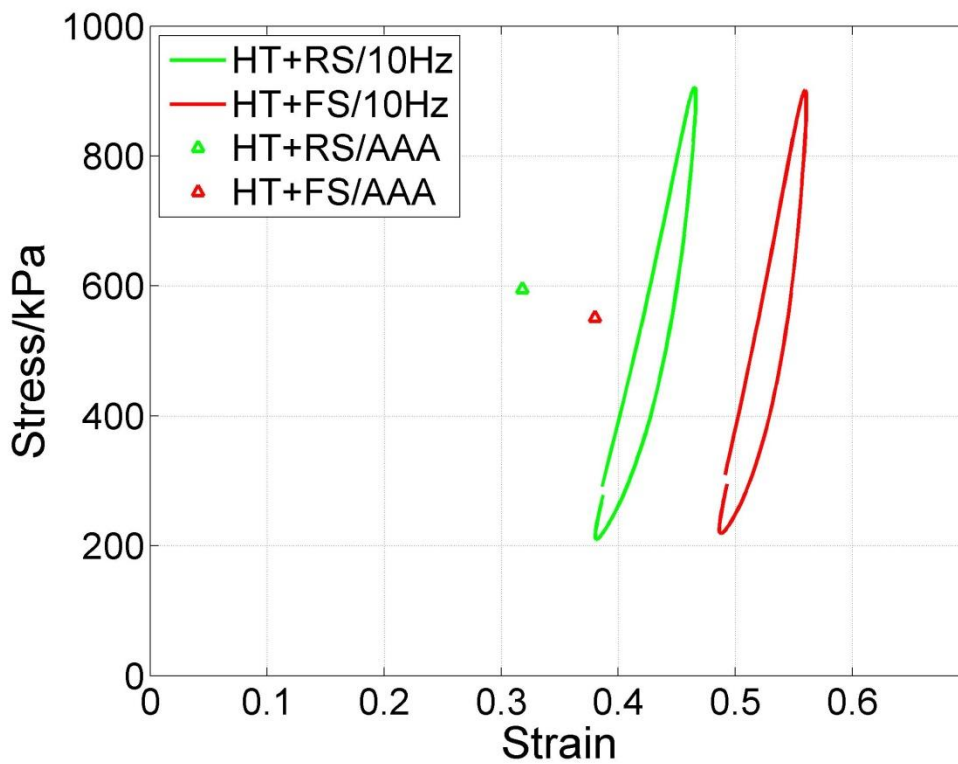


Figure 3.42: Stress-strain relationship of hockey turf systems for 10 Hz loading and the AAA impact

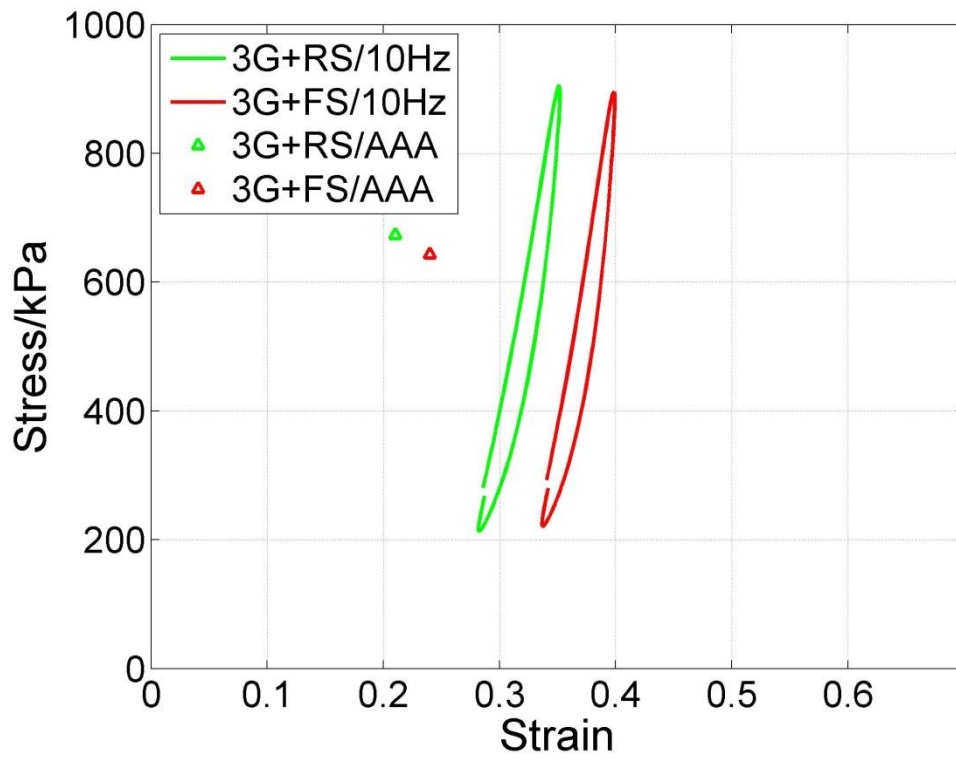


Figure 3.43: Stress-strain relationship of 3G turf systems for 10 Hz loading and the AAA impact

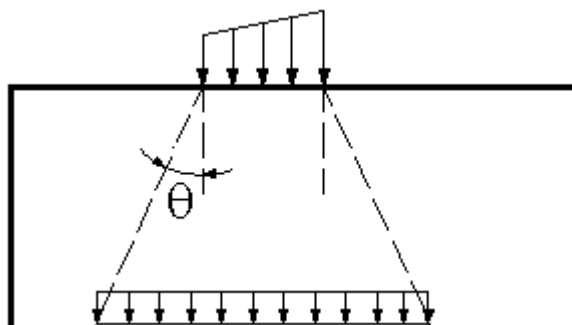


Figure 3.44: Stress distribution angle Θ through surface

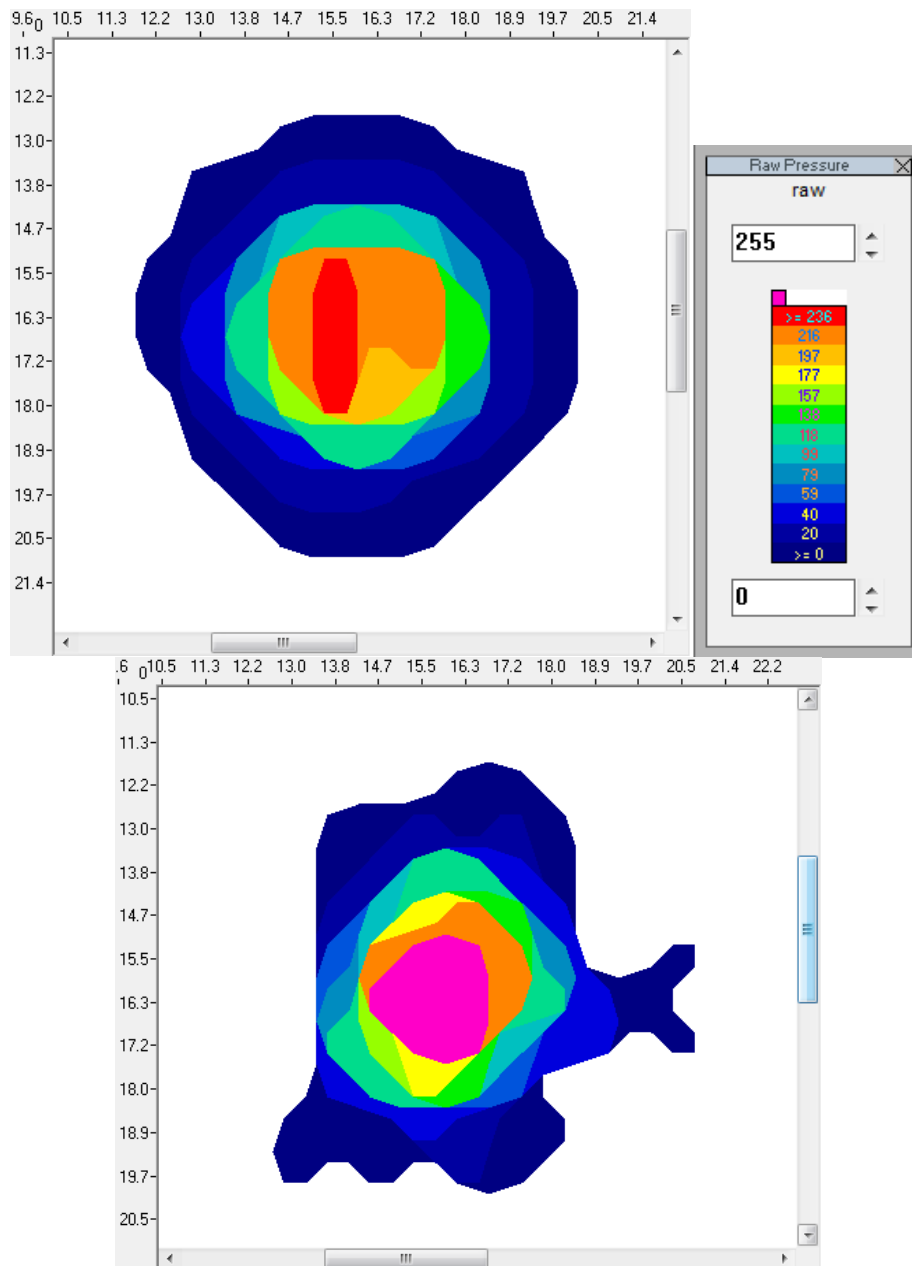


Figure 3.45: Pressure mappings for hockey turf (above) and the 3G turf (below) under 50 mm diameter loading foot

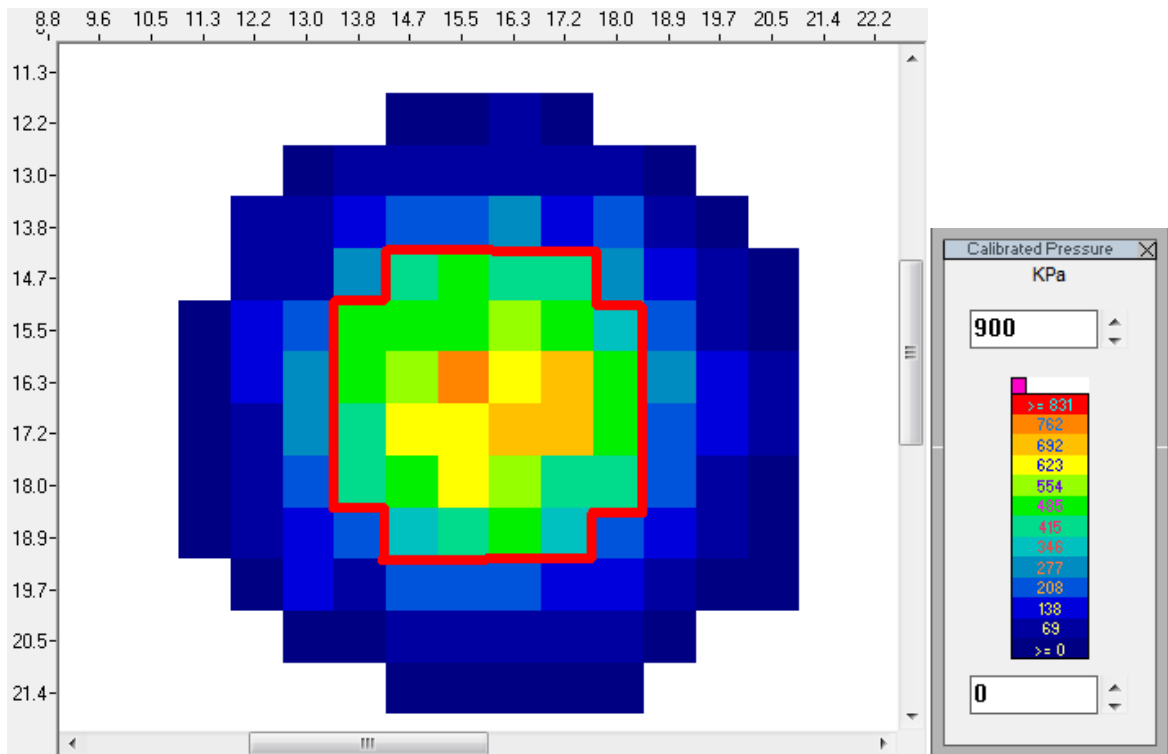


Figure 3.46: Pressure contour at peak stress of 3.3 Hz compressive loading recorded at the bottom of hockey turf + rubber shockpad system under 50 mm diameter loading foot. The high pressure region is displayed by warm colour cells and outlined by the red line.

4. Mechanical behaviour of artificial surface systems under player loading

4.1 Chapter overview

The mechanical behaviour of artificial turf surface system in response to real player loading was not well documented in literature. Previous research of surface system behaviour is mainly based on mechanical compression or impact tests to simulate specific player movement patterns. There is also little published literature surrounding the surface system behaviour at each instant of time throughout a human loading event, and quantifying the surface deformation or load distribution in the system.

This chapter focuses on the development of an experimental programme to investigate the behaviour of four different surface systems under three real-time player movements. This addresses objective 4 of this thesis (Chapter 1). The response of individual surface system under each player movement was analysed from its stress-strain relationship by measuring the force applied and resulting surface deflection. The thin film pressure sensor was used to determine the pressure distribution through the surface system. Results from this chapter are then compared with the mechanical loading measurements (Chapter 3) in Chapter 5.

This chapter is divided into four sections. The experimental methodology section describes the testing programme design and equipment used. Results are then presented including the data analysis methods employed and the identified limitations of this experiment programme. Lastly, the results are discussed to explain the stiffness response and stress distribution in surface system under player loading.

4.2 Experimental methodology

4.2.1 Surface systems

The same four composite carpet-shockpad systems (HT+RS, HT+FS, 3G+RS and 3G+FS) presented in Chapter 3 were used in this player loading experimental programme. Surface samples were cut into the size of 600 mm * 400 mm to fit the size of the FP. The details of the products are listed in Table 3.1. The 3G turf carpet preparation followed the same rule as in the mechanical loading experiment programme. 2.4 kg (10 kg/m²) sand and rubber infill materials were used to fill the carpet sample respectively. The sand and rubber were laid evenly to the carpet in 1.2 kg increments. After each increment the filled material was then further spread and settled down into the carpet by hand (Severn, 2010). The infills

were raked after the specified filling amount reached until the surface visually even. Two filled 3G turf carpets were prepared at least one day before testing for infills stabilisation without conditioning using a weighted studded roller.

To assess the uniformity and repeatability of the 3G turf sample preparation, the infill depth and force reduction by the AAA were measured in multiple locations illustrated in Figure 4.1. Before player loading tests, five infill depth measurements were taken at each location and then averaged. The player was instructed to make foot contact near the centre of the sample. Hence three test locations along the longitudinal axis of the sample were determined for force reduction measurement before player loading tests. Standard FIFA test procedure applied, three drops by the AAA on the same location were recorded. The percentage force reduction value was reported as the average of the second and third drops. After all the player loading trials finished, the infill depth and force reduction measurements were repeated at the same locations to assess the infills condition and surface system property changes before and after the player impacts. The averaged infill depth and force reduction measured in each test location of the 3G turf surface systems before and after player testing are listed in Table 4.1. The heights of the hockey turf with rubber shockpad and with foam shockpad were 33 mm and 30 mm respectively. For both hockey turf systems, force reduction measured before and after player testing remained the same, 69% for HT+RS and 71% for HT+FS.

4.2.2 Player, shoe and movement patterns

Previous biomechanical studies indicated that the same instructed movement performed by multiple subjects generated different kinematic results due to their different movement habits (Korhonen, 2010; Stiles and Dixon, 2007). Therefore, depending on the focus and purpose of the research, it is necessary to minimise the number of subjects (players) if it encourages variability. The purpose of the present study was to analyse the mechanical behaviour of the surface systems under the loading from player ‘in-game’ movements. The biomechanical responses of players to different surface systems or players’ performance comparison were not considered in this study. Hence, an amateur level player with regular training and match playing experience on artificial turf pitch was selected to perform three typical ‘in-game’ movements across four different surface systems.

One 26 year old injury-free male (body weight: 80 kg, height: 1.85 m) provided informed voluntary consent to join this experiment programme in accordance to the protocol

designed by the Loughborough University Ethical Advisory Committee. The subject played on the 3G turf pitches at least two hours per week. The boots worn by the player were soccer boots designed for artificial turf pitch with moulded rubber studs on the outsole (Nike FTII 5, Figure 4.2) in UK size 10. These boots were used in the testing mainly because noticed from a pilot experiment, their large number of shorter moulded studs (nubs) configuration comparing with other boots with cleats and blades generated larger contact areas under player foot strikes instead of only few high pressure spots under several large studs. The short multi stud configuration was also similar to the hockey boots designed for artificial hockey turf surfaces, so was deemed appropriate for both surfaces.

The shod player performed three basic movement patterns involved in sports: heel-toe walking, forefoot running and forefoot single leg drop jump landing. The mechanical behaviour of the four selected surface systems was analysed under the three player loading patterns. Heel-toe walking is one of the most basic human movements, consists of two peaks of vertical impact force from heel strike and push-off respectively. In order to generate a higher single peak in the vertical impact force and shorter boot-surface contact time, the running pattern with forefoot strike was selected. Landing practised by the player was jumping off from a 20 cm height deck and single leg landed on the forefoot with bended knee. Forefoot landing was intended to apply a player loading to the surface systems with the least force in horizontal directions compared with the other two movement patterns (Yeow et al., 2009).

Due to the size of the pressure mat sensing area (436 mm * 369 mm) it was only possible to record data of one foot strike for all these movements. For walking and running, the player was informed to make a left foot contact with the target surface without adjusting his movement stride and rhythm. To prevent the player altering his natural walking and running motions to hit the target area with left foot, practice trials for each movement were taken prior to the trials for data collection. Marks were made on the laboratory floor during the practice trials to help the player to hit the instrumented surface sample naturally with the desired foot. The equipment used and measurement set-up are described in Section 4.2.3.

To compare with the mechanical loading measurements, the magnitude of peak vertical impact force and foot contact time of each movement pattern were controlled to select 4 successful trials with each surface system condition. The maximum vertical impact force

for walking was required to be in the range of $900 \text{ N} \pm 10\%$. The peak vertical impact force for forefoot running and landing was controlled within the range of $1900 \text{ N} \pm 10\%$. Testing was carried out in four days over a period of two consecutive weeks (2 days in each week) with one surface system per day. A pilot experiment was undertaken in a month before testing to ensure that the player was comfortable and confident to practise the required movements in the laboratory. Prior to each test session, the player performed basic warm-up based on his own standard routines. In the pilot experiment, the walking and running speed was measured and informed the player to help generate the required peak force. The benchmark speed of walking and running were 1.6 m/s and 2.7 m/s ($\pm 5\%$) respectively for successful trials.

4.2.3 Equipment & measurement set-up

4.2.3.1 Force/pressure measurement devices

Force plate

The Kistler 9821B FP was used, as that in the mechanical loading test (Section 3.2.3.3) programme, to define the ground contact phase and calibrate the pressure mat. Force data was collected in 'x' medial-lateral (M-L), 'y' anterior-posterior (A-P) and 'z' vertical, 3 components. Centre of pressure (CoP) position during the foot impact event was recorded. The sampling rate was set at 1000 Hz. Force and CoP data recorded for each trial were saved and exported to .csv files. The FP was situated flush within the laboratory floor under the surface systems. The layout is presented in subsection 4.2.3.3.

Pressure mat

The same Tekscan Matscan transducer with VersaTek system used in the mechanical loading test programme (Section 3.2.3.2) was also applied in the player loading experiment programme. It provided contact area and pressure information versus time about the player's walking, running and landing throughout the duration of the ground contact. The thin mat transducer is flexible and able to deform along with its contact surface in the testing environment. As the carpet-shockpad surface system was built on top of the FP, the pressure mat was inserted at the carpet-shockpad interface and under the surface system respectively, as shown in Figure 4.3. The pressure mat was used here to illustrate how the pressure applied on top of the surface system developed and was distributed over the enlarged contact area as it penetrated through the layers. The highest sampling rate at 440 Hz was used. Two-load Frame Calibration was performed for the pressure mat under each

surface system placed flat on the FP, loaded by each movement pattern, using the corresponding instantaneous vertical force reading from the FP as explained in Section 3.2.3.2. Pressure and contact area values recorded for each trial were exported to .csv files and pressure contour graphs for further analysis.

4.2.3.2 Motion analysis systems

Vicon system

Vicon is a passive motion analysis system which tracks the motion of retroreflective markers and reports their 3D locations in real-time using cameras with LEDs (Tsu, 2010). A network of 12 MX cameras operating at the frame (sampling) rate of 500 Hz was used in this research, as the layout shown in Figure 4.4. After all the cameras were placed facing the motion capture space and the zoom and focus were adjusted, a two-stage calibration process was conducted. Firstly, during the dynamic stage of the system calibration, a 5-marker T frame wand was waved around in the capture volume ensuring the markers on the wand visible to the cameras until enough wand counts were taken and spread evenly across the viewing field of each camera, the Vicon Nexus software (1.7.1) calculated the physical position and orientation of each camera. When the progress bar indicates the complete of the dynamic stage of calibration, the image error of each camera needs to be less than 0.3. The purpose of the dynamic stage is to describe the capture volume to the Vicon system (Vicon, 2007). Secondly, in the static stage of calibration, the T frame wand was placed in a corner on top of the FP to set the global coordinates system for the capture volume as illustrated in Figure 4.5.

A pilot experiment was carried out to determine the position of markers on the left boot. In order to measure the vertical deflection of the surface system underfoot, three 14 mm diameter markers were attached to the forefoot and rearfoot of the player's left boot respectively, as shown in Figure 4.6. The player touchdown technique and CoP trajectory of the movement patterns were studied. In the forefoot running and landing movements, it was noticed that the left foot touchdown happened first at the metatarsals towards midfoot and the CoP at the peak vertical force also located at this segment. However, the 3 markers around forefoot in Figure 4.6 only covered the phalangeal segment, so the vertical deflection of the surface system at touchdown and under the peak vertical force could be miscalculated. In accordance with the Heidelberg Foot Measurement Method (Simon et al., 2006), an improved markers configuration around forefoot and rearfoot was used. Two

more markers were added to both sides of the metatarsals and other two more markers were attached to both sides of the calcaneus towards the midfoot, as in Figure 4.7. All the markers used were placed at least 2.5 cm apart from each other to avoid the confusion of the Vicon system to identify each marker. Every marker attached must have a unique identification in order to be tracked by the Vicon software within the capture volume. A generic kinematic model, Vicon Skeleton Template (VST) file was created prior to data collection by the software. It described the relationship between foot segments and the markers attached to the boot of player. The name of each marker (Figure 4.7) and the relationship between markers were programmed and saved as a separate .vst file (Toon, 2008). The created VST file was referenced for each trial, facilitating the post processing of captured data.

Vicon captured data was automatically stored in a database with separate session for each surface system and individual trial for each loading event. By referring to the VST file, raw trial data was reconstructed within the software to automatically create 3D labelled markers and trajectories. The reconstructed and labelled trial data was cropped down to the 'region of interest', which was the ground contact phase in this study. The markers trajectories were reviewed to check if there was any gap or spurious data point. With high frequency sampling rate captures over 250 Hz, it is common to have gaps or spurious data points in the trajectories in a trial (Toon, 2008). Small gaps less than 5 frames were filled automatically by the software. Larger gaps or reoccurring spurious data points were required for manual procedures. There are two gap-filling tools provided by the software. Spline fill tool uses data before and after the gap and generates a smooth interpolation to complete the trajectory. Pattern fill tool requires an alternative marker to be selected as reference and fills the gap based on the data before and after this region (Vicon, 2007). The fully labelled marker trajectories without gap were then exported into American Standard Code for Information Interchange (ASCII) and .c3d files for Matlab post-processing.

High speed camera

The Photron FASTCAM SA1.1 (Photron Limited, Tokyo, Japan) high-speed camera system was used to provide synchronised high speed video (HSV) footage for each trial. The camera was orientated laterally to the surface system and captured at 500 frames per second at its full screen resolution of 1024 * 1024 pixels. Extra lighting was required to illuminate the foot contact area to obtain high quality images, as shown in Figure 4.8.

The camera was connected with a laptop with a LAN cable. The calibration and capturing were conducted through the Photron Fastcam Viewer (3.0) software. To maximise the image quality, a calibration (image initialisation) was executed. By using the lens cap to cover the lens, the resultant black image was employed as a correction standard to correct the output value for each pixel. Recording was first stored in a built-in processor until the user selected the required duration (frames) to save to hard disk, in .avi form.

4.2.3.3 Measurement set-up

The experiments were carried out in the biomechanics laboratory at the Sports Technology Institute, Loughborough University. A total 10.6 m long straight runway was used for the player practising the movements. The surface system with pressure mat installed was placed on top of the FP fixed with double-sided tape on the edges. According to the manufacturer's suggestion, double-sided tape needs to be used avoiding the sensing area and cables across the Tekscan pressure mat. Hence the pressure mat was affixed at three locations, two corners at the bottom and the middle point at the top under the L shape connector, as in Figure 3.3. The first 8 m of the runway prior the FP was designed to provide enough distance for the player to achieve the required walking and running speed and approach the FP naturally. Behind the FP, a 2 m runway was reserved to allow the player to decelerate and stop safely. Two sets of reflective laser timing gates were aligned in front and behind the FP at 5 m apart. The speed of walking and running trials was controlled at 1.6 m/s and 2.7 m/s ($\pm 5\%$) respectively. A picture of the laboratory set-up is shown in Figure 4.9. The use of a multi-output TTL trigger box (Figure 4.10) enabled the synchronisation of the Vicon, FP, Tekscan pressure mat and high-speed camera.

Before taking the dynamic trials on each surface system, a static trial with the player standing still alongside the FP on the laboratory floor (the floor was at the same level of FP) wearing the boot with markers on was recorded by Vicon. As shown in Figure 4.11, the markers were identified and labelled according to the arrangement previously defined in the VST file. The dynamic trials of three movement patterns were first practised on the surface system with the pressure mat under the shockpad layer, on top of FP. Then the player repeated the three movement patterns when the pressure mat was sandwiched between the carpet and shockpad layers. Four valid trials of each movement pattern on each surface system instrumented with pressure mat at each interface were recorded (Table 4.2) according to the requirements stated in Section 4.2.2, giving a total of 96 trials. The markers' trajectories during ground contact were recorded by Vicon and used to determine

the surface system vertical deflection in further analysis. Impact forces, contact duration and CoP position were measured by the FP and the vertical force was also used to calibrate pressure mat. Contact area and pressure distribution data (and contours) between and under layers of surface system were provided by the Tekscan pressure mat. Synchronised HSV footages were obtained for each trial to analyse the player's foot strike techniques (boot segment plane angle) and track if there was any wobble or local displacement of the markers due to the deformation of the football boot. A summary Table 4.3 linking the measurement methods to the results is presented.

4.3 Results

This section presents the data determined from the measurement set-up described in the previous section. The results of FP measurements of player loading on different surface systems and HSV footage are used to describe the movement patterns in subsection 4.3.1. Then categorised by each movement pattern, further analysis of data from Vicon, FP and pressure mat is presented in subsection 4.3.2 to report the vertical deflection, force-deflection and stress-strain relationship of surface system under player loading. Finally, subsection 4.3.3 shows the pressure distribution at different interfaces of surface system.

4.3.1 Player movement patterns

For each movement pattern, the peak vertical forces and boot-surface contact time in each surface system condition are summarised in Table 4.4 and 4.5. The movements performed were described in force-time histories and CoP trajectories. For heel-toe walking, two peaks of vertical impact force at heel strike and push-off respectively and horizontal forces were revealed, as shown in Figure 4.12. The difference of magnitude between the two peaks of vertical force was usually less than 100 N. The horizontal force in M-L direction was around 30 N for the majority of stance, whilst the peak force in A-P direction reached 155 N. The CoP position was also reported in Figure 4.12. In the A-P direction, the displacement of CoP was regarded with respect to the 'x' axis coinciding with the longitudinal foot axis and walking direction. The displacement of the CoP in M-L direction was defined with respect to the 'y' axis, perpendicular to the x-axis. It was noticed that the 'x' and 'y' axes were regarded to M-L and A-P directions of FP respectively, which was the opposite of the Vicon set-up. In the following analysis, the coordinates system of FP was corrected to comply with the Vicon global coordinates system. Therefore, the 'x' axis is used to indicate A-P direction and 'y' axis indicates M-L direction. The y component of the CoP started laterally from the foot axis and presented a medial shift after touchdown,

followed by a lateral shift during the weight transfer from rearfoot to forefoot (the first peak). After heel off the surface, the CoP (y) shifted medially for toe off. The curve of the CoP (x) showed a forward motion of the whole stance phase. In A-P direction, the range of CoP displacement is approximately 90% of the foot length. The ground contact time for heel-toe walking was approximately 0.68 s.

For forefoot running, a typical single peak vertical force-time history is shown in Figure 4.13. The vertical peak force recorded in all surface system conditions was averaged 1916 ± 51 N. The horizontal force in M-L direction was smaller than 55 N and the peak force in A-P direction was similar as in the heel-toe walking. Forefoot running ground contact lasted approximately 0.28 s and peak vertical force usually occurred at approximately 0.11 s after initial contact. An initial medial shift of CoP (y) together with an anteriorly oriented peak of CoP (x) after touchdown may represent a braking phase of the player landing on pronation. A further medial shift of the CoP (y) followed during the propulsive phase across the centre of the metatarsals segment. Finally, the CoP reached the hallux area at toe-off indicated by the pronounced increase in CoP (x) and decrease in CoP (y).

Single leg drop jump landing on the forefoot created a single peak vertical force-time history and minimal horizontal forces, as shown in Figure 4.14. The peak vertical force recorded in all surface system conditions was in the range of 1969 ± 113 N. The horizontal forces in both directions were below 90 N. The average ground contact time was 0.34 s, longer than the contact time of forefoot running. The x component of the CoP showed two anteriorly oriented peaks after touchdown and shifted anteriorly again for take-off. The significant decrease of CoP (y) at the take-off phase was because the player bounced off from the surface system to his right diagonal front to land outside the FP area.

The plots of the CoP data showed the data points in early and late stance undergoing random displacements when the vertical force was at low level. So the threshold of vertical force was set at 100 N. The frames of recording with vertical force lower than 100 N were removed before further data analysis.

Table 4.6 shows the mean, standard deviation (SD) and coefficient of variation (COV) of the peak vertical force and contact time for each movement pattern of a total 31 successful trials. The data of walking and running movements suggests minimal variation among the trials. The repeatability of landing movement is relatively lower, because the variations of

angle of knee bending involved absorbing the energy during the impact. However, the variation is still in the acceptable range.

4.3.2 Surface system mechanical behaviour

4.3.2.1 Under forefoot running

Surface system vertical deflection

During forefoot running, Vicon captured the motion of the player's left foot through the markers on the boot. At the ground contact phase, the forefoot compressed and released the surface system through the loading and unloading process. As the forefoot remained in contact with surface through the duration of ground contact, the vertical deflection of surface system, in time, was identified by displacement of the forefoot in 'z' axis throughout the ground contact phase compare to its position at the touch down instant (frame). The following post-processing of motion captured data was done by Matlab.

Step 1, the static trial was analysed to get the average static position of the forefoot markers during the captured period. A plane in 3D space was fitted to the 5 forefoot markers (Figure 4.15) to estimate 'z' value using the least squares method to minimise the perpendicular distances of the markers to the plane. The estimated 'z' suggested the elevation of the forefoot plane above the laboratory floor while player standing for any 'x', 'y' position.

Step 2, for dynamic trial, the three dimensional kinematic data of the whole trial was linearly interpolated to the same time base (to 1000 Hz frequency) as the CoP and force data. The initiation of ground contact phase was identified when the vertical force measured greater than 10 N. The kinematic data during ground contact was filtered using a zero-lag 4th order low pass Butterworth filter with a cut off frequency of 20 Hz. Alternative cut-off frequency either side of 20 Hz were investigated. However, 20 Hz was chosen because it best removed the deemed noise from the data. After filtering, the kinematic data was further cropped with a vertical force threshold of 100 N to identify the valid region of ground contact phase for further analysis. Because the CoP data showed lower reliability at force level lower than 100 N.

Step 3, a series of CoP calculations was made to obtain the optimised dynamic CoP position at each time step throughout the identified ground contact phase. Firstly, the CoP data was altered to account for the top platform offset as the vertical distance from the

force sensors to the FP surface (48 mm) and the artificial turf system resting on top of the FP using a fixed offset as the height of the surface system. It was feasible to use the rigid body transformation technique (Challis, 1995) to determine the translation of the forefoot plane from one reference frame to another about the desired axis which was the ‘z’ axis in this study. The transformation matrix was determined using the static and instantaneous dynamic marker positions. Secondly, as the surface systems on top of the FP were compliant, an ‘fmin’ Matlab function was used to optimise the dynamic CoP position at each time instant considering surface system compliance when the transformation matrix was applied. Finally, the forefoot plane position in the ‘z’ axis was calculated relative to the resting surface system level in each frame during the identified ground contact phase, by Equation 4.1.

$$D_v = Z_d - (Z_s + h) \quad (4.1)$$

Where:

D_v = Vertical deflection (mm)

Z_d = Forefoot plane in ‘z’ axis of dynamic CoP (mm)

Z_s = Forefoot plane in ‘z’ axis of static CoP (mm)

h = Total thickness of the surface system (mm)

Figure 4.16 shows the vertical deflection calculated for the hockey turf surface systems composed with rubber shockpad (a) and foam shockpad (b) respectively. Figure 4.17 presents the vertical deflection of 3G+RS system (a) and 3G+FS system (b) under player forefoot running. The solid line at 0 mm deflection represents the resting surface system level without any load. The development of the vertical deflection of surface system was illustrated by the green curve in each graph. Because the foot flexion at touchdown, the angle between forefoot and surface level (as horizontal = 0°) in sagittal plane was larger than 25° which was measured from the HSV images. As a result, the position of toe marker had significant influence on the vertical deflection calculated at the beginning of the identified ground contact phase. At touchdown, before a flat forefoot stance reached, the position of toe marker was higher above the surface level. So the vertical deflection at the first approximately 8 ms was positive, as shown in Figure 4.16 (a) and 4.17 (a). These errors in early and late stance were caused by the limitation of the markers configuration

and the rigid body transformation method to measure vertical deflection. The robustness of results is further discussed in the Section 4.4.

The player completed 4 repeat runs on each surface system with pressure mat at the bottom. The graphical data of vertical deflection shown in Figure 4.16 and 4.17 is one representative trial selected for each surface system condition. For the hockey turf systems, the maximum vertical deflection achieved with the foam shockpad was 12.8 mm, 4.4 mm larger than with rubber shockpad. For the 3G turf systems, the 3G turf with foam shockpad system experienced larger vertical deflection than with rubber shockpad, 10.5 mm compared to 9.2 mm, as shown in Figure 4.17. Mean maximum vertical deflection for each surface system under player forefoot running is given in Table 4.7.

Force-deflection relationship

The vertical deflection result calculated from the marker position during the identified ground contact phase was synchronised with the vertical force measured by the FP to obtain the force-deflection relationship of each surface system in response to player running. Figure 4.18 and 4.19 present the force-deflection relationship of player forefoot running on HT+RS and HT+FS respectively. As shown in Figure 4.18, the maximum vertical deflection of HT+RS at 8.4 mm was achieved at the peak force 1919 N. A peak vertical force of 2013 N was reached on the hockey turf with foam shockpad system resulting in a peak deflection of 12.8 mm, as shown in Figure 4.19. Figure 4.20 and 4.21 present the force-deflection relationship of player forefoot running on the surface systems of the 3G turf with rubber and foam shockpad respectively. In Figure 4.21, the 3G turf with foam shockpad system reached a transition point between high and low stiffness at approximately 4.5 mm deflection. Generally, the force-deflection relationship of the tested surface system shows a nonlinear behaviour during loading and unloading following different paths due to energy loss during the impact.

It is noticed that in Figure 4.18 as the vertical force was in the range from around 1000 N to 1150 N, the deflection remained at approximately 5.7 mm. This was caused by the effect of some mid-rear foot contact involved during this period, suggested by the CoP position. The same effect was also found in Figure 4.20 when the force was in the range from 550 N to 700 N. The vertical deflection decreased approximately 0.3 mm. The CoP position may locate out of the forefoot plane as the mid-rear foot in contact with surface. Hence the

vertical deflection reported was smaller than the actual deflection under the CoP, causing a decrease of vertical deflection in the loading path.

Impact area and stress-strain relationship

Force-deflection of carpet-shockpad surface systems was converted to stress-strain relationship to observe the mechanical behaviour of the surface systems after normalising for their thickness and considering the loading area. Force was converted into stress using the Equation 3.4. The impact area of the player's forefoot running strike was measured separately using Tekscan pressure mat. The player was instructed to practise the movement with the same technique directly on the pressure mat resting on the FP. The area-time relationship was identified from a selected trial which was closest to the mean peak vertical force of the recorded running trials. It was assumed this boot-surface contact area history was representative of the development of contact area under forefoot in the recorded running trials. Because the Tekscan system measuring at a sampling rate of 440 Hz, the data was also interpolated to the same time base as the force data of FP and filtered with a zero-lag 4th order low pass Butterworth filter with a cut off frequency of 15 Hz. The processed boot contact area-time relationship of forefoot running is shown in Figure 4.22. The same vertical force threshold of 100 N was used to correlate contact area with force in the same identified stance. Strain of the surface systems was determined by Equation 3.5 where D_v is the vertical deflection of the surface system calculated using Equation 4.1.

The stress-strain relationship of hockey turf surface systems with rubber and foam shockpad are shown in Figure 4.23 and 4.24 respectively. Larger maximum strain (0.42) was reached on the system with foam shockpad than with rubber shockpad (0.26). The stress-strain relationship of the 3G turf surface systems with rubber and foam shockpad are shown in Figure 4.25 and 4.26 respectively. Due to the difference of surface system total thickness, the maximum strain on both 3G turf surface systems was lower than 0.22. The 3G turf with rubber shockpad system had maximum strain lower than 0.18. As expected, the stress-strain relationship demonstrates a similar nonlinear loading and unloading event to the force-deflection relationship presented above during the identified ground contact phase.

4.3.2.2 Under forefoot landing

Surface system vertical deflection

The vertical deflection of surface systems under player's forefoot landing trials was calculated by the same method introduced in Section 4.3.2.1. Matlab code was edited to process the motion capture data of landing movement on each surface system and plotted the results.

The vertical deflection of hockey turf systems in response to player forefoot drop jump landing is shown in Figure 4.27. The HT+FS system reached maximum deflection of 13.0 mm, which was 3 mm larger than the deflection of HT+RS. In Figure 4.28, the maximum deflections of the 3G turf with rubber and foam shockpad systems were 9.5 mm and 11.9 mm respectively. 4 successful trials on each surface system were analysed. The graphical data shown in Figure 4.27 and 4.28 is one representative trial selected for each surface system condition. Mean maximum vertical deflection for each surface system under player forefoot landing is listed in Table 4.8.

Large vertical deflection was observed at the beginning of ground contact phase on both 3G turf systems. The touchdown deflection on 3G+RS was approximately the same as the maximum value measured under peak vertical force. The deflection reached 7.7 mm at the touchdown on 3G+FS. As shown in Figure 4.29, the boot significantly deviated from horizontal (not a flat-foot landing) resulting in a small contact area at the boot-surface interface. Therefore, even under small load, large deflection was recorded on the 3G turf systems with their loose infills condition.

Force-deflection relationship

By incorporating the vertical force measured by the FP, the force-deflection relationship of each surface system in response to the player forefoot landing was produced. Figure 4.30 and 4.31 present the force-deflection relationship of player forefoot landing on HT+RS and HT+FS respectively. As shown in Figure 4.30, the maximum vertical deflection 9.8 mm was achieved at the peak force 2218 N. A vertical force of 2108 N was reached on the hockey turf with foam shockpad system resulting in a peak deflection of 13.0 mm, as shown in Figure 4.31. Under similar peak vertical force around 2000 N, 3G+RS deformed up to 9.5 mm (Figure 4.32) and 3G+FS maximum deflection was nearly 12 mm (Figure 4.33). The increase of deflection at take-off from 3 mm to 7 mm shown in Figure 4.32 was also because of the increase in forefoot sagittal angle. The relationship between this angle and surface deflection in early and late stance is discussed in subsection 4.4.1.

Impact area and stress-strain relationship

The impact area of the player's left forefoot landing was measured by Tekscan pressure mat placed on top of the FP with the player directly landing on it. The closest trial measuring boot contact area to the mean peak vertical force and contact time of the recorded trials on surface systems was exported from Tekscan. The area data was then interpolated to the same time base as the force data of FP and filtered with a zero-lag 4th order low pass Butterworth filter with a cut off frequency of 10 Hz by Matlab. The area-time history of the player forefoot landing is shown in Figure 4.34. The stress and strain were calculated using Equation 3.4 and 3.5 respectively.

The stress-strain relationship of hockey turf surface systems with rubber and foam shockpad are shown in Figure 4.35 and 4.36 respectively. Larger maximum strain (0.43) was reached on the system with foam shockpad than with rubber shockpad (0.3). In Figure 4.35, the peak stress of 340 kPa was reached when the strain of the surface system was between 0.21-0.24. The peak stress was measured before the maximum force achieved due to the increase of contact area lagged behind the increase of force during loading. The stress-strain relationship of the 3G turf surface systems with rubber and foam shockpad are shown in Figure 4.37 and 4.38 respectively. The smallest maximum strain 0.175 among the surface systems under player forefoot landing was observed in Figure 4.37, but the total thickness of 3G+RS was the thickest, 54 mm. The maximum strain of the 3G turf combined with foam shockpad was larger than 0.24.

4.3.2.3 Under heel-toe walking

Surface system vertical deflection

As shown in Figure 4.11, a typical force-time history of heel-toe walking consists of two peaks. The 1st peak and the 2nd peak are observed at the heel strike and forefoot push-off respectively. Unlike the forefoot movements with only one foot segment involved during ground contact, the contact time of rearfoot and forefoot with the surface systems was different during walking. In order to measure the deflection of surface systems under the rearfoot and forefoot area in their contact duration respectively, three independent planes (Figure 4.39) were built with 3 heel markers (Heel, Lateral Heel, Medial Heel), 5 rear and mid foot markers (Lateral Heel, Lateral M, Heel, Outer M, Instep M) and 5 forefoot markers (Toe, Outer, Instep, Outer M, Instep M). The ground contact of a walking trial was divided into three phases (percentage of the complete ground contact) according to the

different contact segments of the foot identified by the HSV images and the CoP trajectory. The first phase of the initial 10% of ground contact was touchdown phase (TD). The deflection of surface system during this phase was measured by the displacement of the plane made by 3 heel markers in axis 'Z' comparing to its static position offset the surface system height. The second phase was the mid-stance phase (MS) situated from 10% to 55% of the ground contact. The deflection was measured using the 5 rear and mid foot markers plane as the whole rear and mid foot stayed in contact with the surface system. The MS phase was followed by the push-off phase (PO) which took place from 55% till the end of the ground contact. As the rearfoot lifted off the surface in this phase, the plane of 5 forefoot markers was used to calculate the deflection of the surface system with the method introduced in Section 4.3.2.1. Table 4.9 summarises the vertical deflection in different phases for each surface system under multiple walking trials.

Figure 4.40 shows the vertical deflection of HT+RS during the three phases of a heel-toe walking trial. At the beginning of the TD phase, because the boot was at its most inclined to the horizontal and the heel contact area was small, the maximum vertical deflection measured up to 19.6 mm. During the MS phase, both the rearfoot and mid foot were in contact with the surface and the CoP was shifting through the rearfoot towards forefoot. The vertical deflection measured using the 5 rear and mid foot markers plane varied little during MS with an average of 5.7 mm. During the PO phase, the maximum vertical deflection measured under the forefoot was 5.9 mm.

The vertical deflection-time relationship of HT+FS is presented in Figure 4.41. In the TD phase, the maximum vertical deflection was 12.8 mm. The vertical deflection averaged 8.6 mm during the MS phase. With the 2nd peak vertical force reached in the PO phase, the maximum vertical deflection increased to 9.2 mm.

Figure 4.42 shows the vertical deflection of 3G+RS during the three phases of a heel-toe walking trial. In the TD phase, the vertical deflection decreased from 8 mm to 2.8 mm. The average vertical deflection during the MS phase was 4.5 mm. During the PO phase, the maximum vertical deflection reached 5.4 mm at 1.62 s.

Figure 4.43 presents the vertical deflection-time relationship of 3G+FS under player heel-toe walking. In the TD phase, the maximum vertical deflection was 17.7 mm. The average vertical deflection during the MS phase was 5.1 mm. With the 2nd peak vertical force reached in the PO phase, the maximum vertical deflection increased to 5.3 mm at 0.54 s.

Force and deflection

Because the vertical force recorded by the synchronised FP had two peaks in the identified ground contact phase and the change of vertical deflection did not follow a single increase and decrease trend, so for clearer presentation, the relationship of force and deflection for heel-toe walking was plotted on the same time base by two separate curves. A comparison of vertical force and deflection on the hockey turf in combination with the rubber shockpad below is shown in Figure 4.44. The deflection decreased from maximum 19.6 mm to 5.3 mm as the vertical force reached 619 N in the TD phase. During the MS phase, though the vertical force varied from 876 N to 530 N, the deflection remained at 5.7 mm under the rear and mid foot. During the PO phase, there was a small gradual increase of the deflection from 4.9 mm to 5.9 mm under the forefoot from 1.5 s to 1.64 s along with the raising of the vertical force to the 2nd peak of 944 N. Then both vertical force and deflection decreased from 1.67 s as the foot pushed off and left the surface.

The vertical force and deflection behaviour against time for heel-toe walking on HT+FS are shown in Figure 4.45. At the end of the TD phase, the vertical deflection reached 7.7 mm at 670 N. The first peak of vertical force was 877 N in the second (MS) phase causing a small peak surface deflection of 9.4 mm at 0.26 s. The average vertical deflection in the MS phase was 8.6 mm. In the PO phase, both peak vertical force (931 N) and deflection (9.2 mm) reached at 0.6 s.

The vertical force and deflection of the 3G turf with rubber shockpad surface system during the player heel-toe walking ground contact are shown in Figure 4.46. At the end of the TD phase, the vertical force reached 637 N and the deflection was 2.8 mm. It is observed in the MS phase the peak vertical force and deflection almost synchronously occurred. The vertical deflection was 5.4 mm at peak in this phase, and then it dropped to 4 mm as the decrease in force. During the PO phase, the vertical force and deflection increased again to the 2nd peak of 860 N and 5.4 mm.

A comparison of vertical force and deflection on the 3G turf in combination with the foam shockpad below is shown in Figure 4.47. At the end of TD phase, the vertical force and deflection were 681 N and 4.8 mm at 0.08 s. During the MS phase, the maximum deflection reached 6.3 mm at 891 N. In the PO phase, the peak force was 894 N which was similar to the 1st peak. But the maximum deflection was 5.3 mm, 1 mm smaller than in the MS phase.

Impact area and stress-strain relationship

The impact area of the foot strike by the shod player practising heel-toe walking was measured by Tekscan pressure mat. The player was required to use the same heel-toe walking technique to walk directly on the pressure mat supported by the FP below as he did on the surface systems. The boot contact area-time history of a representative trial was presented in Figure 4.48. Matlab was employed to interpolate and filter the data from Tekscan using the same method in Section 4.3.2.2. The boot contact area increased gradually during the initial 0.2 s and plateaued from 7.2 s to 7.5 s at around 51 cm². The contact area decreased rapidly during the final push-off. The contact area during the identified ground contact was used to calculate the stress applied by the player using Equation 3.4. The strain of the surface system was obtained by Equation 3.5.

The applied stress and resulting strain of HT+RS were shown in Figure 4.49 on the same time base. The maximum stress of 370 kPa was rapidly achieved, only 0.024 s after the initial touchdown of the heel. The vertical force at this time was 464 N, which was much smaller than the first peak of force 876 N, but the limited contact area of 12.5 cm² contributed to the maximum stress. Due to the increase of contact area to 51 cm² in the MS phase, the stress decreased with time 104 kPa at the end of the MS phase. During the PO phase, the 2nd peak of stress 201 kPa reached simultaneously with the 2nd peak of vertical force. The largest strain at the beginning of the TD phase was 0.58. From 1.2 s to 1.65 s, the strain did not significantly change and remained at an average of 0.17.

The stress-time and strain-time histories of HT+FS were presented in Figure 4.50. The maximum stress applied on this surface system by player heel-toe walking was 363 kPa, occurred 0.025 s after the initial touchdown, similar to the maximum stress measured on the hockey turf with rubber shockpad system. The stress decreased gradually afterwards but with a small increase at 0.16 s. During the PO phase, the stress raised up to approximately 200 kPa again. The strain-time history curve shows two peaks in the MS and PO phases, coincidence with the two peaks of vertical force during the ground contact. Both the peaks were in the range of 0.3 to 0.31.

The stress-time and strain-time histories of 3G+RS under player heel-toe walking were presented in Figure 4.51. There are two peaks of stress showing on the graph during the heel strike. The second peak reached the maximum stress of 332 kPa at the surface system strain of 0.07. The maximum strain was 0.15 under the applied stress of 240 kPa. It is

observed that the in the MS phase, after the maximum stress reached, there is still a 0.03 increase of strain before declining together with stress. During the PO phase, the stress and strain raised up to 182 kPa and 0.1 respectively.

The stress-time and strain-time histories of 3G+FS under player heel-toe walking were shown in Figure 4.52. An initial peak stress of 306 kPa was followed by the maximum stress 328 kPa during the heel strike. The stress dropped to 92 kPa at the transition from the MS phase to the PO phase and increased to 190 kPa in the PO phase. The maximum strain of this surface system was 0.36, much larger than the system of the 3G turf combined with rubber shockpad. The strain reduced pronouncedly to 0.07 at the transition from the MS phase to the PO phase.

4.3.3 Pressure distribution in surface system

A summary Table 4.10 lists the peak pressure and contact area measured by the pressure mat inserted at different interfaces of surface systems under player running, landing and walking. Generally, the results show the load applied by the player on top of surface system over a specific area is distributed over an increasing area as it penetrates through the carpet layer and then the shockpad, reducing the stress.

4.3.3.1 Under forefoot running

Average peak boot-surface contact area was 70 cm² during player forefoot running. For HT+RS, the peak contact areas measured between the layers and underneath the system were 172 cm² and 169 cm² respectively. The peak contact area recorded between the hockey turf and foam shockpad was approximately 2.6 times larger than the initial peak contact area underfoot. Peak contact area at the bottom of this system was slightly increased further to 188 cm². The peak contact areas measured underneath the 3G turf with rubber and foam shockpad were 200 cm² and 197 cm² respectively.

Average peak stress applied on the four surface systems underfoot was in the range of 271-278 kPa. Peak stress measured at the bottom of HT+RS was 124 kPa, which was larger than 115 kPa recorded between the layers. Because as shown in Figure 4.53, larger high pressure region in a similar contact area measured at the bottom of the surface system in comparison to at the carpet-shockpad interface. For the HT+FS system, peak stress between the layers was 138 kPa, larger than the peak stress at the bottom with the difference of 24 kPa. Peak stress recorded at the bottom of the two 3G turf systems (around

100 kPa) indicates no significant difference between the two shockpad used in terms of pressure distribution.

The pressure mat was also inserted between the carpet and shockpad layers in the 3G turf systems. Due to the influence of unsmooth backing of the 3G carpet discussed in Section 3.3.3, as shown in Figure 4.54, inactive sensing cells are found within the pressure contours when the pressure mat is sandwiched between layers. The sensing cells under the space between two parallel stitch lines were not activated, so caused error in recording contact area and stress. Therefore, the pressure mat is considered not applicable to be used at the 3G carpet and shockpad interface.

Comparison of the peak contact area under boot and at the bottom for the two hockey turf surface systems during player forefoot running indicates the contact area enlarged greater with foam shockpad by 169% than 141% with rubber shockpad. The increase in peak contact area at the bottom of the 3G turf systems compared with underfoot was greater than 180%. As the largest contact area 200 cm² measured at the bottom of 3G+RS, the peak stress recorded at this interface was the lowest (99 kPa) for the test surface systems. The peak stress reduced by 55% at the bottom of HT+RS in comparison to 59% of HT+FS. The results indicate that the surface systems are ranked in the same order for enlarging the contact area as reducing the pressure.

4.3.3.2 Under forefoot landing

Average peak boot-surface contact area was 73 cm² during player forefoot landing. The peak contact area between the hockey turf and rubber shockpad was larger than it measured at the bottom of the system (201 cm² in comparison to 193 cm²). Peak contact area increased approximately to the same size, by 171%, between the hockey turf and foam shockpad and under the two layers. The peak contact areas measured underneath the 3G turf with rubber and foam shockpad were 220 cm² and 222 cm² respectively.

Averaged peak stress underfoot applied on the hockey turf systems was around 285 kPa. For both of the two systems, the stress reduced to around 105 kPa through the hockey turf carpet. However, the peak stress at the bottom of HT+RS increased up to 112 kPa while the peak stress at the bottom of HT+FS remained at 105 kPa. This is due to a smaller contact area measured under the hockey turf with rubber shockpad system than between the two layers. Under the same applied peak stress 267 kPa, the peak stress at the bottom

of the 3G turf with rubber shockpad system and the 3G turf with foam shockpad system reduced to 95 kPa and 91 kPa respectively.

Comparison of the peak contact area underfoot and at the bottom for the two hockey turf surface systems during player forefoot landing indicates the contact area enlarged greater with foam shockpad by 171% than 164% with rubber shockpad. There is no significant difference identified for the bottom contact area with the two 3G turf systems. The reductions of peak stress through all the tested surface systems were not significantly different, ranging from 61% to 66%.

Further analysis of pressure contours to compare the pressure in the centre and the outer zone is presented in Subsection 4.4.3.

4.3.3.3 Under heel-toe walking

Under heel-toe walking movement, the peak contact area measured between the layers of hockey turf and rubber shockpad system was about 3 times larger than the boot-surface contact area at peak and slightly larger than the peak contact area measured at the bottom of this surface system by 5 cm². In HT+FS, the peak contact area enlarged as the load penetrating through each layer. The peak contact area increased from 57 cm² under the boot to 179 cm² between the carpet and shockpad layers. The peak contact area further enlarged to 188 cm² at the bottom of the surface system. The results of peak contact area measured at the bottom of the two 3G turf surface systems were similar, over 170 cm² which was over 3 times larger than the boot-surface contact area.

Peak stress applied on top of the surface system was determined by the average value over the four trials for each surface condition. The results show the stress reduced significantly through the layers. For HT+RS, the peak stress between layers recorded slightly higher than at the bottom (73 kPa in comparison to 68 kPa). Peak stress reduced progressively from 365 kPa (on top) to 66 kPa (between layers) and then to 62 kPa (at the bottom) in HT+FS. The applied peak stress 332 kPa on 3G+RS reduced to 56 kPa, up to 83% at the bottom of the system. With approximately the same amount of stress (328 kPa) applied on 3G+FS, the peak stress measured at the bottom of this surface system was 59 kPa.

Comparison of the peak contact area under boot and at the bottom for all the surface systems during player walking suggests HT+FS enlarged the impact area the most, by up to 230%. The 3G turf combined with rubber and foam shockpad increased the contact area

by 202% and 209% respectively. HT+RS was the only one enlarging the peak contact area by less than 200%. Despite the relatively large differences in the enlarged peak contact area through the layers, the reduction of peak stress is 82% - 83% of the applied stress, approximately the same for all the tested surface systems. Peak contact area and stress recorded between the hockey turf and shockpad layers suggest that, regardless of the shockpad used, the hockey turf carpet plays the dominant role in reducing the stress over an increased contact area.

4.4 Discussion

This section discusses the results of artificial turf surface system behaviour under player loading. The discussion is divided into sub sections that determine the validity of the rigid body transformation method for calculating surface system vertical deflection, examine the change of stiffness of surface systems during player loading and further analyse the pressure distribution at each interface in detail using the contours.

4.4.1 Validity of boot segment plane

Measuring the surface system deflection underfoot by tracking the position of segment plane(s) fitted through markers on the boot during player movements provides the ability to characterise the surface system behaviour under realistic player loading conditions. The effectiveness of this method was analysed by calculating the root mean square fit error (RMSFE) between the positions of active segment markers in static and dynamic trials at each time instant using Equation 4.2.

$$RMSFE = \sqrt{\frac{\sum_{i=1}^n (Pd_i - Ps_i)^2}{n}} \quad (4.2)$$

Where:

RMSFE = Root mean square fit error

Pd = Dynamic marker position (mm)

Ps = Static marker position (mm)

For all the movement patterns, the RMSFE for the rigid body transformation of the active segment throughout stance was less than 3 mm with the largest errors occurring in early and/or late stance. The stance average RMSFE was less than 1 mm. The small errors in the

RMSFE suggest this method was able to perform reliably during the majority of stance for measuring surface system deflection.

The errors in the calculation of surface deflection in early and late stance occurred as the active segment plane significantly deviated from horizontal, as mentioned in Subsection 4.3.2.1. Through the initial analysis of the HSV images, it was observed that if the angle between the active segment sagittal plane and surface level was larger than 25° , the errors in estimating the position of the plane in the 'z' axis result in errors in the calculation of surface deflection. In order to identify the effective range of segment plane sagittal angle for measuring reliable surface deflection, a programme was written in Matlab to calculate the instantaneous angle of rotation of the active segment plane in sagittal plane throughout stance using the rigid body transformation technique (Ahmadi et al., 2010; Challis, 1995).

The unloaded surface level was defined as horizontal (0°) and zero deflection. The compression of the surface system underfoot was indicated by negative values for vertical deflection. Any positive result (above surface level) was considered to be an error. Moreover, to account for the RMSFE in early and late stance, the valid vertical deflections of all the surface systems during walking, running and landing are shown in Figure 4.55, 4.56 and 4.57 respectively. The corresponding segment plane sagittal angle during stance for each movement is presented in Figure 4.58, 4.59 and 4.60. The active boot segment angle results in sagittal plane for walking indicated the plane deviated from horizontal in the range of -20° to 20° , the vertical deflection of HT+FS was reliably calculated. The vertical deflection of three other surface systems was considered to be reliable when the active plane sagittal angle was in the range of -20° to 10° . Generally, the forefoot plane sagittal angle for running was small in early stance showing the subject had an almost flat forefoot strike pattern. The errors in the calculation of vertical deflection occurred when the forefoot plane angled over 20° from horizontal. The segment plane sagittal angle for forefoot landing was approximately smaller than 10° and 14° in early and late stance respectively. These results suggest that measuring compliant surfaces vertical deflection by tracking the CoP position on the boot segment plane during foot strike for this marker configuration, is only effective when the foot plane during the stance of movement pattern deviated from horizontal no larger than 20° . Dividing the foot into smaller segment with more markers may help to expand the range of effectiveness of this measurement method. However, in this study, only the angle in sagittal plane was considered. In order to better

understand the effect of human joint movement on this method, the segment plane angle in coronal (frontal) plane also needs to be determined.

4.4.2 Stiffness of surface systems

The force-deflection relationship of surface systems presented in Section 4.3 shows nonlinear behaviour during the player loading. In order to compare the behaviour of different surface systems, the stiffness in a specified range of force (i to i+1) was calculated using Equation 4.3. The changes in stiffness at different compression stages provide a measurement of nonlinearity, but the extent of nonlinearity is further discussed using nonlinear mathematical model in Chapter 5.

$$k_i = \frac{F_{i+1} - F_i}{x_{i+1} - x_i} \quad (4.3)$$

Where:

k_i = Stiffness (N/mm)

F_i = Force (N)

x_i = Deflection (mm)

Since both running and landing movements were using forefoot strike technique, to compare the stiffness of surface systems for different movements, the stiffness during heel strike of walking movement was not calculated. During the PO phase of walking, the vertical force mostly increased from approximately 600 N to the 2nd peak. The slope of the rising (loading) curve of walking at this force range was calculated. A summary Table 4.11 is listed the average stiffness of each surface system under different player movements.

The force-deflection relationship of surface systems during the PO phase of walking was presented in Figure 4.61. The stiffness of surface systems ranged from 211 N/mm (3G+FS) to 331 N/mm (HT+RS). The stiffness of HT+FS and 3G+RS was 214 N/mm and 228 N/mm respectively. Compared to rubber shockpad, using the foam shockpad reduced the stiffness of hockey turf system and 3G turf system by 35% and 7% respectively. It is also highlighted that the shockpad played a more significant role in the change of stiffness in hockey turf system than the 3G turf system.

A comparison of force-deflection relationship for running on four surface systems is shown in Figure 4.62. It is observed that initially the surface systems are easily deformed with the

application of small force. The stiffness was low when the applied vertical force was less than 600 N. Thereafter, a clear trend of increasing stiffness was visually identified for all the surface systems. Because of the variation in deflection measured in early stance on 3G+RS, the deflection decreased whilst the force increasing in the load range of 600 to 900 N. Surface system stiffness was calculated when the vertical force was higher than 900 N during loading. The stiffness of the HT+RS was 276 N/mm, slightly higher than the 3G+RS of 270 N/mm. The stiffness of the 3G+FS was 234 N/mm compared with 199 N/mm for the HT+FS. The foam shockpad used in the hockey turf system presented a significant reduction in stiffness due to the large deflection produced under the similar peak force.

The force-deflection relationship of the surface systems under landing is shown in Figure 4.63. As the large surface deflection reached in the touchdown due to the small contact area under boot, the deflection decreased until the vertical force reached 600 N. The stiffness of surface systems was calculated at the force ranged from 600N to peak. The rankings of stiffness of surface systems remained the same as for player running. The HT+RS behaved as the stiffest system with 272 N/mm, followed by the 3G+RS with 265 N/mm. The stiffness of foam shockpad added with the 3G carpet on top was 256 N/mm, higher than combined with hockey turf (194 N/mm). In the same range of applied load, compared to the stiffness determined during running, the stiffness of each surface system under landing measured without significant difference. For the HT+RS, 3G+RS and HT+FS, the stiffness under running was around 5 N/mm higher than the stiffness under landing. With the exception of the 3G+FS, landing stiffness was 22 N/mm higher than the running stiffness. This may be explained by the stronger nonlinearity recorded in landing movement in the specified force range.

4.4.3 Pressure contour

Peak pressure and contact area results from Tekscan pressure mat reported in Section 4.3.3 reveal that the applied load underfoot is distributed over enlarged contact area through the layers of surface system, consequently, reducing the pressure measured at different interfaces. Impact of foot strike on the compliant surface systems created a deflection bowl around the boot-surface contact spot. The enlarged contact area measured at each surface system interface reflected the size of the deflection bowl containing a high pressure region in the centre with similar size as the boot-surface contact area and a lower pressure region around it as the perimeter zone (see Section 3.4.4). The F-Scan software was used to define

the shape and size of the centre high pressure region, isolate it from the pressure contour and compare the pressure in this centre area with the outer zone.

Boot-surface contact area for player forefoot running was recorded as introduced in Subsection 4.3.2.1. Peak contact area contour and the CoP position were exported as shown in Figure 4.64. Eight points were used to define a polygon for describing the area which was 75 cm². The relative coordinates of the eight points to the CoP position were determined in the matrix of sensing cells. Thereafter, the polygon of the peak boot-surface contact area was applied to the pressure contours measured at the carpet-shockpad interface and the bottom of HT+RS (Figure 4.65). It is noticed that in the enlarged contact areas, the high pressure region (indicated by warmer colours) is still concentrated within the polygon and the blue colour in the outer zone shows lower pressure values. The applied peak pressure over the boot-surface contact area on HT+RS was 277 kPa (Table 4.10). As shown in Figure 4.66, at the carpet-shockpad interface, the peak pressure over the whole enlarged contact area was 115 kPa. However, over the impact area size polygon, the peak pressure measured significantly higher at 182 kPa. The pressure measured in the outer zone surrounding the polygon showed a lower value at 47 kPa. At the bottom of the surface system, the peak pressure over the whole enlarged area was 124 kPa in comparison to 187 kPa recorded in the centre polygon area. The area surrounding the polygon indicated by colder colours in Figure 4.65 (right) had an average pressure at 60 kPa. Pressure measured in the polygon region directly under the surface loaded area is similar at both interfaces of HT+RS, around 185 kPa, reduced by 33% from the applied peak pressure. Compared with the average pressure of the whole enlarged area, the applied pressure is reduced by approximately 55%. The results show a slight increase of pressure in the polygon area at the bottom of the surface system compared with in between the layers. The increase of pressure in the outer zone is relatively larger at 13 kPa. It is also observed in Figure 4.65 that more sensing cells with warmer colours showing higher pressure displayed in the pressure contour at the bottom of surface system.

The applied pressure on HT+FS under player forefoot running was 278 kPa, similar to the applied pressure on HT+RS. At the carpet-shockpad interface, the pressure at peak over the whole enlarged contact area was 138 kPa (refer to Table 4.10). In the impact area size polygon, the peak pressure measured notably higher at 198 kPa. The pressure measured in the outer zone (106 cm²) surrounding it showed a lower value of 96 kPa. At the bottom of the surface system, the peak pressure over the whole enlarged area was 114 kPa in

comparison to 156 kPa recorded in the centre polygon area. The area (113 cm²) surrounding the polygon measured an average pressure at 86 kPa.

HT+FS showed gradual pressure reduction through the layers in both polygon region in the centre and the outer zone. However, the results measured for HT+RS did not show gradual pressure reduction through carpet and then shockpad layer. Pressure results measured in the polygon region at the two interfaces of HT+RS varied only around 3% showing no further load spreading through the rubber shockpad.

Table 4.1: Averaged infill height and force reduction measured on the test locations (marked in Figure 4.1) of the 3G turf surface systems before and after player testing trials

Test location	Before player testing trials				After player testing trials			
	3G turf + Rubber shockpad		3G turf + Foam shockpad		3G turf + Rubber shockpad		3G turf + Foam shockpad	
	Ave. Force reduction	Ave. infill height (mm)	Ave. Force reduction	Ave. infill height (mm)	Ave. Force reduction	Ave. infill height (mm)	Ave. Force reduction	Ave. infill height (mm)
1	69%	38.8	70%	35.9	66%	37.5	69%	34.6
2	68%	39.5	71%	35.5	65%	37.9	68%	35
3	68%	38.4	69%	37.2	68%	37.6	69%	35
4	N/A	37.9	N/A	36.4	N/A	37.5	N/A	35.6
5	N/A	39.8	N/A	38.2	N/A	37.6	N/A	34.6

Table 4.2: Player movement patterns/surface systems tested in the laboratory

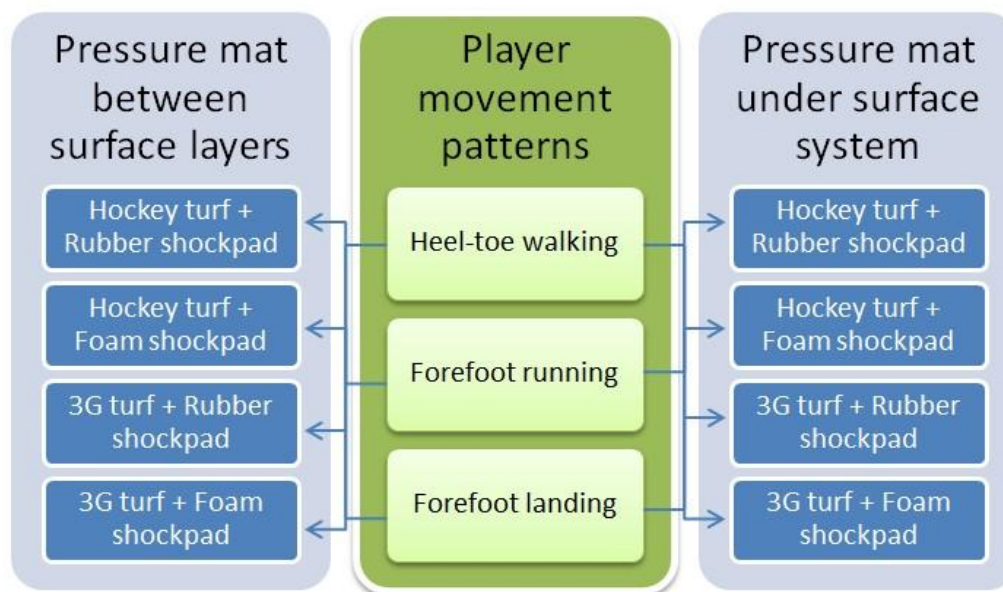


Table 4.3: A summary table linking the measurement methods to the results

Measurement method	Result
Vicon + force plate	Surface deflection
Force plate	Forces
	Contact duration
Tekscan pressure mat	Contact area
	Pressure distribution
Vicon + HSV	Boot segment plane angle
Timing gates	Movement speed

Table 4.4: A summary of peak vertical force and contact time for each player movement pattern on each surface system with pressure mat placed at the bottom

Player movement pattern		Pressure mat at the bottom of surface systems											
		Hockey turf + Rubber shockpad			Hockey turf + Foam shockpad			3G turf + Rubber shockpad			3G turf + Foam shockpad		
		Peak vertical force (N)		Contact time (s)	Peak vertical force (N)		Contact time (s)	Peak vertical force (N)		Contact time (s)	Peak vertical force (N)		Contact time (s)
Heel-toe walking	Trial 1	825	865	0.71	826	973	0.68	870	861	0.69	849	854	0.69
	Trial 2	877	945	0.7	901	952	0.65	897	860	0.69	891	894	0.67
	Trial 3	849	880	0.7	879	932	0.68	882	859	0.72	893	867	0.68
	Trial 4	800	885	0.69	894	950	0.68	912	884	0.7	846	876	0.69
	Average	837.75	893.75	0.7	875	951.75	0.67	890.25	866	0.7	869.75	872.75	0.68
Forefoot running	Trial 1	1932		0.27	1998		0.28	2022		0.26	1914		0.27
	Trial 2	1922		0.28	2013		0.29	1853		0.28	1863		0.27
	Trial 3	1919		0.3	1896		0.32	1892		0.27	1909		0.28
	Trial 4	1987		0.3	1890		0.3	1894		0.28	1896		0.27
	Average	1940		0.29	1949.25		0.30	1915.25		0.27	1895.5		0.27
Forefoot landing	Trial 1	2055		0.35	2137		0.3	2048		0.32	1900		0.37
	Trial 2	1777		0.37	1775		0.36	1864		0.35	2018		0.33
	Trial 3	2218		0.34	1793		0.37	1857		0.37	1958		0.34
	Trial 4	N/A		N/A	2025		0.32	2020		0.33	1912		0.35
	Average	2016.67		0.35	1932.5		0.34	1947.25		0.34	1947		0.35

Table 4.5: A summary of peak vertical force and contact time for each player movement pattern on each surface system with pressure mat placed between the layers

Player movement pattern		Pressure mat between the layers of surface systems											
		Hockey turf + Rubber shockpad			Hockey turf + Foam shockpad			3G turf + Rubber shockpad			3G turf + Foam shockpad		
		Peak vertical force (N)		Contact time (s)	Peak vertical force (N)		Contact time (s)	Peak vertical force (N)		Contact time (s)	Peak vertical force (N)		Contact time (s)
Heel-toe walking	Trial 1	807	894	0.66	863	908	0.67	868	873	0.67	832	849	0.7
	Trial 2	865	886	0.64	834	869	0.7	886	835	0.63	818	891	0.67
	Trial 3	867	936	0.65	919	879	0.69	888	821	0.69	883	830	0.67
	Trial 4	N/A	N/A	N/A	869	877	0.71	862	846	0.7	911	870	0.65
	Average	846.33	905.33	0.65	871.25	883.25	0.69	876	843.75	0.67	861	860	0.67
Forefoot running	Trial 1	1895		0.26	1919		0.29	1830		0.26	1870		0.28
	Trial 2	1919		0.28	1958		0.29	1942		0.26	2005		0.28
	Trial 3	1880		0.29	1824		0.31	1947		0.27	1879		0.31
	Trial 4	N/A		N/A	1900		0.29	1858		0.27	1965		0.3
	Average	1898		0.28	1900.25		0.30	1894.25		0.27	1929.75		0.29
Forefoot landing	Trial 1	2125		0.32	1952		0.33	2036		0.34	1936		0.33
	Trial 2	2034		0.32	2039		0.33	1861		0.37	1875		0.34
	Trial 3	1820		0.35	2180		0.31	2011		0.36	1960		0.35
	Trial 4	2072		0.32	1880		0.34	1959		0.37	1952		0.34
	Average	2012.75		0.33	2012.75		0.33	1966.75		0.36	1930.75		0.34

Table 4.6: Player movement repeatability analysis for all the trials

Player movement pattern		Peak vertical force (N)		Contact time (s)
Heel-toe walking	Mean	Heel strike	Push-off	0.681
		866.548	883.903	
	SD	30.911	36.979	0.021
	COV	0.036	0.042	0.031
	p-value	0.436	0.024	0.095
Forefoot running	Mean	1915.839		0.283
	SD	50.965		0.016
	COV	0.027		0.055
	p-value	0.489		0.728
Forefoot landing	Mean	1969.323		0.342
	SD	113.092		0.019
	COV	0.057		0.057
	p-value	0.737		0.568

Table 4.7: Maximal vertical deflection for each surface system under player forefoot running

Surface condition	Max vertical deflection (mm)		
	Mean	SD	COV
hockey turf + rubber shockpad system	8.6	0.2	0.02
hockey turf + foam shockpad system	12.5	0.2	0.02
3G turf + rubber shockpad system	8.8	0.3	0.03
3G turf + foam shockpad system	10.2	0.6	0.06

Table 4.8: Maximal vertical deflection for each surface system under player forefoot landing

Surface condition	Max vertical deflection (mm)		
	Mean	SD	COV
hockey turf + rubber shockpad system	10.3	0.3	0.03
hockey turf + foam shockpad system	12.9	0.2	0.01
3G turf + rubber shockpad system	9.0	0.3	0.04
3G turf + foam shockpad system	11.3	0.9	0.08

Table 4.9: Vertical deflection of each surface system during three phases of player heel-toe walking

Surface condition	Max vertical deflection (mm) in touchdown phase (TD)			Ave vertical deflection (mm) in mid-stance phase (MS)			Max vertical deflection (mm) in push-off phase (PO)		
	Mean	SD	COV	Mean	SD	COV	Mean	SD	COV
hockey turf + rubber shockpad system	18	3	0.17	5.5	0.2	0.03	5.9	0.2	0.04
hockey turf + foam shockpad system	13.2	2.8	0.21	8.5	0.2	0.03	9.2	0.2	0.02
3G turf + rubber shockpad system	9.4	1.9	0.2	4.9	0.9	0.19	6.0	0.6	0.11
3G turf + foam shockpad system	14.2	2.7	0.2	5.0	0.6	0.11	5.6	0.2	0.04

Table 4.10: Peak contact area and stress (+ standard deviation) measured by the pressure mat placed at different positions in the surface systems under three player movement patterns

Surface system	Parameters		Movement patterns		
			Heel-toe walking	Forefoot running	Forefoot landing
Hockey turf + rubber shockpad system	Peak contact area (cm ²)	Top	54 ± 2	70 ± 5	73 ± 3
		Between	169 ± 3	169 ± 6	201 ± 4
		Bottom	164 ± 6	169 ± 5	193 ± 5
	Peak stress (kPa)	Top	370 ± 5	277 ± 7	284 ± 6
		Between	73 ± 2	115 ± 3	105 ± 2
		Bottom	68 ± 3	124 ± 4	112 ± 4
Hockey turf + foam shockpad system	Peak contact area (cm ²)	Top	54 ± 2	70 ± 5	73 ± 3
		Between	179 ± 7	181 ± 4	197 ± 3
		Bottom	188 ± 3	188 ± 6	198 ± 3
	Peak stress (kPa)	Top	365 ± 2	278 ± 8	285 ± 8
		Between	66 ± 1	138 ± 2	106 ± 1
		Bottom	62 ± 2	114 ± 3	105 ± 2
3G turf + rubber shockpad system	Peak contact area (cm ²)	Top	54 ± 2	70 ± 5	73 ± 3
		Between	N/A	N/A	N/A
		Bottom	172 ± 8	200 ± 7	220 ± 7
	Peak stress (kPa)	Top	332 ± 8	274 ± 9	267 ± 12
		Between	N/A	N/A	N/A
		Bottom	56 ± 3	99 ± 4	95 ± 5
3G turf + foam shockpad system	Peak contact area (cm ²)	Top	54 ± 2	70 ± 5	73 ± 3
		Between	N/A	N/A	N/A
		Bottom	176 ± 4	197 ± 4	222 ± 5
	Peak stress (kPa)	Top	328 ± 7	271 ± 3	267 ± 6
		Between	N/A	N/A	N/A
		Bottom	59 ± 2	100 ± 2	91 ± 3

Note: 'Top' suggests the applied stress and boot-surface contact area at the topside of surface system. 'Between' indicates the stress and contact area were measured as the pressure mat sandwiched between carpet and shockpad layer. 'Bottom' means the stress and contact area were measured as the pressure mat placed underneath the surface system on top of the force plate.

Table 4.11: Average stiffness of surface systems under different player movements in the range of vertical force from 600 N to peak

Player movement pattern	Stiffness (N/mm)			
	HT + RS	HT + FS	3G + RS	3G + FS
Walking	331	214	228	211
Running*	276	199	270	234
Landing	272	194	265	256

Note: for running, the stiffness was calculated in the vertical force range of 900 N to peak.

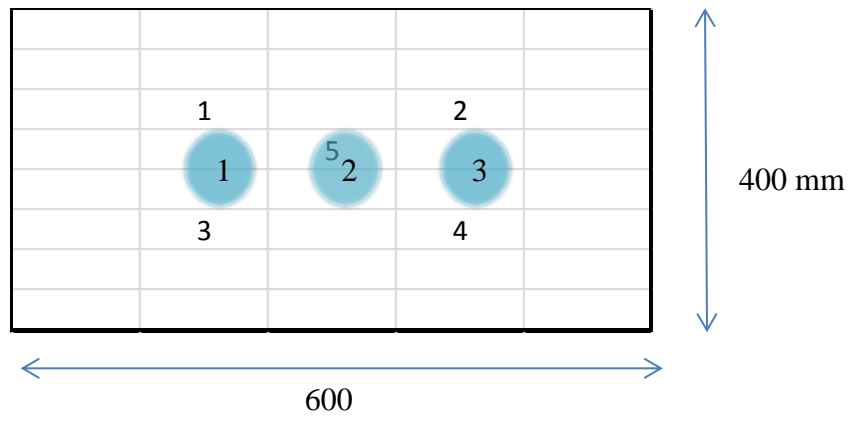


Figure 4.1: Test locations for infill height (numbered cells) and the AAA (numbered circles)



Figure 4.2: Picture of the soccer boots used in the experiment programme

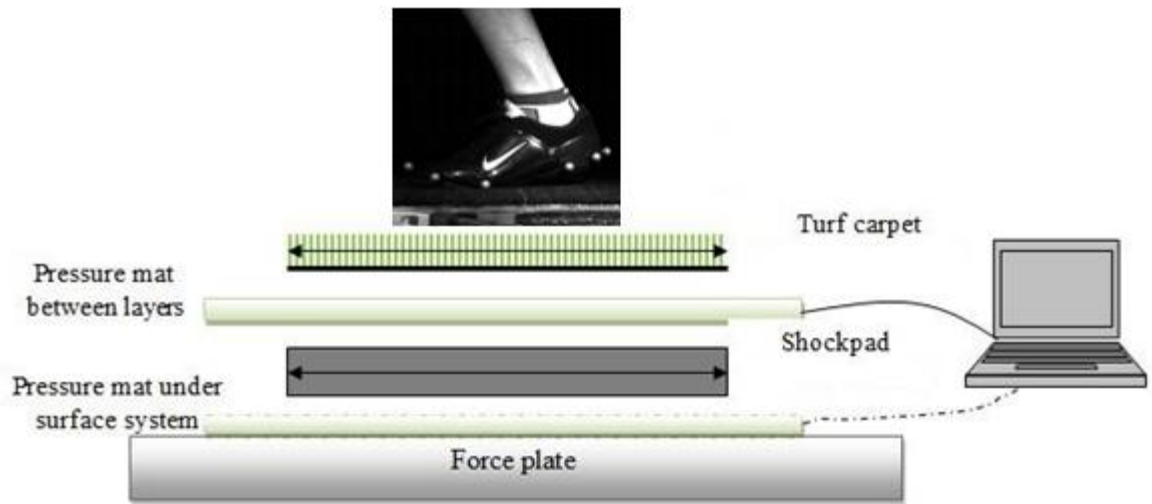


Figure 4.3: Schematic graph (above) and picture (below) of the pressure mat position in the measurement set-up

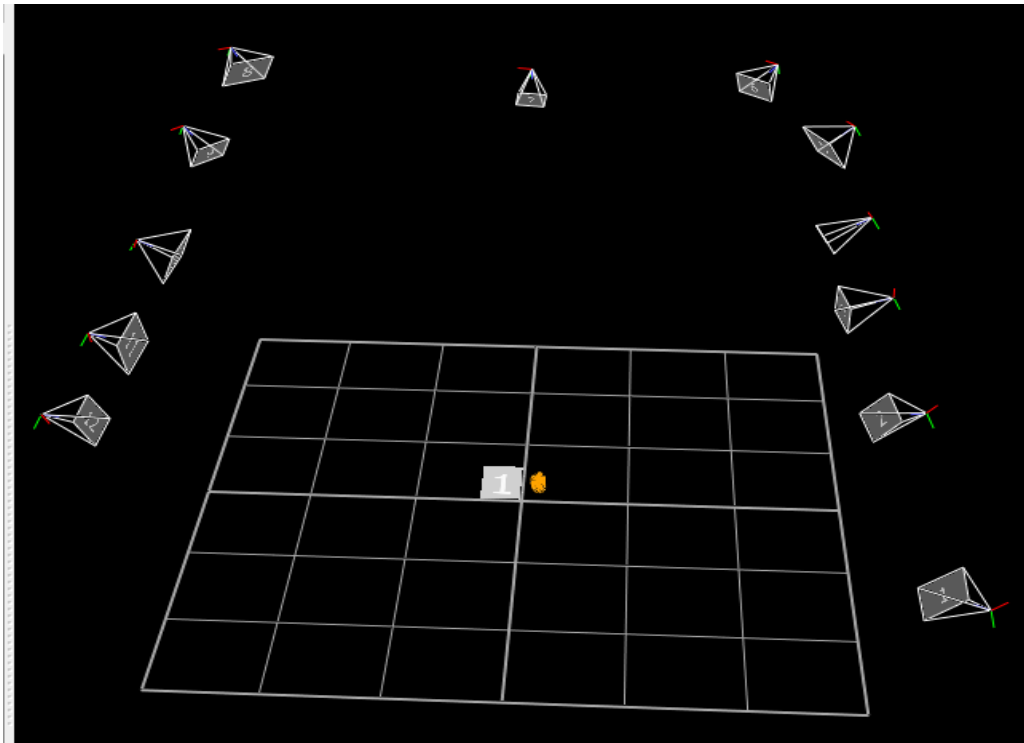


Figure 4.4: Screen-shot of the layout of 12 Vicon cameras and capture volume including the force plate and markers in the centre of laboratory floor map

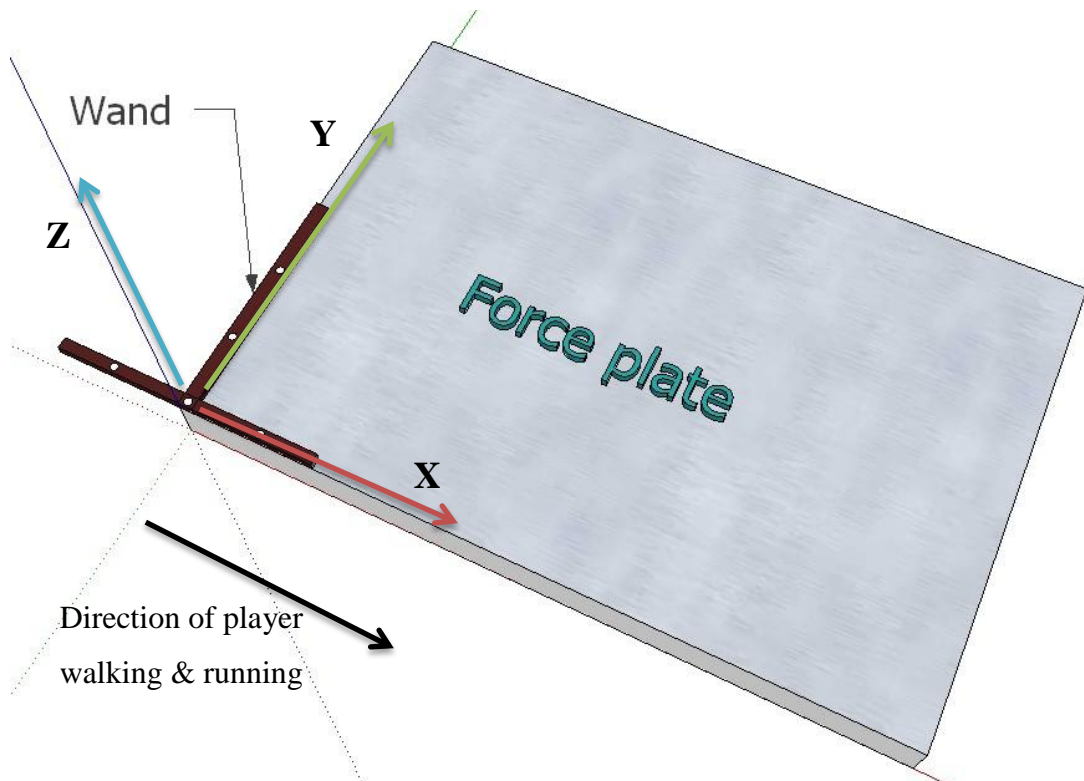


Figure 4.5: The static stage of calibration of the Vicon system to set the global coordinates system



Figure 4.6: Position of markers on the left boot of player in the pilot experiment

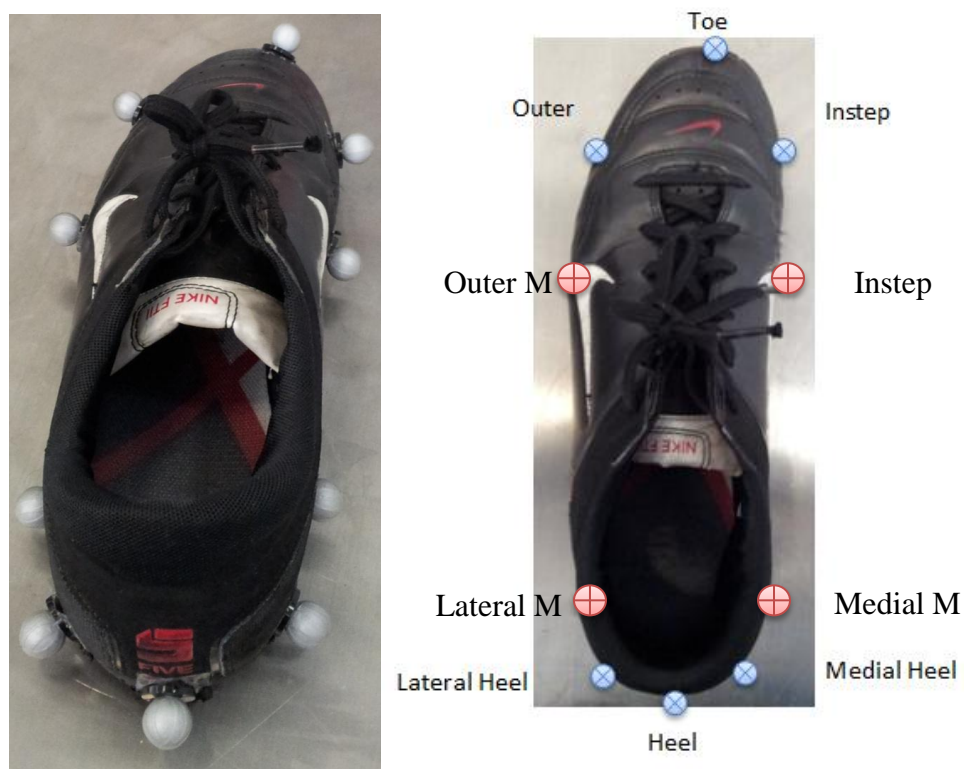


Figure 4.7: Improved markers configuration of the left boot with four additional markers (red)



Figure 4.8: High speed camera with lighting system orientated laterally to the surface system

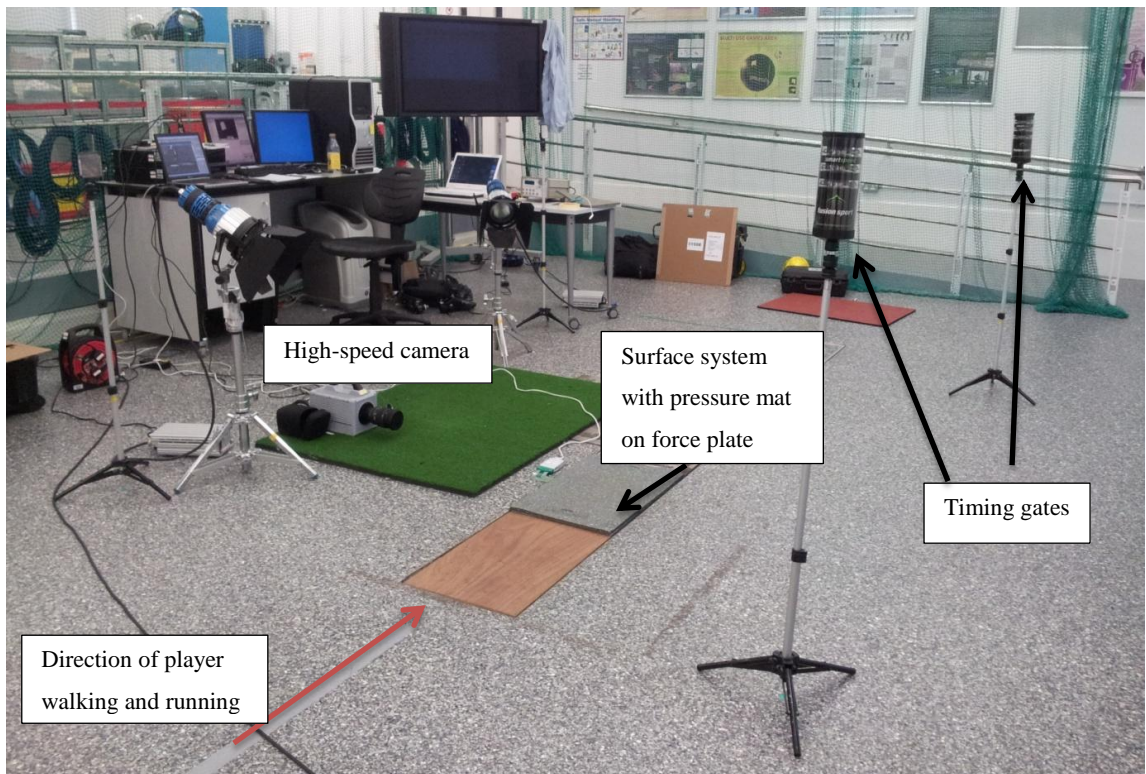


Figure 4.9: Measurement set-up for player loading tests in laboratory



Figure 4.10: Multi-output trigger box for various devices (Vicon, force plate, pressure mat and high-speed camera)

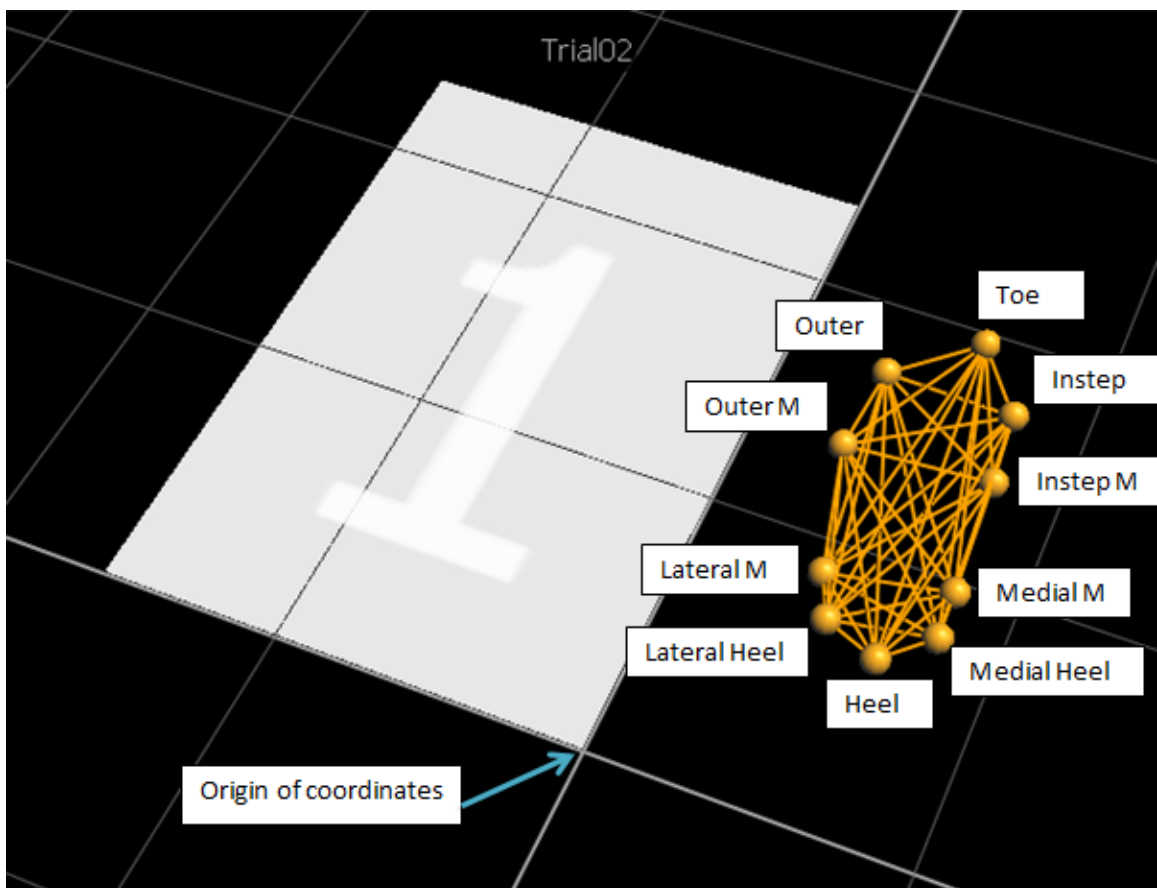


Figure 4.11: Static trial capture with player standing alongside the force plate and labelled markers

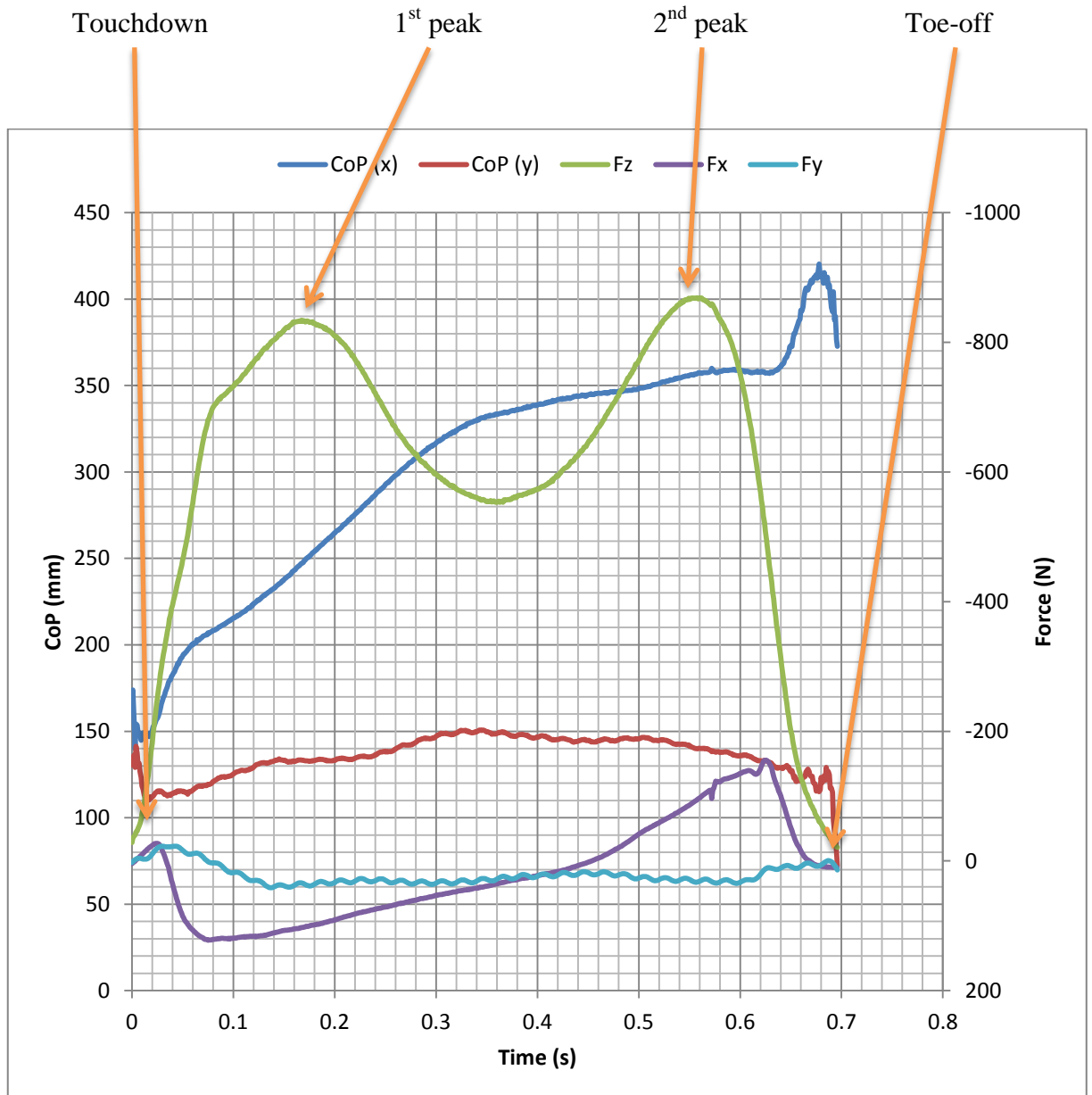


Figure 4.12: Representative vertical force (F_z), horizontal forces (F_x , F_y) and CoP (x,y)-time history profiles for heel-toe walking with images from high-speed camera taken at the frames of touchdown, first peak, second peak and toe-off

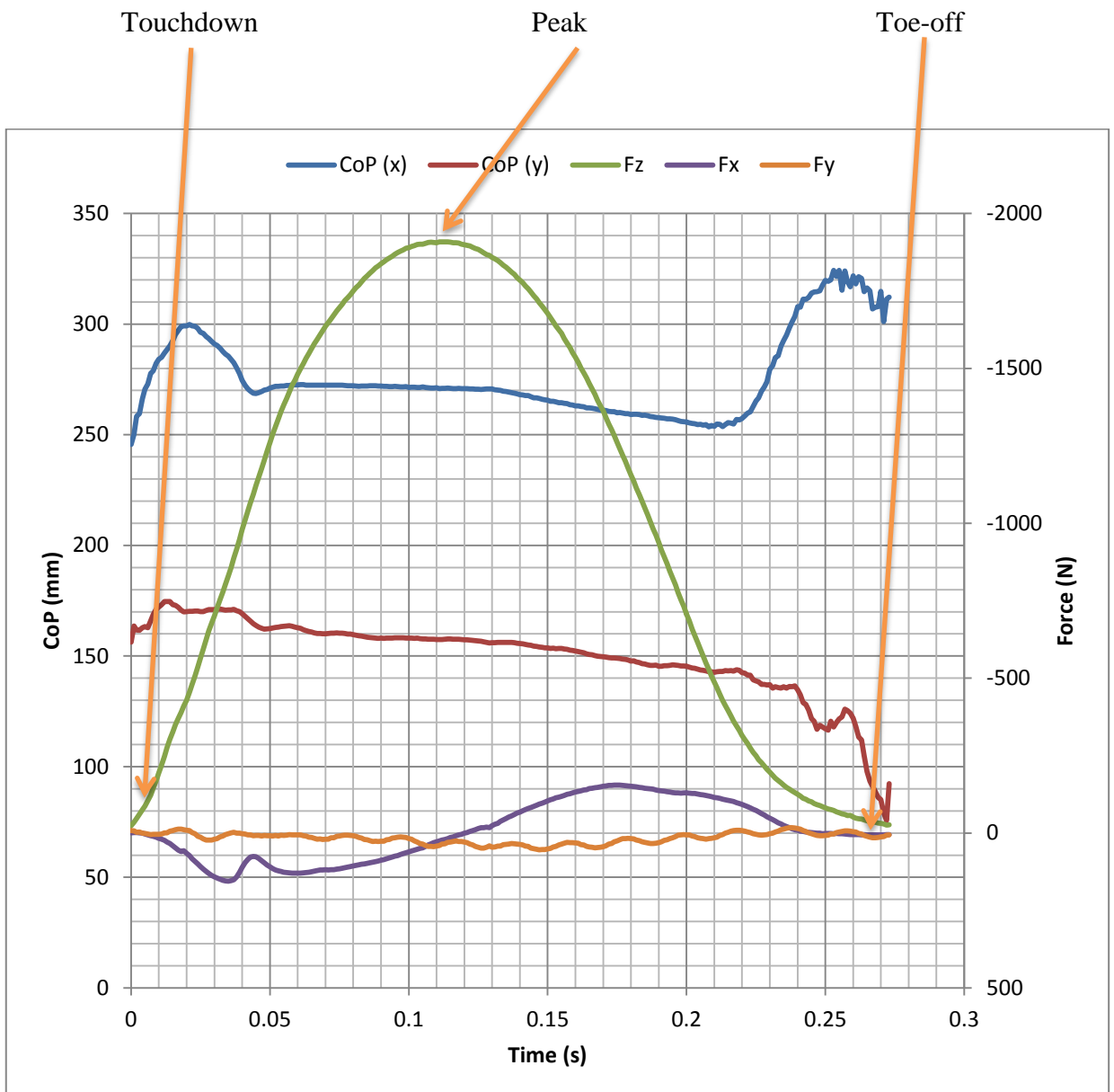


Figure 4.13: Representative vertical force (F_z), horizontal forces (F_x , F_y) and CoP (x,y)-time history profiles for forefoot running with images from high-speed camera taken at the frames of touchdown, peak force and toe-off

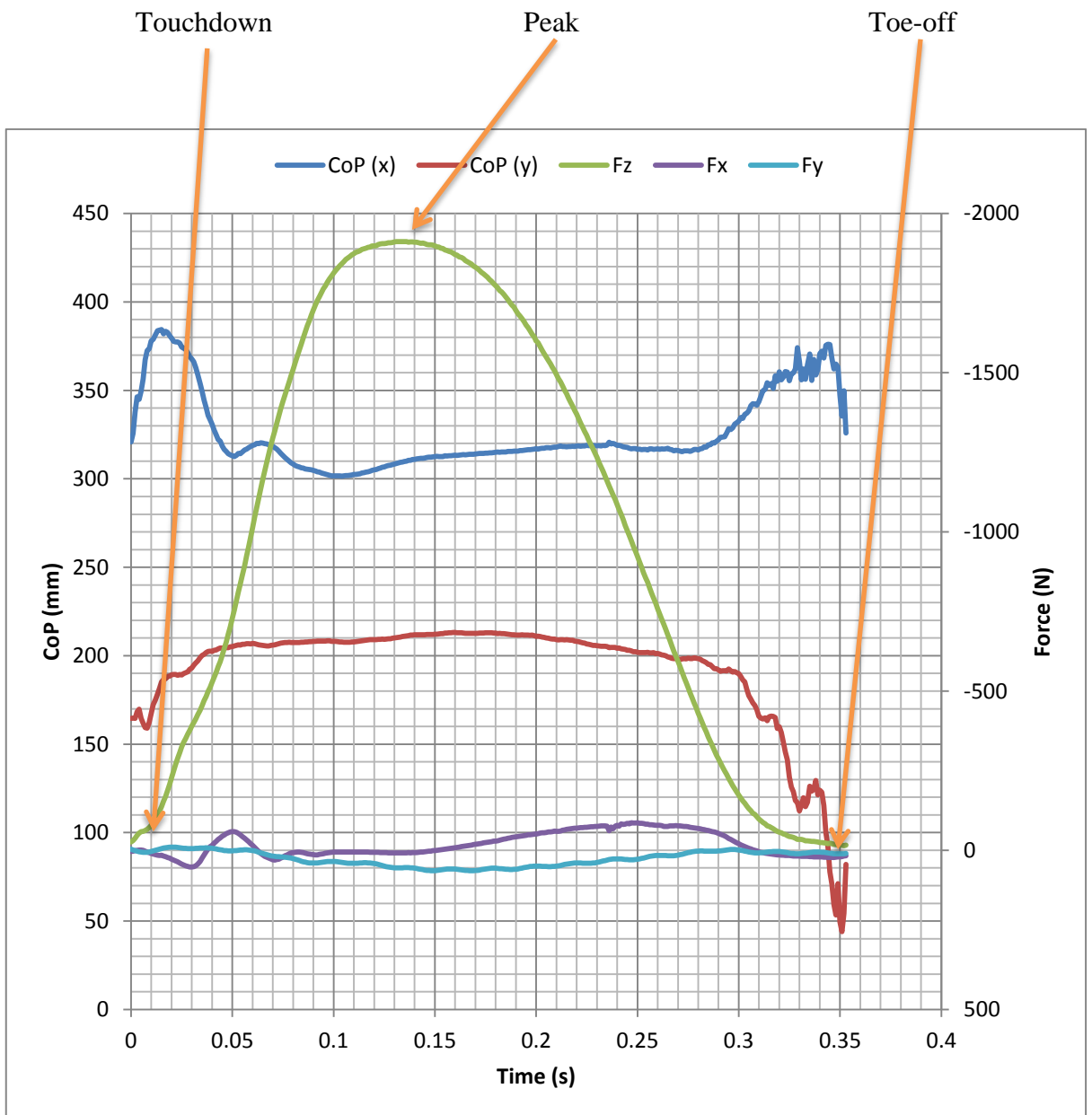
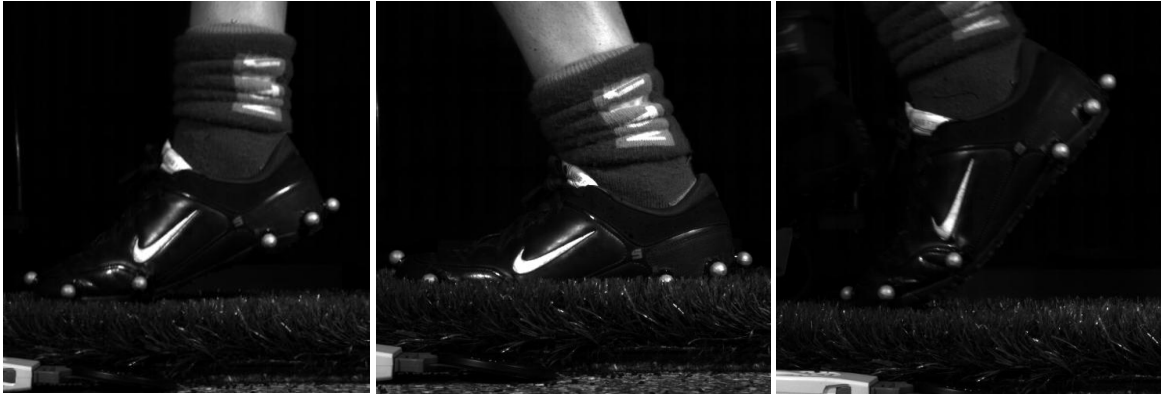


Figure 4.14: Representative vertical force (F_z), horizontal forces (F_x , F_y) and CoP (x,y)-time history profiles for forefoot landing with images from high-speed camera taken at the frames of touchdown, peak force and toe-off

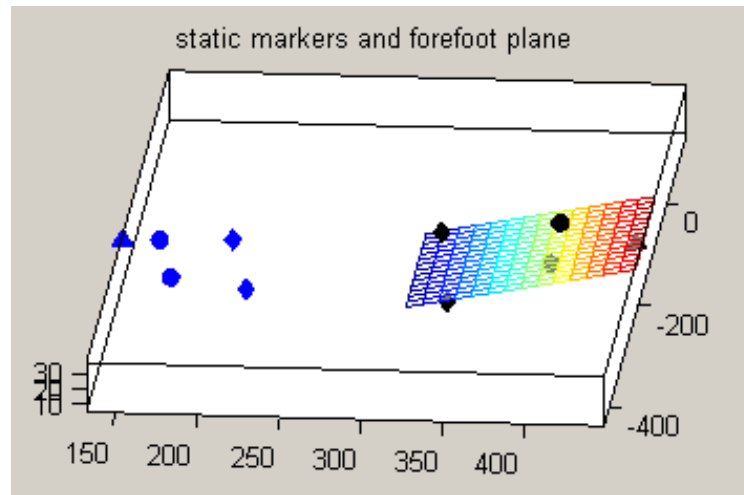


Figure 4.15: A plane fitted through the 5 forefoot markers (black) in the static trial

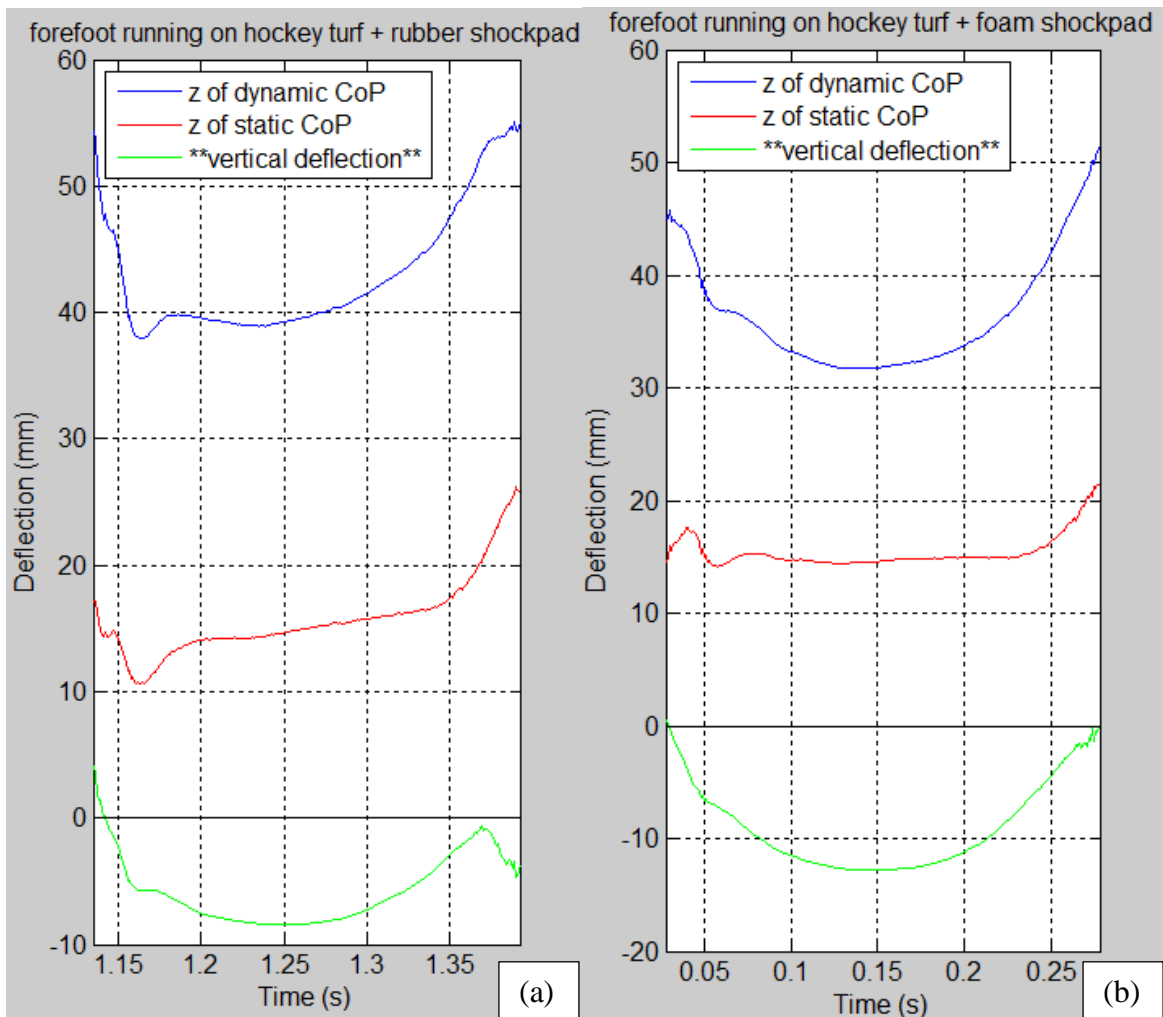


Figure 4.16: Vertical deflection (green curve) of hockey turf + rubber shockpad system (a) and hockey turf + foam shockpad system (b) under player forefoot running

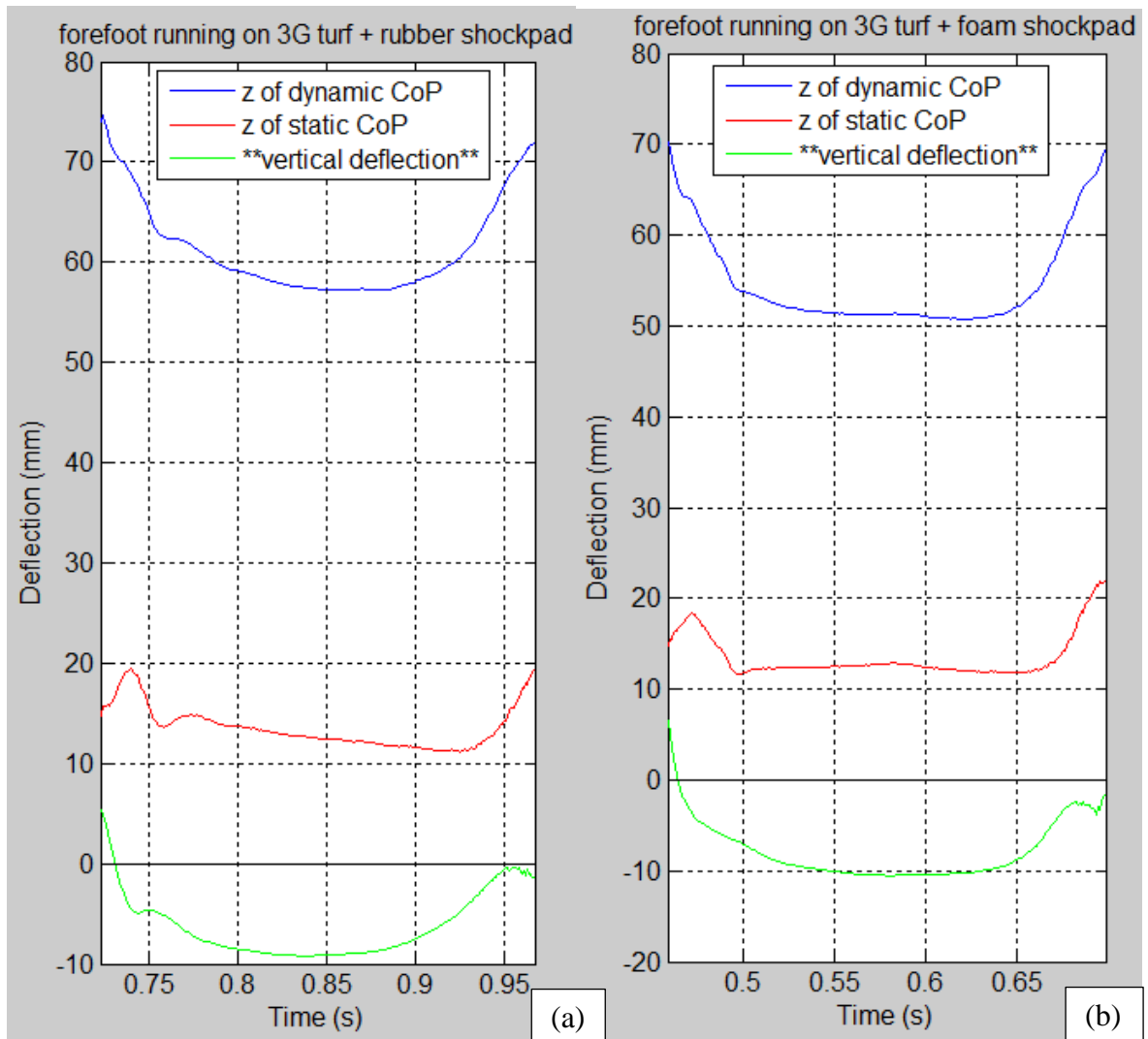


Figure 4.17: Vertical deflection (green curve) of 3G turf + rubber shockpad system (a) and 3G turf + foam shockpad system (b) under player forefoot running

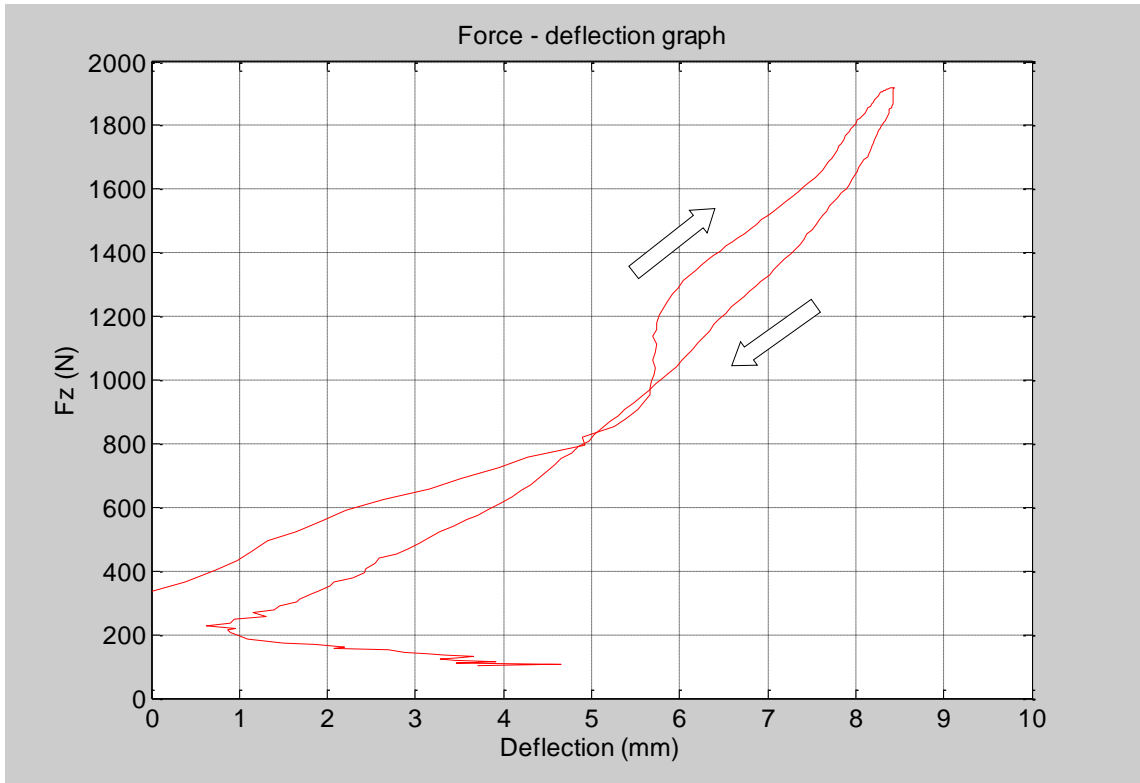


Figure 4.18: Force-deflection relationship of player forefoot running on hockey turf + rubber shockpad system

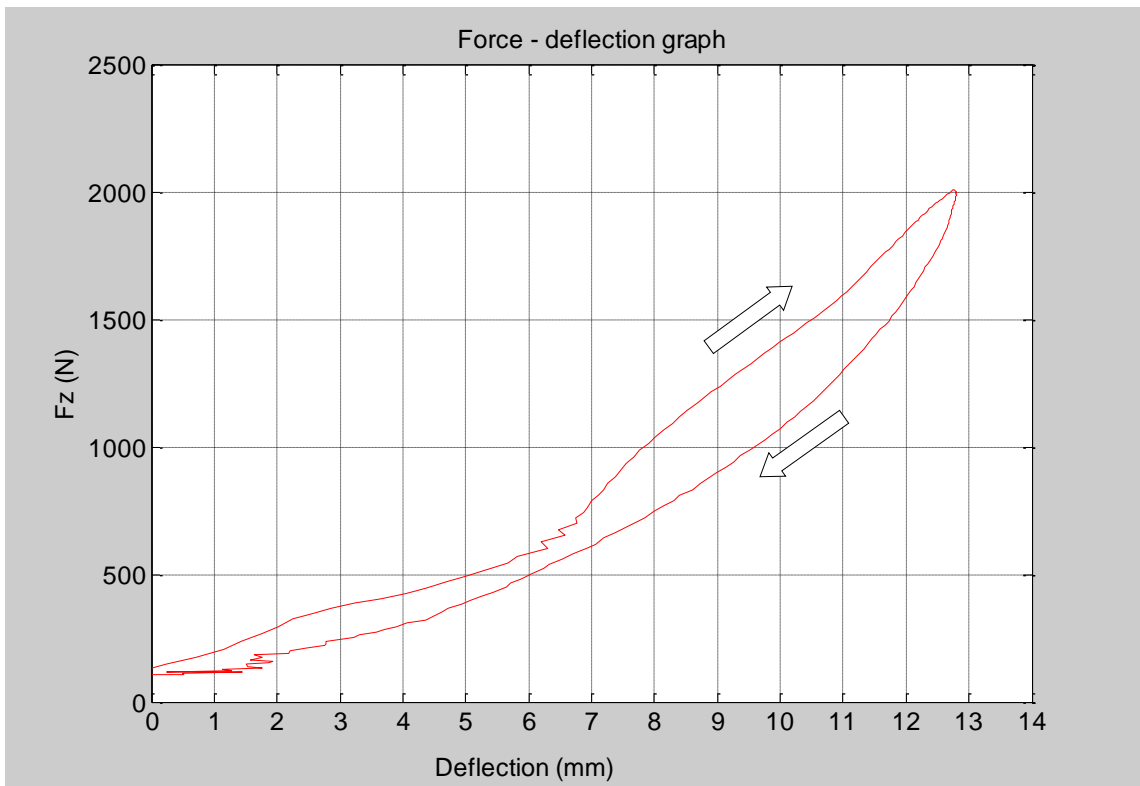


Figure 4.19: Force-deflection relationship of player forefoot running on hockey turf + foam shockpad system

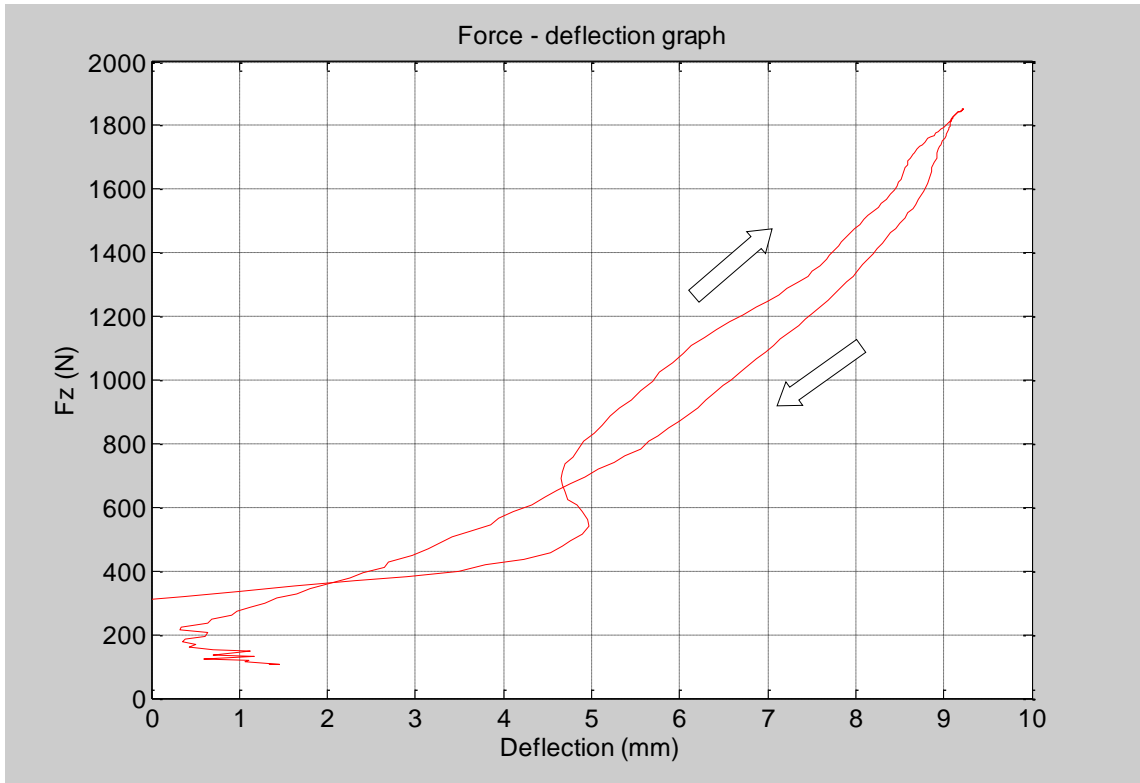


Figure 4.20: Force-deflection relationship of player forefoot running on 3G turf + rubber shockpad system

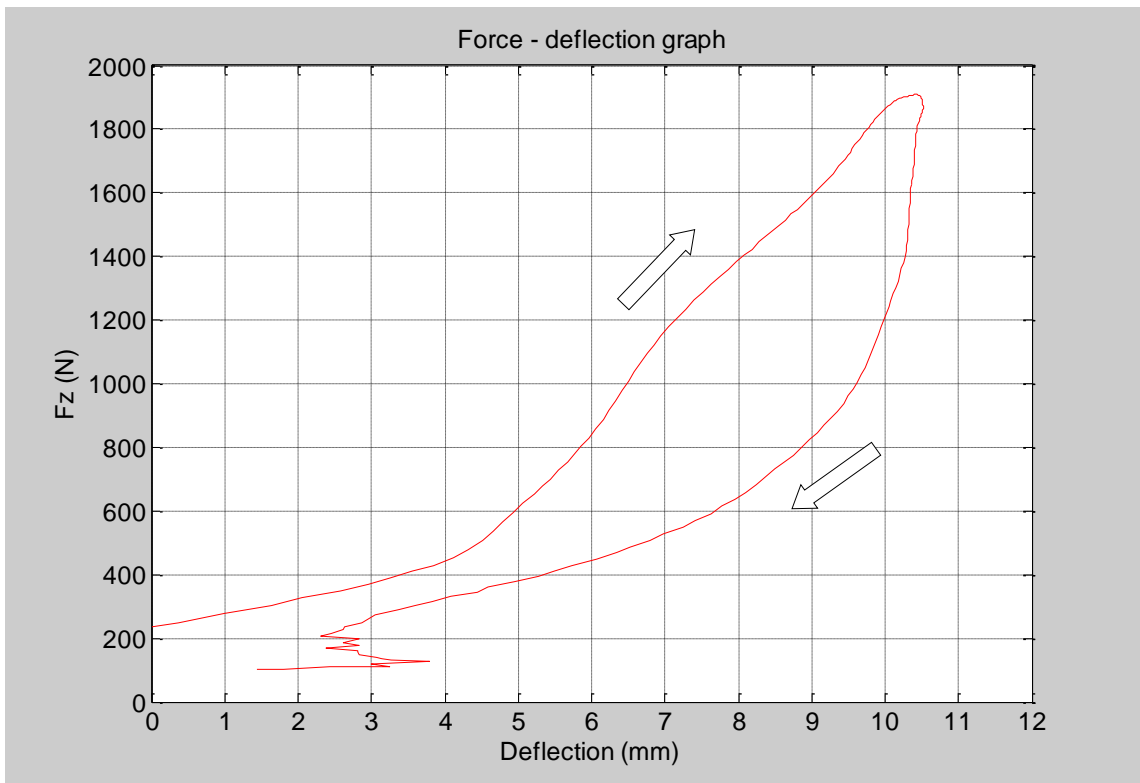


Figure 4.21: Force-deflection relationship of player forefoot running on 3G turf + foam shockpad system

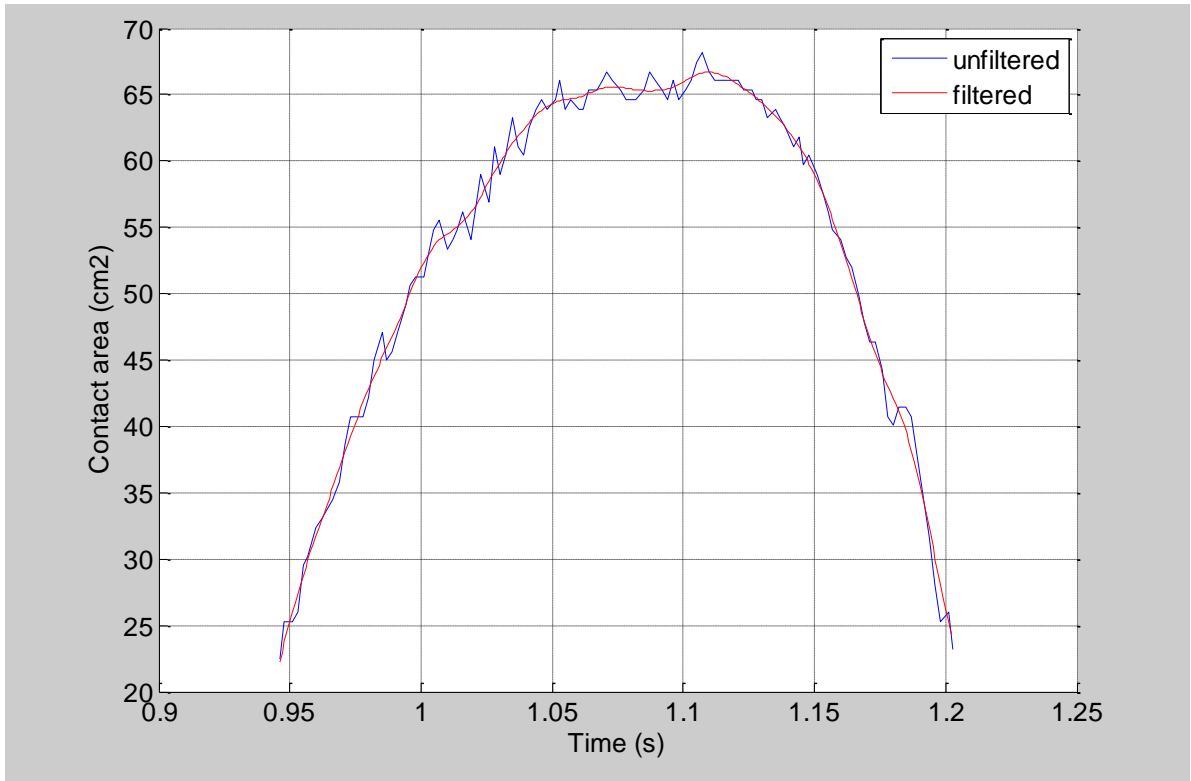


Figure 4.22: Boot contact area-time relationship of player forefoot running

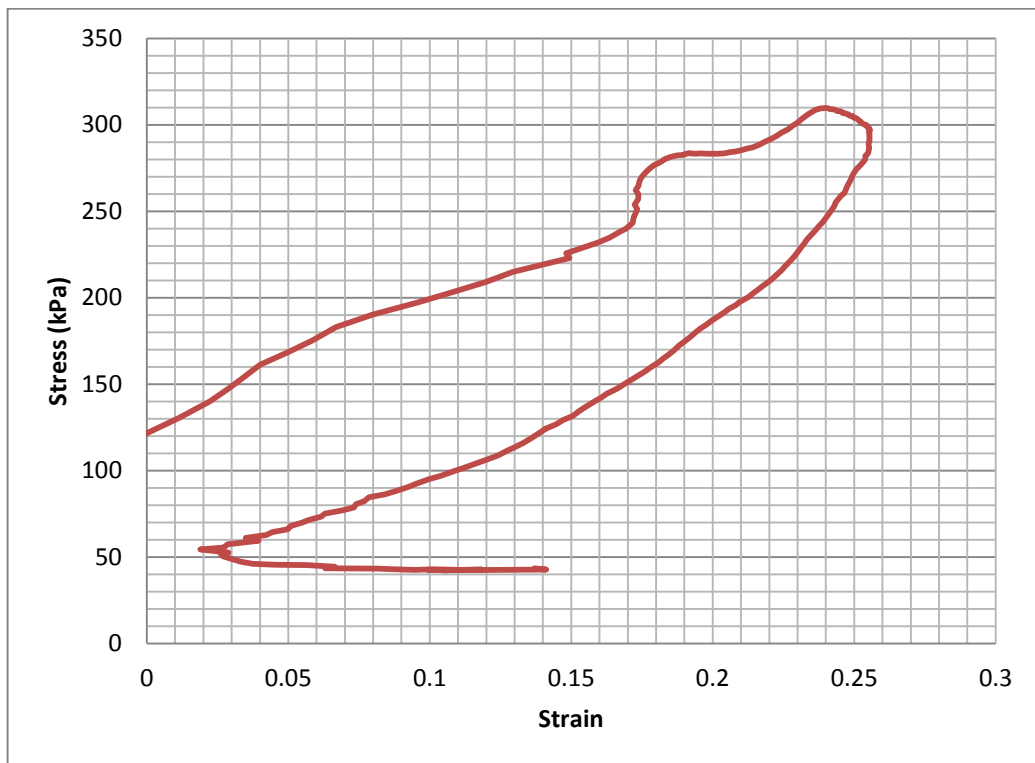


Figure 4.23: Stress-strain relationship of player forefoot running on hockey turf + rubber shockpad system

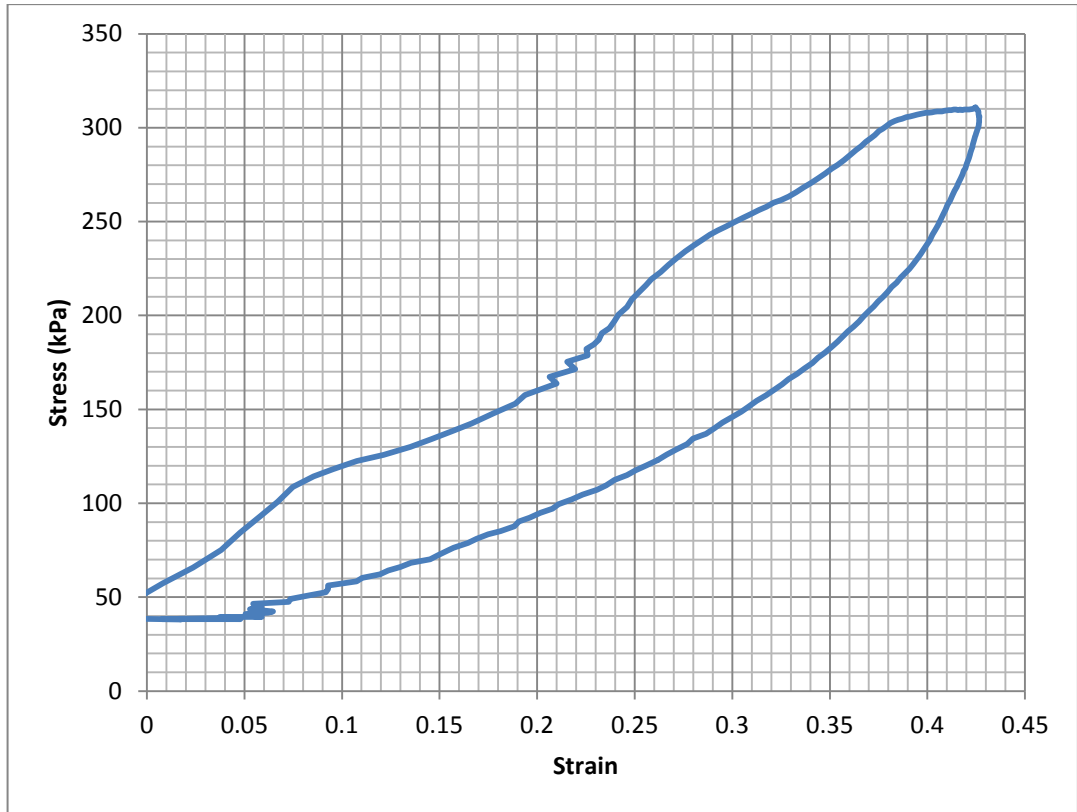


Figure 4.24: Stress-strain relationship of player forefoot running on hockey turf + foam shockpad system

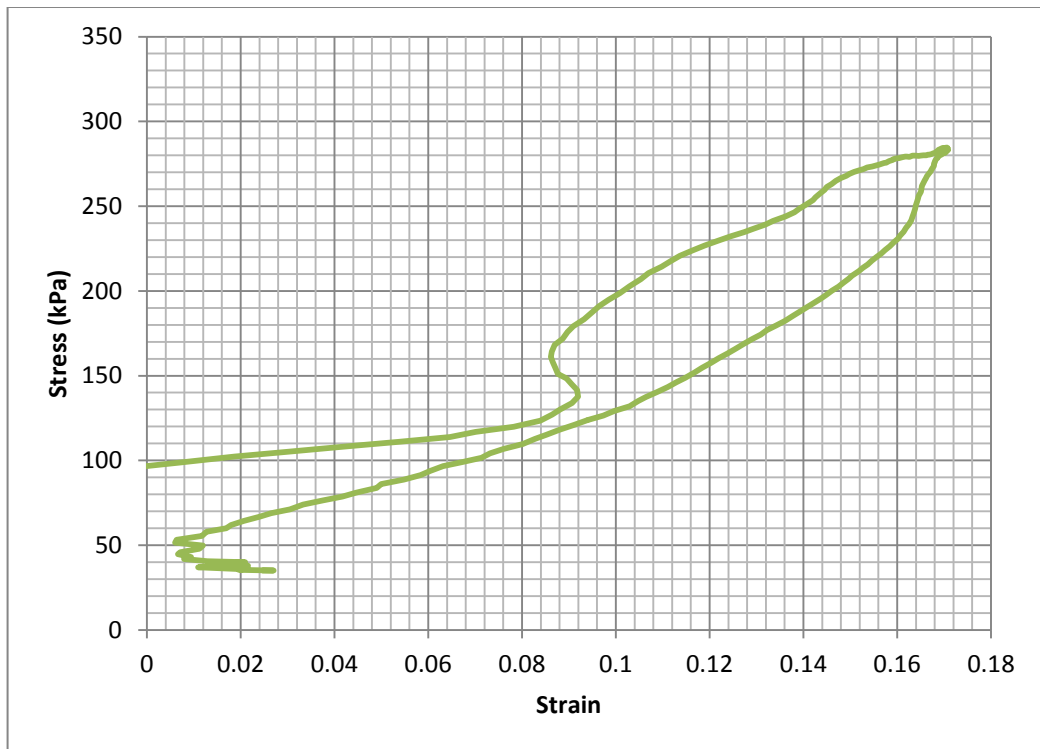


Figure 4.25: Stress-strain relationship of player forefoot running on 3G turf + rubber shockpad system

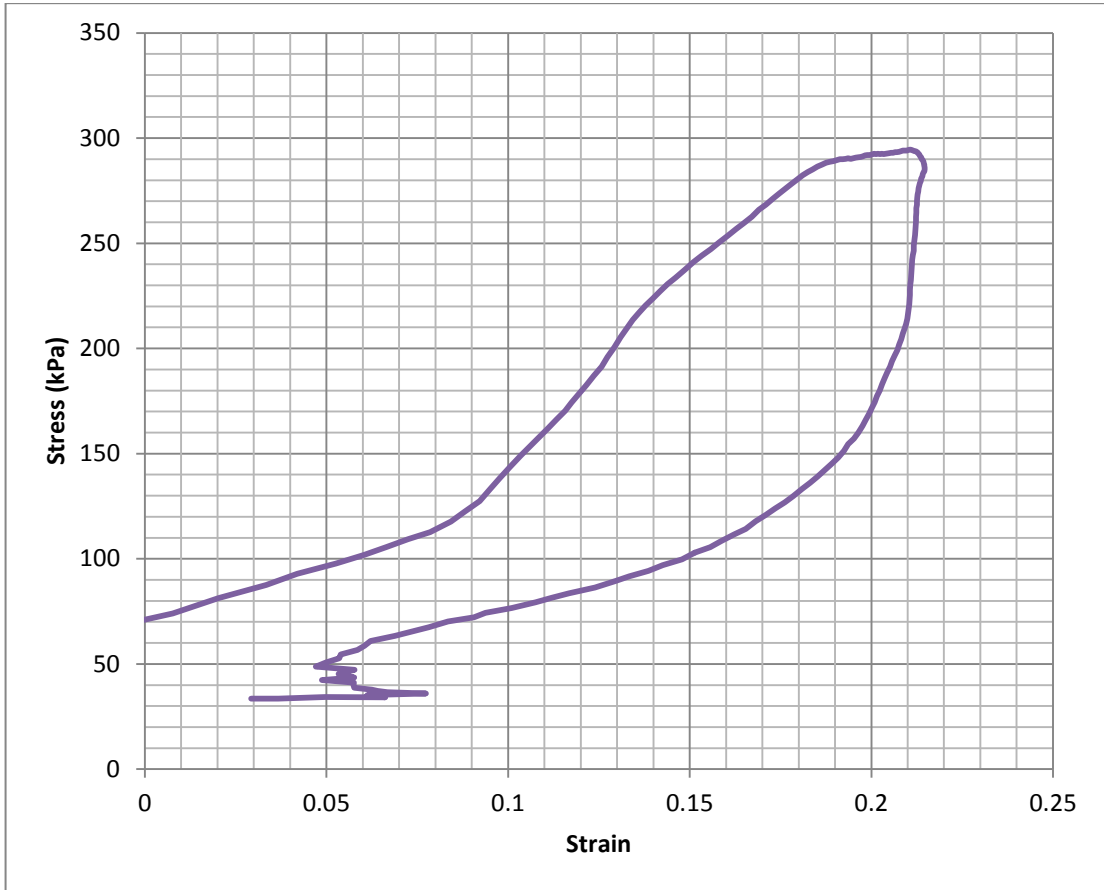


Figure 4.26: Stress-strain relationship of player forefoot running on 3G turf + foam shockpad system

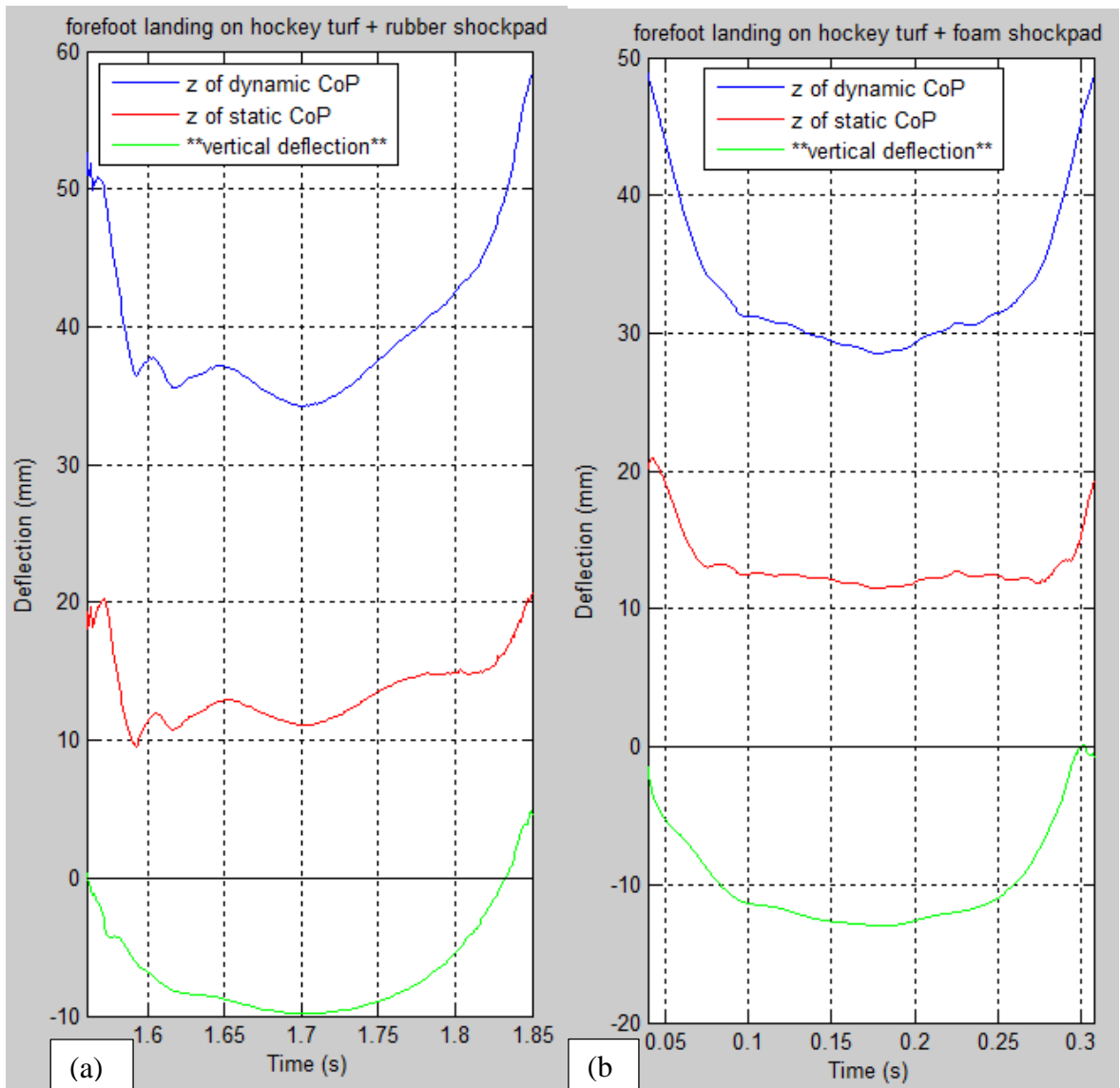


Figure 4.27: Vertical deflection (green curve) of hockey turf + rubber shockpad system (a) and hockey turf + foam shockpad system (b) under player forefoot landing

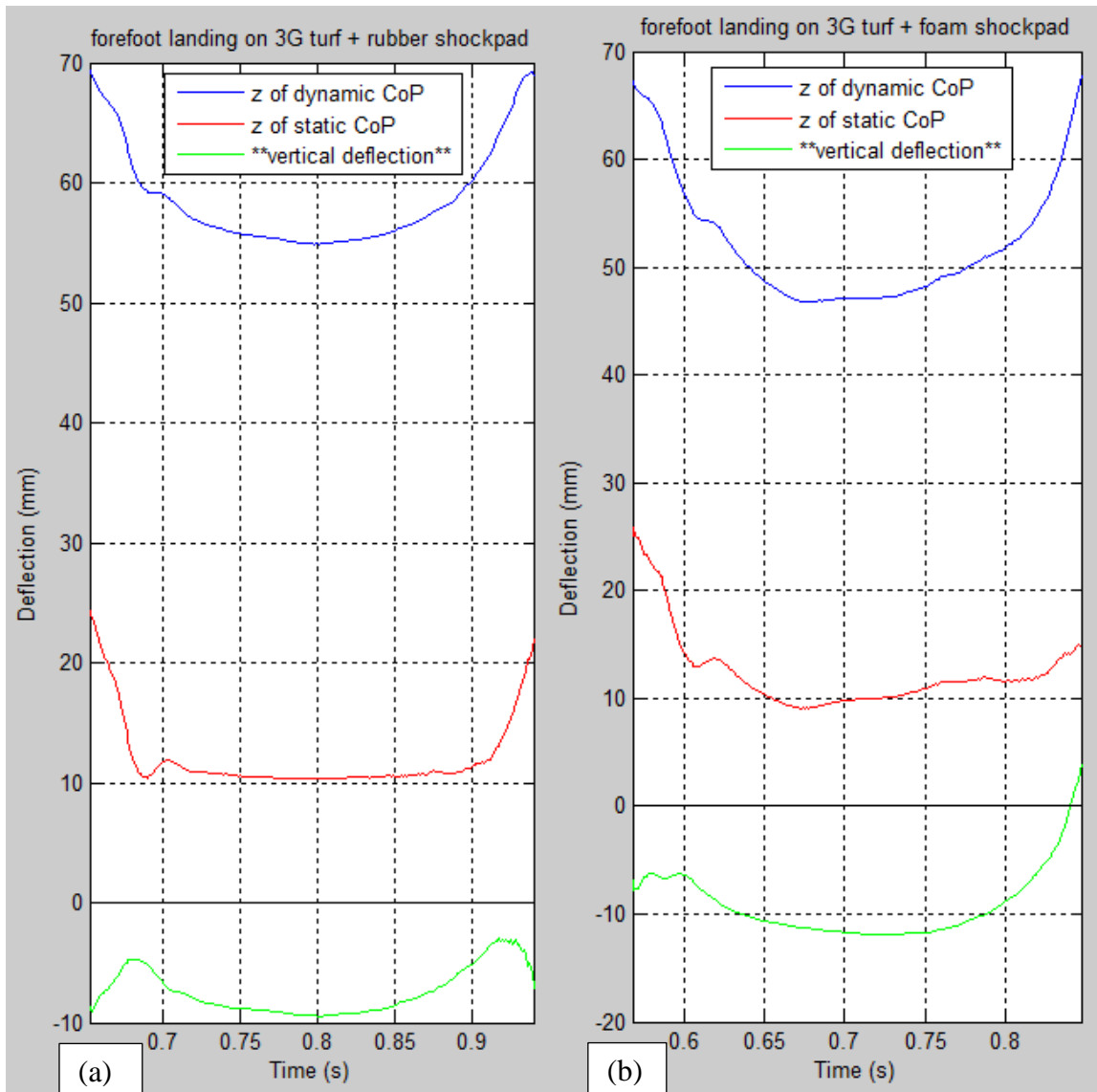


Figure 4.28: Vertical deflection (green curve) of 3G turf + rubber shockpad system (a) and 3G turf + foam shockpad system (b) under player forefoot landing



Figure 4.29: HSV footage shows the large surface deflection on 3G turf system at touchdown where the boot was inclined to the horizontal and boot-surface contact area was small

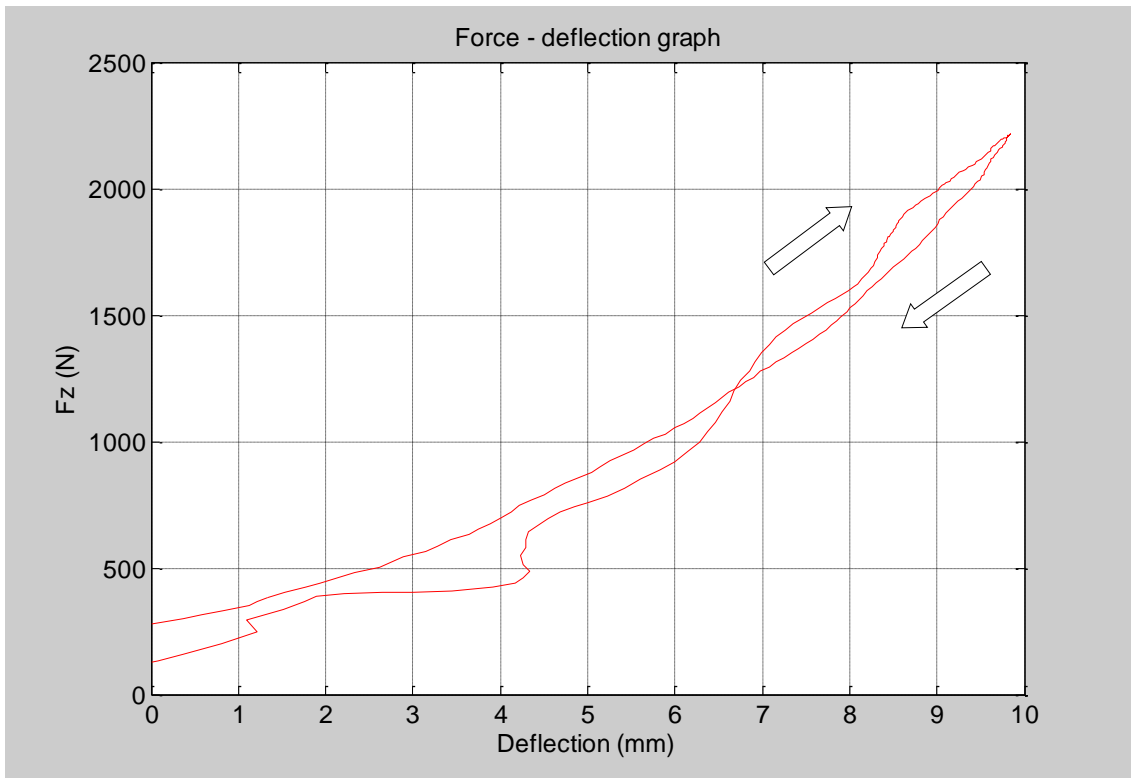


Figure 4.30: Force-deflection relationship of player forefoot landing on hockey turf + rubber shockpad system

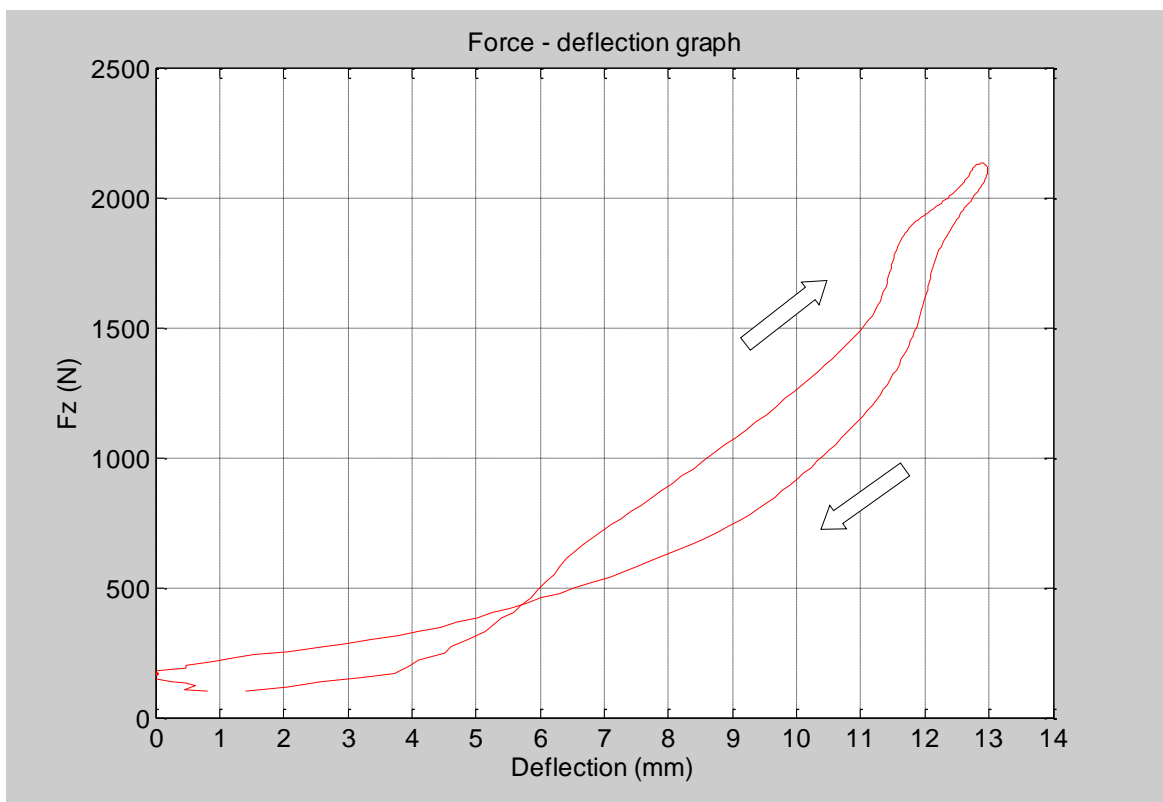


Figure 4.31: Force-deflection relationship of player forefoot landing on hockey turf + foam shockpad system

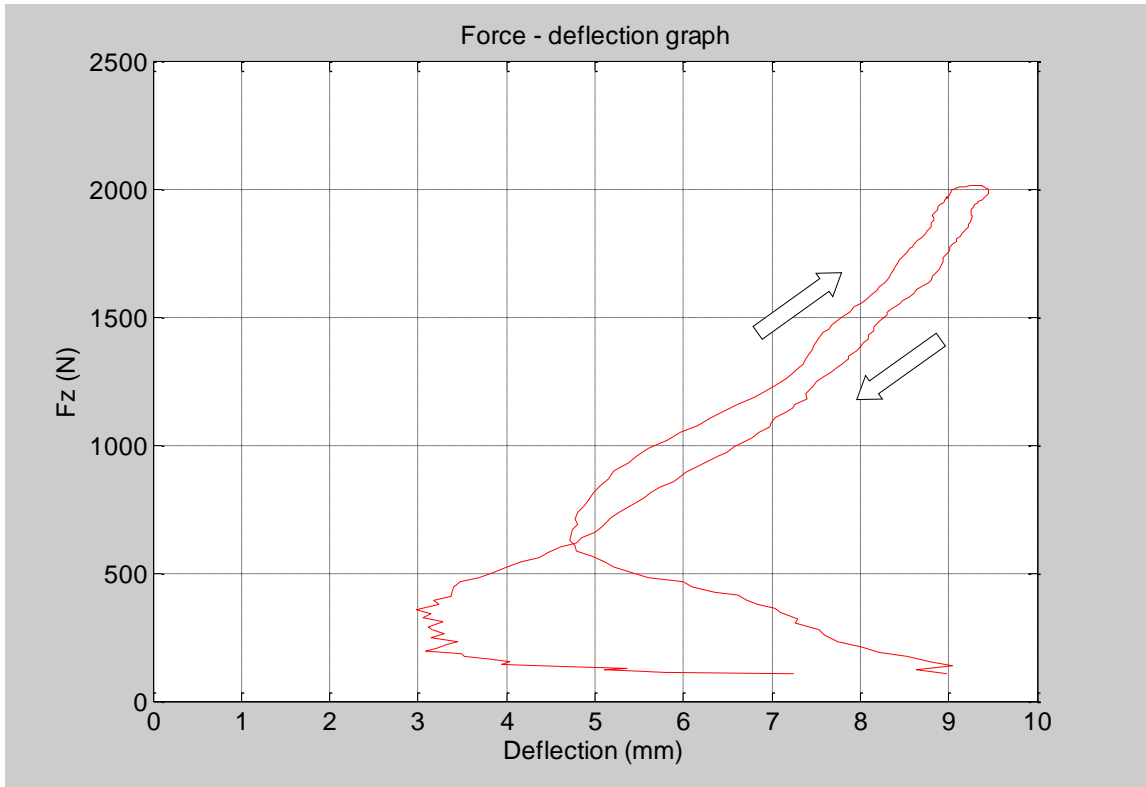


Figure 4.32: Force-deflection relationship of player forefoot landing on the 3G turf + rubber shockpad system

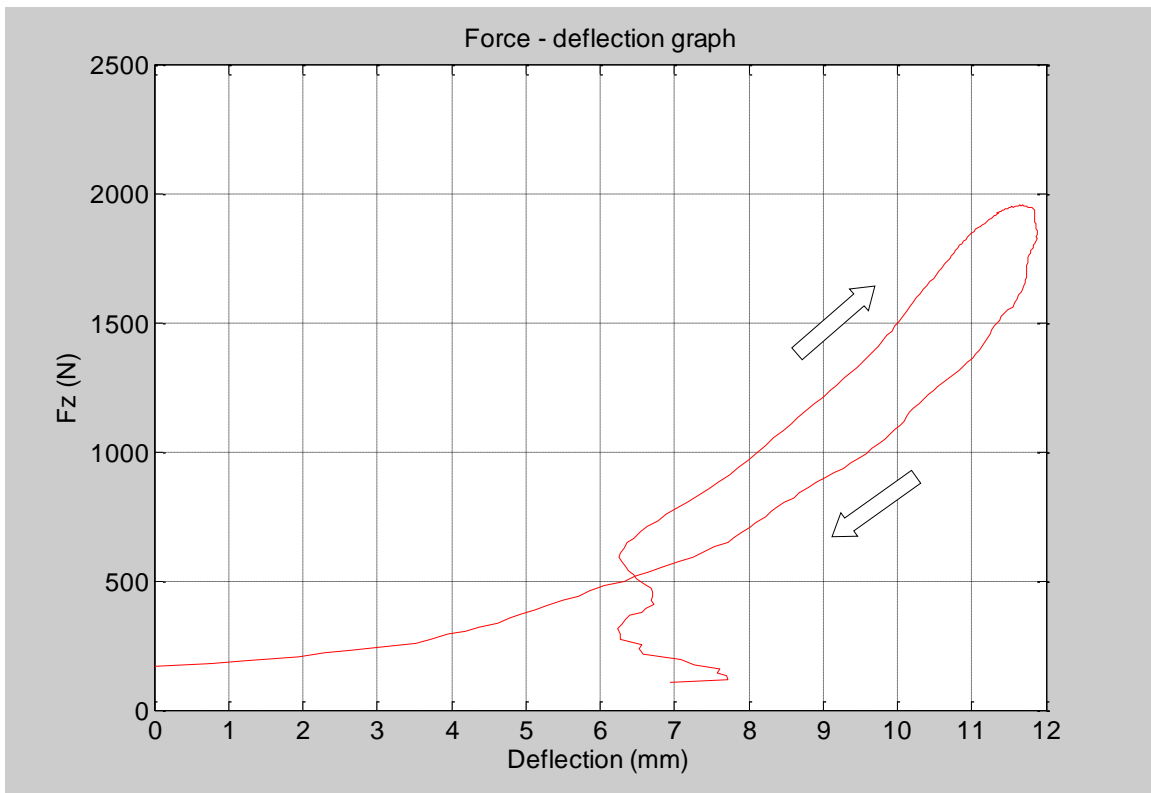


Figure 4.33: Force-deflection relationship of player forefoot landing on 3G turf + foam shockpad system

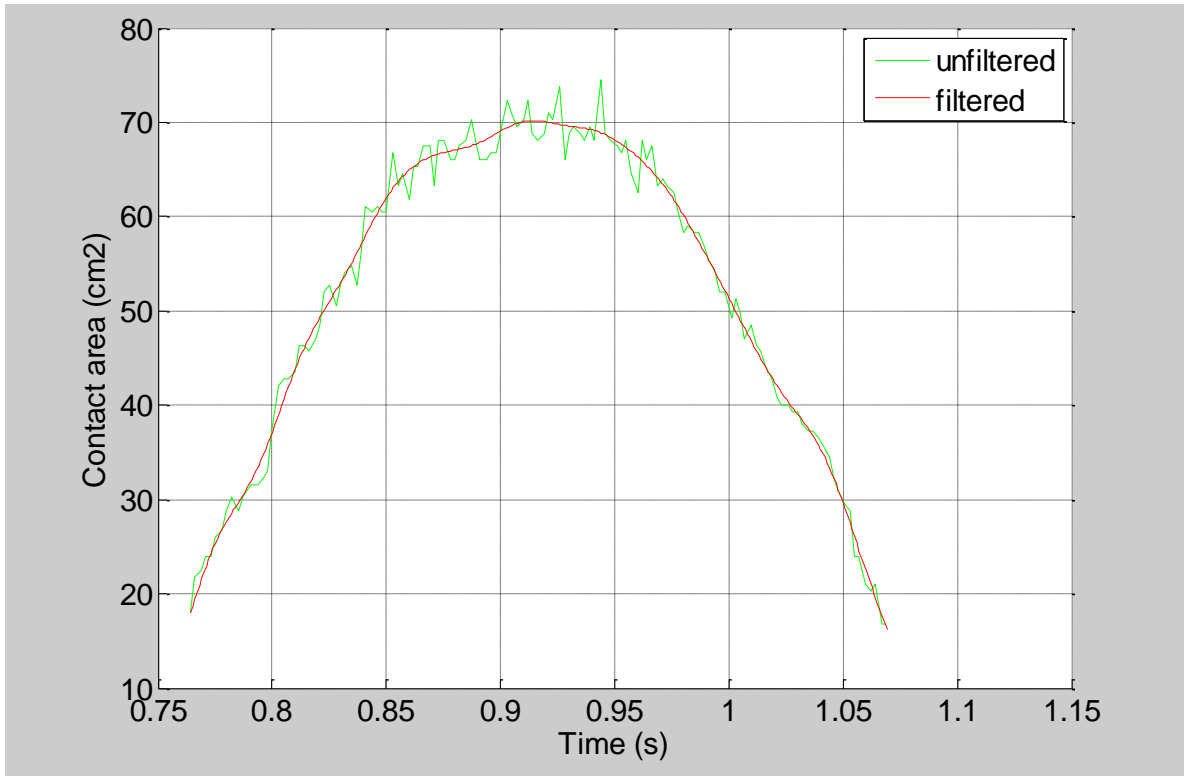


Figure 4.34: Boot contact area-time relationship of player forefoot landing

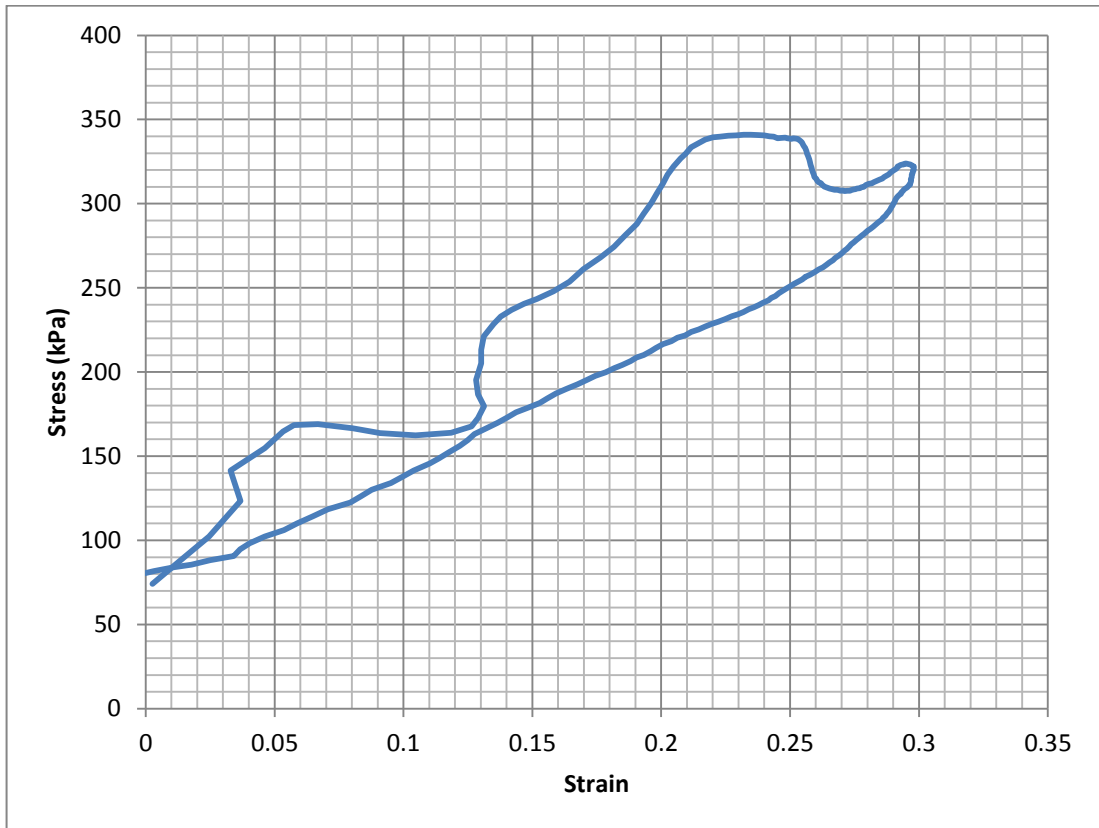


Figure 4.35: Stress-strain relationship of player forefoot landing on hockey turf + rubber shockpad system

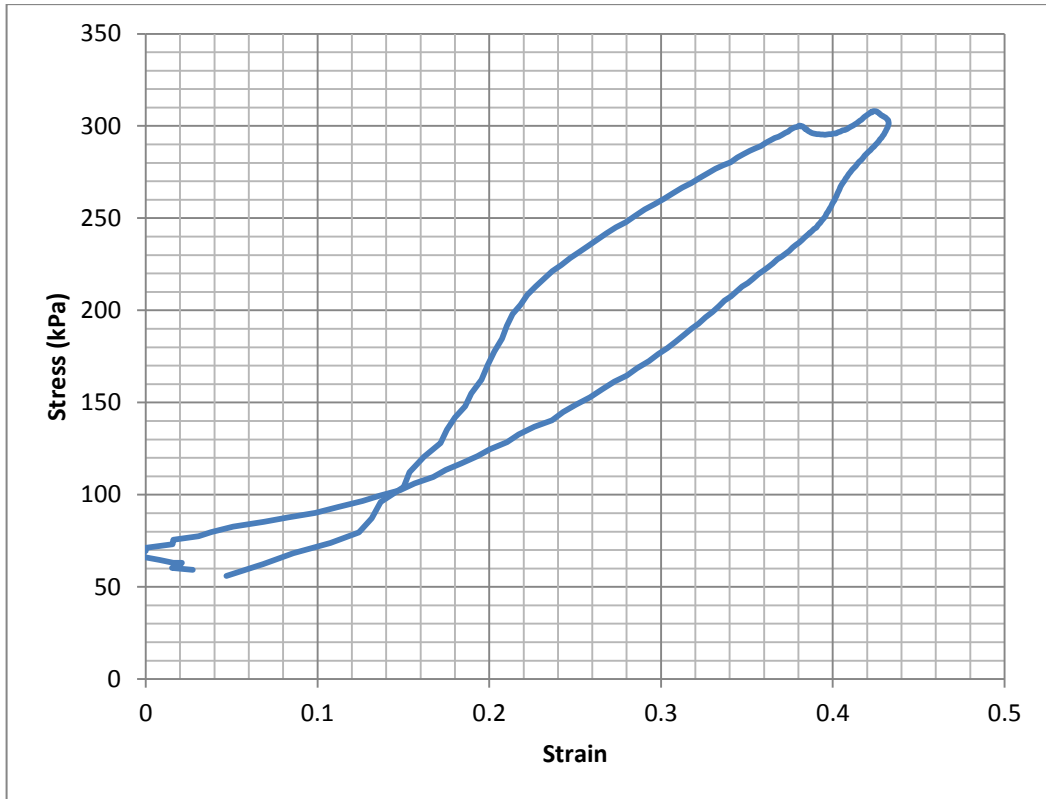


Figure 4.36: Stress-strain relationship of player forefoot landing on hockey turf + foam shockpad system

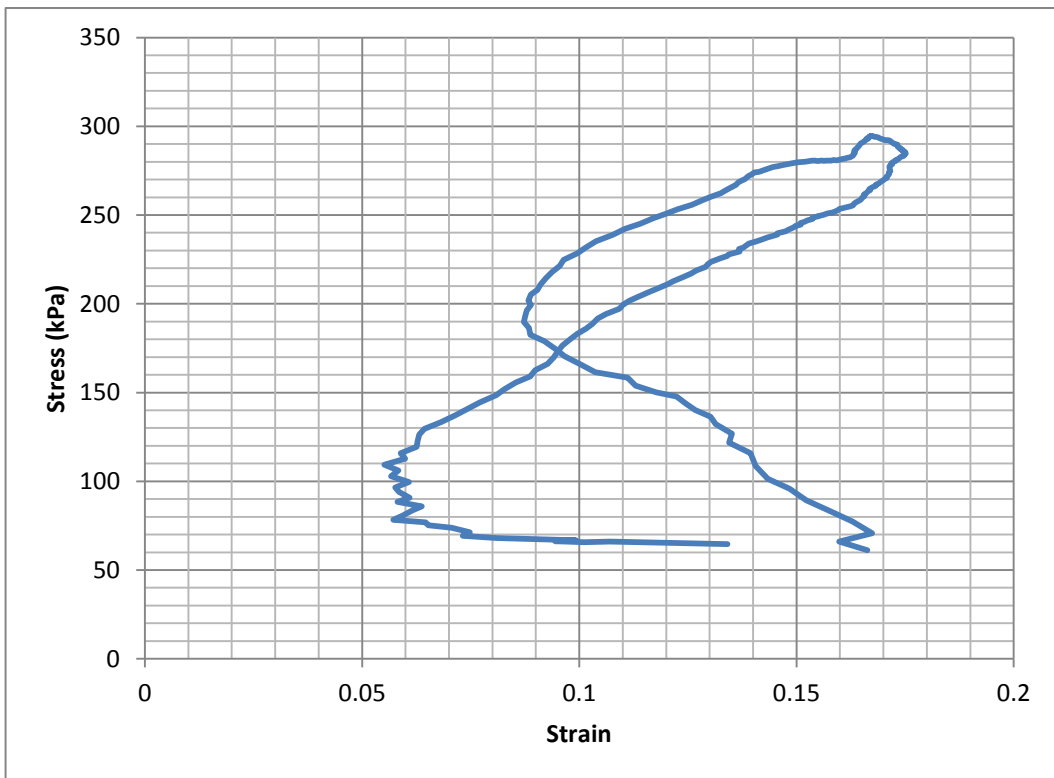


Figure 4.37: Stress-strain relationship of player forefoot landing on 3G turf + rubber shockpad system

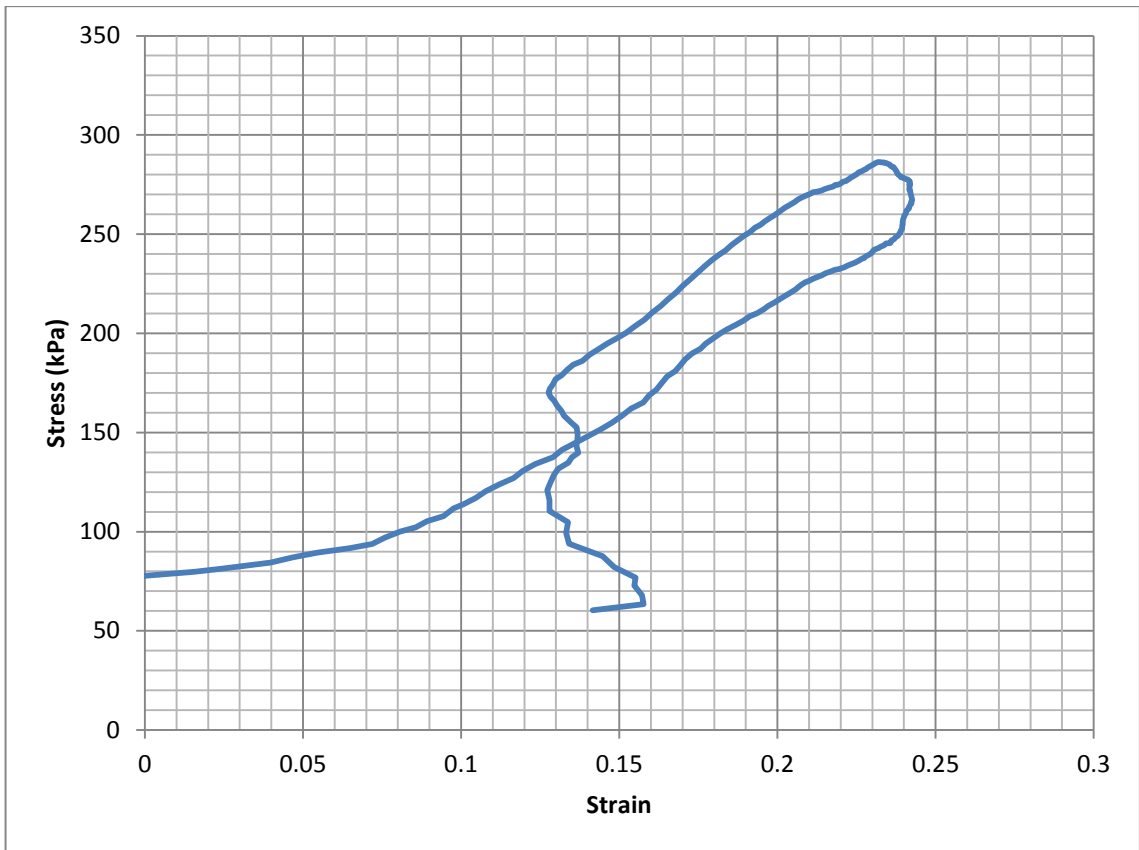


Figure 4.38: Stress-strain relationship of player forefoot landing on 3G turf + foam shockpad system

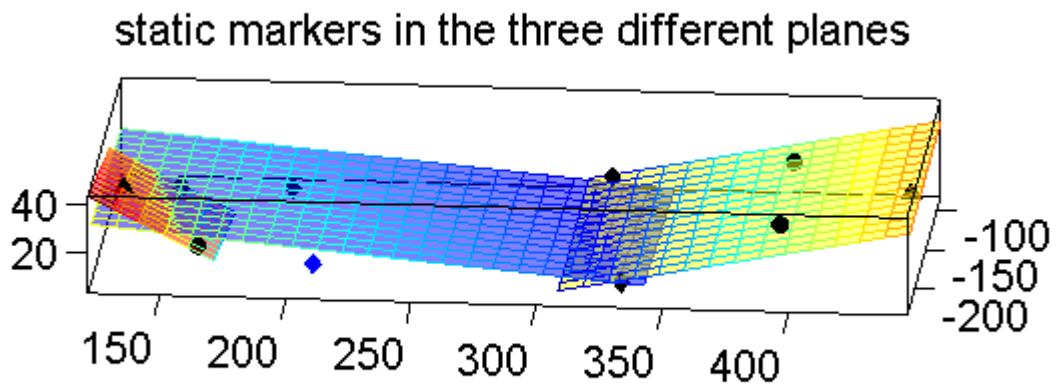


Figure 4.39: Planes fitted through 5 forefoot markers (yellow), 5 rear and mid foot markers (blue) and 3 heel markers (red) in the static trial

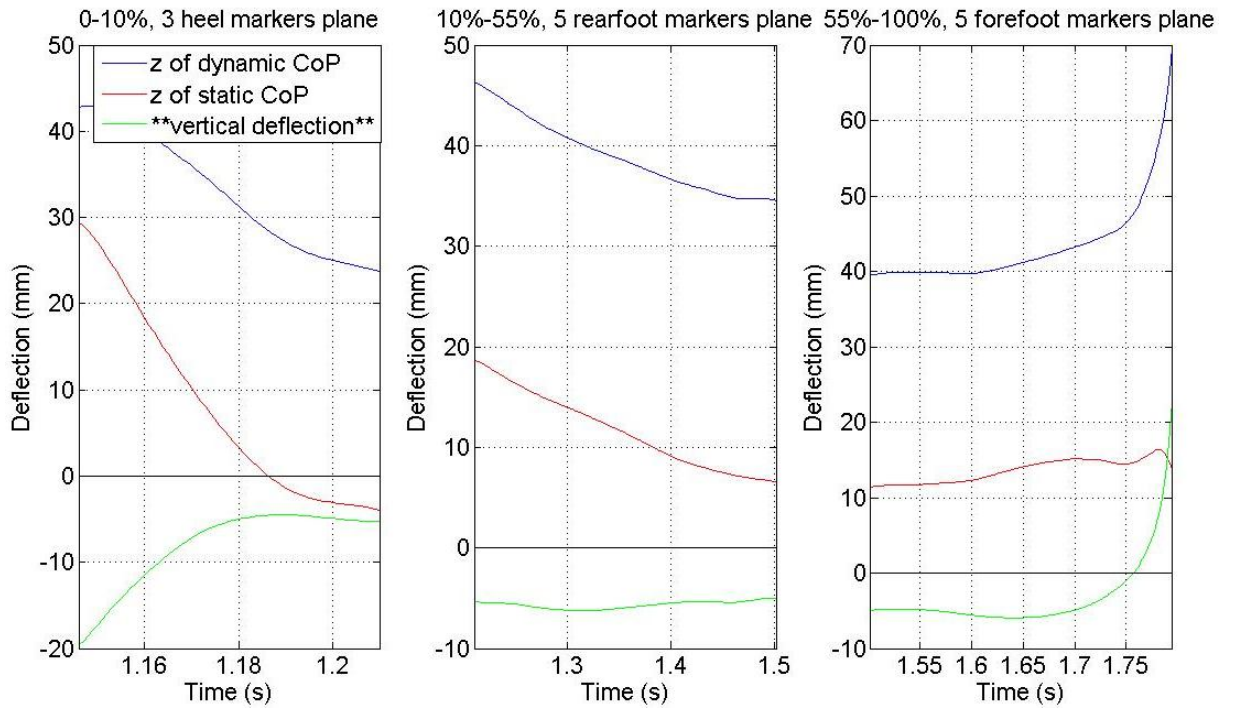


Figure 4.40: Vertical deflection (green curve) of hockey turf + rubber shockpad system measured at 0-10%, 10%-55% and 55%-100% of ground contact under player heel-toe walking

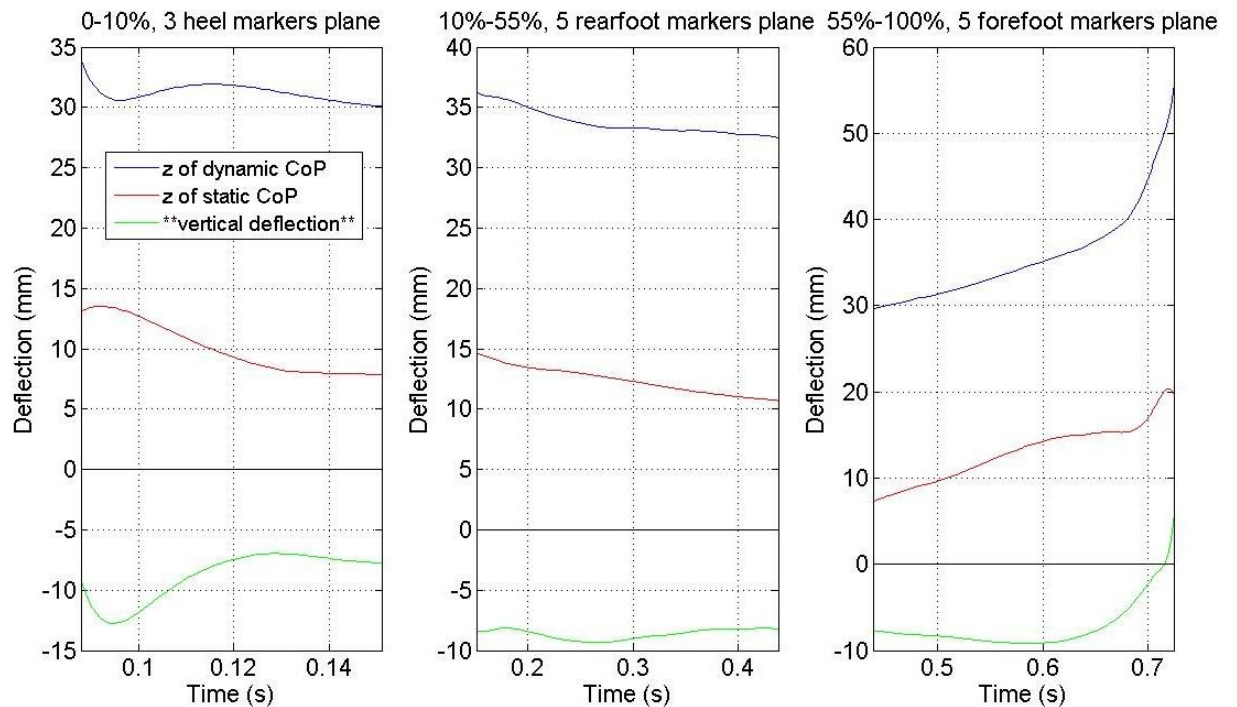


Figure 4.41: Vertical deflection (green curve) of hockey turf + foam shockpad system measured at 0-10%, 10%-55% and 55%-100% of ground contact under player heel-toe walking

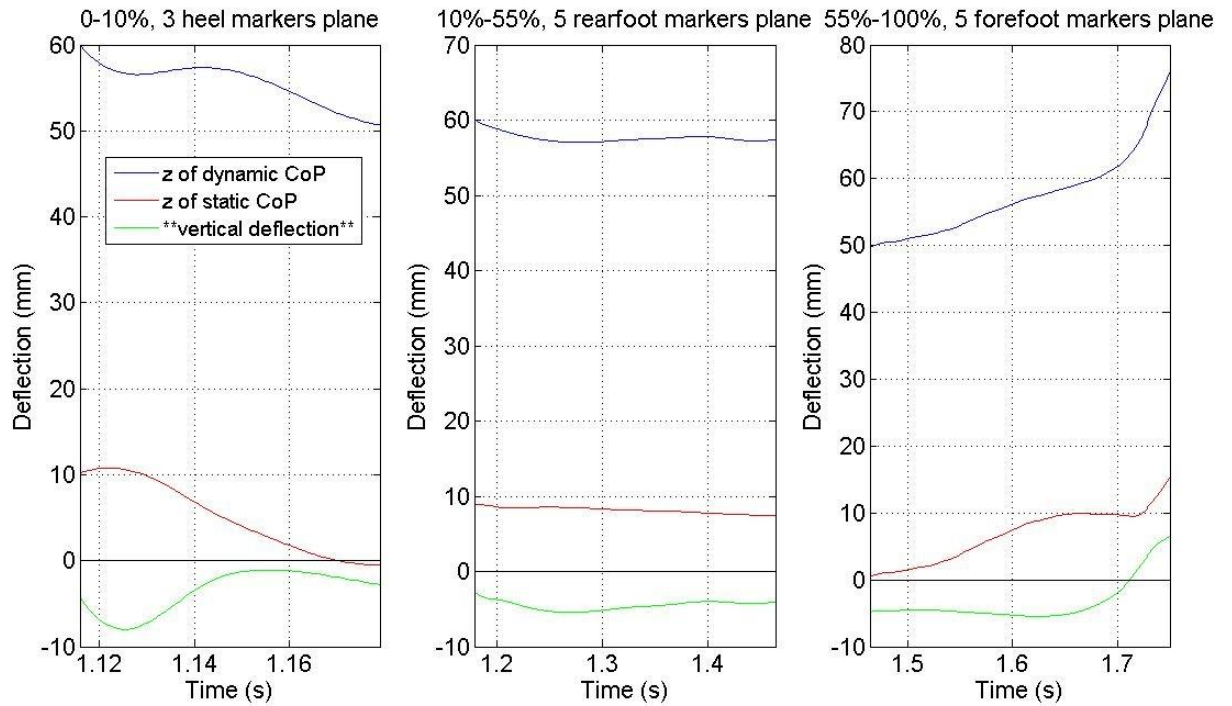


Figure 4.42: Vertical deflection (green curve) of 3G turf + rubber shockpad system measured at 0-10%, 10%-55% and 55%-100% of ground contact under player heel-toe walking

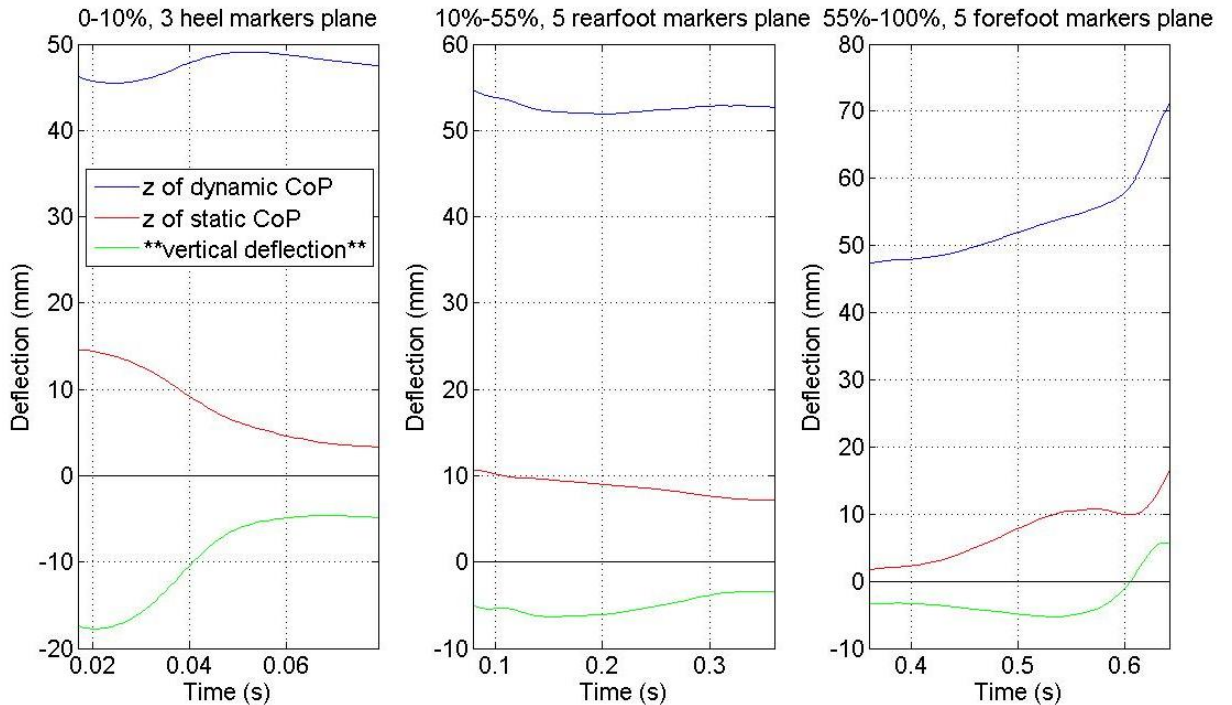


Figure 4.43: Vertical deflection (green curve) of 3G turf + foam shockpad system measured at 0-10%, 10%-55% and 55%-100% of ground contact under player heel-toe walking

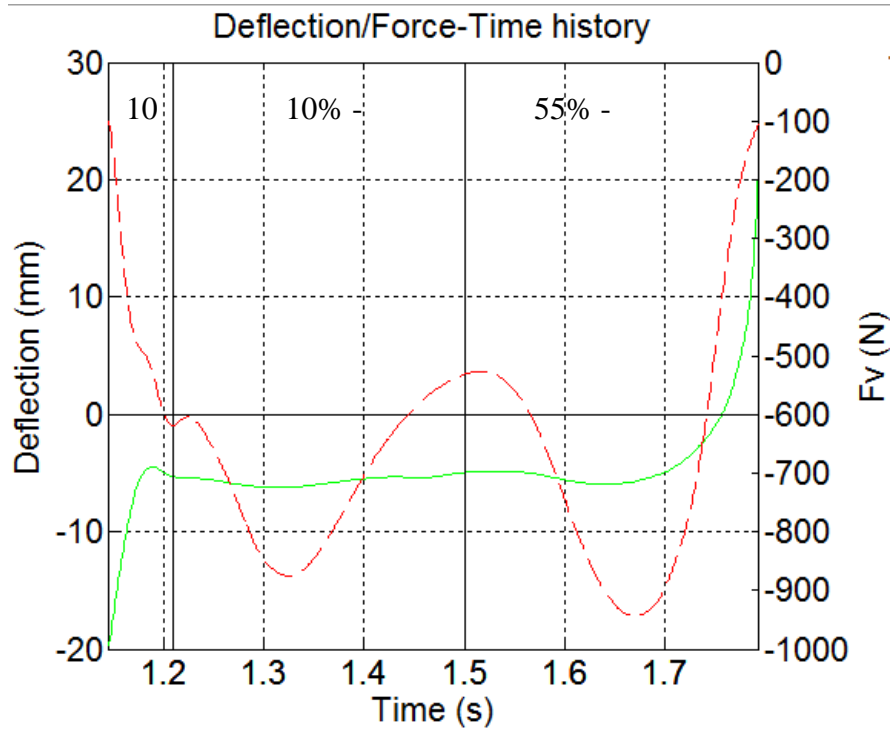


Figure 4.44: Force (red dash curve) and deflection (green curve) in touchdown phase (10%), mid-stance phase (10%-55%) and push-off phase (55%-100%) during ground contact of player heel-toe walking on hockey turf + rubber shockpad system

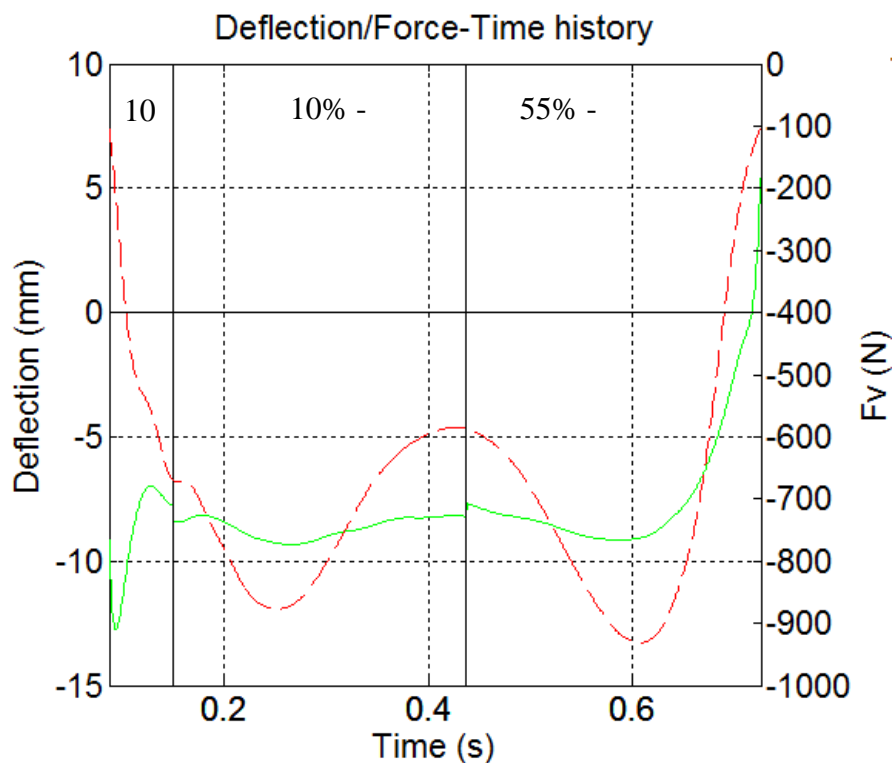


Figure 4.45: Force (red dash curve) and deflection (green curve) in touchdown phase (10%), mid-stance phase (10%-55%) and push-off phase (55%-100%) during ground contact of player heel-toe walking on hockey turf + foam shockpad system

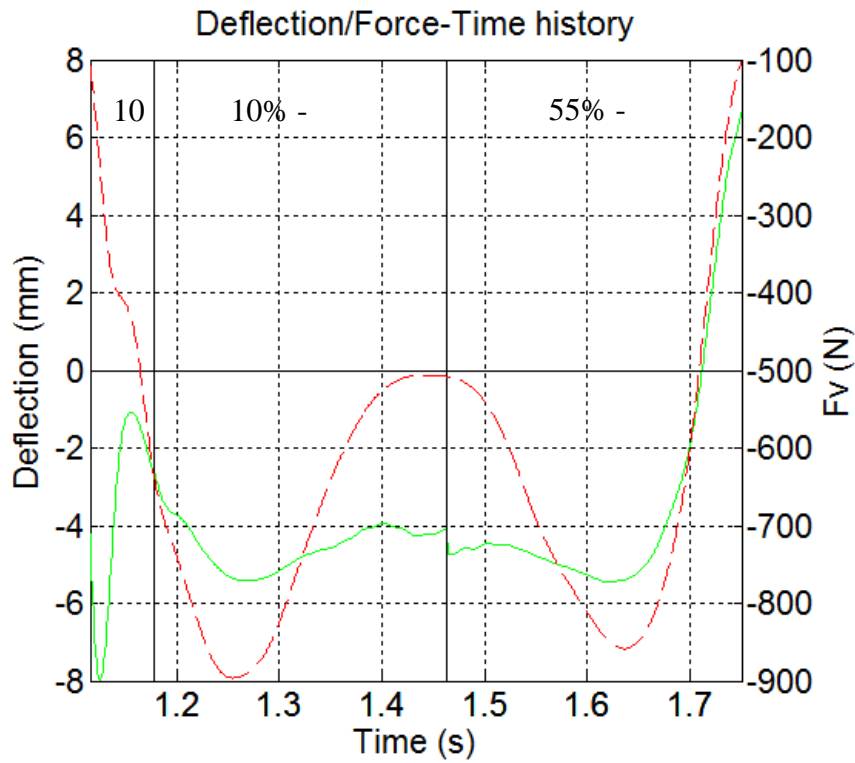


Figure 4.46: Force (red dash curve) and deflection (green curve) in touchdown phase (10%), mid-stance phase (10%-55%) and push-off phase (55%-100%) during ground contact of player heel-toe walking on 3G turf + rubber shockpad system

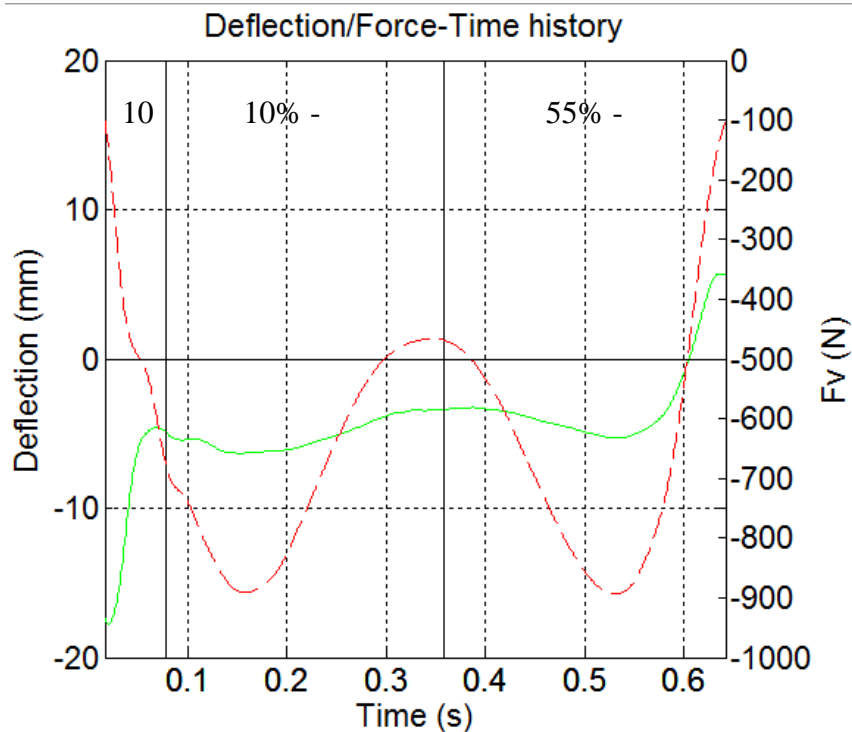


Figure 4.47: Force (red dash curve) and deflection (green curve) in touchdown phase (10%), mid-stance phase (10%-55%) and push-off phase (55%-100%) during ground contact of player heel-toe walking on 3G turf + foam shockpad system

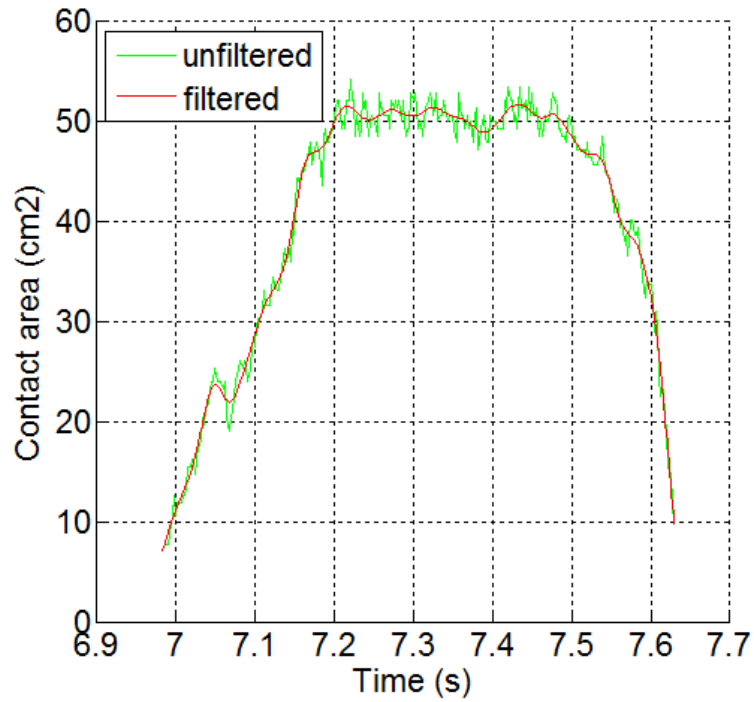


Figure 4.48: Boot contact area-time relationship of player heel-toe walking

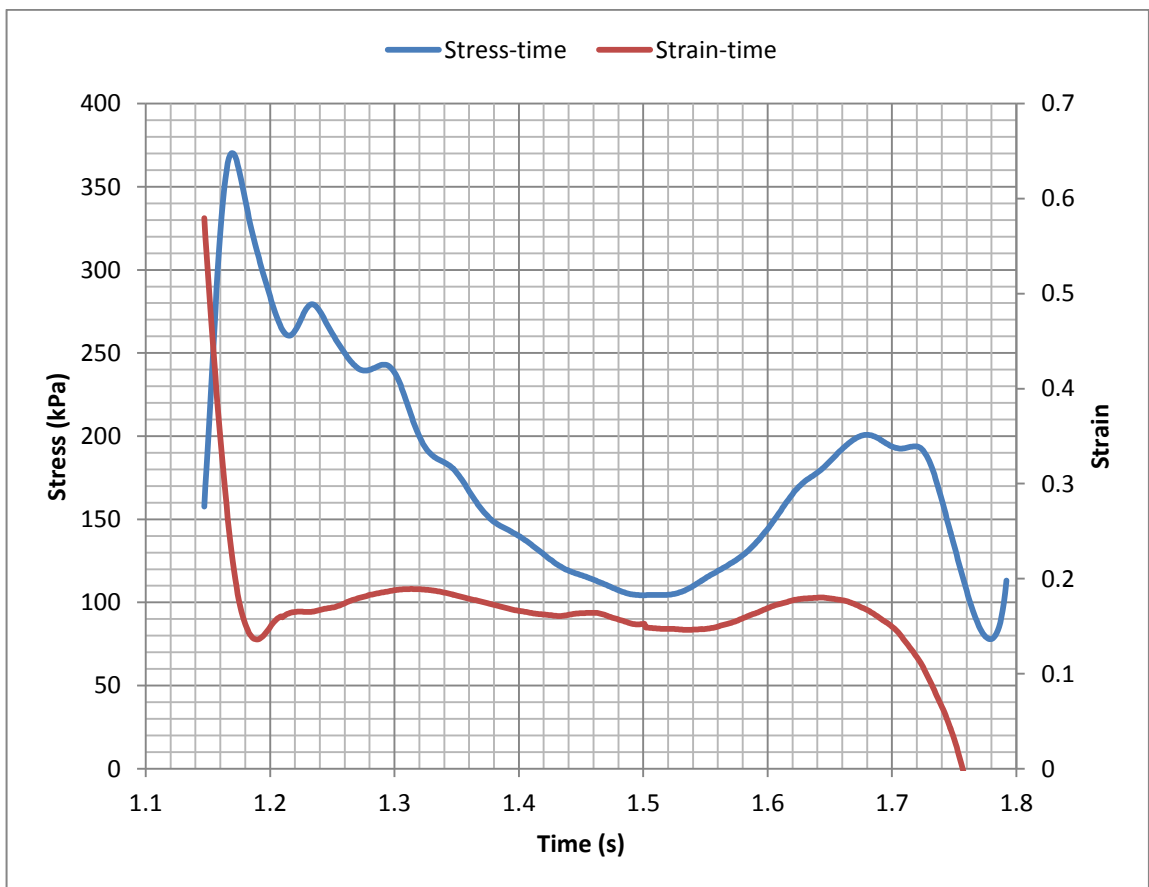


Figure 4.49: Stress-time and strain-time histories of player heel-toe walking on the hockey turf + rubber shockpad surface system

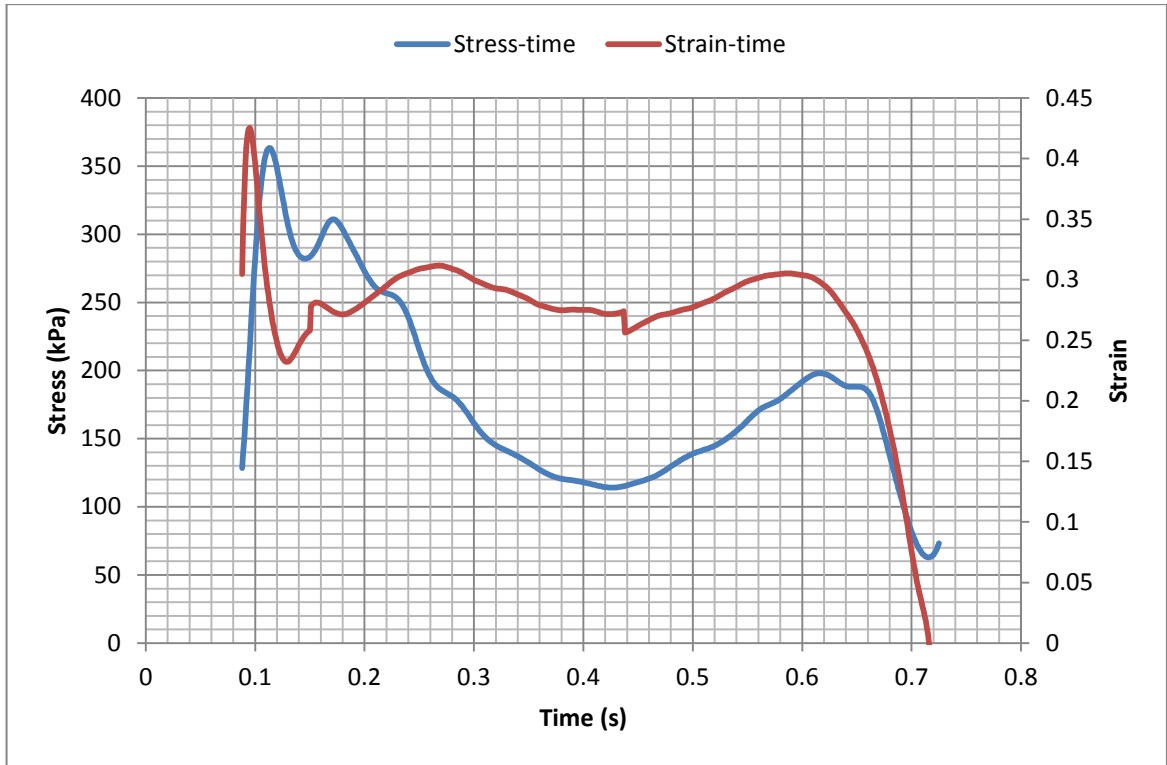


Figure 4.50: Stress-time and strain-time histories of player heel-toe walking on the hockey turf + foam shockpad surface system

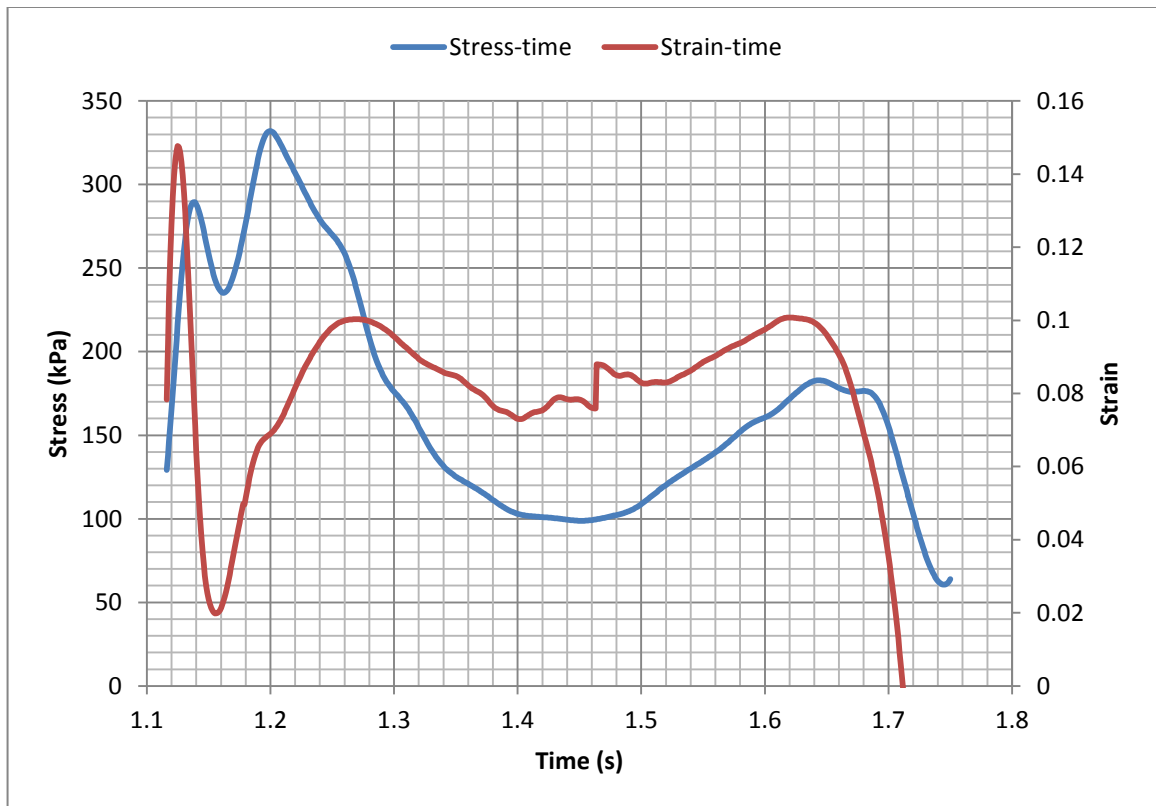


Figure 4.51: Stress-time and strain-time histories of player heel-toe walking on the 3G turf + rubber shockpad surface system

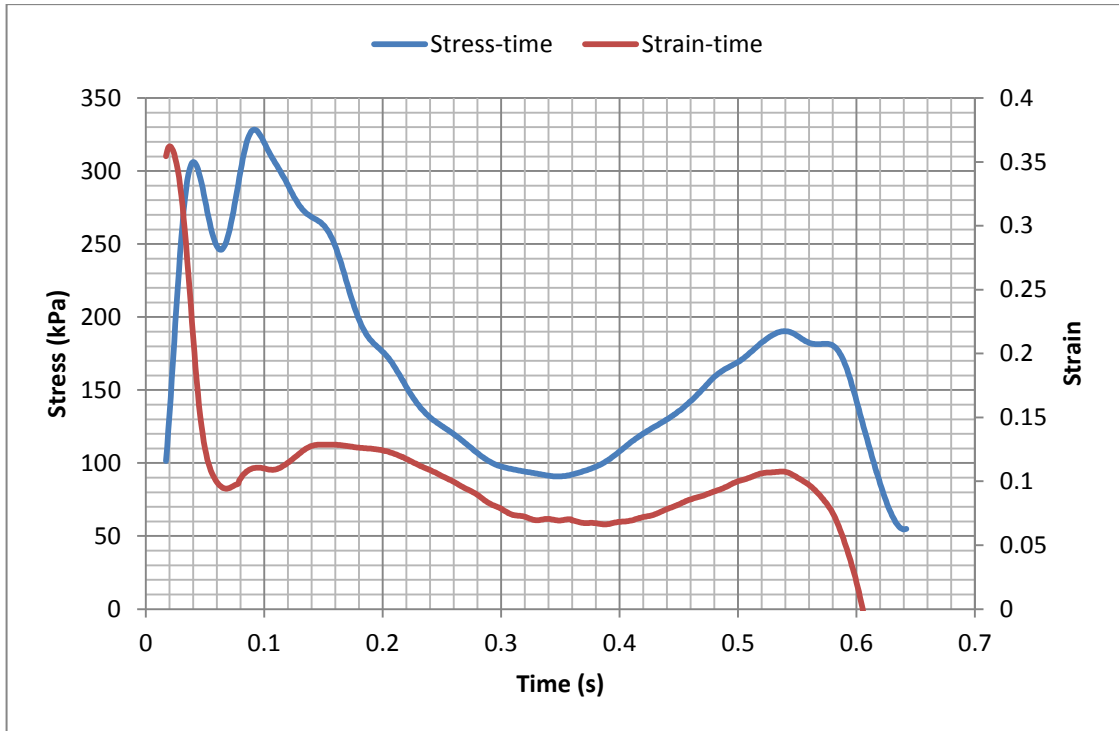


Figure 4.52: Stress-time and strain-time histories of player heel-toe walking on the 3G turf + foam shockpad surface system

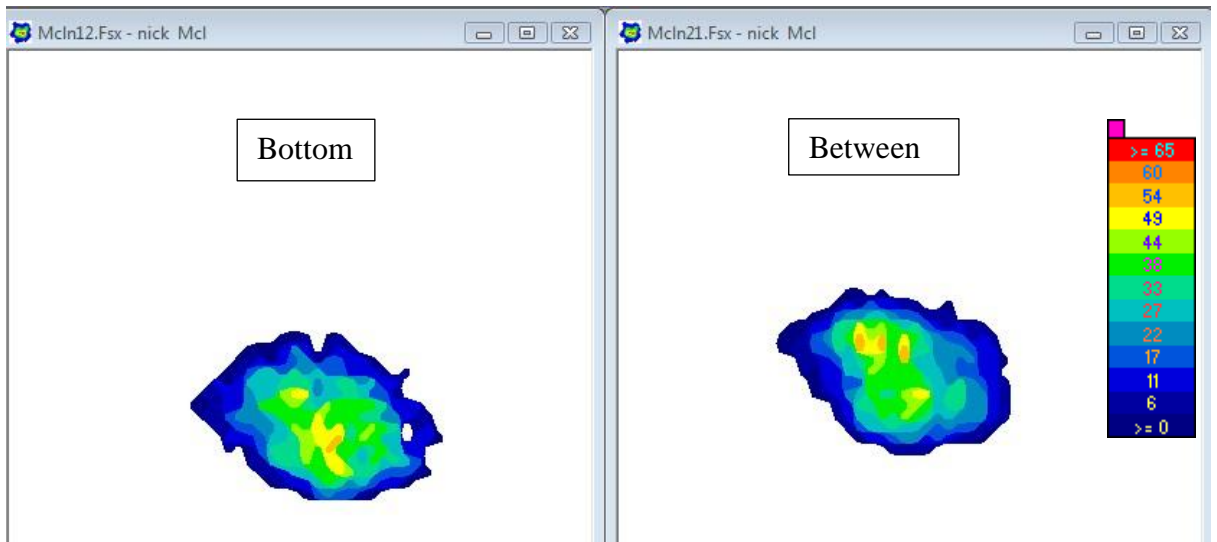


Figure 4.53: Pressure maps recorded at the bottom of hockey turf + rubber shockpad system and between the two layers. Larger high pressure region (warm colour) measured at the bottom than between the layers over similar contact area

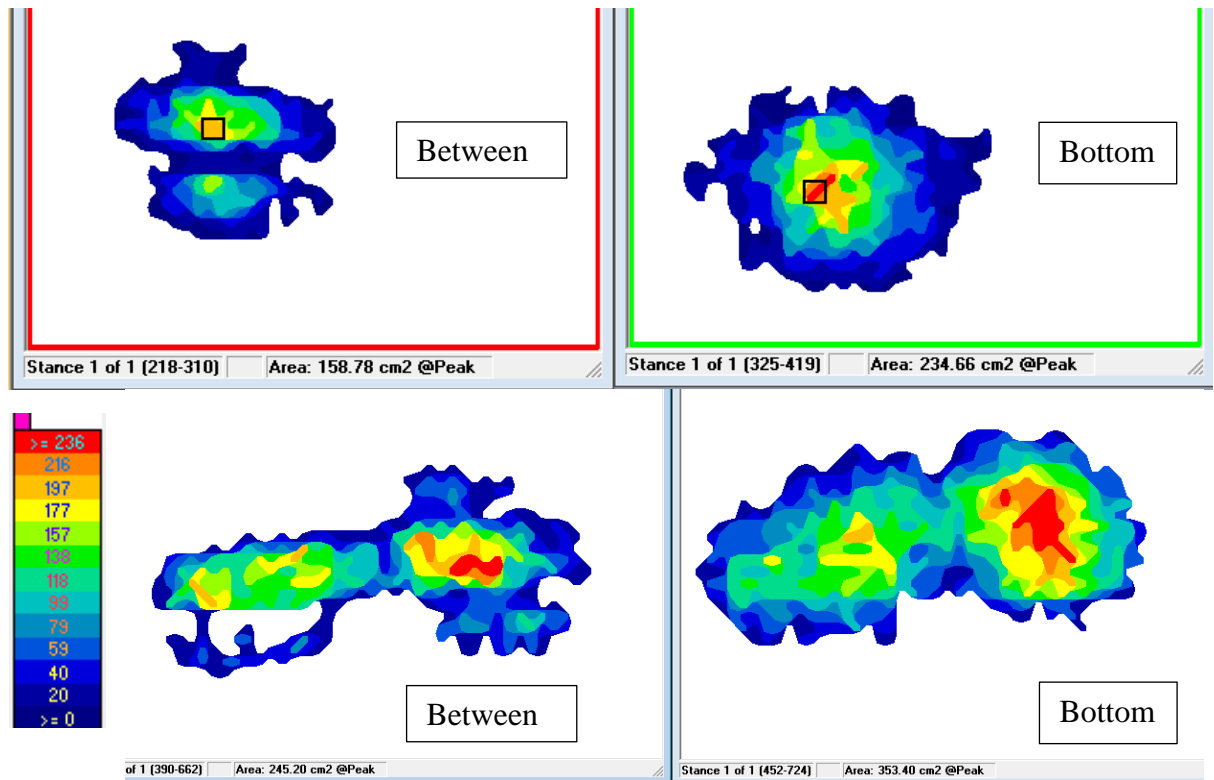


Figure 4:54: Pressure contours show the peak contact area between the layers and underneath the 3G turf systems under player running (above) and walking (below)

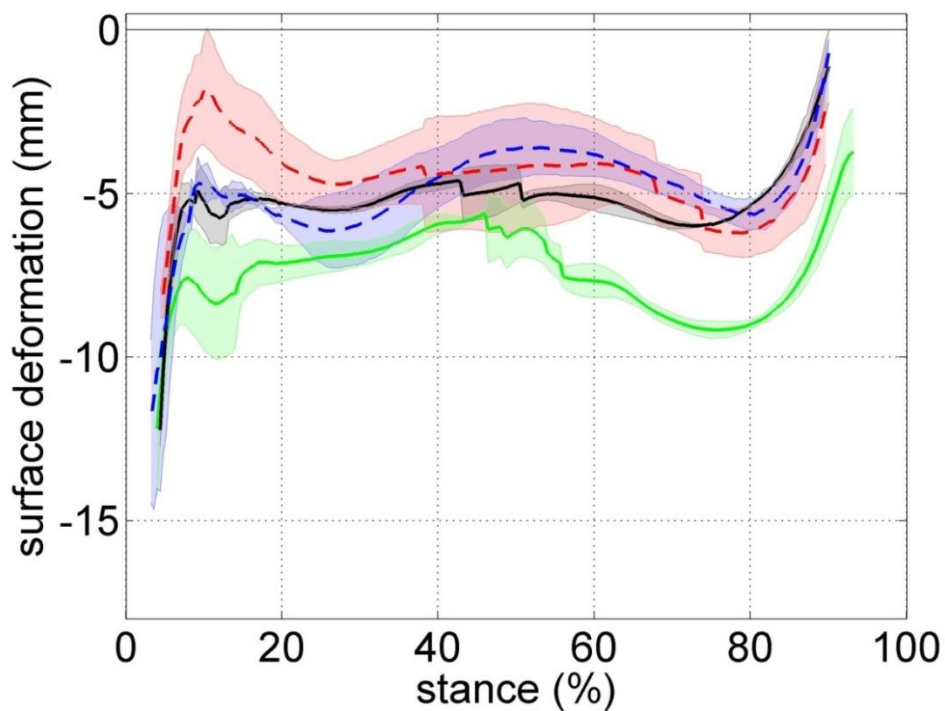


Figure 4.55: Valid surface vertical deflection for player walking on hockey turf + rubber shockpad system (black), hockey turf + foam shockpad system (green), 3G turf + rubber shockpad system (red) and 3G turf + foam shockpad system (blue). All show the mean (solid/dashed line) \pm SD (shaded area)

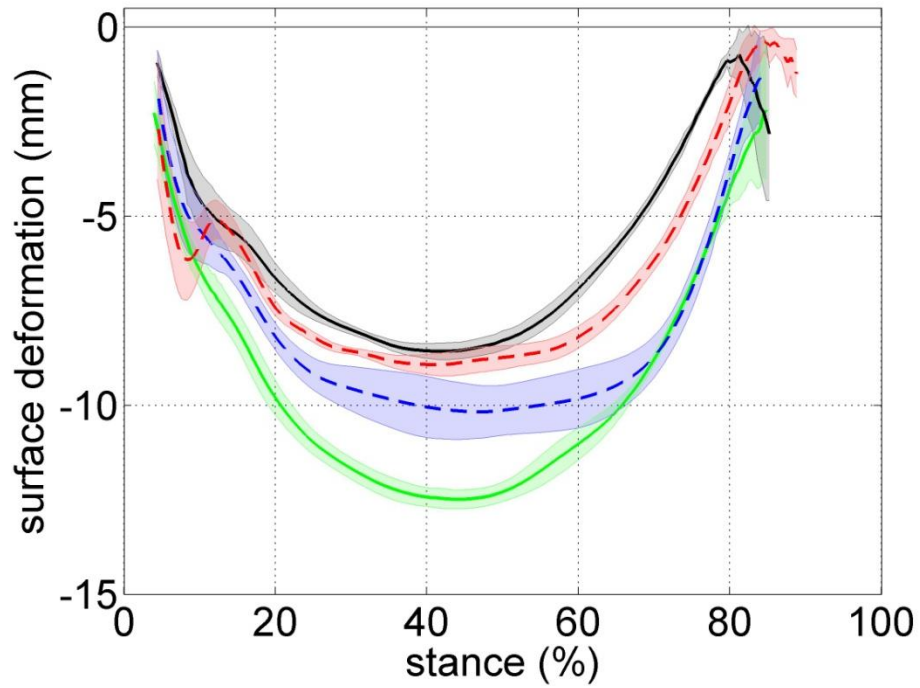


Figure 4.56: Valid surface vertical deflection for player running on hockey turf + rubber shockpad system (black), hockey turf + foam shockpad system (green), 3G turf + rubber shockpad system (red) and 3G turf + foam shockpad system (blue). All show the mean (solid/dashed line) \pm SD (shaded area)

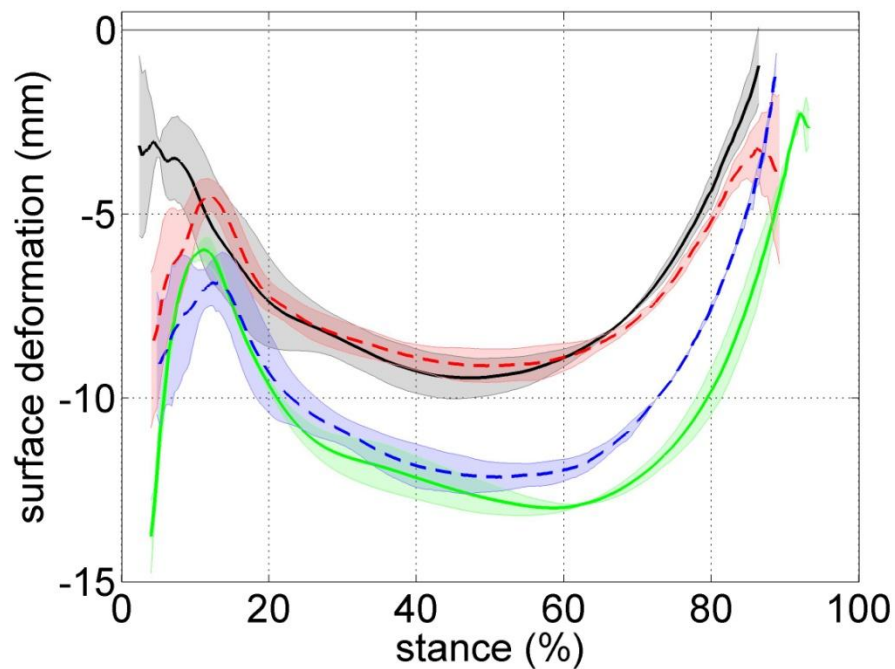


Figure 4.57: Valid surface vertical deflection for player landing on hockey turf + rubber shockpad system (black), hockey turf + foam shockpad system (green), 3G turf + rubber shockpad system (red) and 3G turf + foam shockpad system (blue). All show the mean (solid/dashed line) \pm SD (shaded area)

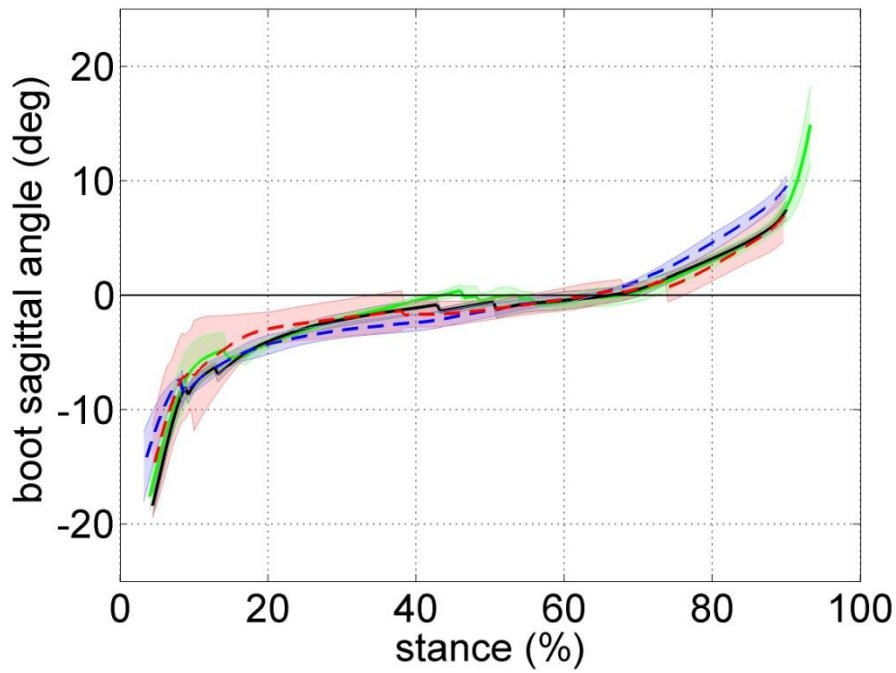


Figure 4.58: The active boot segment angle in sagittal plane for walking on hockey turf + rubber shockpad system (black), hockey turf + foam shockpad system (green), 3G turf + rubber shockpad system (red) and 3G turf + foam shockpad system (blue). All show the mean (solid/dashed line) \pm SD (shaded area)

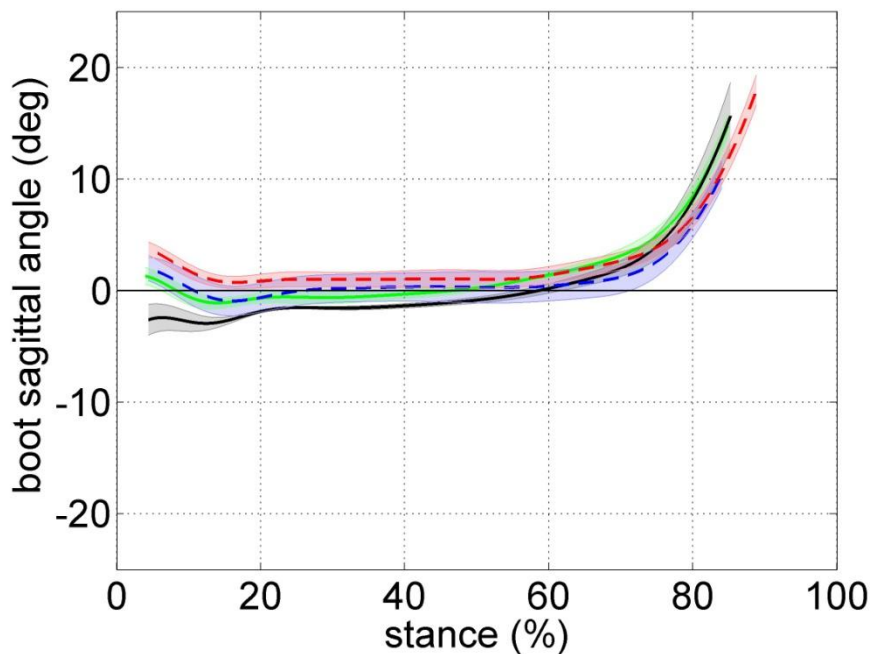


Figure 4.59: The active boot segment angle in sagittal plane for running on hockey turf + rubber shockpad system (black), hockey turf + foam shockpad system (green), 3G turf + rubber shockpad system (red) and 3G turf + foam shockpad system (blue). All show the mean (solid/dashed line) \pm SD (shaded area)

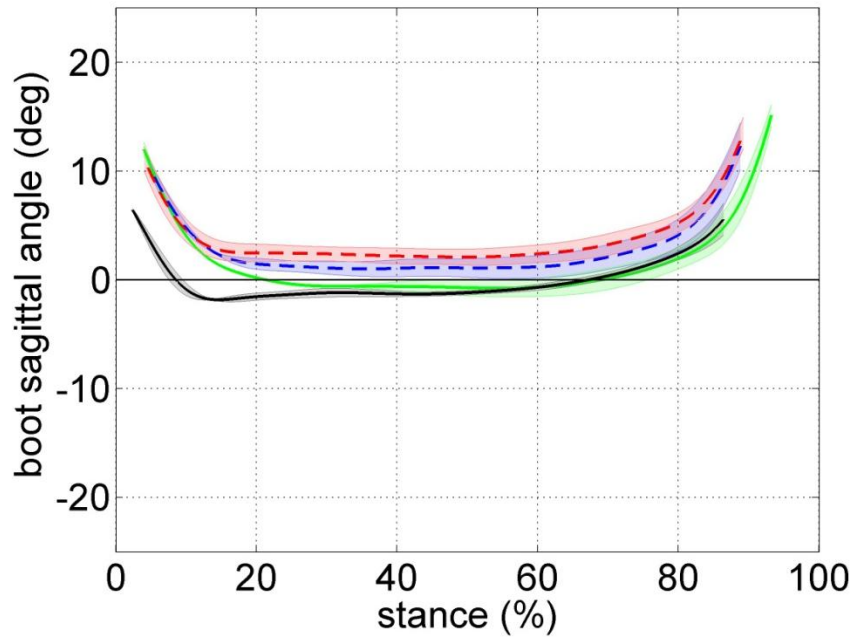


Figure 4.60: The active boot segment angle in sagittal plane for landing on hockey turf + rubber shockpad system (black), hockey turf + foam shockpad system (green), 3G turf + rubber shockpad system (red) and 3G turf + foam shockpad system (blue). All show the mean (solid/dashed line) \pm SD (shaded area)

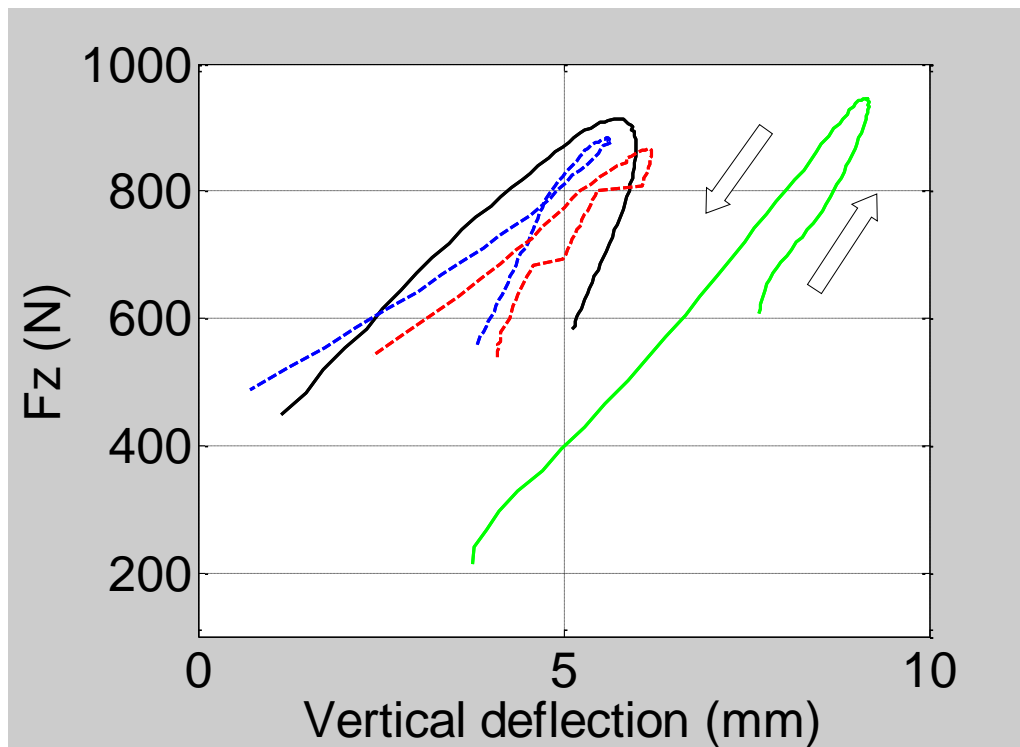


Figure 4.61: A comparison of force-deflection relationship for the push-off phase of walking on hockey turf + rubber shockpad system (black), hockey turf + foam shockpad system (green), 3G turf + rubber shockpad system (red) and 3G turf + foam shockpad system (blue)

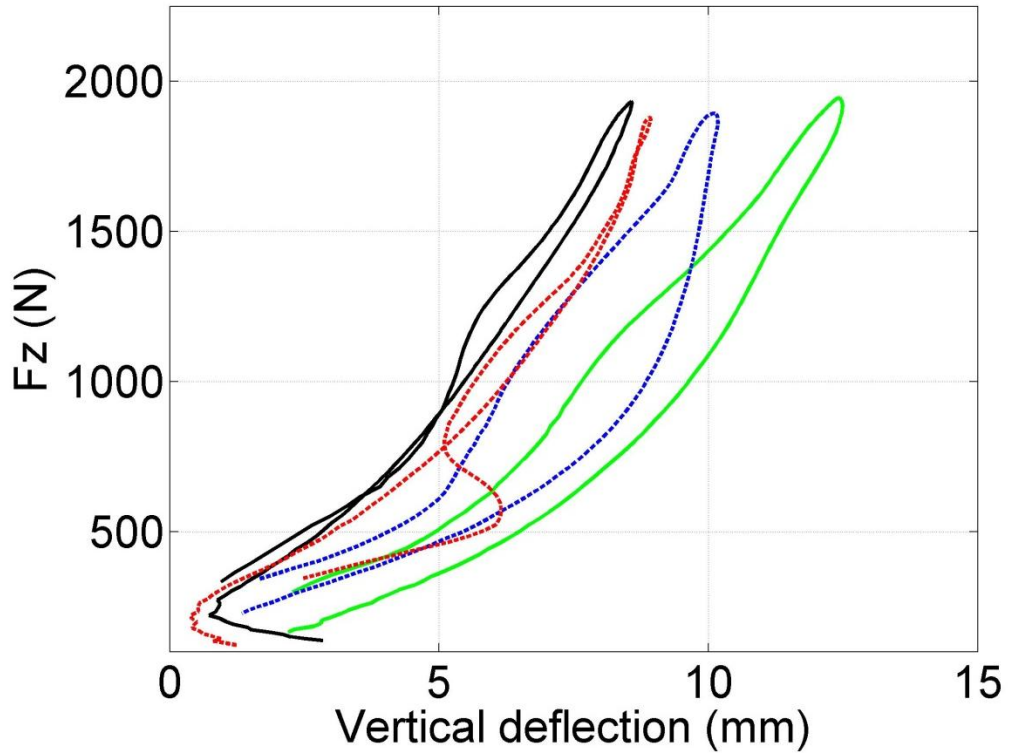


Figure 4.62: A comparison of force-deflection relationship for running on hockey turf + rubber shockpad system (black), hockey turf + foam shockpad system (green), 3G turf + rubber shockpad system (red) and 3G turf + foam shockpad system (blue)

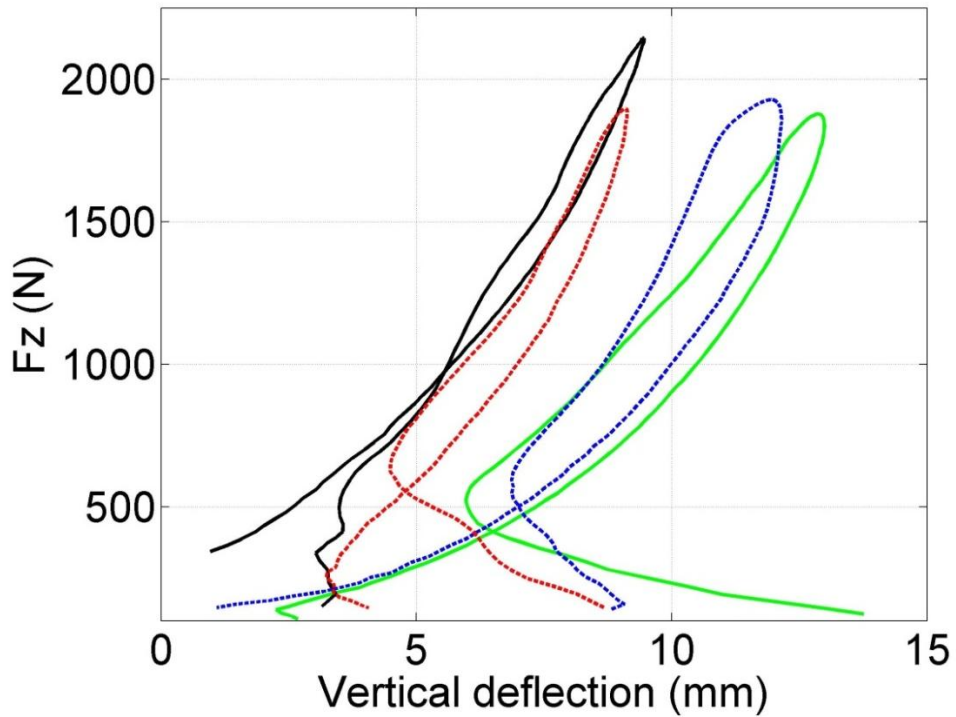


Figure 4.63: A comparison of force-deflection relationship for landing on hockey turf + rubber shockpad system (black), hockey turf + foam shockpad system (green), 3G turf + rubber shockpad system (red) and 3G turf + foam shockpad system (blue)

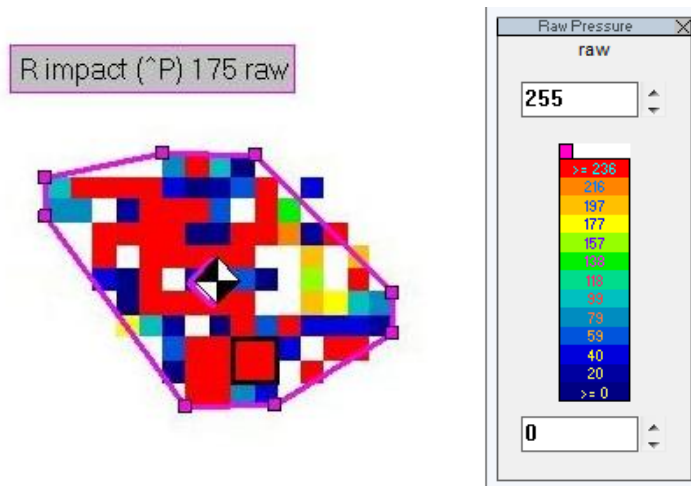


Figure 4.64: Contact area measured by pressure mat at boot-surface interface and delineated by a polygon. The CoP was indicated by the black and white square.

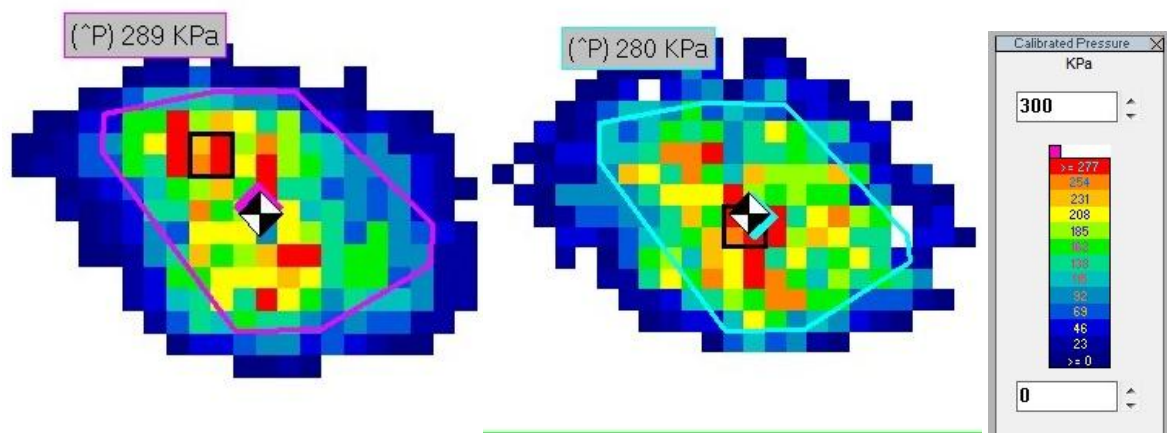


Figure 4.65: Pressure contour measured at the carpet-shockpad interface (left) and the bottom of hockey turf + rubber shockpad system (right), with the impact area polygon and the CoP position

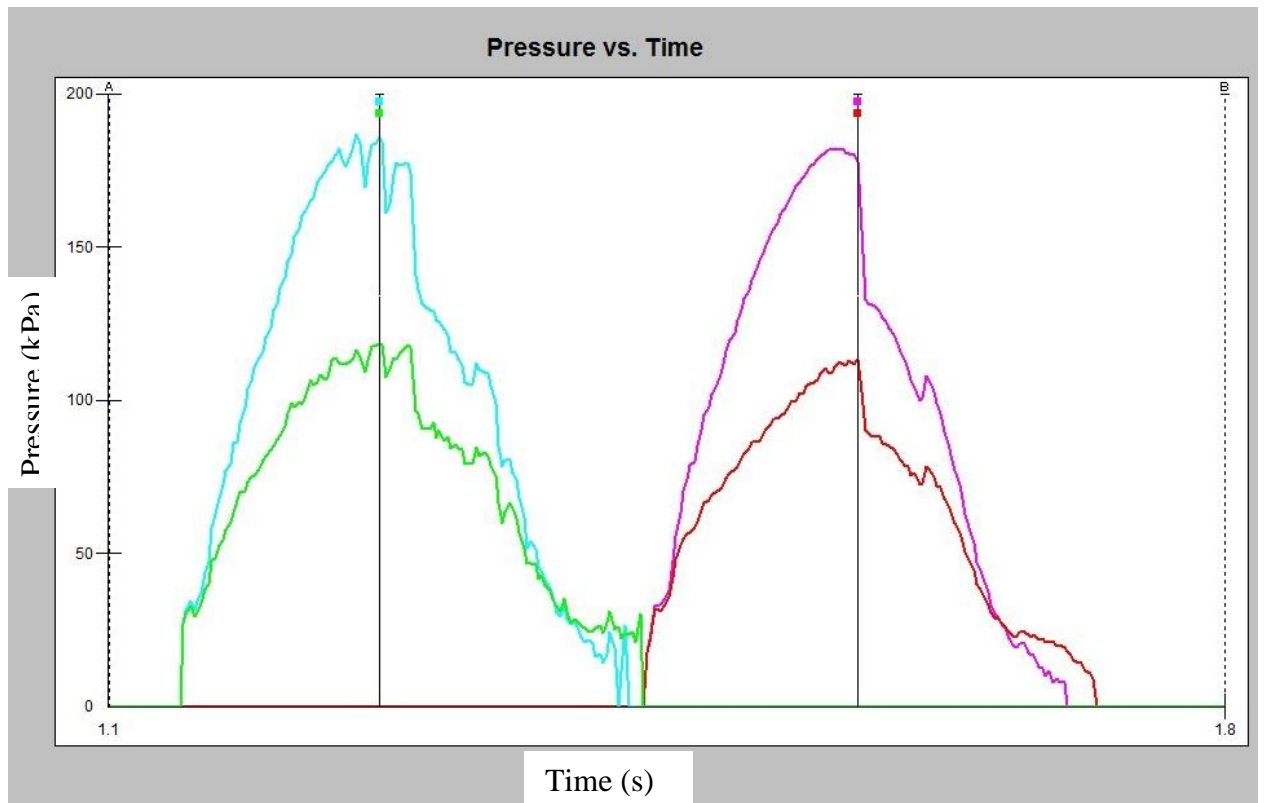


Figure 4.66: In hockey turf + rubber shockpad system, the pressure history measured at carpet-shockpad interface over whole contact area (red) and polygon area (magenta), and at the bottom of the surface system over whole contact area (green) and polygon area (cyan)

5. Discussion

5.1 Chapter overview

This chapter provides an overall discussion of the experimental work carried out in the thesis and specifically compares the mechanical behaviour of artificial turf systems under mechanical loading (presented in Chapter 3) and player loading (shown in Chapter 4). The comparison is focused on the results of the 10th cycle of mechanical test simulation of running (a steady-state dynamic compression at 3.3 Hz loading frequency with a 50 mm diameter loading foot) and player forefoot running trials. The discussion explains the differences of surface system behaviour under different loading conditions and identifies the factors that influence its behaviour. Both address objective 5 of this thesis (Chapter 1). Key loading parameters of different test approaches used in this research project are contrasted. Compressive properties to assess the mechanical behaviour of each surface system in terms of strain, modulus, stress distribution and energy behaviour derived from stress-strain and force-deflection relationships and pressure mat data are compared in Section 5.2. In Section 5.3, the use of two suitable numerical models to describe and predict surface system behaviour is discussed to address objective 6 of this thesis (drawing and expanding upon literature presented in Chapter 2).

5.2 Linking research findings

The summary Table 5.1 details the compressive properties of each surface system which are discussed in detail in the following subsections. The numbers and comparisons presented in this section are between the average values.

5.2.1 Differences between test approaches

Surface system mechanical behaviour has been measured using three different approaches, mechanical cyclic loading, the AAA impact test and player loading. The mechanical cyclic loading experimental programme evaluated and analysed the mechanical behaviour of the individual layers and surface systems in response to cyclic loading at different frequencies based on previous biomechanical research data and compared to the AAA test according to industry standard. The player loading experiment programme was aimed to understand the player-surface interactions under different human movement patterns and examine the correlation to the findings of the mechanical simulation methods.

The applied loads differed in terms of magnitude, impact area and rate of loading. An understanding of the effect of each loading variable was gained from comparing the mechanical behaviour of specific surface systems to various loading regimes. Impact magnitude and loading rate were shown to be the key variables in previous studies of material properties (Gross and Bunch, 1989; Davidson, 2012). The loading is different in the form of control. The target maximum vertical impact force for mechanical cyclic loading at each frequency was set at 1900 N to load and unload surface specimens through a sine wave. The magnitude of uncontrolled player loading was maintained at consistent levels when practising movements on different surface systems due to the occurrence of subject kinematic adjustments (Dixon et al., 1999). These two loading regimes resulted active response of surface system as unloading was driven by the material testing machine and the player push-off. The free falling impact test using AAA was controlled to be consistent transferring input energy of 11 J to the surface specimens through a linear spring resulting passive response relative to other loading regimes. The impact magnitudes of the AAA were dependent on the stiffness of specimens, hence the peak varied with the surface systems tested (as listed in Table 3.6). Surface vertical deformation response depends on the corresponding force acting during compressive loading.

It was also identified that the properties (deflection, stiffness and nonlinearity) of viscoelastic materials were affected by the loading rate and area (Gross and Bunch, 1989; Yukawa et al, 2011). Results presented in Chapter 3 show that increased loading rate leads to stiffer response for the surface systems, especially in the lower load range, narrower hysteresis loop and decrease of maximum strain. These findings are consistent with damping theory and previous work by McCullagh and Graham (1985). The mechanical behaviour of surface systems under 3.3 Hz mechanical loading at the rate of 12.7 kN/s is compared with it under player running at the average loading rate of 17.4 kN/s in this chapter. In contrast, the loading rate of the AAA impact was in the range of 105.1 – 126.3 kN/s, significantly higher than the other two types of loading. Therefore the effect of variation in loading rate needs to be considered when comparing the surface system mechanical behaviour measured with different test approaches in the following subsections.

Impact area during loading was measured to convert the force into stress. A change in area was shown to have pronounced effect on the deflection, stiffness response and nonlinearity of surface system (as presented in Chapter 3). Previous biomechanical research mostly focused on impact force measurement instead of stress and the size of foot impact area was

not well documented, so the effect of impact area was not determined. Yukawa et al (2011) tested an athletic track surface using a shock tester with eight different test feet whose diameters varied from 30 to 59.5 mm (7 to 28 cm²). Force-deflection relationship presented in graph suggested that increased impact area led to stiffer response for the surface and decrease of deflection. However, the reasoning behind the effect of changing impact areas on the surface behaviour was not discussed in their study. In the mechanical cyclic loading tests (Chapter 3), two sizes of circular loading feet available to Instron machine, 50 and 125 mm diameters (20 and 123 cm²) were selected to simulate player's heel and forefoot respectively, based on data from previous studies using mechanical test methods to represent human foot impact (Dura et al., 2002; McCullagh and Graham, 1985). The results shown in Section 3.3.2.1 exhibit the response of surface systems with these two loading feet agrees with the trend obtained by Yukawa et al (2011). The impact area of the AAA was a circle of 70 mm (38 cm²). These impact areas of mechanical loading were treated as constant terms due to the flat face of the cyclic loading feet and the assumption of negligible lower side rounded radius of the AAA test foot. However, the impact area of player's foot strike varied with the deflection of surface system during loading and unloading. The peak impact areas under three player movement patterns were in the range of 54 – 73 cm². The difference in impact areas led to variation in the level of stress applied, which made it only possible to compare the chord modulus of surface system under different loading conditions in a relatively narrow stress range.

The ability of surface system to deflect from its original shape to the maximum strain can be described using strain rate. The strain rates of the 3G turf systems under 3.3 Hz mechanical loading with 50 mm diameter foot were similar to those under player running movement. The strain rates of the hockey turf systems under player running movement were higher than those under 3.3 Hz mechanical loading with 50 mm diameter foot (refer to Table 5.1). This parameter is related with the viscous behaviour of surface system under loading (Miller et al., 2000) and therefore could affect the energy flow within the surface system. In addition, all the mechanical loading tests carried out only delivered force in vertical direction, but forces in horizontal direction also occurred simultaneously with vertical force during the selected player movements (as shown in Chapter 4). Although the impact loads were predominantly compressive and horizontal forces were relatively low (less than 250 N) in the selected movement patterns, the possible effects of the horizontal forces on stiffness response and energy behaviour of surface system have not been

analysed in this research project due to the limitations in measurement systems to measure surface strain and pressure distribution caused by horizontal components.

With these differences between test approaches discussed above, it was expected to observe differences in surface system behaviour comparing the results between experiment programmes. The identified loading variables were shown to influence the mechanical behaviour of surface system and necessary to be considered in developing test methods and mathematical models to determine and describe player-surface interaction. Further work should try to restrict the number of loading variables in view of comparing the results from mechanical dynamic loading tests and actual human movements. Chapter 6 provides additional details of recommendations to further research.

5.2.2 Compressive strain

The maximum compressive strain of the surface systems (under mechanical, player loading and the AAA impact) shows the ability of each surface system to accommodate the applied load by deforming to large strains. The 3.3 Hz mechanical compressive loading with 50 mm diameter loading foot provided the largest vertical contact stress (968 kPa). The maximum strain of 0.60 was observed for the HT+FS system (Chapter 3), the largest strain at peak stress among all tested surface systems. The 3G+RS system gave the smallest strain of 0.35 at peak stress. Although the peak stress applied by the player forefoot running was lower, around 275 kPa, the strain ranking was consistent with the trends from the mechanical loading (refer to Table 5.1). It is noted that surface systems using foam shockpad experience greater strain than using rubber shockpad (presented in Chapter 3 and 4). Hockey turf system with foam shockpad showed the strain more than 0.1 larger than with rubber shockpad whilst the difference in strain is 0.05 for the 3G turf systems with different shockpads under both loading regimes. It agrees with the individual shockpad layer's deformation response, as presented in Section 3.3.1, the peak strain of foam shockpad was 0.65, 0.24 larger than the peak strain of rubber shockpad under 3.3 Hz loading. With carpet layer laid on top, the difference in peak compressive strain between surface systems using the two shockpads is reduced.

The strain values calculated from the peak vertical deformations of the AAA impacts are also able to rank the four surface systems in the same order. However, from the AAA data the difference in peak strain between the rubber and foam shockpads is underestimated in comparison to the other loading conditions. Strain values of hockey turf system and 3G

turf system with foam shockpad are 0.06 and 0.03 larger than using rubber shockpad respectively (refer to Table 5.1). These results indicate that compared to the dynamic mechanical compressive loading and real player loading, the AAA test method is less able to contrast the strain behaviour of the surface systems with different shockpads. The lower sensitivity of the AAA may be explained by the shorter rising time to peak force (i.e. higher loading rate) of the impact that is less able to mobilise the shockpad response to contribute to the overall surface system strain, so the peak strain (deformation) recorded is mainly determined by the properties of carpet layer. It shows another limitation of the AAA test method for assessing the strain (deformation) behaviour of multi-layer surface system in contrast to player loading.

5.2.3 Chord modulus

The surface systems show nonlinear stress-strain behaviour under selected mechanical and player loading conditions during loading and unloading in Figure 5.1 and 5.2 (as discussed in Chapter 3 and 4). The value of Young's modulus is a material property useful for calculating compliance of structural materials that follow Hooke's law when subjected to uniaxial loading (that is, the strain is proportional to the applied force). For materials that follow nonlinear stress-strain behaviour, the value of chord modulus is appropriate for estimating the change in strain for a specified range in stress. Therefore, chord modulus of each surface system under 3.3 Hz mechanical loading with 50 mm loading foot in the range of 170 – 300 kPa is compared to the chord modulus estimated for the same stress range under player forefoot running (see Table 5.1). All the tested surface systems demonstrated a stiffer response under the mechanical loading compared to player impact. In the specified range in stress, the chord modulus for HT+RS under 3.3 Hz mechanical loading was 4.2 times the modulus with player running. The chord modulus for HT+FS under 3.3 Hz mechanical loading was 3.7 times the modulus with player running. For the 3G turf systems, the chord modulus with mechanical loading increased by a factor ranged from 2.5 to 2.9, compared to the modulus with player running.

The large difference in stiffness response under the two loading conditions is considered to be caused by several factors including variations in contact areas at the boot-carpet interface and horizontal forces. The size of impact area was identified as one of the factors that can affect the stiffness response in Section 5.2.1 and its influence on the stress-strain relationship of surface systems was shown in Chapter 3. The impact area of the selected mechanical loading was constant at 20 cm² whilst the area under player forefoot impact

varied during the stance with the peak value measured as approximately 70 cm² (refer to Chapter 4). The findings in Chapter 3 showing the strain and peak stress reduced as the impact area increased and a decrease in chord modulus of surface systems in the stress range of 10 – 155 kPa under larger contact area (see Figure 3.27 and 3.28). This behaviour is consistent with the changes in chord modulus of surface systems with player running and mechanical loading due to contact area difference. A further source of differences in response of the surface systems under the two loading conditions may be introduced by differences in the horizontal forces generated by the player during running, whilst only vertical force was delivered in mechanical loading test. Theory of elastic materials suggests vertical force applied on elastic materials in an unconfined compression test will induce horizontal forces and hence horizontal strains and affect the material behaviour in the vertical direction (Miller et al., 2000). The magnitudes of horizontal strains are related with the Poisson's ratio of the material and the vertical strain. Artificial turf system has low Poisson's ratio that results from a high void-volume fraction in the carpet-shockpad combined structure (Anderson, 2007; Severn, 2010) makes the horizontal strains relatively small in the mechanical loading (Thomson et al., 2001). During running, the player exerts a three-dimensional force on the ground; the surface system experiences deformations in three directions and the horizontal strains are expected to be larger, and therefore have larger influence on the stiffness behaviour in the vertical direction. However, the effects of horizontal forces/strains on the stiffness response of surface system are unable to be quantified from the current data alone. Further research could develop measurement systems to determine the horizontal/shear forces at the carpet-shockpad interface and horizontal strain of each layer in order to facilitate assessment of surface system's response to horizontal forces and their effects on the stiffness of surface system.

5.2.4 Stress distribution

Stress and pressure contours recorded by the pressure mat at the bottom of surface systems under mechanical and player loading conditions are presented in Chapter 3 and 4 respectively. The surface contact stress is greatly reduced with depth as the load is distributed through the surface system over an increasing contact area. Under 3.3 Hz mechanical loading with 50 mm diameter foot, the applied stress was 968 kPa at peak. For all the surface systems, the peak stress measured at the bottom/underneath the system was reduced by 75 – 78% (Table 5.1). The peak stress applied by the player during his forefoot running strike was much lower, around 275 kPa. The reduction in stress at the bottom of

the surface systems was in the range of 55 – 64%. The reduction was less than 60% for both hockey turf systems, whilst both 3G turf systems reduced the stress by approximately 63%. The AAA delivered the impact stress in the range of 550 – 675 kPa on the tested surface systems. The applied stress reduced by 64% and 66% through HT+RS and HT+FS respectively, and the reduction in stress for the 3G turf systems was similar, around 69%.

It is noted that surface systems using the foam shockpad reduce the surface contact stress at depth more than for the rubber shockpad under 3.3 Hz mechanical loading test.

Determining the stress distribution angle is a suggested way to compare the stress reduction differences observed previously used in geotechnical engineering (Section 3.4.4). It demonstrates that surface systems with foam shockpad develop angles approximately 5° larger (43.9° for HT+FS and 33.4° for 3G+FS) compared to the rubber shockpad (38.3° for 3G+RS and 28.2° for 3G+RS). This difference in stress distribution angles results in a further reduction in stress by 2 – 3% for the surface systems with foam shockpad. This behaviour is consistent with the findings of the other mechanical loading tests at 0.9 and 10 Hz (Section 3.4.4). Differences in the stress reduction ability between the surface systems with different shockpads result primarily from variations in the thickness of shockpads and stiffness of surface systems. The foam shockpad is thinner than the rubber shockpad as listed in Table 3.1, and surface systems with foam shockpad behave stiffer than with rubber shockpad at the higher load range (> 1000 N) under 50 mm test foot as presented in Section 3.3.2. Therefore, the same compressive load applied over the specific area on the compliant surface system with foam shockpad caused a larger deflection bowl than with rubber shockpad and distributed the load over a larger area. Hence greater stress reduction was measured at the bottom of the surface systems using foam shockpad.

This difference in stress reduction introduced by different shockpad used in hockey turf systems under player running is also prominent with 4% greater stress reduction measured for HT+FS than HT+RS. But the difference between the two 3G turf systems under the player running tests is less than 1%. It is assumed in the analysis that the forefoot impact area and the enlarged contact area recorded are in circular shape in order to calculate stress distribution angle of each surface system using the method described in Section 3.4.4. Under player forefoot running, the stress distribution angle for HT+FS is 45° compared to 38° for HT+RS. For the AAA test, the stress distribution angle measured in HT+FS is 39.8°, 4.5° larger than in HT+RS, resulting 2% difference in stress reduction. For both player running and the AAA tests, the differences in stress distribution angles between the

3G turf systems are around 1° , which lead to similar stress reduction performances. The relationship between stress distribution angle and stress reduction found in mechanical loading tests is also noted in player loading and the AAA tests.

Overall, the findings indicate that the stress reduction ability of surface system is related to the degree of the stress distribution angle as the applied load is transmitted through the surface system and the contact area increases in size. The hockey turf systems showed a 2 – 4 % difference in stress reduction under the three different loading regimes due to different properties of the shockpads underneath. The behaviour of both 3G turf systems in terms of stress distribution showed little difference except under mechanical loading test (3% difference in stress reduction). These findings indicate that both shockpads used have similar effect on stress distribution in 3G turf systems. Considering the infill depth of 3G carpet layer (more than twice the thickness of rubber shockpad) and its load spreading effect, it may suggest that the shockpad response to further distribute stress could only be mobilised when the surface contact stress is at a higher level such as in the mechanical compressive loading reaching 968 kPa.

These findings highlight how these surface systems distribute the applied stress in response to different loading regimes and the shockpad layer response and contribution to this behaviour.

5.2.5 Energy behaviour

Energy characteristics of the materials under deformation can be determined by considering the area under or enclosed by various portions of the force-deflection curve for loading and unloading (Davidson, 2012). With reference to literature (Chapter 2, Figure 2.15), the area contained below the loading curve represents the input energy absorbed during compression. The area below the unloading curve shows the energy returned. The area enclosed by these two curves is the difference between energy input and energy returned, so corresponds to the energy lost from the compression cycle – often termed the hysteresis. These areas have been calculated using the trapezium rule at a time interval resolution of 10 ms. The hysteresis energy ratio (HER) is the ratio of energy loss to the input energy, varying between 0 and 100%; 0 indicates a perfectly elastic response and 100% denotes no energy returned (Davidson, 2012). This parameter was calculated for the surface systems and is used to compare the energy behaviour of surface systems tested.

Table 5.1 presents average HER values at the 10th cycle of 3.3 Hz mechanical loading with the 50 mm diameter test foot and for the player loading for each surface system. Force-deflection profiles under player loading shown in Section 4.3.2.1 (Figure 4.18 – 4.21) revealed much narrower hysteresis loops compared with the profiles under mechanical loading presented in Section 3.3.2.2 (Figure 3.25 and 3.26), therefore indicating a more elastic response where the majority of input energy was returned upon unloading. This is the case for every surface system tested, with HER values in the range of 7 – 34% under player forefoot running, whilst HER between 36% and 50% for 3.3 Hz mechanical loading. The energy storage and return of a surface depends on the deformations and corresponding forces acting during the total compression history (Baroud et al., 1999). Although the impact force peaks for both loading conditions were controlled to be the same magnitude of 1900 N, the deflection of each surface system reached at peak load was different due to the variation in contact area, thus the peak strains were different. Surface system under 3.3 Hz mechanical loading with 50 mm diameter test foot experienced greater strain and more energy lost than under player running. The mechanical loading exhibited a higher level of densification reached (closer to ‘bottom out’) upon impact, therefore losing more energy which could possibly be returned. It may suggest that higher stress through smaller contact area or higher load on the same area will cause more energy lost through work done in deforming the materials to higher strains which exceed air voids compression into compressing a structure similar to a solid block of elastomer (rubber) once void spaces sufficiently filled.

Furthermore, energy loss is a viscoelastic phenomenon which is time dependent. The total contact duration of 3.3 Hz mechanical loading was 0.3 s, almost the same as the average ground contact duration 0.28 s in player forefoot running, though the vertical peak forces occurred at different times during the compression. The vertical peak force of 3.3 Hz mechanical loading was controlled to occur at 50% of the total time of compression whilst the vertical peak of player running (uncontrolled) occurred at approximately 40% of the total contact time. The slower rate of unloading in player running may result in more energy return, thus a lower amount of energy loss. It suggests that improvement can be made to employ custom loading wave pattern in future mechanical testing regime to better reproduce the force-time relationship of player forefoot running instead of using the sine wave loading pattern.

Although energy is a scalar quantity, the forces that are exerted by a surface as energy returned are vector quantities. In comparison to purely vertical force applied in mechanical loading, horizontal forces during player running may also contribute to the player performance. Baroud et al. (1999) showed the energy return was maximal in the vertical direction contributing about 85% of the total energy return in all directions using a finite element modelling approach to determine energy return in forefoot running on sport surface. Hence only the energy behaviour of surface systems in vertical direction is measured, its behaviour in the horizontal directions is outside the scope of this study.

Differences in HER between the variants of rubber and foam shockpads used in surface systems are also noted. Carpet layers combined with the foam shockpad exhibit wider hysteresis loops, i.e. more energy loss, in comparison to surface system with rubber shockpad. Under 3.3 Hz mechanical loading with 50 mm diameter test foot, surface systems with foam shockpad have HER values approximately 7% higher than those with rubber shockpad showing more energy loss. The HER for 3G+FS under player running is around 2 times the HER for 3G+RS. The HER for HT+FS is larger than the HER for HT+RS by a factor of 3.4. However, the loading and unloading curves at low force level have not been plotted for the player running as a result of the raw data of early and late stance of player forefoot running been removed before analysing the force and deflection behaviour for the reason stated in Chapter 4. This limitation of the analysis may result in underestimating the HER for surface systems under the player loading. This error is comparable between the running data for the four surface systems as the same analysis method used to exclude the first 5% of stance from the calculation.

More elastic response (less energy loss) with the rubber shockpad under the systems may be further explained by the structure of the shockpad and material properties. The intrinsic stiffness of the bonded rubber shreds and lower volume of air voids in the rubber shockpad result in a stiffer response and smaller compressive strain of the surface system and therefore lead to less energy loss. The rubber shockpad may absorb the energy primarily by elastic buckling of the bonded rubber shred structure and return the majority of this energy upon unloading. The foam shockpad has open cells and lower density which indicates higher volume fraction of air-filled (porosity). McCullagh and Graham (1985) explained energy loss in terms of the heat generated in the air pockets due to deformation of the cell walls. The intrinsic stiffness of the cell walls/rubber shreds may be associated with the element of elasticity and the viscous resistance to be associated with air pressure within the

air cell/internal pore configuration. More energy loss with foam shockpad may be explained as the pressure of the air pockets giving less support to the cell walls and less stiff of the walls themselves, resulting in larger strain of the surface system (as discussed in Section 5.2.2). In such a case the energy loss would be increase. In addition, the open-cell structure of foam shockpad suggests the cells may be connected by side channels through walls. So it is possible that under compressive loads, air may flow from one cell to another through these side channels giving rise to another source of energy loss due to shearing of the exchanging air. Further work could explore how the microstructure of shockpad is associated with energy behaviour by using the scanning electron microscope to support this discussion.

The amount of energy lost at a particular impact force (1900 N) is found to be loading rate dependent as it decreases with an increase in the rate observed in Section 3.4.2. This energy characteristic of surface systems tested is consistent with the findings of previous study carried out by McCullagh and Graham (1985). It may be explained as the loading rate increases, an increase in the viscous resistance (the pressure of the air cells) leads to an increase in the stiffness of surface system and a reduction in the deformation, therefore the energy loss is reduced. Stress relaxation tests could be performed in further research to determine the viscous damping properties of surface systems.

5.3 Modelling surface system mechanical behaviour

Understanding of the mechanical behaviour of surface systems gained through the results of experiment programmes in this research project allows a set of model coefficients to be identified and mathematical models to be developed. Development of the models could assist the engineering of surface system to exhibit the required behaviour for predictable player-surface interaction.

Various mathematical models have been used to assess compliant surface and elastomeric materials mechanical properties under drop weight, ball and human impacts as presented in Chapter 2. Basic models contained only a linear or nonlinear spring to represent the material's elastic behaviour (Robinovitch and Chiu, 1998; Shorten and Himmelsbach, 2002). These materials were found to possess elements of both elasticity and viscosity from experiments (McCullagh and Graham, 1985). More advanced approaches considered the combination of the elastic and viscous components to represent the material's viscoelasticity by using a nonlinear (power) spring in parallel with a viscous damper (Carré

et al., 2006; Anderson, 2007). These spring-damper models were evaluated for their ability to reproduce the experimental force-deflection impact curves determined from laboratory drop tests. Davidson et al (2009) found an exponential spring and depth damper combination best replicated the surface characteristics of the tested gymnastic mat under a head form impact. Kobayashi and Yukawa (2011) also incorporated an exponential function in the model to improve the stability of simulation.

An exponential model is compared with an exponential damped model in this section to fit the experimental stress-strain loading curves of 3.3 Hz mechanical loading with 50 mm diameter test foot and player forefoot running for each surface system tested. Stress-strain models in comparison to force-deflection models provide more parameters corresponding to impact area and strain rate, which could affect the surface system mechanical behaviour to be inferred. The equations for the two models are given by Equations 5.1 and 5.2.

$$\text{Exponential Model:} \quad \sigma = E e^{\alpha \varepsilon} + \sigma_0 \quad (5.1)$$

$$\text{Exponential Damped Model:} \quad \sigma = E e^{\alpha \varepsilon} + 10d\dot{\varepsilon} + \sigma_0 \quad (5.2)$$

Where:

σ = Stress (kPa)

ε = Strain

E = Modulus of elasticity (kPa)

α = Nonlinearity Coefficient

d = Damping Coefficient (N.s/cm²)

$\dot{\varepsilon}$ = Strain Rate (1/s)

σ_0 = Stress Offset (kPa)

The need for the stress offset parameter to translate the model data to coincide with experimental data at the initial stage of impact was a result of using a constant damping

coefficient to describe all stages of surface behaviour. The elastic component of the model was small due to low strain in the initial stage, however, the viscous component was relatively large and therefore an offset stress was needed to cancel the large viscous term (Anderson, 2007).

The parameters for each model were optimised using the Curve Fitting Toolbox run through Matlab (Mathworks, Vers. R2009a) to provide the best correlation to the experimental data and evaluated by the root mean squared error (RMSE) and the adjusted square of correlation (Adj R-sq).

The exponential model uses an exponential spring to describe and predict surface system stress-strain behaviour for the loading section. The correlation for the loading behaviour between the exponential model adding a damper and the experimental data is also analysed. Figure 5.3 compares the two models to the mechanical loading data at 3.3 Hz with 50 mm loading foot for hockey turf systems. Figure 5.4 shows a comparison of the two models to the loading behaviour of 3G turf systems under the same loading condition. Both exponential and exponential damped models demonstrate good correlations with the experimental data of each surface system during the loading phase. The RMSE of each model compared to the peak loading stress (968 kPa) is less than 1.4%. Parameters of models are given in Table 5.2. The nonlinearity coefficient showing the curvature of the stress-strain behaviour is similar in both models for each surface system. This parameter is larger for the 3G turf systems than hockey turf systems by approximately 4. Surface systems using foam shockpad have the nonlinearity coefficient larger than using rubber shockpad by around 1. The addition of a damper to the exponential model reduces the modulus with an exception for 3G+FS showing the modulus of the damped model slightly larger than for the exponential model.

Exponential and exponential damped models compared to player loading data for forefoot running movement on hockey turf and 3G turf systems are presented in Figure 5.5 and 5.6 respectively. Parameters of models are listed in Table 5.3. Generally, the exponential damped model shows stronger nonlinearity than exponential model and significantly reduces the modulus. The damping coefficient is related with the impact area on top of surface system and varies with the strain rate (Carré et al., 2006). The relationship is unclear at this stage for damping coefficient and stress offset. Good correlations are demonstrated with similar errors between the two models and stress-strain data during

loading phase. As the experimental data of player forefoot running covers a relatively narrow range in stress lower than 300 kPa and strain less than 0.5, it is difficult to identify which model could provide a stronger fit to the data at higher stress level (over 400 kPa). But it is anticipated the nonlinearity and slope of stress-strain curve increase with increasing applied stress under player loading as observed under mechanical loading. In this case, the exponential damped model may be better for predicting the surface system stress-strain behaviour during loading phase at higher stress level for player running movement. Another advantage of adding a damper to the exponential model is its potential to account for the energy return during unloading (Davidson et al., 2009; Anderson, 2007). It is indicated that both of the models are better at describing the surface systems with rubber shockpad (low in errors). This may be explained when modelling the carpet-shockpad system as a single element, the combination of carpet layer and rubber shockpad acts more like one element.

These models developed at this stage are capable of describing and predicting the surface system nonlinear behaviour during loading phase. However, the parameters determined are dependent on loading type and surface system strain rate (for exponential damped model). In addition, the models are limited as assuming the combined layers surface system to be homogeneous that strain occurs at different layers simultaneously, and only describing two dimensional behaviour. Thus, in the present forms, the models are not ideal for modelling surface system behaviour independently of design and loading type. Development of finite element model would address these issues and provide detailed description of the strain gradients through the surface system and the area of deflection bowl under impact.

5.4 Summary

The findings from all experimental chapters are discussed collectively in this chapter and give an insight into how surface systems respond under actual player loading and the effects of loading variables on the mechanical behaviour of surface system.

As a player carries out a movement, he/she produces forces in three directions as the foot is planted onto the surface. For straight line movement without changing direction such as running, the force applied in the vertical direction is the largest component. Without considering the surface response to horizontal forces, the surface undergoes deformation in the vertical direction to accommodate the vertical force component. Energy input from the player into the surface is a function of the applied force and the duration. The larger the

force, the greater the potential for energy stores in the surface. However, the actual amount of energy storage depends on the surface stiffness and deformation (Stefanyshyn and Nigg, 2003). Results in this research show nonlinear behaviour of the surface system as the stiffness increases with an increase in applied load and this in turn reduces the rate of increase of deformation with increasing force of the surface system. This then suggests a more rapid stiffening of the surface system at higher vertical applied loads results in reduced energy storage ability. As the surface is unloaded, due to the viscous property of the surface, some of the energy is lost in deforming the surface. The viscous behaviour of the surface is associated with the structure and composition of the surface.

The specific surface response to a loading event depends on the loading variables including the mass of the player, movement speed, loading rate, type or style of foot contact, contact time and foot contact area with the surface.

In lower speed rearfoot strike running (as shown in Figure 2.8), the heel impact generates high rate of loading with high stress, the surface may experience large strains within a short rise time to peak stress and thus respond relatively stiffly, and therefore return the majority of the stored energy to the player. In the following propulsion phase, the forefoot is in contact with surface over a larger contact area and produces a lower rate of loading relative to the heel impact phase such that the peak surface strain is smaller than in the impact phase. This may be true even if the peak forces are similar or larger than the heel impact loads.

To increase the running speed, players usually alter the foot contact style to perform a forefoot dominated strike for running/sprinting with little or no heel impact phase. This then generates higher magnitude of loading and higher rate of loading with a single peak vertical force compared to the propulsion peak in rearfoot strike running. An increase in the loading rate results in a stiffer response of the surface system and a reduction in energy loss. The change in contact area from a heel to forefoot is shown to have a large influence under loading on the stiffness response and the surface vertical deflection (Chapter 3). For the same maximum vertical load, as the contact area increases the contact stress and compressive strain reduce, and the surface stiffness response at lower load range (< 1000 N) increases showing a more linear force-deflection loading curve. The research demonstrates that the stiffness response is dependent on contact area, thus the stress applied and rate of loading, and hence the contact area is necessary to be considered in the analysis of surface

mechanical behaviour under player loading. The area of contact and the stress-strain behaviour of the surface materials has not been identified or quantified in most of the previous studies into surface behaviour under (vertical) loading. However, unlike the constant test foot area in mechanical loading experiments, the contact area in a player foot strike varies during the stance, reaching the peak under the maximum vertical force in forefoot running and landing. Introducing the foot contact area as another variable during the loading history adds more complexity in the analysis of surface stress-strain behaviour under player movements.

The surface contact stress under the foot during contact has been demonstrated in this work to greatly reduce with depth, as the load is distributed through the surface system thickness over an increasing contact area with depth – a form of load spreading. This stress distribution of surface system may be expressed for convenience as an ‘angle of load spreading’ to describe the size of the enlarged contact area at depth, which was observed to be dependent on the stress applied, properties of shockpad used and thickness of each layer. Pressure distribution contours showed the stress was not distributed evenly over the enlarged contact area. In the centre region directly under the surface load area the pressure at depth was still relatively large and that outside of this area the pressure was much lower. This shows the average stress is reduced, but the stress concentration directly under the surface load area also indicates that these surface systems can be described as ‘point elastic’. Shockpad layer used in the system was expected to further distribute the load after it passing through carpet layer. Hockey turf system with foam shockpad demonstrated gradual stress distribution through carpet and then shockpad layer under player forefoot running. However, similar stress distribution was measured at the hockey carpet-rubber shockpad interface and at the bottom of this system.

The complexity of player loading and the influence of the identified loading variables on the surface system response further highlight the drawbacks of relying on current simple industry standard drop weight impact tests such as the AAA to simulate the athlete in its assessment of surface performance. The AAA test is designed to reproduce the initial impact of heel strike in rearfoot running with generally high contact loads and high loading rate over a small contact area. With its current design, this drop test is inappropriate for measuring the surface system response during forefoot push-off phase in rearfoot running or under forefoot strike movement patterns. Relative to the AAA, a player forefoot running or sprinting exhibits larger contact area, a lower rate of loading, higher magnitude of

loading and longer ground contact time such that the surface system is expected to respond differently and is likely to show a less stiff response and larger energy loss compared to its behaviour under heel strike. Player forefoot strike movement patterns such as sprinting and acceleration are frequently performed in a match. This contrast in behaviour may be expected to contribute to a difference in what a player may 'feel' about surface hardness in comparison to the AAA grading, and although the industry standards do not yet include for energy loss, this is clearly an area for consideration regarding player energy expenditure. The AAA is used in standards to measure surface shock absorbency and vertical deformation, and whilst these quantities have been contrasted to 'good quality' natural grass, there is no published evidence of the suitability of the acceptable ranges to player performance.

Improving the current drop test set-up and method to adequately reproduce player forefoot loading patterns and assess the resulting surface system properties appears a suitable direction to further evaluate surface system deformation ability and energy behaviour. Hence a more comprehensive assessment of surface system could be proposed to improve the industry player-surface related performance standards. More detailed recommendations are suggested in Section 6.4.2.

Attempts to employ two stress-strain models to describe surface systems behaviour during loading phase show good correlation between models and experimental stress-strain data. Exponential damped model is considered to be suitable to predict the stress-strain behaviour of surface systems under player loading at higher stress level and has the potential to reproduce unloading curve showing the energy returned. The findings of this model provide a good basis to the development of finite element model which is capable of describing the player-surface interaction in further details.

Table 5.1: Summary table of compressive properties for each surface system under different loading types

Surface system	Loading type	Peak contact area (cm ²)	Strain rate (1/s)	Compressive strain	Chord modulus	Stress reduction	Hysteresis energy ratio
HT+RS	3.3 Hz	20	1.81	0.49	2785.6	76%	42.3%
	Player running	70	2.19	0.26	662.0	55%	5.8%
	AAA	38	N/A	0.32	N/A	64%	N/A
HT+FS	3.3 Hz	20	2.06	0.60	2293.6	78%	49.5%
	Player running	70	3.34	0.42	615.2	59%	23.6%
	AAA	38	N/A	0.38	N/A	66%	N/A
3G+RS	3.3 Hz	20	1.41	0.35	3987.2	75%	36.0%
	Player running	70	1.4	0.16	1378.1	64%	15.7%
	AAA	38	N/A	0.21	N/A	68%	N/A
3G+FS	3.3 Hz	20	1.62	0.40	3279.8	78%	42.2%
	Player running	70	1.55	0.21	1307.5	63%	33.9%
	AAA	38	N/A	0.24	N/A	69%	N/A

Table 5.2: Parameters and error values for stress-strain models to describe the loading phase of the 10th cycle of 3.3 Hz mechanical loading with 50 mm diameter foot on each surface system

Surface system	Model	Parameters				RMSE (kPa)	Adjusted square of correlation
		E (kPa)	α	d (N.s/cm ²)	σ_0 (kPa)		
Hockey turf + Rubber shockpad	Exponential	30	7.4	N/A	-141	7	0.999
	Exponential Damped	23.6	7.8	7.9	-255	8	0.999
Hockey turf + Foam shockpad	Exponential	6.2	8.5	N/A	-48	13.2	0.998
	Exponential Damped	5.5	8.7	10.4	-255	13.3	0.998
3G turf + Rubber shockpad	Exponential	16.6	11.4	N/A	-109	6.3	0.999
	Exponential Damped	14.8	11.7	20.8	-391	6.6	0.999
3G turf + Foam shockpad	Exponential	3.6	12.9	N/A	-29	12.7	0.998
	Exponential Damped	3.8	12.8	27.4	-475	12.7	0.998

Table 5.3: Parameters and error values for stress-strain models to describe the loading phase of player forefoot running movement on each surface system

Surface system	Model	Parameters				RMS E (kPa)	Adjusted square of correlation
		E (kPa)	α	d (N.s/cm ²)	σ_0 (kPa)		
Hockey turf + Rubber shockpad	Exponential	1066	0.7	N/A	-939	8	0.971
	Exponential Damped	212.5	2.5	30	-731	8.6	0.967
Hockey turf + Foam shockpad	Exponential	10150	0.1	N/A	-10100	8.2	0.987
	Exponential Damped	488.8	1	9.8	-751	9.3	0.983
3G turf + Rubber shockpad	Exponential	616.8	1.7	N/A	-535	4.7	0.988
	Exponential Damped	317.1	2.9	9.8	-365	4.9	0.987
3G turf + Foam shockpad	Exponential	1078	1.1	N/A	-1044	11.8	0.971
	Exponential Damped	372	2.6	15.6	-565	12.2	0.969

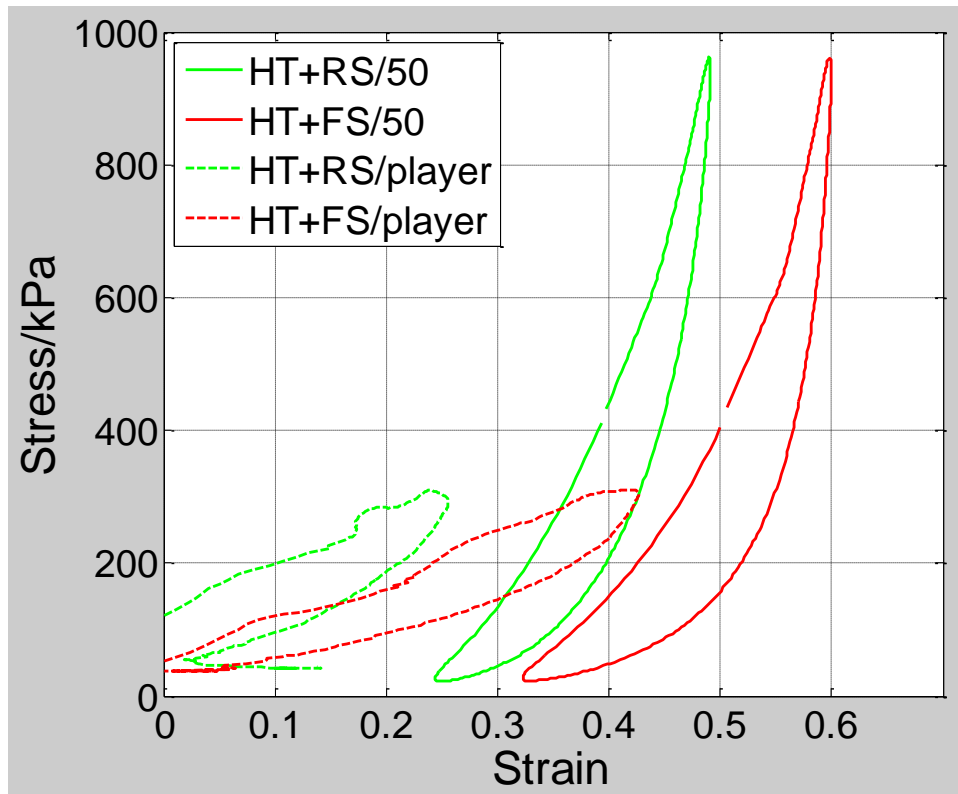


Figure 5.1: Stress-strain relationship of hockey turf surface systems for 3.3 Hz mechanical loading with 50 mm test foot (solid lines) and player forefoot running impact (dashed lines)

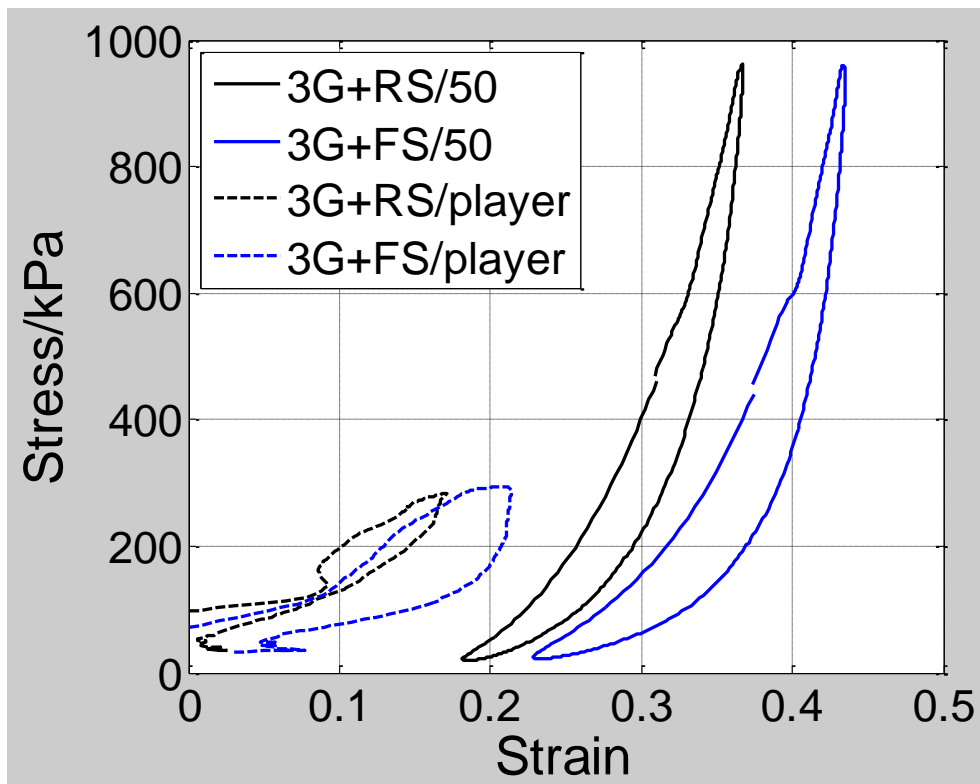


Figure 5.2: Stress-strain relationship of 3G turf surface systems for 3.3 Hz mechanical loading with 50 mm test foot (solid lines) and player forefoot running impact (dashed lines)

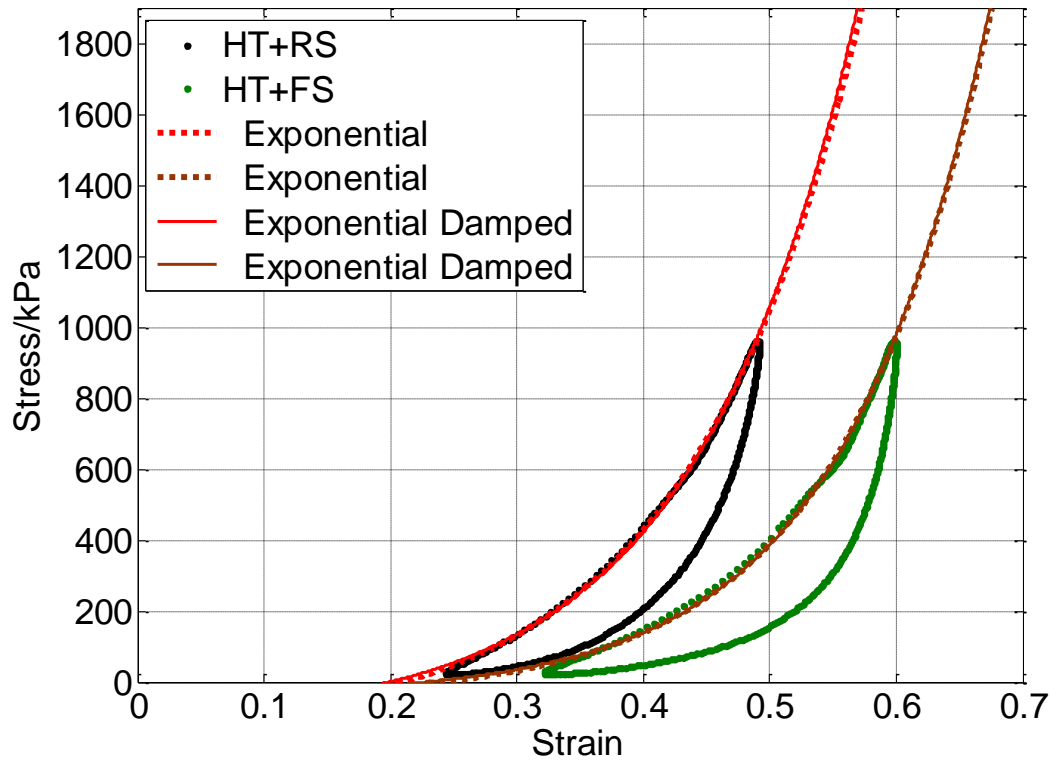


Figure 5.3: Comparison of stress-strain models for 3.3 Hz mechanical loading with 50 mm diameter loading foot on the hockey turf systems

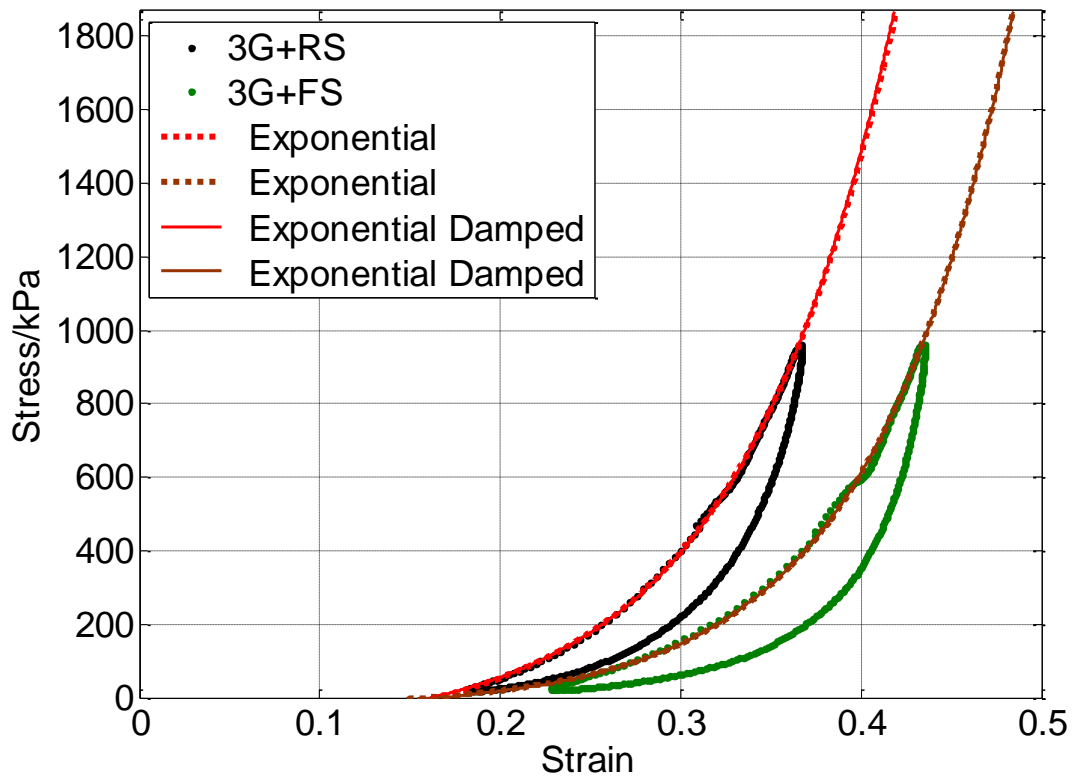


Figure 5.4: Comparison of stress-strain models for 3.3 Hz mechanical loading with 50 mm diameter loading foot on the 3G turf systems

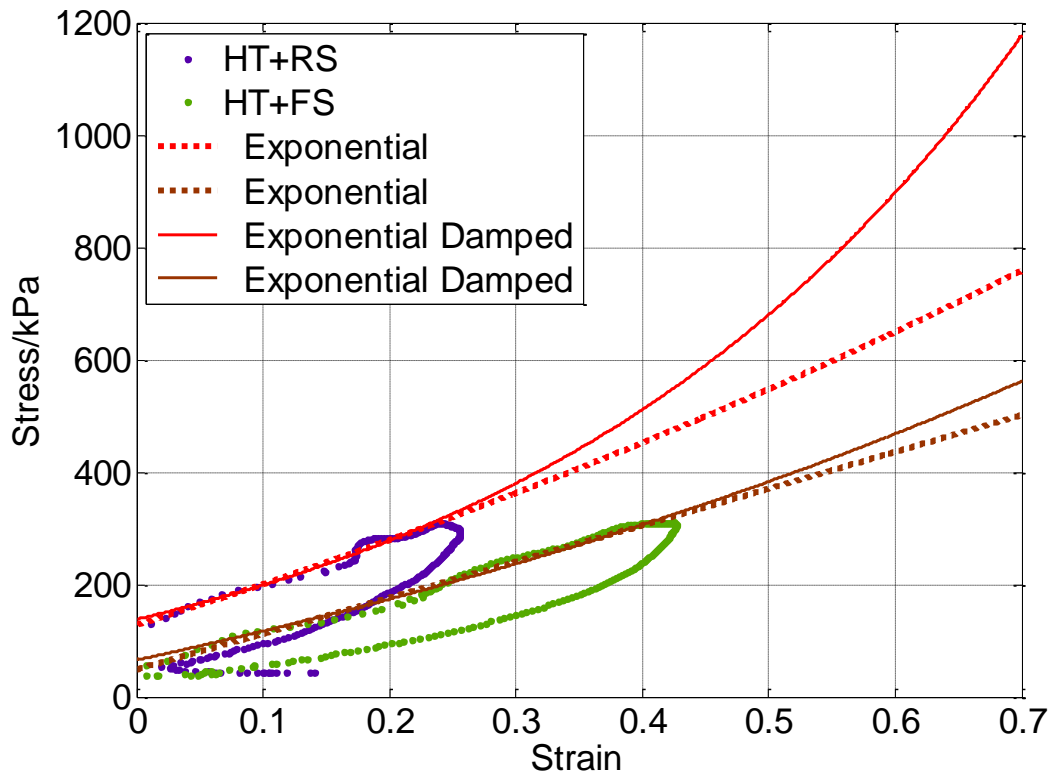


Figure 5.5: Comparison of stress-strain models for player forefoot running on the hockey turf systems

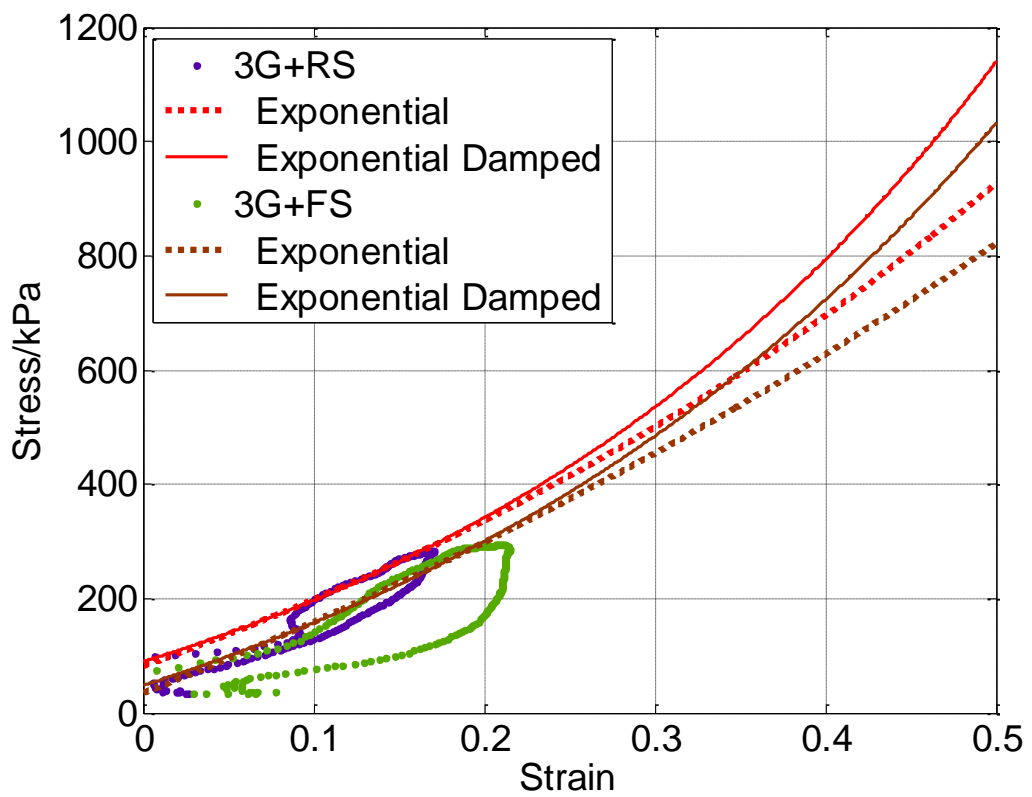


Figure 5.6: Comparison of stress-strain models for player forefoot running on the 3G turf systems

6. Conclusions

6.1 Chapter overview

This chapter provides a concise set of conclusions setting out the key findings of this research which address objective 7 of this thesis (Chapter 1) and lead into implications for the artificial turf surface system research area and industry. Limitations of this study are discussed, followed by a selection of further work recommendations.

6.2 Conclusions

The literature review concluded that there was a lack of knowledge within the interaction between player and sports surface regarding the effects of real player loading on the mechanical response behaviour of artificial turf systems. Current mechanical tests using drop weight tests and material testing machines were identified as unable to represent player loading. Few if any were biomechanically validated in their loading variables nor incorporated the complexities of player movements and therefore were considered in general as inappropriate for measuring the behaviour of sports surface in-service condition. To determine the surface response in actual player-surface interactions, measurements needed to be complemented with real subject tests. However, no published research was found to investigate the mechanical behaviour of artificial turf system during player locomotion, such as deformation response.

The aim of this research was to quantify the previously unreported mechanical behaviour of artificial turf surface systems under a range of real player movements, and the contribution of component layers to the surface system response using advanced measurement systems. The following conclusions derived from the key findings of this research achieved the objectives outlined in Chapter 1.

This research introduced a mechanical loading programme to measure the behaviour of the component layers and surface systems using dynamic cyclic compressive loading with changes in impact areas and loading frequencies to evaluate the effects of these loading variables (Chapter 3). All tested layers and surface systems showed nonlinear stress-strain behaviour with hysteresis loops during compressive loading and unloading. A reduction in the loading foot size from 125 mm to 50 mm diameter resulted in an increase in surface system vertical deflection and stronger nonlinearity of the surface system response. Hockey turf systems experienced vertical deflections at the same peak load under 50 mm

loading foot 70 – 110% larger than under the 125 mm loading foot. The peak vertical deflections of 3G turf systems under 50 mm loading foot were increased by 30 – 80% compared to under 125 mm foot. An increase of the number of loading cycles applied caused an accumulation of residual strain for the individual layers. From the initial to the 40th cycle at 3.3 Hz under 50 mm loading foot, the residual strain developed approximately 0.01 for foam shockpad and 0.05 for both rubber shockpad and hockey carpet. The 3G carpet exhibited a prominent accumulation of residual strain of 0.12 due to gradual compaction of the infill materials. Increasing the loading frequency (0.9, 3.3 and 10 Hz) led to stiffer behaviour in the lower stress range (< 400 kPa) for all surface systems under the 50 mm loading foot. 3G turf systems showed also an increase in stiffness at higher stress range (> 600 kPa) and a decrease in maximum strain as the loading frequency increased. Hysteresis loops obtained at different loading frequencies indicated that the amount of energy loss by each surface system decreased with an increase in loading rate (for the same maximum load of 1900 N).

Measurement system and data analysis methods presented in Chapter 4 were developed to investigate how artificial turf surface systems respond under real player loading. The Centre of Pressure (CoP) position during player walking, running and landing on surface systems was determined to assist in analysing the displacements of Vicon markers on the shoe, such that surface vertical deflection history for each movement could be determined.

The heel-toe walking results on all surface systems indicated that the maximum applied stress (in the range of 328 to 370 kPa) and surface strain (0.55 for HT+RS, 0.44 for HT+FS, 0.17 for 3G+RS and 0.29 for 3G+FS) occurred in very early stance (first 10%) when the boot-surface contact area was small (less than 10 cm²). Thereafter, the peak stress (180 – 200 kPa) observed during the push-off phase (55% - 100% of stance) resulted in a slight increase in strain to a peak value (0.18 for HT+RS, 0.31 for HT+FS and 0.11 for both 3G turf systems). For forefoot running and landing, the peak surface strain occurred around mid-stance concurrent with the time of peak applied stress. The strain measured at peak stress (271 – 278 kPa) under average forefoot running contact area of 70 cm² was in the range of 0.16 to 0.42 for all surface systems. The strain of each surface system under forefoot landing with an averaged contact area of 73 cm² at peak stress (267 – 285 kPa) was slightly larger than under running with a difference within 0.05, but still remained in the similar range of 0.16 to 0.43.

Peak vertical deformation data recorded under the AAA impacts was converted into strain and compared with the results under player forefoot running in Table 5.1. The AAA applied much higher peak stress in the range of 550 to 675 kPa on surface systems compared to player forefoot running, resulting surface strain in the range of 0.21 to 0.38. The strain under the AAA impacts was 0.05 and 0.03 larger than under forefoot running for 3G+RS and 3G+FS respectively. The strain of HT+RS was also observed as 0.06 larger under the AAA. However, the strain of HT+FS under the AAA impacts was 0.04 smaller than under forefoot running whilst the peak impact stress was the lowest at 551 kPa. As a stiffer surface would provide increased impact force magnitude and thus stress measured using the AAA, assuming that a "bottoming out" of the surface does not occur (Dixon et al., 1999). In contrast, the surface applied stress variations in subject testing were not found to be correlated to the stiffness of the surface. Therefore, the surface strain (deformation) measured by the AAA is unable to represent the actual surface response during player loading.

Pressure mat measuring system was validated for use in both mechanical and player loading experimental programmes and proved to be a useful tool for evaluating the pressure distributions and contact areas at different interfaces of the surface system. The surface applied stress was observed to greatly reduce with depth over increasing contact area through the surface systems. The Pressure mat data, placed at the bottom of the surface system, showed that the surface applied stress of 968 kPa (mechanical loading at 3.3 Hz) was reduced by approximately 77% for all surface systems. The Player running applied stress of around 275 kPa was reduced by approximately 60% at the base of the surface system in comparison. Although the average pressure was reduced, more detailed analysis of the pressure distribution contours showed that directly under the surface load area the pressure at depth was still relatively large and that outside of this centre area the pressure was much lower. This shows a deflection bowl in the surface system spreading some of the applied load, but also reinforces that these surface systems can be described as 'point elastic'. When the pressure mat was sandwiched between hockey carpet and shockpad layer, gradual pressure reduction was observed through carpet and then shockpad under mechanical loading with 125 mm test foot. Compared to the pressure measured at carpet-shockpad interface, it was slightly further reduced by shockpad no more than 18%. The gradual pressure reduction through HT+FS was also observed under player forefoot running, but not with HT+RS. This inconsistency may be caused by the limitation of using

a single pressure mat at each interface in separate repeat trials, which is discussed in Section 6.3.

Measurements of mechanical behaviour of the surface systems gained through the experimental programmes assisted in the development of exponential (damped) stress-strain models to describe and predict surface system behaviour under compressive loading. Key parameters of the models were identified including modulus of elasticity, nonlinearity coefficient, damping coefficient and strain rate. Exponential damped model developed stronger nonlinearity than exponential model and reduced the modulus of elasticity.

Implications

The findings of this research are distilled into the following primary implications for academic research and sports surface industry.

In the research into the mechanism of sports surface response to vertical loads, the disparity of mechanical behaviour of surface system under drop weight impact testing, mechanical compressive cyclic loading and actual player movements has been identified due to differences between test boundary conditions. Drop weight test devices fail to replicate player loading and do not measure any aspects of the surface nonlinear behaviour. Mechanical compressive loading using advanced material testing machines is useful for analysing the effect of each influential loading parameter (e.g. loading magnitude, rate, area) and surface physical property (e.g. thickness, density and temperature) on the mechanical behaviour of sports surface only when biomechanically validated loading inputs are used in test design. Ideally mechanical behaviour of surface for in-service play conditions could be assessed simultaneously during real player movements using the measurement systems and methods developed in this project (possibly with some modification to address the issues discussed in Section 6.3).

The importance of recording the surface nonlinear response during the whole dynamic compressive loading is highlighted again in this research. Section 3.4.2 showed hockey turf systems reached approximately the same strain at the same peak stress for different loading frequencies, but the stiffness and energy loss were evidently different. Measuring only the peak force/stress and deflection/strain clearly does not contrast the different surface response in such a case. Therefore, complete loading and unloading histories should be obtained for evaluating surface behaviour in further studies.

Contact area under compressive loading is found to affect surface system vertical deflection and stiffness; hence it needs to be considered within measured mechanical behaviour in further studies. Few previous research studies either provided detail of this important parameter or evaluated its effect on surface behaviour. The surface systems with a rubber shockpad used in this project exhibited lower stress distribution (smaller stress distribution angles) and less energy loss (more elastic response) compared with using foam shockpad. Intrinsic material properties and microstructure of shockpad were employed to explain the observed differences in surface system behaviour. These aspects such as cellular structure, air void ratio, stiffness of cell walls and infill bulk density also should be assessed by microscopic examinations to be associated with surface apparent response in further research.

Surface system under player movements also experience horizontal forces together with vertical forces. The evaluation of horizontal forces and their effects was outside the scope of this project. However, comparison between surface behaviour under player loading and vertical mechanical loading suggested horizontal forces are expected to have some influence on the stiffness and energy behaviour. Further work could develop current measurement systems to examine horizontal forces and resulting surface deformation and how they affect the surface behaviour in the vertical direction to more comprehensively understand of surface behaviour in service conditions. Section 6.4.1 provides additional details relating to test design for further research.

Shockpads help to regulate the surface system stiffness and reduce the applied peak stress by deforming. Stress distribution results presented in Chapter 3 and 4 showed that the applied stress could be reduced by carpet layer on top by more than 40%. Therefore the design and manufacture of shockpad should be directed towards optimising its mechanical behaviour at a lower stress level (< 300 kPa) and under larger contact area to consider the stress distribution effect of carpet layer, instead of sharing the same criteria used to assess carpet layer or composite surface system. Pressure distribution contours showed high stress concentration directly under the surface load area in the centre region and a much lower pressure measured in the outer zone of the enlarged contact area recorded at the bottom of surface system. Shockpad could evenly distribute the compressing/impacting load over an increased contact area may reduce energy loss and improve durability of the product. Shockpads designed in this way would contribute to better overall surface system response under player loading.

6.3 Study limitations

The methods and technologies for obtaining the results have their limitations, which are discussed in the following.

With a focus on proposing improvements upon measurement and data analysis methods, only a selection of four surface systems was investigated in this project. The shockpads, artificial turf carpets and component materials used for building the tested surface systems ensured a good representation of products on the market for different sports. A large variety of artificial turf surface products with different properties exists within the industry. However trying to examine all these categories in one research project would be inconceivable. This project investigated the behaviour and contribution of two prefabricated shockpads and within surface systems. A cast in-situ shockpad was not included due to difficulties in constructing this type of shockpad in the laboratory. Various combinations of sand and rubber infills can be used for 3G carpet layer. In this research only one combination was selected without changing the materials and quantities of infills.

The advanced material testing machine (Instron ElectroPuls E3000) used in this research enables highly dynamic testing with force and displacement parameters recorded at a high sampling rate. But as presented in Section 3.3, the need of several initial cycles to achieve the target peak force (1900 N) was identified, especially for higher loading frequency, more initial cycles were required. Therefore, a resulting limitation was the results were presented from the first cycle achieved the target peak force which varied with the loading frequency (2nd cycle for 0.9 Hz, 10th cycle for 3.3 Hz and 20th cycle for 10 Hz). The analysis of loading frequency effects on mechanical behaviour of surface systems compared the data from the 19th cycle for all frequencies. Comparison of data from the outset through all the cycles would have been preferable.

The player loading experimental programme was limited to analyse only one subject with one pair of boots practising three basic movement patterns (walking, running and drop-landing) that generated moderate forces and rates of loading. Variations in multiple players, different types of boots and for more extreme sport-specific movements and their effects on surface system response were not investigated in this research project. Since the measurement system and data analysis methods proved to be able to quantify surface system stress-strain relationship (in vertical direction only) under these selected player movements, the current work can be extended to include a larger subject population size,

more types of boots and movement patterns, thus furthering the understanding of surface responses to different player loading conditions.

Measuring the pressure distribution at two interfaces of surface system using a single pressure mat introduced a limitation to the player loading experimental programme. In order to analyse the applied loading distribution through the carpet layer and then the shockpad it would be ideal to have two pressure mats measuring simultaneously, one placed at the carpet-shockpad interface and the other one at the bottom of the surface system. However, as only one pressure mat was available the pressure distribution at each interface was measured in separate repeat trials. The player was instructed to use the same technique and be consistent, however a lower repeatability was observed as expected for the human movements in comparison to the mechanical loading and the COV of peak vertical force, for example, was 0.057 (Table 4.6) for landing for all the subject trials. This effect was lessened, however, by using the averaged values for peak stress and contact area of four repeats. Effectiveness and calibration issues of the pressure mat used in this study are presented in Chapter 3. More advanced pressure sensing system in the future with improved calibration methods and faster sampling rate, less affected by shear force and intrusion effect would be expected to provide more accurate pressure distribution results.

The three segment boot planes fitted to the markers were found to be valid for measuring surface system vertical deflection with acceptable small errors under the selected player movements throughout the majority of stance. However, it was observed that as the angle of the boot sagittal plane deviated more from the absolute horizontal, for example in very early and late stance, the errors in the calculation of surface deflection were larger due to much of the boot being out of contact with the surface. A resulting limitation was the inability to present accurate vertical deflection of the surface in the early touch-down and late toe-off phases. In addition, each segment boot plane was considered as a rigid body for data analysis of the three movements, so the slight deformation of the boot outsole where Vicon markers were attached to during foot impact was ignored.

An additional shortcoming was the lack of control of the foot-surface impact area. It is one of the identified variables that affect the response of surface system. In comparison to the results from mechanical loading to the player loading, the variations in mechanical loading feet sizes (20 and 123 cm²) and peak player foot contact areas (ranged from 54 to 73 cm² for the three movement patterns) made it difficult to explain the different surface system

responses and assess the effects of other loading parameters (e.g. loading rate and horizontal forces). Section 6.4 provides recommendations to address this problem.

Preliminary modelling work presented in Section 5.3 employed two exponential models to fit only the loading curves of mechanical and player loading events. Further work could explore the use of exponential damped model to describe a whole loading event including the unloading phase.

6.4 Recommendations

This section covers a selection of recommendations for further work based on the outcomes of this research project. Some build upon aspects discussed in this thesis that could benefit from additional investigation, whilst others relate to new areas of research which fell outside the scope of this project. Recommendations are provided in the context of further academic research, which looking at improving the measurement systems and methods to further understand the player-surface interactions, and suggestions to the sports surface industry concerning improvements to standard test method.

6.4.1 Further academic research

Issues with achieving target peak force in initial cycles for mechanical cyclic loading tests are highlighted in Section 3.3 and 6.3. Further work in conjunction with the testing machine manufacturer could perhaps develop a feedback loop which compares actual and target force values on a per cycle basis and adjusts automatically in order to achieve this parameter accurately (Davidson, 2012). It would be an invaluable feature to the current control software and ensure the validity of data from every cycle, especially at high loading frequency.

In order to further analyse the effect of each influential loading variable (e.g. loading magnitude, rate, area and stud configuration) on the mechanical behaviour of surface system under mechanical and player loading, it is recommended to control relevant variables and compare the experimental results in the remaining variable. For example, mechanical loading foot area could be designed to match the peak boot-surface contact area of a specific movement, ideally also in the same shape and stud configuration. By controlling other variables such loading magnitude, rate and contact time together, the response of the surface system under mechanical simulated and actual player loading could be contrasted to evaluate the representativeness of the mechanical test method and identify

other possible factors that affect the surface behaviour during player loading that are important.

This research project has focused on the effects of player loading on the mechanical behaviour of surface system. Further work could consider an integrated study that investigates the surface behaviour and player performance simultaneously. By attaching markers to player's joints such as ankle and knee, biomechanical data such as joint flexion angle and acceleration could be obtained during a loading event on sports surface to assess player kinematic adjustments in response to changes in surface properties. Using multiple pressure sensors (insole and mat) placed at each level of the foot/shoe/carpet/shockpad system allows the stresses on the player and the surface to be assessed simultaneously. Such integrated studies allow the simultaneous evaluation of surface-related injury risk, surface behaviour and player performance.

Further research could develop and introduce horizontal loading into the current mechanical loading test, for example, by using angled load platens as illustrated in Figure 6.1 (Anderson, 2007; Davidson, 2012). This arrangement for the component and system material testing machine could be used to simultaneously impart both normal and shear force components on the surface sample. Player loading data from Chapter 4 can help inform the design of platen angle (γ) and magnitude of applied vertical force (F) to create realistic loading.

6.4.2 Industry

The updated standard test device used by the sport governing bodies for measuring force reduction and vertical deformation still has limitations in the replication of actual player loading. In comparison to player running/sprinting, this drop test from constant height delivers much higher rate of loading and shorter contact time which results in stiffer surface response and smaller vertical deformation than under player movements.

Improvements could be made to use biomechanical data to incorporate a range of loads (900 – 3000 N), contact areas (50 – 100 mm diameter) and load durations (0.1 – 1 s) to measure the resulting surface response. In addition, reported results could present the force-deflection (stress-strain) relationship for loading phase instead of only the peak values to exhibit the surface nonlinear stiffness behaviour.

6.5 List of publications

Wang, X., Fleming, P.R. and Dixon, N., 2012, Advanced Measurement for Sports Surface System Behaviour. 9th International Conference of the International Sports Engineering Association, Lowell, USA, July 2012

Forrester, S., Wang, X. and Fleming, P.R., 2013, Quantifying the dynamic errors in centre of pressure position during human locomotion on compliant surfaces. *Journal of Biomechanics*, 2013 (submitted)

Wang, X., Fleming, P.R. and Forrester, S., 2014, Advanced Measurement for Sports Surface System Behaviour under player loading. 10th International Conference of the International Sports Engineering Association, Sheffield, UK, July 2014 (abstract accepted)

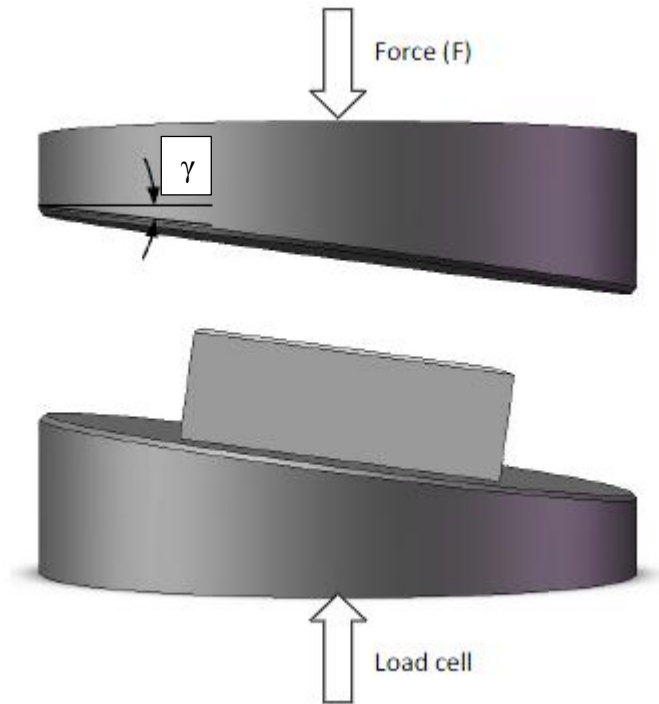


Figure 6.1: Angled load platens design facilitating simultaneous application of multiple GRF components (modified from Davidson, 2012)

Reference

- Adrian, M., Xu, D., 1990. Matching the Playing Field to the Player. In: Natural and Artificial Playing Fields: Characteristics and Safety Features (ED. R. C. Schmidt), American Society for Testing and Materials, Philadelphia, USA: 10-19.
- Ahmadi, A., Rowlands, D., James, D., 2010. Development of inertial and novel marker-based techniques and analysis for upper arm rotational velocity measurements in tennis. *Sports Engineering* 12, 179–188.
- Alcántara, E., Gámez, J., Rosa, D., Sanchis, M., 2009. Analysis of the influence of rubber infill morphology on the mechanical performance of artificial turf surfaces for soccer. *Proceedings of the Institution of Mechanical Engineers, Part P: Journal of Sports Engineering and Technology* 223, 1–9.
- Allgeuer, T., Torres, E., Bensason, S., Chang, A., Martin, J., 2008. Study of shockpads as energy absorption layer in artificial turf surfaces. *Sports Technology* 1, 29–33.
- Anderson, L., 2007. *Elastomeric Shockpads for Outdoor Synthetic Sports Pitches*, PhD Thesis, Loughborough University, Loughborough, UK.
- Andersson, H., Ekblom, B., Krustup, P., 2008. Elite football on artificial turf versus natural grass: movement patterns, technical standards, and player impressions. *Journal of sports sciences* 26, 113–22.
- Bartlett, R., 1999. *Sports Biomechanics: Reducing Injury and Improving Performance*, E & FN Spon, London, UK.
- Barnett, S., Cunningham, J.L., West, S., 2001. A comparison of vertical force and temporal parameters produced by an in-shoe pressure measuring system and a force platform. *Clinical biomechanics (Bristol, Avon)* 16, 353–7.
- Baroud, G., Nigg, B., Stefanyshyn, D., 1999. Energy storage and return in sport surfaces. *Sports Engineering* 173–180.
- Blackburn, S., Nicol, A. C., Walker, C., 2005. Development of a Biomechanically Validated Turf Test Rig, Research Poster, University of Strathclyde, Glasgow, UK.
- Bloomfield, J., Polman, R., O'Donoghue, P., 2004. The 'Bloomfield Movement Classification': Motion Analysis of Individual Players in Dynamic Movement Sports. *International Journal of Performance Analysis in Sport*. 4 (2), 20–31.
- Bobbert, M. F., Yeadon, M.R., Nigg, B.M., 1992. Mechanical analysis of the landing phase in heel-toe running. *Journal of Biomechanics* 25(3): 223-234.
- Brachet, P., 2004. *An Experimental / Computational investigation of the interaction between athletes and playing surfaces*. PhD Thesis, University of Strathclyde, UK.

- Brandrup, J., Immergut, E. H., 1975. Polymer handbook, J. Brandrup, E. H. Immergut, editors, with the collaboration of W. McDowell Wiley New York.
- Brimacombe, J.M., Wilson, D.R., Hodgson, A.J., Ho, K.C.T., Anglin, C., 2009. Effect of calibration method on Tekscan sensor accuracy. *Journal of biomechanical engineering* 131, 034503.
- Bryant, J.T., Reid, S.A., Stevenson, J.M., 1999. Contact Pressure Calibration Method: Development of a Calibration Jig, DCIEM Contractor Report, submitted in partial fulfillment of PWGSC Contract No. W7711-7-7405/SRV. Report submitted to the Defence and Civil Institute of Environmental Medicine.
- Brown, R.P., 1987. Performance tests for artificial sports surfaces, *Polymer Testing*, vol. 7, no. 4, pp. 279-292.
- Carré, M. J., Dodd, D., Senior, T., Haake, S. J., 2004. A System for Predicting the Impact Between a Ball and a Sports Surface, In: *The Engineering of Sport 5*, (Eds M. Hubbard, R. D. Mehta, and J. M. Pallis) pp. 45-51.
- Carré, M.J., Haake, S.J., 2004. An examination of the Clegg impact hammer test with regard to the playing performance of synthetic sports surfaces. *Sports Engineering* 7, 121–129.
- Carré, M.J., James, D.M., Haake, S.J., 2006. Hybrid Method for Assessing the Performance of Sports Surfaces During Ball Impacts. *Proceedings of the Institution of Mechanical Engineers, Part L: Journal of Materials: Design and Applications* 220, 31–39.
- Carvalho, V., Bucklin, R., 2005. Effects of trimming on dairy cattle hoof weight bearing and pressure distributions during the stance phase. *Transactions of the ...* 48, 1653–1660.
- Cavanagh, P.R., Lafortune, M.A., 1980. Ground reaction forces in distance running. *Journal of Biomechanics* 13: 397-406.
- Cavanagh, P.R., 1980. *The Running Shoe Book*, Anderson World, Mountain View, CA, USA.
- Challis, J., 1995. A procedure for determining rigid body transformation parameters. *Journal of biomechanics* 28.
- Chuckpaiwong, B., Nunley, J.A., Mall, N.A., Queen, R.M., 2008. The effect of foot type on in-shoe plantar pressure during walking and running. *Gait & Posture* 28, 405–411.
- Clegg, B., 1976. An impact testing device for in situ base course evaluation. *Australian Road Research Bur. Proc.*, 8, 1-6.
- Cotton, R.T., 2008. Surface interactions of soccer balls, PhD Thesis, Loughborough University, Loughborough, UK.

- Crawshaw, G. H. 1989, *Textile Sports Surfaces and Artificial Grass*, Elsevier Science Publishers Ltd, Oxford, UK.
- Davidson, C., 2012. *Investigating the Suitability of Laser Sintered Elastomers for Running Footwear Applications*, PhD Thesis, Loughborough University, Loughborough, UK.
- Davidson, P.L., Wilson, S.J., Wilson, B.D., Chalmers, D.J., 2009. An approach to modeling impact energy absorption by surfaces. *Journal of applied biomechanics* 25, 351–9.
- Desso 2007, - <http://www.dessosports.com/en/home/> - Accessed 3rd November 2010
- De Wit, B., De Clercq, D., 1997. Differences in sagittal plane kinematics between barefoot and shod running. In J. Bangsbo, B. Saltin, H. Bonde, Y. Hellsten, B. Ibsen, M. Kjaer, & G. Sjogaard (Eds.), *Proceedings of the Second Annual Congress of the European College of Sport Science*, Copenhagen, Denmark (pp. 790-791). Copenhagen: University of Copenhagen.
- De Wit, B., De Clercq, D., Aerts, P., 2000. Biomechanical analysis of the stance phase during barefoot and shod running. *Journal of biomechanics* 33, 269–78.
- Dixon, S. J., Batt, M. E., Collop, A. C., Singleton, T. M., 1998. The biomechanical and mechanical performance of Sureflex sports surface material. In S. J. Haake (Ed.), *The engineering of sport* (pp. 191 – 198). Oxford: Blackwell.
- Dixon, S.J., Batt, M.E., Collop, A.C., 1999. Artificial playing surfaces research: a review of medical, engineering and biomechanical aspects. *International journal of sports medicine* 20, 209–18.
- Dixon, S.J., Collop, A.C., Batt, M.E., 2000. Surface effects on ground reaction forces and lower extremity kinematics in running. *Medicine & Science in Sports & Exercise* 32.
- Dragoo, J.L., Braun, H.J., 2010. The effect of playing surface on injury rate: a review of the current literature. *Sports medicine (Auckland, N.Z.)* 40, 981–90.
- Dura, J. V., Garcia, a. C., Solaz, J., 2002. Testing shock absorbing materials: the application of viscoelastic linear model. *Sports Engineering* 5, 9–14.
- Duthie, G., Pyne, D., Hooper, S., 2003. Applied physiology and game analysis of rugby union, *Sports Medicine*, vol. 33, no. 13, p. 973-991.
- Eaves, D., 2004. Foam fundamentals. In: Eaves D, editor. *Handbook of polymer foams*. Shawbury: Rapra Technology, p. 1–8.
- Ekstrand, J., Timpka, T., Hägglund, M., 2006. Risk of injury in elite football played on artificial turf versus natural grass: a prospective two-cohort study. *British journal of sports medicine* 40, 975–80.
- El Kati, R., 2012. *Effect of mechanical behaviour of artificial turf on player-surface interaction in soccer*. PhD Thesis, Loughborough University. Loughborough, UK.

- FIFA, 2012. FIFA Quality Concept for Football Turf: Handbook of Test Methods & Handbook of Requirements. Zurich, Switzerland.
- FIH, 1999. Handbook of Requirements for Synthetic Hockey Pitches Outdoor, Brussels, Belgium.
- FIH, 2008. Handbook of Performance Requirements for Synthetic Hockey Pitches: The Pitch Handbook. Lausanne, Switzerland.
- Fleming, P., Dixon, N., Lambert, J., Young, C., 2002. Monitoring the Performance of Hockey Pitches During Construction, In: Engineering of Sport 4 (Eds. S. Ujihashi and S. J. Haake), Blackwell Publishing, Oxford, UK, pp. 545-552.
- Fleming, P. R., Young, C., Dixon, N., 2004. Performance Measurements of Synthetic Turf Hockey Pitches. In Engineering of Sport 5 (Eds. M. Hubbard, R. D. Mehta, and J. m. Pallis), Vol 2: 524 – 531.
- Fleming, P., 2011. Artificial turf systems for sport surfaces: current knowledge and research needs. Proceedings of the Institution of Mechanical Engineers, Part P: Journal of Sports Engineering and Technology 225 , 43–63.
- Ford, K.R., Manson, N. a, Evans, B.J., Myer, G.D., Gwin, R.C., Heidt, R.S., Hewett, T.E., 2006. Comparison of in-shoe foot loading patterns on natural grass and synthetic turf. Journal of science and medicine in sport / Sports Medicine Australia 9, 433–40.
- Fuller, C.W., Dick, R.W., Corlette, J., Schmalz, R., 2007. Comparison of the incidence, nature and cause of injuries sustained on grass and new generation artificial turf by male and female football players. Part 1: match injuries. British journal of sports medicine 41 Suppl 1, i20–6.
- Göbel, E.F., 1974. Rubber springs design. John Wiley & Sons, Incorporated.
- Gottschall, J.S., Kram, R., 2005. Ground reaction forces during downhill and uphill running. Journal of Biomechanics 38, 445–452.
- Gross, T., Bunch, R., 1989. Material moderation of plantar impact stress. Medicine & Science in Sports & Exercise 21 (5): 619-624.
- Grund, T., Senner, V., 2010. Traction behavior of soccer shoe stud designs under different game-relevant loading conditions. Procedia Engineering 2, 2783–2788.
- Hagel, B.E., Fick, G.H., Meeuwisse, W.H., 2003. Injury Risk in Men’s Canada West University Football. American Journal of Epidemiology 157 , 825–833.
- Halkon, B., Webster, J., Mitchell, S., Mientjes, M., 2012. Development of a test methodology for the assessment of human impacts in sport, in: Procedia Engineering. pp. 813–818.
- Hitoshi, K., 1995. Patent application JP7150437, Low-crimped pile yarn for artificial turf (nylon 6 and/or nylon 66).

- Innovene, 2006. Patent application EP1672020, Polyethylene composition for artificial turf.
- IRB, 2012. IRB Artificial Rugby Turf Performance Specification: One Turf Technical Manual. Dublin, Ireland.
- ITF, 1997. An initial ITF study on performance standards for tennis court surfaces. London.
- Jin, H., Lu, W.-Y., Scheffel, S., Hinnerichs, T.D., Neilsen, M.K., 2007. Full-field characterization of mechanical behavior of polyurethane foams. *International Journal of Solids and Structures* 44, 6930–6944.
- John Tyson and Timothy Schmidt, K.G., 2003. *Optical Deformation & Strain Measurement in Biomechanics*.
- Kaila, R., 2007. Influence of modern studded and bladed soccer boots and sidestep cutting on knee loading during match play conditions. *The American journal of sports medicine* 35, 1528–36.
- Kim, W., Voloshin, A., 1992. Dynamic loading during running on various surfaces, *Human Movement Science* 11, pp. 675-689.
- Kirk, R.F., Noble, I.S.G., Mitchell, T., Rolf, C., Haake, S.J., Carré, M.J., 2007. High-speed observations of football-boot-surface interactions of players in their natural environment. *Sports Engineering* 10, 129–144.
- Kobayashi, K., Yukawa, H., 2011. Identification of the Exponential Function Type Nonlinear Voigt Model for Sports Surfaces by Using a Multi-Intensity Impact Test. *Journal of System Design and Dynamics* 5, 1326–1336.
- Kolitzus, H.J., 1984. Functional standards for playing surfaces. In: *Sports Shoes and Playing Surfaces: Biomechanical Properties*. (ed. Frederick, E.C.). Human Kinetics Publishers, Champaign, IL, USA.
- Korhonen, M.T., Suominen, H., Viitasalo, J.T., Liikavainio, T., Alen, M., Mero, A. a, 2010. Variability and symmetry of force platform variables in maximum-speed running in young and older athletes. *Journal of applied biomechanics* 26, 357–66.
- Lieberman, D.E., Venkadesan, M., Werbel, W. a, Daoud, A.I., D’Andrea, S., Davis, I.S., Mang’eni, R.O., Pitsiladis, Y., 2010. Foot strike patterns and collision forces in habitually barefoot versus shod runners. *Nature* 463, 531–5.
- Livesay, G.A., Reda, D.R., Nauman, E.A., 2006. Peak Torque and Rotational Stiffness Developed at the Shoe-Surface Interface: The Effect of Shoe Type and Playing Surface *The American Journal of Sports Medicine* 34 , 415–422.
- Luo, Z.P., Berglund, L.J., An, K.N., 1998. Validation of F-scan pressure sensor system: a technical note, *J. Rehab. Res. Devel.*, 35: 186-191.

- MacLeod, H., Morris, J., Nevill, A., Sunderland, C., 2009. The Validity of A Non-differential Global Positioning System for Assessing Player Movement Patterns in Field Hockey, *Journal of Sports Sciences*, 27: 2, pp. 121-128.
- McCullagh, P.J.J., Graham, I.D., 1985. A preliminary investigation into the nature of shock absorbency in synthetic sports materials. *Journal of Sports Sciences* 3, 103–114.
- McGhie, D., Ettema, G., 2013. Biomechanical analysis of surface-athlete impacts on third-generation artificial turf. *The American journal of sports medicine* 41, 177–85.
- McMahon, T.A., Greene, P.R., 1979. The influence of track compliance on running. *Journal of Biomechanics* 12, 893–904.
- Meyers, M.C., Barnhill, B.S., 2004. Incidence, Causes, and Severity of High School Football Injuries on FieldTurf Versus Natural Grass: A 5-Year Prospective Study *The American Journal of Sports Medicine* 32 , 1626–1638.
- Miller, J.E., Baroud, G., Nigg, B.M., 2000. Elastic behaviour of sport surface materials. *Sports Engineering* 3, 177–184.
- Morvan, T., 2012. Tekscan pressure sensor used in assessment of personal protective equipment, MSc Final Report, Loughborough University, Loughborough, UK.
- Müller, C., Sterzing, T., Lange, J., Milani, T.L., 2010. Comprehensive evaluation of player-surface interaction on artificial soccer turf. *Sports biomechanics / International Society of Biomechanics in Sports* 9, 193–205.
- Mueller, M., Strube, M., 1996. Generalizability of in-shoe peak pressure measures using the F-scan system. *Clinical Biomechanics*.
- Munro, C.F., Miller, D.I., Fuglevand, A.J., 1987. Ground reaction forces in running: a reexamination, *Journal of Biomechanics*, vol. 20, no. 2, pp. 147-155.
- Murin, E., Bryant, J., Reid, S., Whiteside, R., 2001. Calibration issues of Tekscan systems for human pressure assessment. Defense Technical Information Center.
- Nigg, B.M.; Denoth, J., Neukomm, P.A, 1981. Quantifying the load on the human body: Problems and some possible solutions; in Morecki et al. (Eds) *Biomechanics VII*, pp. 88–99.
- Nigg, B.M., Denoth, J., Kerr, B., Luethi, S., Smith, D., & Stacoff., 1984. Load, Sports Shoes and Playing Surfaces. In: *Sports Shoes and Playing Surfaces* (Ed. Frederick, E.C), Human Kinetics Publishers, IL, USA: pp 1-23
- Nigg, B. M., Frederick, E. C., Hawes, M. R., Luethi, S. M., 1986. Factors influencing short-term pain and injuries in tennis. *International Journal of Sport Biomechanics*, 2, 156-165.

- Nigg, B. M., Bahlsen, H.A., Luethi, S.M., Stokes, S., 1987. The influence of running velocity and midsole hardness on external impact forces in heel-toe running. *Journal of Biomechanics* 20: 951-959.
- Nigg, B.M., Yeadon M.R., 1987. Biomechanical Aspects of Playing Surfaces. *Journal of Sports Science* 5: 117-145.
- Nigg, B., Bahlsen, H., 1988. Influence of heel flare and midsole construction on pronation, supination, and impact forces for heel-toe running. *International Journal of Sport Biomechanics* 4, 205–219.
- Nigg, B. M., 1990. The validity and relevance of tests used for the assessment of sports surfaces. *Medicine and Science in Sports and Exercise* 22(1): 131-139.
- Nigg, B. M., Anton, M., 1995. Energy aspects for elastic and viscous shoe soles and playing surfaces. *Medicine and Science in Sport and Exercise* 27(1): 92-97.
- Nigg, B. M., Cole, G.K., Bruggemann, P., 1995. Impact forces in heel-toe running. *Journal of Applied Biomechanics* 11: 407-432.
- Orchard, J., 2002. Is there a relationship between ground and climatic conditions and injuries in football? / Existe-t-il des correlations entre la nature du sol, les conditions climatiques et les traumatismes au football ? *Sports Medicine* 32, 419–432.
- Pain, M.T.G., Tsui, F., Cove, S., 2008. In vivo determination of the effect of shoulder pads on tackling forces in rugby. *Journal of sports sciences* 26, 855–62.
- Peikenkamp, K., Fritz, M., Nicol, K., 2002. Simulation of the vertical ground reaction force on sport surfaces during landing. *Journal of Applied Biomechanics*, 18, 122–134.
- Petersen, C.J., Pyne, D., Dawson, B., Portus, M., Kellett, A., 2010. Movement patterns in cricket vary by both position and game format, *Journal of sports sciences*, vol. 28, no. 1, pp. 45-52.
- Petrass, L. a, Twomey, D.M., 2013. The relationship between ground conditions and injury: what level of evidence do we have? *Journal of science and medicine in sport / Sports Medicine Australia* 16, 105–12.
- Queen, R.M., Haynes, B.B., Hardaker, W.M., Garrett, W.E., 2007. Forefoot loading during 3 athletic tasks. *The American journal of sports medicine* 35, 630–6.
- Robinovitch, S.N., Chiu, J., 1998. Surface stiffness affects impact force during a fall on the outstretched hand. *Journal of Orthopaedic Research*, 16, 309–313.
- Ronkainen, J. a, El-Kati, R.F., Fleming, P.R., Forrester, S.E., 2010. Application of an industrial robot in the sports domain: simulating the ground contact phase of running. *Proceedings of the Institution of Mechanical Engineers, Part P: Journal of Sports Engineering and Technology* 224, 259–269.

- SAPCA 2005, Code of Practice for the Construction and Maintenance of Synthetic Turf Sports Pitches, Second Edition.
- Schoukens, G., 2009. Developments in textile sport surfaces, *Advances in carpet Manufacture*, Woodhead Publishing Com., Cambridge, UK, Chapter 5, pp.102-137.
- Schwanitz, S., Odenwald, S., 2008. Long-term Cushioning Properties of Running Shoes (P152), in: *The Engineering of Sport 7 SE - 11*. Springer Paris, pp. 95–100.
- Severn, K.A., 2010. Science of Synthetic Turf Surfaces: Player-Surface Interactions. PhD Thesis, Loughborough University, Loughborough, UK.
- Shorten, M. R., Hudson, B., Himmelsbach, J. A., 2003. Shoe-Surface Traction of Conventional and In-Filled Synthetic Turf Football Surfaces. In *Proceedings of the XIX International Congress of Biomechanics*.
- Shorten, M., Himmelsbach, J., 2002. Shock attenuation of sports surfaces. *The Engineering of Sport* 3–6.
- Simon, J., Doederlein, L., McIntosh, a S., Metaxiotis, D., Bock, H.G., Wolf, S.I., 2006. The Heidelberg foot measurement method: development, description and assessment. *Gait & posture* 23, 411–24.
- Sport England, 2003. A Guide to Design, Specification & Construction of Multi-Use Games Areas Including Multi-Sport Synthetic Turf Pitches – Pt. 1, London, UK
- Stefanyshyn, D., Nigg, B., 2003. Energy and performance aspects in sports surfaces. *Sport Surfaces*, 31–46.
- Stefanyshyn, D.J., Lee, J.-S., Park, S.-K., 2010. The influence of soccer cleat design on resultant joint moments. *Footwear Science* 2, 13–19.
- Stiles, V., Dixon, S., 2006. The influence of different playing surfaces on the biomechanics of a tennis running forehand foot plant. *Journal of applied biomechanics* 14–24.
- Stiles, V., Dixon, S., 2007. Biomechanical response to systematic changes in impact interface cushioning properties while performing a tennis-specific movement. *Journal of sports sciences* 25, 1229–39.
- Stiles, V.H., James, I.T., Dixon, S.J., Guisasola, I.N., 2009. Natural turf surfaces: The Case for Continued Research 39, 65–84.
- Stiles, V., Guisasola, I.N., James, I.T., Dixon, S., 2011. Biomechanical Response to Changes in Natural Turf During Running and Turning. *Journal of Applied Biomechanics*. 27, 54-63.
- Synthetic Grass Info, 2010. - <http://grasssyntheticinfo.com/> - Accessed 3rd November 2010.

- Tekscan, 2003. I-Scan Equilibration and Calibration Practical Suggestions. Revision A - personal communication with company representative by email - Received March 2012.
- TenCate, 2010. - <http://www.tencate.com/> - Accessed 3rd November 2010.
- Thomson, R.D., Birkbeck, A.E., Lucas, T.D., 2001. Hyperelastic modelling of nonlinear running surfaces. *Sports Engineering* 4, 215–224.
- Tipp, G. & Watson, V. 1982, *Polymeric Surfaces for Sports and Recreation*, Applied Science Publishers, London, UK.
- Tipp, G. & Watson, V. 1988, *Synthetic Surfaces*, National Turfgrass Council.
- Toon, D., 2008. Design and analysis of sprint footwear to investigate the effects of longitudinal bending stiffness on sprinting performance, PhD Thesis, Loughborough University, Loughborough, UK.
- Torres, E., Sandkuehler, P., Allgeuer, T., 2010. Polyolefin Materials in Artificial Turf II: Infill Developments, *Sports Technology*.
- Tsu, F., 2010. Determining Impact Intensities in Contact Sports, PhD Thesis, Loughborough University, Loughborough, UK.
- Twomey, D.M., Finch, C.F., Lloyd, D.G., Elliott, B.C., Doyle, T.L. a, 2012. Ground hardness and injury in community level Australian football. *Journal of science and medicine in sport / Sports Medicine Australia* 15, 305–10.
- Tyson, J., Schmidt, T. & Galanulis, K. 2003, *Optical Deformation & Strain Measurement in Biomechanics*. GOM user report, Accessed 5th November 2010.
- United European Football Association (UEFA), 2003. *Artificial Turf Requirements and Recommendations*, Nyon, Switzerland.
- Vetrano, K., 2009. Air Quality Survey of Synthetic Turf Fields Containing Crumb Rubber Infill, New York City Department of Health and Mental Hygiene, New York, USA.
- Vicon, 2007. *Vicon MX Hardware System Reference*. Revision 1.7, Oxford, UK.
- Villwock, M. R., Meyer, E. G., Powell, J.W., Fouty, A. J., Haut, R. C., 2008. The effects of various infills, fibre structures and shoe designs on generating rotational traction on artificial surfaces, *Journal of Sports Engineering and Technology*, 223 (Part P), pp. 11-19.
- Villwock, M.R., Meyer, E.G., Powell, J.W., Fouty, A.J., Haut, R.C., 2009. Football Playing Surface and Shoe Design Affect Rotational Traction. *The American Journal of Sports Medicine* 37 , 518–525.
- Walker, C. A., 1996. *Experimental Mechanics and Artificial Turf*, In: *The Engineering of Sport* (Ed. S. J. Haake), Balkema, Rotterdam, p. 239-242.

- Walker, C., 2003. Performance of sports surfaces. *Materials in Sports Equipment*, Abington, Cambridge, Woodhead Publishing, 47-64.
- Walker, C., 2006. The effect of cyclic loading on the stiffness and damping factors in the midsoles of running shoes. *Proceedings of the Institution of Mechanical Engineers, Part L: Journal of Materials: Design and Applications*, 220(1):41–7.
- Wannop, J.W., Worobets, J.T., Stefanyshyn, D.J., 2010. Footwear Traction and Lower Extremity Joint Loading. *The American Journal of Sports Medicine* 38 , 1221–1228.
- Watson, V., 1986. Synthetic Surfaces for Sport Outdoor, *Leisure Management*, Feb 1986: pp. 45-49.
- Watson, V., Tipp, G., 1987. *Impact Absorbing Surfaces, National Playing Fields Association*, London, UK.
- Webster, J.M., Roberts, J.R., 2010. Comfort of cricket leg guards: a study of strap contact pressure, in: *Procedia Engineering*. Elsevier, pp. 3385–3390.
- Willems, T., Witvrouw, E., Delbaere, K., De Cock, a, De Clercq, D., 2005. Relationship between gait biomechanics and inversion sprains: a prospective study of risk factors. *Gait & posture* 21, 379–87.
- Williams, S., Hume, P. a, Kara, S., 2011. A review of football injuries on third and fourth generation artificial turfs compared with natural turf. *Sports medicine (Auckland, N.Z.)* 41, 903–23.
- Yeow, C.H., Lee, P.V.S., Goh, J.C.H., 2009. Effect of landing height on frontal plane kinematics, kinetics and energy dissipation at lower extremity joints. *Journal of biomechanics* 42, 1967–73.
- Young, C., 2006, *Mechanical and Perceived Behaviour of Synthetic Turf Field Hockey Pitches*, PhD Thesis, Loughborough University, Loughborough, UK.
- Young, C., Fleming, P. R., 2007. A Review of Mechanical Impact Testing Devices for Sports Surfaces. In *Proceedings of the First International Conference on Science, Technology and Research into Sport Surfaces (STARSS)*. Loughborough University, UK.
- Yukawa, H., Kobayashi, K., Kawamura, S., 2012. Identification of Viscoelastic Model for Long Pile Synthetic Turf by using Multi-intensity Impact Test. *Procedia Engineering* 34, 849–854.
- Yukawa, H., Murai, T., Nishimura, H., Kawamura, S., Kobayashi, K., 2011. Parameter identification of nonlinear viscoelastic model with impact area parameter for sport surface by using multi-intensity multi-area impact test. *Procedia Engineering* 13, 395–401.

- Zammit, G. V, Menz, H.B., Munteanu, S.E., 2010. Reliability of the TekScan MatScan(R) system for the measurement of plantar forces and pressures during barefoot level walking in healthy adults. *Journal of foot and ankle research* 3, 11.
- Zanetti, E.M., Bignardi, C., Franceschini, G., Audenino, A.L., 2013. Amateur football pitches: mechanical properties of the natural ground and of different artificial turf infills and their biomechanical implications. *Journal of sports sciences* 31, 767–78.